

Discrete Dynamics in Nature and Society

# Discrete Dynamics of Nonlinear Systems in Nature and Society

Lead Guest Editor: J. E. Macías-Díaz

Guest Editors: Qin Sheng, Stefania Tomasiello, and Ahmed S. Hendy





---

# **Discrete Dynamics of Nonlinear Systems in Nature and Society**

Discrete Dynamics in Nature and Society

---

## **Discrete Dynamics of Nonlinear Systems in Nature and Society**

Lead Guest Editor: J. E. Macías-Díaz

Guest Editors: Qin Sheng, Stefania Tomasiello,  
and Ahmed S. Hendy



Copyright © 2019 Hindawi. All rights reserved.

This is a special issue published in “Discrete Dynamics in Nature and Society.” All articles are open access articles distributed under the Creative Commons Attribution License, which permits unrestricted use, distribution, and reproduction in any medium, provided the original work is properly cited.



## Editorial Board

Douglas R. Anderson, USA  
David Arroyo, Spain  
Viktor Avrutin, Germany  
Stefan Balint, Romania  
Kamel Barkaoui, France  
Gian I. Bischi, Italy  
Gabriele Bonanno, Italy  
Florentino Borondo, Spain  
Driss Boutat, France  
Filippo Cacace, Italy  
Pasquale Candito, Italy  
Giulio E. Cantarella, Italy  
Antonia Chinnì, Italy  
Cengiz Çinar, Turkey  
Carmen Coll, Spain  
Giancarlo Consolo, Italy  
Alicia Cordero, Spain  
Giuseppina D'Agui, Italy  
Manuel De la Sen, Spain  
Beatrice Di Bella, Italy  
Luisa Di Paola, Italy  
Josef Diblík, Czech Republic  
Xiaohua Ding, China  
Tien Van Do, Hungary  
Marcio Eisencraft, Brazil  
Elmetwally Elabbasy, Egypt  
Hassan A. El-Morshedy, Egypt  
D. Fournier-Prunaret, France  
Genni Fragnelli, Italy  
Ciprian G. Gal, USA  
Marek Galewski, Poland  
Caristi Giuseppe, Italy  
David M. Goldsman, USA  
Gisèle R Goldstein, USA  
Vladimir Gontar, Israel  
Chris Goodrich, USA

Pilar R. Gordo, Spain  
Kannan Govindan, Denmark  
Luca Guerrini, Italy  
Juan L. G. Guirao, Spain  
Antonio Iannizzotto, Italy  
Giuseppe Izzo, Italy  
Sarangapani Jagannathan, USA  
Jun Ji, USA  
Emilio Jiménez Macías, Spain  
Nikos I. Karachalios, Greece  
Eric R. Kaufmann, USA  
Nickolai Kosmatov, USA  
Victor S. Kozyakin, Russia  
Mustafa R. S. Kulenovic, USA  
Kousuke Kuto, Japan  
Aihua Li, USA  
Xiaohui Liu, UK  
Francesco Longo, Italy  
Miguel Ángel López, Spain  
Ricardo López-Ruiz, Spain  
Rodica Luca, Romania  
Agustin Martin, Spain  
Akio Matsumoto, Japan  
Rigoberto Medina, Chile  
Driss Mehdi, France  
Vicenç Méndez, Spain  
Dorota Mozyrska, Poland  
Yukihiko Nakata, Japan  
Luca Pancioni, Italy  
G. Papashinopoulos, Greece  
Juan Pavón, Spain  
Ewa Pawluszewicz, Poland  
Alfred Peris, Spain  
Allan C. Peterson, USA  
Adrian Petrusel, Romania  
Andrew Pickering, Spain



Chuanxi Qian, USA  
Morteza Rafei, Netherlands  
Youssef N. Raffoul, USA  
Maria Alessandra Ragusa, Italy  
Mustapha A. Rami, Spain  
Aura Reggiani, Italy  
Pavel Rehak, Czech Republic  
Paolo Renna, Italy  
Marko Robnik, Slovenia  
Yuriy Rogovchenko, Norway  
Silvia Romanelli, Italy  
Christos J. Schinas, Greece  
Daniel Sevcovic, Slovakia  
Leonid Shaikhet, Israel  
Seenith Sivasundaram, USA  
Charalampos Skokos, South Africa  
Piergiulio Tempesta, Spain  
Tetsuji Tokihiro, Japan  
J. R. Torregrosa, Spain  
Delfim F. M. Torres, Portugal  
Fabio Tramontana, Italy  
Firdaus Udwadia, USA  
Jose C. Valverde, Spain  
Antonia Vecchio, Italy  
Rafael J. Villanueva, Spain  
Francisco R. Villatoro, Spain  
Hubertus Von Bremen, USA  
Abdul-Aziz Yakubu, USA  
Bo Yang, USA  
Guang Zhang, China  
Zhengqiu Zhang, China  
Lu Zhen, China  
Yong Zhou, China  
Zuonong Zhu, China

# Contents


## **Discrete Dynamics of Nonlinear Systems in Nature and Society**

Jorge E. Macías-Díaz , Qin Sheng , Stefania Tomasiello , and Ahmed S. Hendy  
Editorial (2 pages), Article ID 2801806, Volume 2019 (2019)

## **Optimal Control Strategy for a Discrete Time Smoking Model with Specific Saturated Incidence Rate**

Abderrahim Labzai , Omar Balatif , and Mostafa Rachik  
Research Article (10 pages), Article ID 5949303, Volume 2018 (2019)

## **Evolution of Electoral Preferences for a Regime of Three Political Parties**

María Guadalupe Medina Guevara , Héctor Vargas Rodríguez, Pedro Basilio Espinoza Padilla,  
and José Luis Gozález Solís  
Research Article (9 pages), Article ID 2989851, Volume 2018 (2019)

## **Positive Periodic Solutions for an Generalized SIS Epidemic Model with Time-Varying Coefficients and Delays**

Zhiwen Long   
Research Article (5 pages), Article ID 7296320, Volume 2018 (2019)


## **Uniqueness and Novel Finite-Time Stability of Solutions for a Class of Nonlinear Fractional Delay Difference Systems**

Danfeng Luo and Zhiguo Luo   
Research Article (7 pages), Article ID 8476285, Volume 2018 (2019)

## **A Hybrid Ant Colony Optimization for Dynamic Multidepot Vehicle Routing Problem**

Haitao Xu , Pan Pu , and Feng Duan  
Research Article (10 pages), Article ID 3624728, Volume 2018 (2019)


## **Laplace Transform Method for Pricing American CEV Strangles Option with Two Free Boundaries**

Zhiqiang Zhou  and Hongying Wu  
Research Article (12 pages), Article ID 5908646, Volume 2018 (2019)

## **A Solvable Time-Inconsistent Principal-Agent Problem**

Chao Li  and Zhijian Qiu  
Research Article (15 pages), Article ID 8512608, Volume 2018 (2019)




## **Ising Model of User Behavior Decision in Network Rumor Propagation**

Chengcheng Li, Fengming Liu , and Pu Li  
Research Article (10 pages), Article ID 5207475, Volume 2018 (2019)

## **Spatial Dynamics for a Generalized Solow Growth Model**

Yue Zhong  and Wenyi Huang   
Research Article (8 pages), Article ID 6945032, Volume 2018 (2019)

## **Research on a Triopoly Dynamic Game with Free Market and Bundling Market in the Chinese Telecom Industry**

Junhai Ma , Tiantong Xu , and Wandong Lou   
Research Article (11 pages), Article ID 5720392, Volume 2018 (2019)

---

**The Uniqueness Theorem of the Solution for a Class of Differential Systems with Coupled Integral Boundary Conditions**

Shuman Meng and Yujun Cui 

Research Article (7 pages), Article ID 9601868, Volume 2018 (2019)

**Applications of General Residual Power Series Method to Differential Equations with Variable Coefficients**

Bochao Chen, Li Qin, Fei Xu, and Jian Zu 

Research Article (9 pages), Article ID 2394735, Volume 2018 (2019)

**Asymptotic Properties of Solutions to Second-Order Difference Equations of Volterra Type**

Janusz Migda, Małgorzata Migda , and Magdalena Nockowska-Rosiak

Research Article (10 pages), Article ID 2368694, Volume 2018 (2019)

**Nonsmooth Vibration Characteristic of Gear Pair System with Periodic Stiffness and Backlash**

Minjia He, Shuo Li , Zhenjun Lin, Jinjin Wang, Shuang Liu , and Ruolan Hao 

Research Article (13 pages), Article ID 3498057, Volume 2018 (2019)

## Editorial

# Discrete Dynamics of Nonlinear Systems in Nature and Society

**Jorge E. Macías-Díaz** <sup>1</sup>, **Qin Sheng** <sup>2</sup>, **Stefania Tomasiello** <sup>3</sup>, and **Ahmed S. Hendy**<sup>4,5</sup>

<sup>1</sup>Departamento de Matemáticas y Física, Universidad Autónoma de Aguascalientes, Ags. 20131, Mexico

<sup>2</sup>Department of Mathematics, Baylor University, Waco, TX 76798-7328, USA

<sup>3</sup>Consorzio di Ricerca Sistemi ad Agenti, Università degli Studi di Salerno, 84084 Fisciano, Salerno, Italy

<sup>4</sup>Department of Computational Mathematics and Computer Science, Institute of Natural Sciences and Mathematics, Ural Federal University, 19 Mira St., Yekaterinburg 620002, Russia

<sup>5</sup>Department of Mathematics, Faculty of Science, Benha University, Benha, 13511, Egypt

Correspondence should be addressed to Jorge E. Macías-Díaz; jemacias@correo.uaa.mx

Received 9 December 2018; Accepted 10 December 2018; Published 3 January 2019

Copyright © 2019 Jorge E. Macías-Díaz et al. This is an open access article distributed under the Creative Commons Attribution License, which permits unrestricted use, distribution, and reproduction in any medium, provided the original work is properly cited.

Discrete nonlinear systems have become increasingly important in the past decades. To understand them, new analytical and numerical methodologies have been proposed. More accurate predictions of the solutions of systems related to physical problems are investigated in that way. It is worth noting that qualitative and quantitative features of discrete nonlinear modeling problems and simulation techniques have attracted a significant amount of attention from researchers in different branches of applied sciences. This is due to the fact that features of the solutions are crucial to our understanding of many important phenomena in nature and society. In fact, the science and engineering communities have benefited tremendously from recent progress in the area. Interactions between the praxis and new mathematical methodologies have also reached a new high level.

Based on the above, this special issue aims at keeping track of the most relevant developments in the analysis and simulations of discrete nonlinear systems that appear in nature and society. More precisely, we pay special attention to analytical features of the solutions of the systems as well as the analysis of interactive computational strategies. Both deterministic and stochastic paradigms arising from nature and society are of interest, and pertinent applications to the resolution of realistic problems are studied. Continuous methods are within our interest as far as they provide helpful or insightful tools for the analysis. Challenging issues pertaining to the analysis of (integer- and fractional-order) partial differential equations and underlying approximation techniques are also of high relevance.

There are 49 research papers being received and undergone thorough peer-reviewing processes. There are 15 articles accepted and published in this special issue. They represent the most recent developments in the fields, with applications to sciences and technologies. The contributions focus primarily on issues that include the following:

- (i) solvable time-inconsistent principal-agent problems;
- (ii) non-smooth vibration characteristics of gear pair systems with periodic stiffness and backlash;
- (iii) applications of the general residual power series method to problems with variable coefficients;
- (iv) Laplace transform method for pricing American CEV Strangles option with two free boundaries;
- (v) Triopoly dynamic games with free or bundling markets in telecommunication industry;
- (vi) Ising models of user behavior decision in network rumor propagation;
- (vii) uniqueness of the solution for a class of differential system with coupled integral boundary conditions;
- (viii) asymptotic properties of solutions to second-order difference equations of Volterra type;
- (ix) positive periodic solutions for generalized epidemic models with time-varying coefficients and delays;
- (x) spatial dynamics for generalized Solow growth models;

- (xi) uniqueness and finite-time stability of solutions for nonlinear fractional delay difference systems;
- (xii) evolution of electoral preferences for regimes of three political parties;
- (xiii) hybrid ant colony optimization for dynamic multidepot vehicle routing problem;
- (xiv) optimal control strategies for discrete-time smoking models with saturated incidence rates;
- (xv) mean-square stability of semi-implicit Euler methods for the model of technology innovation network.

### **Conflicts of Interest**

The guest editors of this special issue report no potential conflicts of interest.

*Jorge E. Macías-Díaz*  
*Qin Sheng*  
*Stefania Tomasiello*  
*Ahmed S. Hendy*

## Research Article

# Optimal Control Strategy for a Discrete Time Smoking Model with Specific Saturated Incidence Rate

Abderrahim Labzai <sup>1</sup>, Omar Balatif <sup>2</sup> and Mostafa Rachik<sup>1</sup>

<sup>1</sup>Laboratory of Analysis Modeling and Simulation, Department of Mathematics and Computer Science, Faculty of Sciences Ben M'Sik, Hassan II University Mohammedia, Sidi Othman, Casablanca, Morocco

<sup>2</sup>Mathematical Engineering Team (INMA), Department of Mathematics, Faculty of Sciences El Jadida, Chouaib Doukkali University, El Jadida, Morocco

Correspondence should be addressed to Abderrahim Labzai; labzaiabdo1977@gmail.com

Received 4 August 2018; Revised 6 October 2018; Accepted 4 November 2018; Published 15 November 2018

Academic Editor: Qin Sheng

Copyright © 2018 Abderrahim Labzai et al. This is an open access article distributed under the Creative Commons Attribution License, which permits unrestricted use, distribution, and reproduction in any medium, provided the original work is properly cited.

The aim of this paper is to study and investigate the optimal control strategy of a discrete mathematical model of smoking with specific saturated incidence rate. The population that we are going to study is divided into five compartments: potential smokers, light smokers, heavy smokers, temporary quitters of smoking, and permanent quitters of smoking. Our objective is to find the best strategy to reduce the number of light smokers, heavy smokers, and temporary quitters of smoking. We use three control strategies which are awareness programs through media and education, treatment, and psychological support with follow-up. Pontryagin's maximum principle in discrete time is used to characterize the optimal controls. The numerical simulation is carried out using MATLAB. Consequently, the obtained results confirm the performance of the optimization strategy.

## 1. Introduction

Following the WHO report on the global tobacco epidemic, which was published on 19 July 2017 in the United Nations High-Level Political Forum for Sustainable Development in New York, tobacco consumption is the world's leading cause of death with a rate of more than 7 million deaths a year [1]. Tobacco consumption is known as the main cause of death of lethal diseases such as lung cancer, oral cavity, stomach ulcer, and a probable cause of death for cancers of the larynx, bladder, pancreas, and renal pelvis. Comparative data on smoking show that the risk of heart attack among smokers is 70% higher than that of nonsmokers. In addition to that, the economic costs are also enormous totaling more than 1400 billion dollars (US \$) in health expenditure and loss of productivity [2].

Lung cancer in smokers is ten times higher than in nonsmokers, and one in ten smokers will die of lung cancer. In Spain, it is estimated that about 55,000 deaths a year are attributable to smoking [3]. However, smoking-related illnesses cause more than 440,000 deaths each year

in the United States and more than 105,000 deaths in the United Kingdom each year. Moreover, about 4 million people die from smoking-related diseases worldwide and half of all smokers die from smoking-related diseases, while the number of new smokers continues to increase [4].

As far as Morocco is concerned, a new report by the World Health Organization revealed that the number of smokers has notably risen, expecting it to reach over 7 million by 2025 [5]. The WHO has urged the Moroccan government to increase taxes on cigarettes and other tobacco products to discourage use and decrease the rising number of smokers across the country. In its Global Report on Trends in Prevalence of Tobacco Smoking in 2015, WHO estimated that up to 21% of Morocco's population (approximately 4,820,500 persons) smoked in 2010.

More specifically, the report noted that about 42% of men and up to 2% of women smoked in Morocco in 2010. It goes on to add that the highest rate of smoking among men was seen in the 25–39 age groups and 15–24 age groups among women. WHO recommends that at least one adult survey



and one youth survey be completed every five years. In the event that the Moroccan government does not adopt new measures to discourage the use of tobacco, the UN estimated that the number of smokers could be over 7 million by 2025. Member states, including Morocco, adopted a voluntary global target to reduce tobacco use 30% (smokers and smokeless) by 2025. However, based on the current smoking trend, Morocco will not achieve the target, WHO concluded [6].

Mathematical modeling of smoking has been studied by many researchers [3, 7–9]. We observe that most of those researchers focused on the continuous-time models described by the differential equations. It is noted that, in recent years, more and more attention has been given to discrete time models (see [10–13] and the references cited therein). The reasons for adopting discrete modeling are as follows: Firstly, the statistical data are collected at discrete moments (day, week, month, or year). So, it is more direct and more accurate and timely to describe the disease using discrete time models than continuous time models. Secondly, the use of discrete time models can avoid some mathematical complexities such as choosing a function space and regularity of the solution. Thirdly, the numerical simulations of continuous time models are obtained by the way of discretization.

Based on the aforementioned reasons, we will develop in this paper a discrete time model studying the dynamics of smokers and introduce a saturated incidence rate to be analysed in detail in the next section. Also, we add to our model two elements which were not taken into consideration in the most previous researches. Those two elements are a group of light smokers who quit smoking permanently and a group of heavy smokers who died due to diseases generated by the excess of smoking.

In addition, in order to find the best strategy to reduce the number of light smokers, heavy smokers, and temporary quitters of smoking we will use three control strategies which are awareness programs through media and education, treatment, and psychological support with follow-up.

In this paper, we construct a discrete PLSQ<sup>t</sup>Q<sup>p</sup> Mathematical Smoking Model with Specific Saturated Incidence Rate and introduce the control of awareness measures. In Section 2, the mathematical model is proposed. In Section 3, we investigate the optimal control problem for the proposed discrete mathematical model. Section 4 consists of numerical simulation through MATLAB. The conclusion is given in Section 5.

## 2. Formulation of the Mathematical Model

In this section, we present a discrete PLSQ<sup>t</sup>Q<sup>p</sup> Mathematical Smoking Model. The population under investigation is divided into five compartments: potential smokers (nonsmokers)  $P_k$ , light smokers  $L_k$ , heavy smokers  $S_k$ , smokers who temporarily quit smoking  $Q_k^t$ , and smokers who permanently quit smoking  $Q_k^p$ , respectively. Following what

has been done in many works [2], we introduce a saturated incidence rate  $\beta_i(X_k Y_k / (1 + m_j Y_k))$  in discrete time (where  $X_k Y_k \in \{P_k L_k, P_k S_k, L_k S_k\}$ ,  $\beta_i$ —for  $i = 1, 2, 3$ —is the contact rate between  $X_k$  and  $Y_k$ ,  $m_j$ —for  $j = 1, 2, 3$ —is a positive constant) to describe the crowding effect among potential smokers, light smokers, and heavy smokers.  $\beta_i X_k Y_k$  measures the infection force of the smoking and  $1/(1 + m_j Y_k)$  describes the crowding effect and the “psychological” effect from the behavioral change of the individuals  $Y_k$  when their number increases.

**2.1. Description of the Model. The compartment P:** the potential smokers (nonsmokers), people who have not smoked yet but might become smokers in the future. This compartment is increased by the recruitment of individuals at rate  $\Lambda$  and  $P$  is decreased with the rates  $\beta_1(1 - \rho)(P_k L_k / (1 + m_1 L_k))$ ,  $\beta_1 \rho(P_k S_k / (1 + m_2 S_k))$  and some of the people vacate at a constant death rate of  $\mu$  due to the total natural death rate  $\mu P_k$ .

**The compartment L:** the occasional smokers whose number increases when the potential smokers start to smoke with a saturated incidence rate  $\beta_1(1 - \rho)(P_k L_k / (1 + m_1 L_k))$ . Some other individuals will leave the compartment with the saturated incidence rate  $\beta_2(L_k S_k / (1 + m_3 S_k))$ , the rate  $\beta_3 L_k$ , and  $\mu L_k$ . Here,  $\beta_3$  is the rate of light smokers who permanently quit smoking.

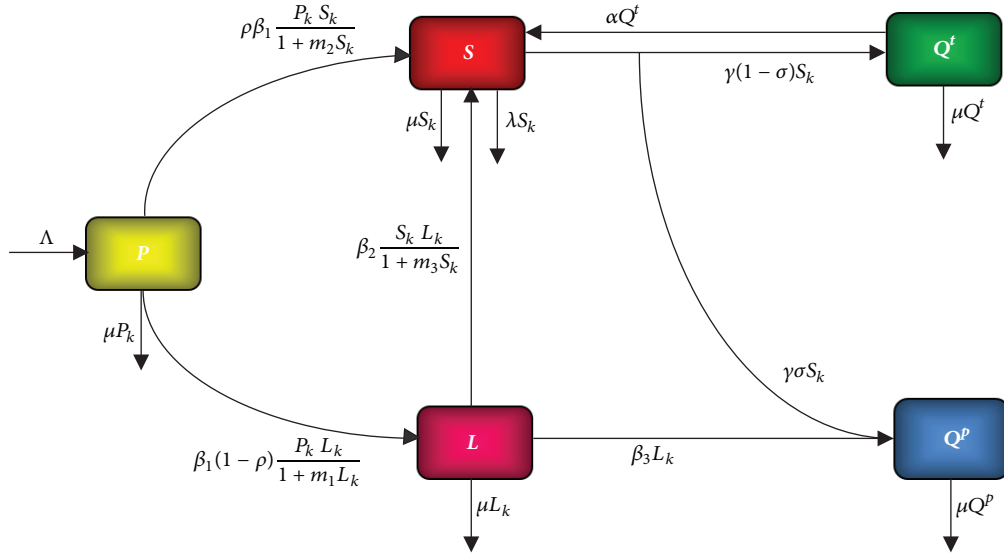
**The compartment S:** the people who are heavy smokers and whose number increases by the saturated incidence rate  $\beta_1 \rho(P_k S_k / (1 + m_2 S_k))$ ,  $\beta_2(L_k S_k / (1 + m_3 S_k))$  and the rate  $\alpha$  of temporary quitters who revert back to smoking. Some others will leave at the rates  $\gamma S_k$ ,  $\lambda S_k$ , and  $\mu S_k$ . Here,  $\lambda$  is the rate of death due to heavy smoking and  $\gamma$  is the rate of quitting smoking.

**The compartment Q<sup>t</sup>:** the individuals who temporarily quit smoking, whose number increases at the rate  $\gamma(1 - \sigma)S_k$  and decreases at the rates  $\mu Q_k^t$  and  $\alpha Q_k^t$ , where  $(1 - \sigma)$  is the fraction of heavy smokers who temporarily quit smoking (at a rate  $\gamma$ ).

**The compartment Q<sup>p</sup>:** the individuals who permanently quit smoking, whose number increases with the rates  $\gamma \sigma S_k$  and  $\beta_3 L_k$ . Some people of this compartment will die with the rate  $\mu Q_k^p$ , where  $\sigma$  is the remaining fraction of heavy smokers who permanently quit smoking (at a rate  $\gamma$ ).

The following diagram will demonstrate the flow directions of individuals among the compartments. These directions are going to be represented by directed arrows in Figure 1.

**2.2. Model Equations.** Through the addition of the rates at which individuals enter the compartment and also by subtracting the rates at which people vacate the compartment, we obtain an equation of difference for the rate at which the individuals of each compartment change over discrete time. Hence, we present the smoking

FIGURE 1: The flow between the five compartments  $PLSQ^tQ^p$ .

infection model by the following system of difference equations:

$$\begin{aligned}
 P_{k+1} &= \Lambda + (1 - \mu) P_k - \beta_1 (1 - \rho) \frac{P_k L_k}{1 + m_1 L_k} \\
 &\quad - \beta_1 \rho \frac{P_k S_k}{1 + m_2 S_k} \\
 L_{k+1} &= (1 - \mu) L_k + \beta_1 (1 - \rho) \frac{P_k L_k}{1 + m_1 L_k} \\
 &\quad - \beta_2 \frac{L_k S_k}{1 + m_3 S_k} - \beta_3 L_k \\
 S_{k+1} &= (1 - \mu - \lambda - \gamma) S_k + \beta_1 \rho \frac{P_k S_k}{1 + m_2 S_k} \\
 &\quad + \beta_2 \frac{L_k S_k}{1 + m_3 S_k} + \alpha Q_k^t \\
 Q_{k+1}^t &= (1 - \mu - \alpha) Q_k + \gamma (1 - \sigma) S_k \\
 Q_{k+1}^p &= (1 - \mu) Q_k^p + \gamma \sigma S_k + \beta_3 L_k
 \end{aligned} \tag{1}$$

### 3. The Optimal Control Problem

The strategies of control that we adopt consist of an awareness program through media and education, treatment, and psychological support with follow-up. Our main goal in adopting those strategies is to minimize the number of occasional smokers, heavy smokers, and the temporarily quitters of smoking during the time steps  $k = 0$  to  $T$  and also minimizing the cost spent in applying the three strategies. In this model, we include the three controls  $u_k$ ,  $v_k$ , and  $w_k$

that represent consecutively the awareness program through media and education, treatment, and psychological support with follow-up as measures at time  $k$ . So, the controlled mathematical system is given by the following system of difference equations:

$$\begin{aligned}
 P_{k+1} &= \Lambda + (1 - \mu) P_k - \beta_1 (1 - \rho) \frac{P_k L_k}{1 + m_1 L_k} \\
 &\quad - \beta_1 \rho \frac{P_k S_k}{1 + m_2 S_k} \\
 L_{k+1} &= (1 - \mu) L_k + \beta_1 (1 - \rho) \frac{P_k L_k}{1 + m_1 L_k} \\
 &\quad - \beta_2 \frac{L_k S_k}{1 + m_3 S_k} - \beta_3 L_k - c_1 u_k L_k \\
 S_{k+1} &= (1 - \mu - \lambda - \gamma) S_k + \beta_1 \rho \frac{P_k S_k}{1 + m_2 S_k} \\
 &\quad + \beta_2 \frac{L_k S_k}{1 + m_3 S_k} + \alpha Q_k^t - c_2 v_k S_k \\
 Q_{k+1}^t &= (1 - \mu - \alpha) Q_k^t + \gamma (1 - \sigma) S_k - c_3 w_k Q_k^t \\
 Q_{k+1}^p &= (1 - \mu) Q_k^p + \gamma \sigma S_k + \beta_3 L_k + c_1 u_k L_k + c_2 v_k S_k \\
 &\quad + c_3 w_k Q_k^t,
 \end{aligned} \tag{2}$$

where

$$c_i = \begin{cases} 1 & \text{for } i = 1, 2, 3. \\ 0 & \end{cases} \tag{3}$$

TABLE 1: Interpretations according to the values of  $c_i$ .

$c_1$	$c_2$	$c_3$	Interpretations
0	0	0	Discrete smoking model (without controls)
1	0	0	Discrete smoking model with awareness program: (u)
0	1	0	Discrete smoking model with treatment: (v)
0	0	1	Discrete smoking model with psychological support along follow-up: (w)
1	1	0	Discrete smoking model with (u) and (v)
1	0	1	Discrete smoking model with (u) and (w)
0	1	1	Discrete smoking model with (v) and (w)
1	1	1	Discrete smoking model with (u), (v) and (w)

There are three controls  $u = (u_0, u_1, \dots, u_T)$ ,  $v = (v_0, v_1, \dots, v_T)$ , and  $w = (w_0, w_1, \dots, w_T)$ . The first control can be interpreted as the proportion to be adopted for the awareness program through media and education. So, we note that  $u_k L_k$  is the proportion of the light smoker individuals who moved to the individuals who permanently quit smoking at time step  $k$ . The second control can be interpreted as the proportion to be subjected to treatment. So, we note that  $v_k S_k$  is the proportion of the individuals who will move from the class of heavy smokers towards the class of the individuals who permanently quit smoking at time step  $k$ . The third control can also be interpreted as the proportion to get psychological support with follow-up. So, we note that  $w_k Q_k^t$  is the proportion of the individuals who temporarily quit smoking and who will transform into the individuals who permanently quit smoking at time step  $k$ . Indeed, the system above (2) presents eight different models as Table 1 explains.

The problem that we face here is how to minimize the objective functional:

$$J(u, v, w) = A_T S_T + B_T L_T + C_T Q_T^t + \sum_{k=0}^{T-1} \left( A_k S_k + B_k L_k + C_k Q_k^t + \frac{D_k}{2} c_1 u_k^2 + \frac{E_k}{2} c_2 v_k^2 + \frac{F_k}{2} c_3 w_k^2 \right), \quad (4)$$

where the parameters  $A_k > 0$ ,  $B_k > 0$ ,  $C_k > 0$ ,  $D_k > 0$ ,  $E_k > 0$ , and  $F_k > 0$  are the cost coefficients; they are selected to weigh the relative importance of  $S_k$ ,  $L_k$ ,  $Q_k^t$ ,  $u_k$ ,  $v_k$ , and  $w_k$  at time  $k$ .  $T$  is the final time.

In other words, we seek the optimal controls  $u_k$ ,  $v_k$ , and  $w_k$  such that

$$J(u^*, v^*, w^*) = \min_{(u, v, w) \in U_{ad}} J(u, v, w), \quad (5)$$

where  $U_{ad}$  is the set of admissible controls defined by

$$U_{ad} = \{(u_k, v_k, w_k) : a \leq u_k \leq b, c \leq v_k \leq d, e \leq w_k \leq f; k = 0, 1, 2, \dots, T-1\} \quad (6)$$

The sufficient condition for the existence of optimal controls  $(u, v, w)$  for problem (2) and (4) comes from the following theorem.

**Theorem 1.** *There exists an optimal control  $(u^*, v^*, w^*)$  such that*

$$J(u^*, v^*, w^*) = \min_{(u, v, w) \in U_{ad}} J(u, v, w) \quad (7)$$

*subject to the control system (2) with initial conditions.*

*Proof.* Since the coefficients of the state equations are bounded and there are a finite number of time steps,  $P = (P_0, P_1, \dots, P_T)$ ,  $L = (L_0, L_1, \dots, L_T)$ ,  $S = (S_0, S_1, \dots, S_T)$ ,  $Q^t = (Q_0^t, Q_1^t, \dots, Q_T^t)$ , and  $Q^p = (Q_0^p, Q_1^p, \dots, Q_T^p)$  are uniformly bounded for all  $(u; v; w)$  in the control set  $U_{ad}$ ; thus  $J(u; v; w)$  is bounded for all  $(u; v; w) \in U_{ad}$ . Since  $J(u; v; w)$  is bounded,  $\inf_{(u, v, w) \in U_{ad}} J(u, v, w)$  is finite, and there exists a sequence  $(u^j; v^j; w^j) \in U_{ad}$  such that  $\lim_{j \rightarrow +\infty} J(u^j, v^j, w^j) = \inf_{(u, v, w) \in U_{ad}} J(u, v, w)$  and corresponding sequences of states  $P^j$ ,  $L^j$ ,  $S^j$ ,  $Q^{tj}$ , and  $Q^{pj}$ . Since there is a finite number of uniformly bounded sequences, there exist  $(u^*, v^*, w^*) \in U_{ad}$  and  $P^*$ ,  $L^*$ ,  $S^*$ ,  $Q^{t*}$ , and  $Q^{p*} \in \mathbb{R}^{T+1}$  such that, on a subsequence,  $(u^j, v^j, w^j) \rightarrow (u^*, v^*, w^*)$ ,  $P^j \rightarrow P^*$ ,  $L^j \rightarrow L^*$ ,  $S^j \rightarrow S^*$ ,  $Q^{tj} \rightarrow Q^{t*}$ , and  $Q^{pj} \rightarrow Q^{p*}$ . Finally, due to the finite dimensional structure of system (2) and the objective function  $J(u; v; w)$ ,  $(u^*; v^*; w^*)$  is an optimal control with corresponding states  $P^*$ ,  $L^*$ ,  $S^*$ ,  $Q^{t*}$ , and  $Q^{p*}$ . Therefore  $\inf_{(u, v, w) \in U_{ad}} J(u, v, w)$  is achieved.  $\square$

In order to derive the necessary condition for optimal control, the pontryagins maximum principle in discrete time given in [10, 11, 14–16] was used. This principle converts into a problem of minimizing a Hamiltonian  $H_k$  at time step  $k$  defined by

$$H_k = A_k S_k + B_k L_k + C_k Q_k^t + \frac{D_k}{2} c_1 u_k^2 + \frac{E_k}{2} c_2 v_k^2 + \frac{F_k}{2} c_3 w_k^2 + \sum_{j=1}^5 \lambda_{j,k+1} f_{j,k+1}, \quad (8)$$

where  $f_{j,k+1}$  is the right side of the system of difference equations (2) of the  $j^{th}$  state variable at time step  $k + 1$ .

**Theorem 2.** Given an optimal control  $(u_k^*, v_k^*, w_k^*) \in U_{ad}$  and the solutions  $P_k^*, L_k^*, S_k^*, Q_k^t$ , and  $Q_k^{p*}$  of the corresponding state system (2), there exist adjoint functions  $\lambda_{1,k}, \lambda_{2,k}, \lambda_{3,k}, \lambda_{4,k}$ , and  $\lambda_{5,k}$  satisfying

$$\begin{aligned} \lambda_{1,k} &= \beta_1 \rho (\lambda_{3,k+1} - \lambda_{1,k+1}) \frac{S_k}{1 + m_2 S_k} \\ &+ \beta_1 (1 - \rho) (\lambda_{2,k+1} - \lambda_{1,k+1}) \frac{L_k}{1 + m_1 L_k} \\ &+ \lambda_{1,k+1} (1 - \mu). \\ \lambda_{2,k} &= B_k + \beta_1 (1 - \rho) (\lambda_{2,k+1} - \lambda_{1,k+1}) \frac{P_k}{(1 + m_1 L_k)^2} \\ &+ \beta_2 (\lambda_{3,k+1} - \lambda_{2,k+1}) \frac{S_k}{1 + m_3 S_k} \\ &+ \lambda_{2,k+1} (1 - \mu) \\ &+ (\lambda_{5,k+1} - \lambda_{2,k+1}) (c_1 u_k + \beta_3). \end{aligned} \quad (9)$$

$$\begin{aligned} \lambda_{3,k} &= A_k + \beta_1 \rho (\lambda_{3,k+1} - \lambda_{1,k+1}) \frac{P_k}{(1 + m_2 S_k)^2} \\ &+ \beta_2 (\lambda_{3,k+1} - \lambda_{2,k+1}) \frac{L_k}{(1 + m_3 S_k)^2} \\ &+ \lambda_{3,k+1} (1 - \mu - \lambda - \gamma) + \gamma \lambda_{4,k+1} (1 - \sigma) \\ &+ (\lambda_{5,k+1} - \lambda_{3,k+1}) c_2 v_k. \\ \lambda_{4,k} &= C_k + \alpha \lambda_{3,k+1} + \lambda_{4,k+1} (1 - \mu) \\ &+ (\lambda_{5,k+1} - \lambda_{4,k+1}) c_3 w_k. \\ \lambda_{5,k} &= \lambda_{5,k+1} (1 - \mu). \end{aligned}$$

With the transversality conditions at time  $T$ ,  $\lambda_{1,T} = \lambda_{5,T} = 0$ ,  $\lambda_{2,T} = B_T$ ,  $\lambda_{3,T} = A_T$ , and  $\lambda_{4,T} = C_T$ .

Furthermore, for  $k = 0, 1, 2, \dots, T - 1$  and  $c_1 = c_2 = c_3 = 1$ , the optimal controls  $u_k^*$ ,  $v_k^*$ , and  $w_k^*$  are given by

$$\begin{aligned} u_k^* &= \min \left[ b; \max \left( a, \frac{1}{D_k} [(\lambda_{2,k+1} - \lambda_{5,k+1}) L_k] \right) \right] \\ v_k^* &= \min \left[ d; \max \left( c, \frac{1}{E_k} [(\lambda_{3,k+1} - \lambda_{5,k+1}) S_k] \right) \right] \end{aligned}$$

$$w_k^* = \min \left[ f; \max \left( e, \frac{1}{F_k} [(\lambda_{4,k+1} - \lambda_{5,k+1}) Q_k^t] \right) \right] \quad (10)$$

*Proof.* The Hamiltonian at time step  $k$  is given by

$$\begin{aligned} H_k &= A_k S_k + B_k L_k + C_k Q_k^t + \frac{D_k}{2} c_1 u_k^2 + \frac{E_k}{2} c_2 v_k^2 + \frac{F_k}{2} \\ &\cdot c_3 w_k^2 + \lambda_{1,k+1} f_{1,k+1} + \lambda_{2,k+1} f_{2,k+1} + \lambda_{3,k+1} f_{3,k+1} \\ &+ \lambda_{4,k+1} f_{4,k+1} + \lambda_{5,k+1} f_{5,k+1} = A_k S_k + B_k L_k \\ &+ C_k Q_k^t + \frac{D_k}{2} c_1 u_k^2 + \frac{E_k}{2} c_2 v_k^2 + \frac{F_k}{2} c_3 w_k^2 + \lambda_{1,k+1} \left[ \Lambda \right. \\ &+ (1 - \mu) P_k - \beta_1 (1 - \rho) \frac{P_k L_k}{1 + m_1 L_k} \\ &- \beta_1 \rho \frac{P_k S_k}{1 + m_2 S_k} \left. \right] + \lambda_{2,k+1} \left[ (1 - \mu) L_k \right. \\ &+ \beta_1 (1 - \rho) \frac{P_k L_k}{1 + m_1 L_k} - \beta_2 \frac{L_k S_k}{1 + m_3 S_k} - c_1 u_k L_k \\ &- \beta_3 L_k \left. \right] + \lambda_{3,k+1} \left[ (1 - \mu - \lambda - \gamma) S_k \right. \\ &+ \beta_1 \rho \frac{P_k S_k}{1 + m_2 S_k} + \beta_2 \frac{L_k S_k}{1 + m_3 S_k} + \alpha Q_k^t - c_2 v_k S_k \left. \right] \\ &+ \lambda_{4,k+1} \left[ (1 - \mu - \alpha) Q_k^t + \gamma (1 - \sigma) S_k - w_k Q_k^t \right] \\ &+ \lambda_{5,k+1} \left[ (1 - \mu) Q_k^p + \gamma \sigma S_k + c_1 u_k L_k + c_2 v_k S_k \right. \\ &+ c_3 w_k Q_k^t + \beta_3 L_k \left. \right] \end{aligned} \quad (11)$$

For  $k = 0, 1, \dots, T - 1$  the optimal controls  $u_k, v_k, w_k$  can be solved from the optimality condition,

$$\begin{aligned} \frac{\partial H_k}{\partial u_k} &= 0, \\ \frac{\partial H_k}{\partial v_k} &= 0, \\ \frac{\partial H_k}{\partial w_k} &= 0 \end{aligned} \quad (12)$$

that are

$$\begin{aligned}
\frac{\partial H_k}{\partial u_k} &= D_k c_1 u_k + (\lambda_{5,k+1} - \lambda_{2,k+1}) c_1 L_k = 0 \\
\frac{\partial H_k}{\partial v_k} &= E_k c_2 v_k + (\lambda_{5,k+1} - \lambda_{3,k+1}) c_2 S_k = 0 \\
\frac{\partial H_k}{\partial w_k} &= F_k c_3 w_k + (\lambda_{5,k+1} - \lambda_{4,k+1}) c_3 Q_k^t = 0
\end{aligned} \tag{13}$$

So, for  $c_1 = c_2 = c_3 = 1$ , we have

$$\begin{aligned}
u_k &= \frac{1}{D_k} (\lambda_{2,k+1} - \lambda_{5,k+1}) L_k \\
v_k &= \frac{1}{E_k} (\lambda_{3,k+1} - \lambda_{5,k+1}) S_k \\
w_k &= \frac{1}{F_k} (\lambda_{4,k+1} - \lambda_{5,k+1}) Q_k^t
\end{aligned} \tag{14}$$

However, if  $c_i = 0$  for  $i = 1, 2, 3$ , the control attached to this case will be eliminated and removed.

By the bounds in  $U_{ad}$  of the controls, it is easy to obtain  $u_k^*$ ,  $v_k^*$ , and  $w_k^*$  in the form of (10).  $\square$

## 4. Simulation

**4.1. Algorithm.** In this section, we present the results obtained by solving numerically the optimality system. This system consists of the state system, adjoint system, initial and final time conditions, and the controls characterization. So, the optimality system is given by the following.

*Step 1.*  $P_0 = p_0$ ,  $L_0 = l_0$ ,  $S_0 = s_0$ ,  $Q_0^t = q_0^t$ ,  $Q_0^p = q_0^p$ ,  $\lambda_{1,T} = \lambda_{5,T} = 0$ ,  $\lambda_{2,T} = B_T$ ,  $\lambda_{3,T} = A_T$ ,  $\lambda_{4,T} = C_T$ , and given  $u_{k,0}^*$ ,  $v_{k,0}^*$ , and  $w_{k,0}^*$

*Step 2.* For  $k = 0; 1; \dots; T-1$  do:

$$\begin{aligned}
P_{k+1} &= \Lambda + (1 - \mu) P_k - \beta_1 (1 - \rho) \frac{P_k L_k}{1 + m_1 L_k} \\
&\quad - \beta_1 \rho \frac{P_k S_k}{1 + m_2 S_k} \\
L_{k+1} &= (1 - \mu) L_k + \beta_1 (1 - \rho) \frac{P_k L_k}{1 + m_1 L_k} - \beta_2 \frac{L_k S_k}{1 + m_3 S_k} \\
&\quad - \beta_3 L_k - c_1 u_k L_k \\
S_{k+1} &= (1 - \mu - \lambda - \gamma) S_k + \beta_1 \rho \frac{P_k S_k}{1 + m_2 S_k} + \beta_2 \frac{L_k S_k}{1 + m_3 S_k} \\
&\quad + \alpha Q_k^t - c_2 v_k S_k
\end{aligned}$$

$$\begin{aligned}
Q_{k+1}^t &= (1 - \mu - \alpha) Q_k^t + \gamma (1 - \sigma) S_k - c_3 w_k Q_k^t \\
Q_{k+1}^p &= (1 - \mu) Q_k^p + \gamma \sigma S_k + \beta_3 L_k + c_1 u_k L_k + c_2 v_k S_k \\
&\quad + c_3 w_k Q_k^t
\end{aligned}$$

$\vdots$   
 $\vdots$

$$\begin{aligned}
\lambda_{1,T-k} &= \beta_1 \rho (\lambda_{3,T-k+1} - \lambda_{1,T-k+1}) \frac{S_k}{1 + m_2 S_k} \\
&\quad + \beta_1 (1 - \rho) (\lambda_{2,T-k+1} - \lambda_{1,T-k+1}) \frac{L_k}{1 + m_1 L_k} \\
&\quad + \lambda_{1,T-k+1} (1 - \mu) \\
\lambda_{2,T-k} &= B_k + \beta_1 (1 - \rho) (\lambda_{2,T-k+1} - \lambda_{1,T-k+1}) \frac{P_k}{(1 + m_1 L_k)^2} \\
&\quad + \beta_2 (\lambda_{3,T-k+1} - \lambda_{2,T-k+1}) \frac{S_k}{1 + m_3 S_k} + \lambda_{2,T-k+1} (1 - \mu) \\
&\quad + (\lambda_{5,T-k+1} - \lambda_{2,T-k+1}) (c_1 u_k + \beta_3) \\
\lambda_{3,T-k} &= A_k + \beta_1 \rho (\lambda_{3,T-k+1} - \lambda_{1,T-k+1}) \frac{P_k}{(1 + m_2 S_k)^2} \\
&\quad + \beta_2 (\lambda_{3,T-k+1} - \lambda_{2,T-k+1}) \frac{L_k}{(1 + m_3 S_k)^2} \\
&\quad + \lambda_{3,T-k+1} (1 - \mu - \lambda - \gamma) + \gamma \lambda_{4,T-k+1} (1 - \sigma) \\
&\quad + (\lambda_{5,T-k+1} - \lambda_{3,T-k+1}) c_2 v_k \\
\lambda_{4,T-k} &= C_k + \alpha \lambda_{3,T-k+1} + \lambda_{4,T-k+1} (1 - \mu) \\
&\quad + (\lambda_{5,T-k+1} - \lambda_{4,T-k+1}) c_3 w_k \\
\lambda_{5,T-k} &= \lambda_{5,T-k+1} (1 - \mu) \\
u_{k+1} &= \min \left[ b; \max \left( a, \frac{1}{D_k} [(\lambda_{2,T-k+1} - \lambda_{5,T-k+1}) L_k] \right) \right] \\
v_{k+1} &= \min \left[ d; \max \left( c, \frac{1}{E_k} [(\lambda_{3,T-k+1} - \lambda_{5,T-k+1}) S_k] \right) \right] \\
w_{k+1} &= \min \left[ f; \max \left( e, \frac{1}{F_k} [(\lambda_{4,T-k+1} - \lambda_{5,T-k+1}) Q_k^t] \right) \right]
\end{aligned} \tag{15}$$

end for

*Step 3.* For  $k = 0; 1; \dots; T$ ; write:

$$\begin{aligned}
P_k^* &= P_k, \\
L_k^* &= L_k,
\end{aligned}$$

TABLE 2: The description of parameters used for the definition of discrete time systems (1). We used just arbitrary academic data.

$P_0$	$L_0$	$S_0$	$Q_0^t$	$Q_0^p$	$\sigma$	$\rho$	$\beta_3$	$\alpha$
$5 \cdot 10^3$	$2 \cdot 10^3$	$1 \cdot 10^3$	$2 \cdot 10^3$	$1 \cdot 10^3$	0.5	0.1	0.01	0.7
$\Lambda$	$\mu$	$\beta_1$	$m_1$	$m_2$	$m_3$	$\lambda$	$\gamma$	$\beta_2$
$8 \cdot 10^2$	0.04	0.6	1	1	1	0.05	0.7	0.05

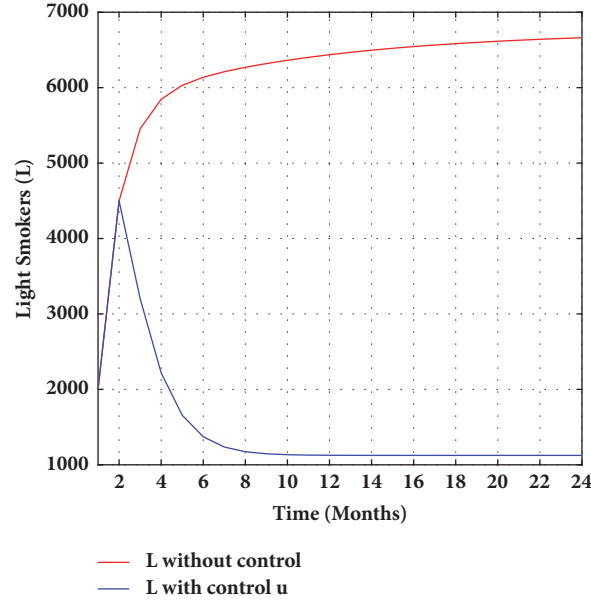


FIGURE 2: The evolution of the light smokers with and without controls.

$$S_k^* = S_k,$$

$$Q_k^{t*} = Q_k^t,$$

$$Q_k^{p*} = Q_k^p,$$

$$u_k^* = u_k,$$

$$v_k^* = v_k,$$

$$w_k^* = w_k$$

(16)

end for

In this formulation, there were initial conditions for the state variables and terminal conditions for the adjoints. That is, the optimality system is a two-point boundary

value problem with separated boundary conditions at time steps  $k = 0$  and  $k = T$ . We solve the optimality system by an iterative method with forward solving of the state system followed by backward solving of the adjoint system. We start with an initial guess for the controls at the first iteration and then before the next iteration we update the controls by using the characterization. We continue until convergence of successive iterates is achieved.

**4.2. Discussion.** In this section, we study and analyse numerically the effects of optimal control strategies such as awareness program through media and education, treatment, and psychological support with follow-up for the infected smokers (Table 2).

**4.2.1. Strategy A: Control with Awareness Program.** Given the importance of the awareness programs in restricting the spreading of smoking, we propose an optimal strategy for this purpose. Hence, we activate the optimal control variable  $u$  which represents the awareness program for light smokers. Figure 2 compares the evolution of light



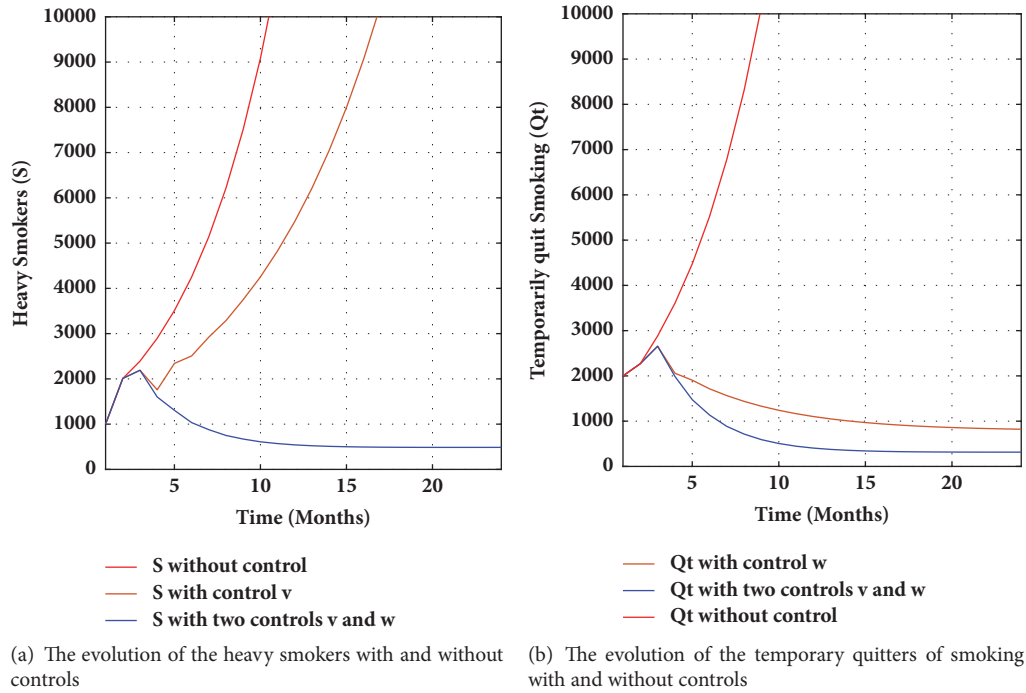


FIGURE 3

smokers with and without control  $u$  in which the effect of the proposed awareness program through media and education is proven to be positive in decreasing the number of light smokers.

**4.2.2. Strategy B: Control with Treatment and Psychological Support with Follow-Up.** When the number of smokers is so high, it is obligatory to resort to some strategies such as treatment in order to reduce the number of smokers. Therefore, we propose an optimal strategy by using the optimal control  $v$  in the beginning. In spite of using the optimal control  $v$ , we observe a temporary decrease of the heavy smokers number which is increased again (Figure 3(a)). The reason of this increase is justified by the fact that heavy smokers revert back to smoking after giving up. For improving the effectiveness of this strategy, we add the elements of follow-up and psychological support which are represented in the proposed strategy by the optimal control variable  $w$  (Figure 3(b)). Combining follow-up and psychological support with treatment results in an obvious decrease in the number of heavy smokers. Also, the proposed strategy has an additional effect in decreasing clearly the number of temporary quitters of smoking.

**4.2.3. Strategy C: Control with Awareness Program, Treatment, and Psychological Support with Follow-Up.** In this strategy, we combine the two previous strategies to achieve better results. We notice that the numbers of light

smokers (Figure 4(a)), heavy smokers (Figure 4(b)), and temporary quitters of smoking (Figure 4(c)) are decreased markedly which leads to satisfactory results.

## 5. Conclusion

In this paper, we introduced a discrete modeling of smokers in order to minimize the number of light smokers, heavy smokers, and temporary quitters of smoking. We also introduced three controls which, respectively, represent awareness program through education and media, treatment, and psychological support with follow-up. We applied the results of the control theory and we managed to obtain the characterizations of the optimal controls. The numerical simulation of the obtained results showed the effectiveness of the proposed control strategies.

## Data Availability

The disciplinary data used to support the findings of this study have been deposited in the Network Repository (<http://www.networkrepository.com>).

## Conflicts of Interest

The authors declare that they have no conflicts of interest.

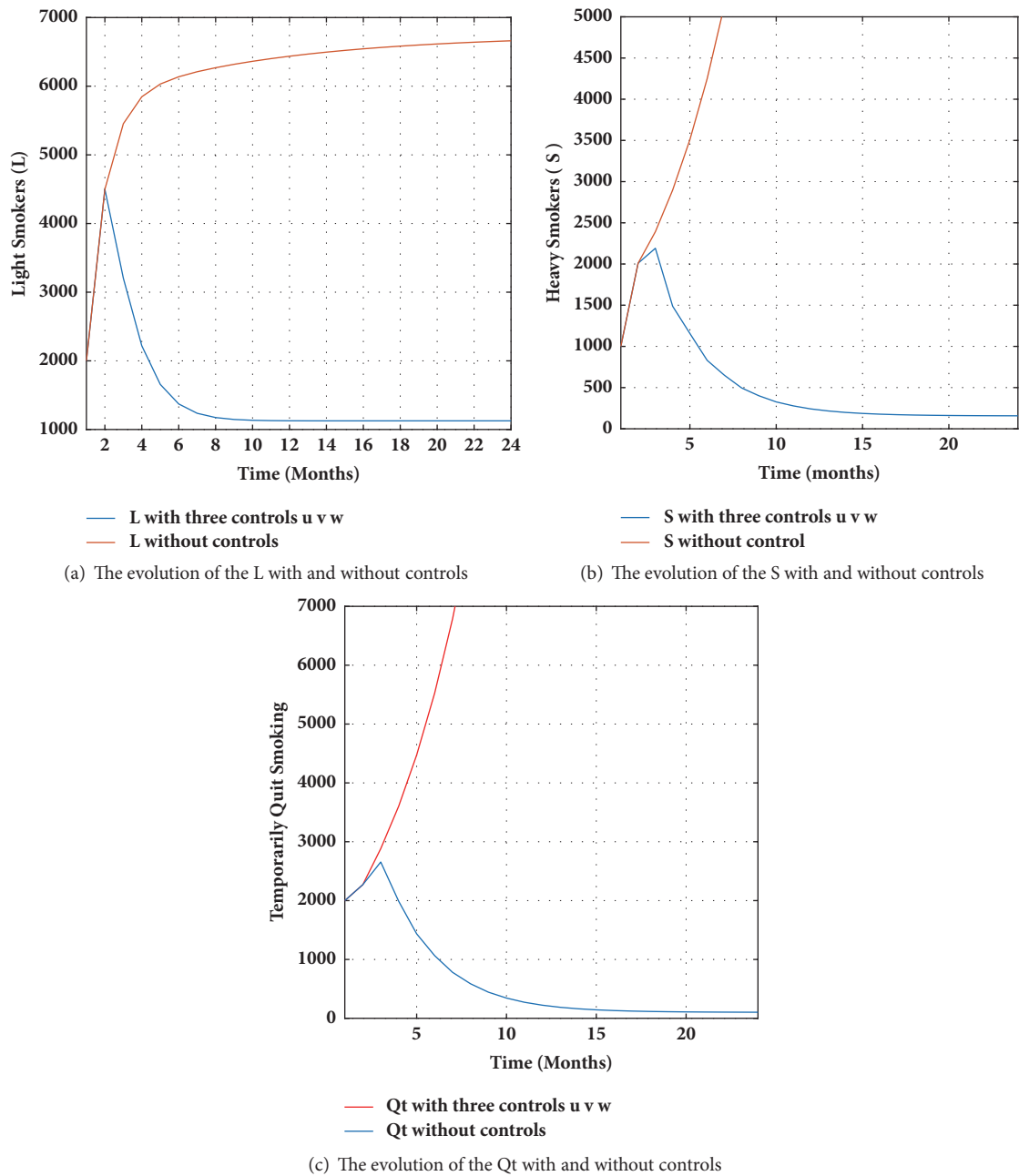


FIGURE 4

## References

- [1] World Health Organization report on the global tobacco epidemic, 2017, <http://apps.who.int/iris/bitstream/10665/255874/1/9789241512824-eng.pdf>.
- [2] V. Capasso and G. Serio, "A generalization of the Kermack-McKendrick deterministic epidemic model," *Mathematical Biosciences*, vol. 42, no. 1-2, pp. 43-61, 1978.
- [3] C. Castillo-Garsow, G. Jordan-Salivia, and A. Rodriguez-Herrera, "Mathematical models for the dynamics of tobacco user recovery and relapse," *Public Health*, vol. 84, no. 4, pp. 543-547, 1997.
- [4] "Cable News Network, China Clouded in Cigarette Smoke," <http://edition.cnn.com/2011/WORLD/asiapcf/01/07/floracruz.china.smokers/index.html?hpt=C2>.
- [5] <https://www.moroccoworldnews.com/2015/07/163058/number-of-smokers-to-reach-7-million-in-morocco-by-2025/>.
- [6] WHO global report on trends in prevalence of tobacco smoking, World Health Organization. WHO Library Cataloguing-in-Publication Data, 2015.
- [7] L. Pang, Z. Zhao, S. Liu, and X. Zhang, "A mathematical model approach for tobacco control in China," *Applied Mathematics and Computation*, vol. 259, pp. 497-509, 2015.
- [8] F. Guerrero, F.-J. Santonja, and R.-J. Villanueva, "Analysing the Spanish smoke-free legislation of 2006: A new method

- to quantify its impact using a dynamic model,” *International Journal of Drug Policy*, vol. 22, no. 4, pp. 247–251, 2011.
- [9] A. Lahrouz, L. Omari, D. Kiouach, and A. Belmaati, “Deterministic and stochastic stability of a mathematical model of smoking,” *Statistics & Probability Letters*, vol. 81, no. 8, pp. 1276–1284, 2011.
  - [10] W. Ding, R. Hendon, B. Cathey, E. Lancaster, and R. Germick, “Discrete time optimal control applied to pest control problems,” *Involve, a Journal of Mathematics*, vol. 7, no. 4, pp. 479–489, 2014.
  - [11] D. C. Zhang and B. Shi, “Oscillation and global asymptotic stability in a discrete epidemic model,” *Journal of Mathematical Analysis and Applications*, vol. 278, no. 1, pp. 194–202, 2003.
  - [12] Z. Hu, Z. Teng, and H. Jiang, “Stability analysis in a class of discrete SIRS epidemic models,” *Nonlinear Analysis: Real World Applications*, vol. 13, no. 5, pp. 2017–2033, 2012.
  - [13] M. D. Rafal and W. F. Stevens, “Discrete dynamic optimization applied to on-line optimal control,” *AIChE Journal*, vol. 14, no. 1, pp. 85–91, 1968.
  - [14] L. S. Pontryagin, V. G. Boltyanskii, R. V. Gamkrelidze, and E. F. Mishchenko, *The Mathematical Theory of Optimal Processes*, John Wiley & Sons, London, UK, 1962.
  - [15] V. Guibout and A. Bloch, “A discrete maximum principle for solving optimal control problems,” in *Proceedings of the 2004 43rd IEEE Conference on Decision and Control (CDC)*, pp. 1806–1811, Bahamas, December 2004.
  - [16] C. L. Hwang and L. T. Fan, “A discrete version of Pontryagin’s maximum principle,” *Operations Research*, vol. 15, pp. 139–146, 1967.

## Research Article

# Evolution of Electoral Preferences for a Regime of Three Political Parties

**María Guadalupe Medina Guevara** , **Héctor Vargas Rodríguez,**  
**Pedro Basilio Espinoza Padilla, and José Luis Gozález Solís**

*Department of Exact Sciences and Technology, University of Guadalajara, Lagos de Moreno, 47460, Mexico*

Correspondence should be addressed to María Guadalupe Medina Guevara; [mguadalupe.medina@lagos.udg.mx](mailto:mguadalupe.medina@lagos.udg.mx)

Received 6 July 2018; Revised 25 September 2018; Accepted 2 October 2018; Published 24 October 2018

Guest Editor: Stefania Tomasiello

Copyright © 2018 María Guadalupe Medina Guevara et al. This is an open access article distributed under the Creative Commons Attribution License, which permits unrestricted use, distribution, and reproduction in any medium, provided the original work is properly cited.

In this article, we use a discrete system to study the opinion dynamics regarding the electoral preferences of a nontendentious group of agents. To measure the level of preference, a continuous opinion space is used, in which the preference (opinion) can evolve from any political option, to any other; for a regime of three parties, a circle is the convenient space. To model a nonbiased society, new agents are considered. Besides their opinion, they have a new attribute: an individual iterative monoparametric map that imitates a process of internal reflection, allowing them to update their opinion in their own way. These iterative maps introduce six fixed points on the opinion space; the points' stability depends on the sign of the parameter. When the latter is positive, three attractors are identified with political options, while the repulsors are identified with the antioptions (preferences diametrically opposed to each political choice). In this new model, pairs of agents interact only if their respective opinions are alike; a positive number called confidence bound is introduced with this purpose; if opinions are similar, they update their opinion considering each other's opinion, while if they are not alike, each agent updates her opinion considering only her individual map. In addition, agents give a certain level of trust (weight) to other agent's opinions; this results in a positive stochastic matrix of weights which models the social network. The model can be reduced to a pair of coupled nonlinear difference equations, making extracting analytical results possible: a theorem on the conditions governing the existence of consensus in this new artificial society. Some numerical simulations are provided, exemplifying the analytical results.

## 1. Introduction

The arising of opinion in society has become a very interesting research topic in the last decades. For example, Ding and Mo [1] have studied how noise, from different sources, like TV, newspaper, and so on, contributes to eliminate the disagreement in a social group; Chen *et al.* [2] have considered how the social similarity influences the opinion dynamics between individuals; D'Aniello *et al.* [3] have used a fuzzy consensus approach to investigate decision-making in a group; Lu *et al.* [4] have investigated the impact of the community structure on the convergence time to reach a consensus in a social group. A recent survey on some opinion dynamics models and their applications is found in [5].

In particular, the opinion dynamics about political options has been studied broadly, using models borrowed

from statistical physics, such as the Ising and Potts ones [6, 7], in which agents are forced to choose between a finite set of options, no matter how much they agree with them. The set of options, naturally, is discrete as the corresponding opinion space for these models too, allowing tendentious agents. An alternative would be the use of a continuous opinion space, in which agents can show their level of agreement regarding the options; this space must also allow opinions to evolve from one option to another, options being equidistant from each other; these requirements suggest that an adequate opinion space, for  $n$ -options, is an  $n - 2$ -sphere. For example, a circle is an appropriate opinion space for three options, while a sphere is suitable for four options. These ideas were used by Medina *et al.* [8] to study the consensus formation on a circle for a regime of three political parties; they used an iterative

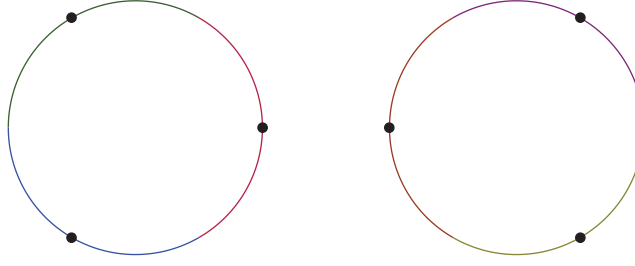


FIGURE 1: The figure shows attractors described by Theorem 2 and their respective attraction basins for system (7). Attractors with  $0 < \kappa < 2/3$  are the associated electoral preferences. Attractors with  $-2/3 < \kappa < 0$ , also called antioptions, are completely opposite to existing options. Agents attracted to one antioption radically refuse the one option remaining half trusting to the other options.

monoparametric map which introduced six fixed points on the opinion space. The stability of these points is governed by the sign of the map's parameter, the personal parameter; if it is positive, the three attractors are identified with the political options, while the remaining three repellers are called the (political) antioptions. An agent having a negative personal parameter rejects all the available political options, being attracted to the antioptions. Since there is an alternating sequence of attractors and repellers on the circle, options and antioptions are diametrically opposed; see Figure 1. Hence an agent whose opinion is attracted to one antioption rejects the diametrically opposed political option, while she (or he) is insecure about the remaining two options. So in contrast, with the discrete option models, these agents are not forced to pick an option. In this sense, the iterative map allows agents to update their opinion taking into account their postures with respect to the choices, emulating an internal reflection process in them. The above agents interact by pairs updating their opinion considering their internal reflection processes and their partners' opinions with some weight (a subjective trust given to each other's opinion); if their opinions are not alike, they update their opinions considering only their own internal reflection processes. A positive number, the confidence bound, is used as a threshold to separate between these two cases.

Although agents, in Medina *et al.* [8] model, have different personal parameters, the same iterative map was used for the opinion updating. However, in a more realistic society, each person forms her opinion differently from others; hence it has sense to consider a different updating rule for each agent. So, in this work, we propose to give each agent a new attribute, a different iterative map that allows them to update their opinion in their own manner. Then we investigate the conditions under which a consensus arises, in this new artificial society, under these new updating rules. Finally, some numerical experiments are performed to validate the analytical results.

This work is sectioned as follows: Section 2 presents a new opinion dynamics model on the circle. Section 3, Main Results, gives a theorem stating the conditions under which the consensus emerges in the social network. Section 4 shows that some simulations with two different opinion updating rules are given. A section of concluding remarks and two appendixes end this communication.

## 2. Opinion Dynamics Modeled on a Circle

Through the work, the opinion space  $X$  is a circle, and it could be identified with the segment  $[0, 2\pi]$  modulus  $2\pi$  in radians or, equivalently, as the segment  $[0, 360]$  modulo 360 in degrees. On it, the opinion updating rules establish three attractors identified with the political options and three antioptions. Options and antioptions are distributed in an alternating sequence; see Figure 1. The antioption opposed to an option corresponds to a total rejection of the latter. The personal parameter space is denoted by  $K$ ; it is identified with the segment  $[-\pi, \pi]$  in radians or  $[-180, 180]$  in degrees. A set with an even number  $N$  of interacting agents is considered. Such interactions take place on discrete times  $t_n$ , for each  $n \in \mathbb{Z}^+ \cup 0$ , so  $(t_n)_{n=0}^\infty$  is a nonbounded sequence of positive real numbers such that  $t_0 = 0$ . Each agent is characterized by three attributes: an opinion  $x_n^i \in X$ ; a constant personal parameter  $\kappa^i \in K$  that allows acceptance or rejection of the presented options (the attracting nature of options and antioptions depends on the sign of  $\kappa^i$ ; see below); and an opinion updating function  $\Xi_i : X \times K \rightarrow \mathbb{R}$ . Like in [8, 9], the social network describing the agent population is governed by the stochastic absolute weights matrix:

$$C = \begin{pmatrix} c_{11} & c_{12} & \cdots & c_{1N} \\ c_{21} & c_{22} & \cdots & c_{2N} \\ \vdots & \vdots & \ddots & \vdots \\ c_{N1} & c_{N2} & \cdots & c_{NN} \end{pmatrix} \quad (1)$$

where its elements are positive real numbers fulfilling  $0 < c_{ii} \leq 1$  and  $0 \leq c_{ij} < 1$ ,  $\forall i, j \in \{1, 2, \dots, N\}$ , in such a way that the sum of each row is equal to one:

$$\sum_{j=1}^N c_{ij} = 1. \quad (2)$$

From a social point of view, a possible interpretation to  $c_{ij}$  could be the credibility given by agent  $i$  to the other agents' opinions in the social network, including his own opinion. The first inequality above  $0 < c_{ii} \leq 1$  establishes that each agent must give a nonzero credibility to its own opinion. Since the matrix rows must add to one, the second inequality

$0 \leq c_{ij} < 1$  establishes that the credibility given to other agent's opinion must be less than one.

Since the interactions between the agents are pairwise, it is necessary to reevaluate the mutual trust between the agents. Hence we use relative weights,

$$\begin{aligned} a_{ii} &= \frac{c_{ii}}{c_{ii} + c_{ij}}, \\ a_{ij} &= \frac{c_{ij}}{c_{ii} + c_{ij}}. \end{aligned} \quad (3)$$

The relative weights fulfill these properties:  $a_{ii} + a_{ij} = 1$ ,  $0 < a_{ii} \leq 1$  and  $0 \leq a_{ij} < 1$ .

On the same manner as well-known models of Deffuant *et al.* [10, 11] and Hegselman-Krause [12], we consider a confidence bound  $\varepsilon > 0$  that determines a criterion to set a limit to agents interaction; i.e., the opinions belonging to agents  $i$  and  $j$  are affine if and only if  $|x_n^i - x_n^j| < \varepsilon$ .

Now we formulate the opinion updating rules on the circle. It is important to distinguish six special points on the opinion space: three options and three antioptions. To do that, we consider iterative monoparametric maps that introduce these six fixed points. As a construction element of the dynamic rules, we use the following functions:

$$\Xi_i(x, \kappa) = x - \kappa^i f_i(x), \quad (4)$$

where

$$f_i(x) = \sin(3x) g_i(\sin(3x)), \quad (5)$$

where  $g_i : [-1, 1] \rightarrow (0, 1]$  is a  $C^1$  class differential function such that  $g_i(0) = 1$ ,  $\forall i \in \{1, 2, \dots, N\}$ ; the sine function,  $\sin(3x)$ , introduces the fixed points,  $p = s\pi/3$  for  $s \in \mathbb{Z}$ ; in the iterative map  $x_{n+1} = \Xi(x_n, \kappa^i)$ :

$$p = \Xi(p, \kappa). \quad (6)$$

Instead of the sine function in (5), it would be possible to use the cosine function with the same purpose. However, this would only move the fixed points on the circle.

Medina *et al.* [8] consider the same updating opinion rule for all agents with  $g_i(x) = 1$ . Now, we propose to use a different function  $g_i(x)$  for each agent, with the purpose to give them a different way to update their opinions; thus the functions  $\Xi_i(x^i, \kappa^i)$  model internal reflection processes for opinion updating in agents; they also provide the knowledge about the options and permit them to keep an attitude regarding these options; see Appendix A. In this sense, the new model introduces a more heterogeneous and less tendentious agent population.

On the recursive model, as initial conditions, a personal parameter and a random opinion are assigned to each agent; aside the stochastic matrix  $C$  is generated too. On the  $n$  temporal step, from the agents population,  $N/2$ -couples are randomly chosen to interact according to these rules:

- (i) When a pair of agents have similar opinions,  $|x_i - x_j| < \varepsilon$ , they update their opinions considering their respective internal reflection processes and considering each other's opinion, with some relative weights:

$$\begin{aligned} x_{n+1}^i &= a_{ii} \Xi_i(x_n^i, \kappa^i) + a_{ij} x_n^j, \\ x_{n+1}^j &= a_{ji} x_n^i + a_{jj} \Xi_j(x_n^j, \kappa^j). \end{aligned} \quad (7)$$

- (ii) But if they do not have similar opinions,  $|x_i - x_j| > \varepsilon$ , every agent in the pair uses only her iterative map to update her opinion, without considering other's opinion, consequently, using  $a_{ii} = a_{jj} = 1$  and  $a_{ij} = a_{ji} = 0$  in (7).

### 3. Main Results

Now, we present the conditions for consensus formation in the artificial society described by the before enunciated model. It is said that model (7) exhibits a strong consensus if the opinions of agents evolve to a stable fixed point.

To simplify our notations and reduce model (7) to a system of only two nonlinear difference equations, we perform the following change of variables:

$$\begin{aligned} x^i &\rightarrow x, \\ \kappa^i &\rightarrow \kappa_x, \\ x^j &\rightarrow y, \\ \kappa^j &\rightarrow \kappa_y, \\ a_{ii} &\rightarrow \alpha, \\ a_{ij} &\rightarrow \beta, \\ a_{ji} &\rightarrow \gamma, \\ a_{jj} &\rightarrow \delta, \\ g_i(x_n^i) &\rightarrow g_{(x)}(x_n), \\ g_j(x_n^j) &\rightarrow g_{(y)}(y_n), \\ f_i(x_n^i) &\rightarrow f_{(x)}(x_n), \\ f_j(x_n^j) &\rightarrow f_{(y)}(y_n), \\ \Xi_i(x_n^i, \kappa^i) &\rightarrow \Xi_{(x)}(x_n, \kappa_x), \\ \Xi_j(x_n^j, \kappa^j) &\rightarrow \Xi_{(y)}(y_n, \kappa_y). \end{aligned} \quad (8)$$

The model becomes into

$$\begin{aligned} x_{n+1} &= \alpha \Xi_{(x)}(x_n, \kappa_x) + \beta y_n, \\ y_{n+1} &= \gamma x_n + \delta \Xi_{(y)}(y_n, \kappa_y), \end{aligned} \quad (9)$$

where  $\alpha + \beta = 1$  and  $\gamma + \delta = 1$ .



Analyzing the fixed points of the previous equations (9), we establish conditions for the existence and stability of the fixed points of the complete system (7), analogously as the model in [8].

**Theorem 1.** *The point  $(p, p)$  is a common fixed point of (7), if and only if  $p = s\pi/3$  for some  $s \in \mathbb{Z}$ .*

*Proof.* Assuming that  $(p, p)$  is a fixed point (9), by direct substitution results,

$$\begin{aligned} p &= \alpha [p - \kappa_x \sin(3p) g_i(\sin(3p))] + \beta p, \\ p &= \gamma p + \delta [p - \kappa_y \sin(3p) g_j(\sin(3p))]. \end{aligned} \quad (10)$$

By definition  $g_i(x) \neq 0$ , then  $\sin(3p) = 0$  or  $p = s\pi/3$  for some  $s \in \mathbb{Z}$ . Conversely, a direct substitution shows that the point  $(p, p)$  is a solution for (9), when  $p$  is an entire multiple of  $\pi/3$ , like it is asked.  $\square$

Note that these fixed points do not depend neither on the relative weights nor on personal parameters, so they are common to all pairs of (9) and they are fixed points of the full set of (7). Of course, (9) have other fixed points. However, when one considers the full system (7), fixed points from one pair of equations are not necessarily the same as another pair, so they may not be fixed points of the complete system. Some examples are presented in Appendix B.

For convenience, the index  $z$  denotes indexes  $x$  or  $y$ . Thus, for example,  $\kappa_z$  represents either  $\kappa_x$  or  $\kappa_y$ .

**Theorem 2.** *Let  $p = s\pi/3$  for some  $s \in \mathbb{Z}$  and  $\eta_z = 1 - \kappa_z f'_{(z)}(p) = 1 - 3(-1)^s \kappa_z$  such that  $|\eta_z| < 1$  and  $\kappa_x, \kappa_y \in K$ . Then  $(p, p)$  is a stable fixed point for (9) if*

- (1)  $0 < \kappa_x, \kappa_y < 2/3$  for  $s$  even,
- (2)  $-2/3 < \kappa_x, \kappa_y < 0$  for  $s$  odd.

*Proof.* For the linearized system (9), the Jacobian matrix is

$$M = \begin{pmatrix} \alpha \eta_x & \beta \\ \gamma & \delta \eta_y \end{pmatrix} \quad (11)$$

Under these considerations, the spectral radius  $\rho(M)$  of  $M$  satisfies

$$\begin{aligned} \rho(M) &\leq \|M\|_\infty = \max \{ \alpha |\eta_x| + \beta, \gamma + \delta |\eta_y| \} \\ &< \max \{ \alpha + \beta, \gamma + \delta \} = 1. \end{aligned} \quad (12)$$

Since all eigenvalues of  $M$  are complex numbers with modulus less than 1, then  $(p, p)$  is a stable fixed point; see [13, 14].

Theorem 2 gives the necessary and sufficient conditions for the existence of a consensus between a pair of agents; now Theorem 3 establishes the necessary and sufficient conditions for the existence of a consensus among all agents in the social web.

**Theorem 3.** *Let  $\kappa^i \in K$  for each  $i \in \{1, 2, \dots, N\}$  and  $p = s\pi/3$  for some  $s \in \mathbb{Z}$ . A strong consensus appears around opinion  $p$  in the next cases:*

- (1) if  $s$  is even and  $0 < \kappa^i < 2/3$  for each  $i \in \{1, 2, \dots, N\}$ ;
- (2) if  $s$  is odd and  $-2/3 < \kappa^i < 0$  for each  $i \in \{1, 2, \dots, N\}$ .

$\square$

This theorem generalizes the one reported in [8] and it could be seen that the consensus in the social network does not depend on  $g_i$  functions, nor absolute weights matrix  $C$ , nor number of agents  $N$ .

A more realistic case is when agents have personal parameters in a subset containing both positive and negative values; then system (9), in general, will have distinct attractors for different couples of agents; see Appendix B. Intuitively, it is expected that these attractors be bounded in some subset of  $X \times X$ ; consequently the agents' opinions will evolve towards a subset  $U \subsetneq X$ ; hence, it is said that a weak consensus is present in the social network [8, 9].

## 4. Some Examples

For the sake of clearance, some simulations are provided. Here we use a social web with 200 agents; it is described by a random matrix of absolute weights. Agents' starting opinions are uniform and randomly distributed on  $X$ . Aside, a uniform time interval partition is considered. The parameters and variables will be expressed in degrees. Considering the same interacting dynamics between agents and two cases for updating rule opinion (5),

$$\begin{aligned} g_1(x) &= \cos^4(x), \\ g_2(x) &= \exp(-x^2). \end{aligned} \quad (13)$$

The simulations use 100 time steps.

*Example 4.* In Figure 2, the personal parameters  $\kappa^i$  are randomly and uniformly distributed on  $[0.5^\circ, 38^\circ]$ . Three different confidence bounds are considered: top rank  $\varepsilon = 180^\circ$ ;  $\varepsilon = 120^\circ$  in middle rank;  $\varepsilon = 60^\circ$  for bottom rank:  $g_1(x)$  to the left and  $g_2(x)$  to the right. When  $\varepsilon = 180^\circ$  all agents interact and one cluster appears. If  $\varepsilon = 120^\circ$ , agents interact with about two-thirds of total population at the most; initially, two clusters appear, but the bigger one absorbs the smaller one. For  $\varepsilon = 60^\circ$ , agents interact with one-third of population, and three clusters arise, each one with about one-third of total population. According to Theorem 3, strong consensus arise for all these cases.

*Example 5.* In Figure 3, the personal parameters  $\kappa^i$  are randomly and uniformly distributed on  $[-10^\circ, 10^\circ]$ . Three different confidence bounds are considered too; top rank  $\varepsilon = 180^\circ$ ;  $\varepsilon = 120^\circ$  in middle rank;  $\varepsilon = 60^\circ$  for bottom rank:  $g_1(x)$  to the left and  $g_2(x)$  to the right. When  $\varepsilon = 180^\circ$ , all agents interact and one cluster appears, but with weak consensus. If  $\varepsilon = 120^\circ$ , the agents interact with about two-thirds of total population at the most, and two weak consensus clusters appear. For  $\varepsilon = 60^\circ$ , agents interact with one-third of population, but now strong and weak consensus states coexist.

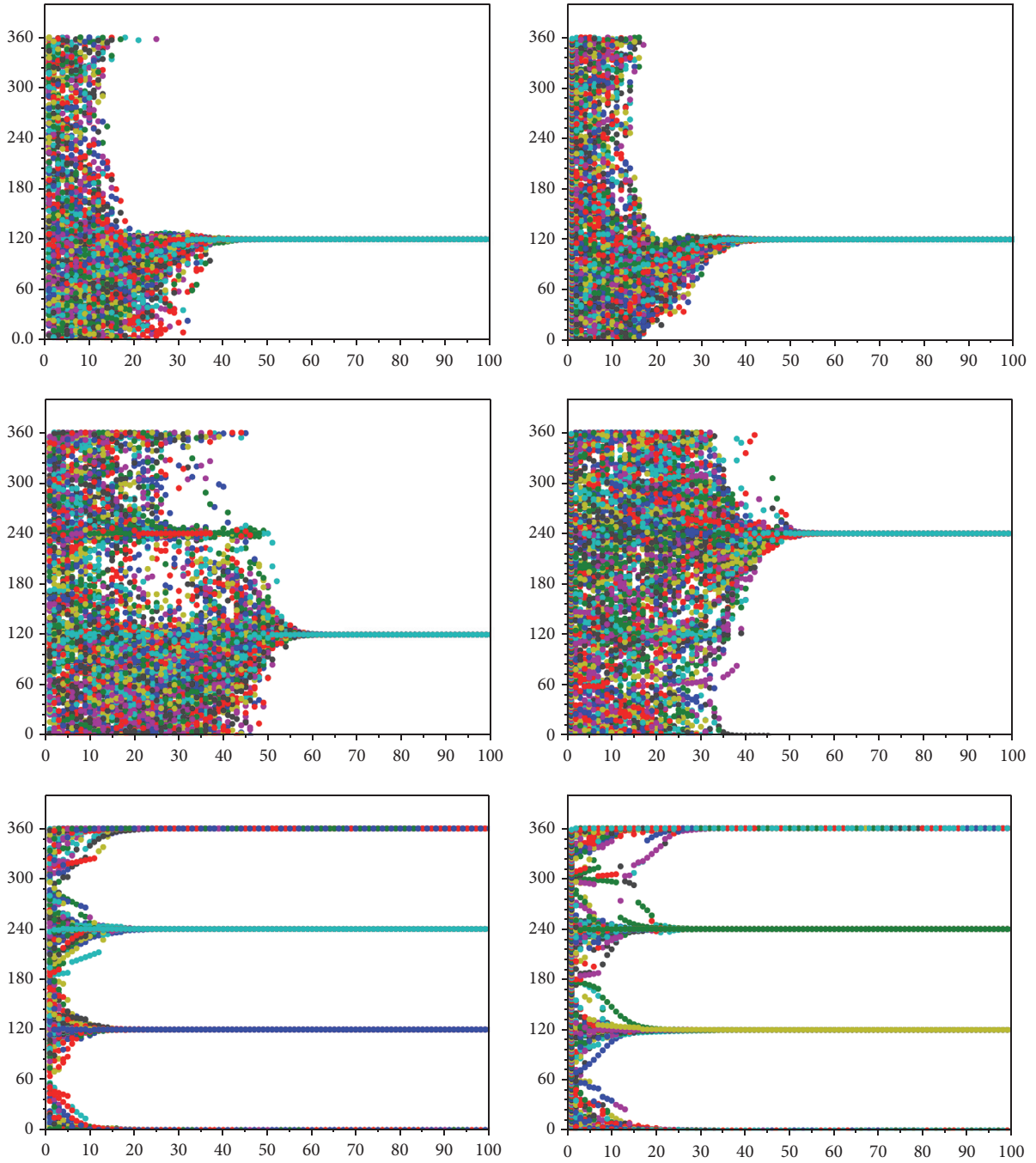


FIGURE 2: The confidence bounds are  $\epsilon = 180^\circ$  (top row);  $\epsilon = 120^\circ$  (middle row), and  $\epsilon = 60$  (bottom row).  $\kappa^i \in [0.5^\circ, 38^\circ]$ . Function  $g_1(x)$  is used on left column and  $g_2(x)$  on the right. In the top row, a single cluster appears. In the middle row, initially two clusters appear, which finally merge. In the lower row, three clusters, with about one-third of the population, appear. Strong consensus appears always, in all three cases, according to Theorem 3.

## 5. Conclusions

In this paper, a new model for opinion dynamics of political preferences about three parties options has been presented; it generalizes the model in Medina *et al.* [8] to include new individual updating rules: a set of monoparametric iterative maps, which emulate different internal reflection processes in

agents. For some positive values of the personal parameter  $\kappa$  (map's parameter), these rules introduce three equidistant attractors on a circular opinion space, which correspond to three choices, that can be interpreted with a different political party. For some negative values of the personal parameter, choices become repulsors, so agents with a negative personal parameter reject the political options. The value of the

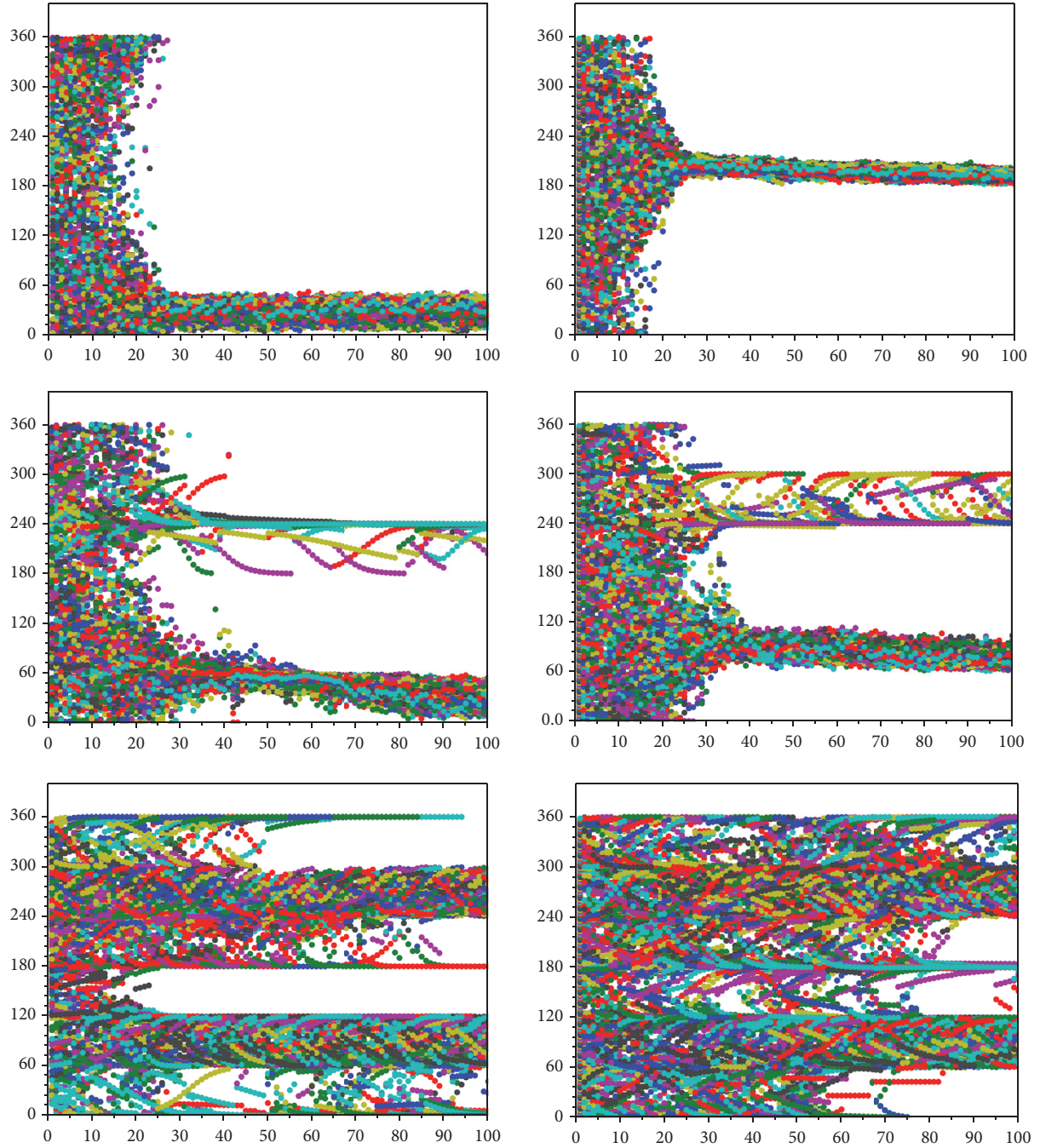


FIGURE 3: The confidence bounds are  $\epsilon = 180^\circ$  (top row),  $\epsilon = 120^\circ$  (middle row), and  $\epsilon = 60$  (bottom row).  $\kappa^i \in [-10^\circ, 10^\circ]$ . Function  $g_1(x)$  is used on left column and  $g_2(x)$  on the right. In the top row, a weak consensus appears throughout the social group. In the middle row, there are two clusters, one grouping most of the opinions and another with a minority of these. In the lower row, the formation, of both weak and strong consensus, can be seen.

personal parameter may lead to a convergence to the fixed points with oscillation or without it; in the first case, the agent is interpreted as a hesitant one, whose opinion consolidates with time, while in the second case the agent is secure about her opinion. At least, for the examples presented here, the fixed points of the iterative maps can bifurcate, for other values of the personal parameter, in  $n$ -cycles and even lead

to chaos (see Appendix A, and Figures 4 and 5). The  $n$ -cycles might be interpreted as a set of  $n$ -postures that an insecure agent can hold; for example, a 2-cycle may be considered a dilemma, while an agent, with a personal parameter in the chaotic regime, is considered an erratic one. In this sense, the personal parameter introduces different behaviors and strong postures in the agents.



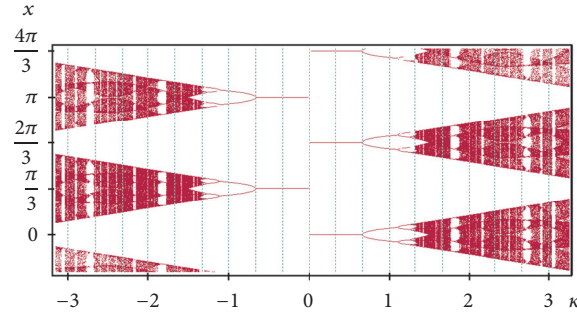


FIGURE 4: The figure shows a bifurcation diagram for the iterative map  $x_{n+1} = x_n - \kappa \cos^4(\sin(3x_n)) \sin(3x_n)$ ; an alternating sequence of tree-like graphs goes upwards and downwards. Here are depicted the options for  $0 < \kappa < 2/3$  and antioptions for  $-2/3 < \kappa < 0$ . Stable fixed points bifurcate in a 2-cycle for  $\kappa = 2/3$ ; then a cascade of bifurcations appears, leading to chaos. The 2-cycle may model a dilemma, since agent's opinion jumps from one posture to another. Other  $n$ -cycles may model other doubt processes in agents.

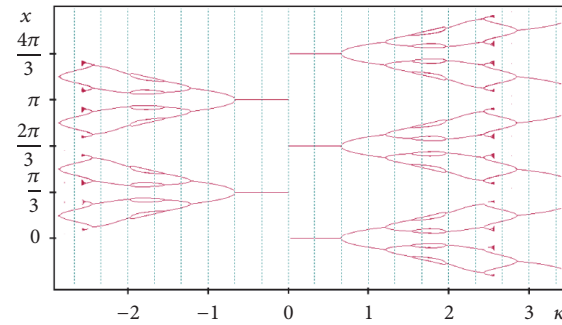


FIGURE 5: The figure shows a bifurcation diagram for the iterative map  $x_{n+1} = x_n - \kappa \exp(-\sin^2(3x_n)) \sin(3x_n)$ ; an alternating sequence of tree-like graphs goes upwards and downwards. Stable fixed points bifurcate in different  $n$ -cycles for  $|\kappa| > 2/3$ . Stable fixed points bifurcate in a 2-cycle for  $\kappa = 2/3$ ; then a cascade of bifurcations appears, leading to chaos, at least in some small regions. The 2-cycle may model a dilemma, since agent's opinion jumps from one posture to another. Other  $n$ -cycles may model other doubt processes in agents.

So, the key point of the present model is a new agent who is characterized by three attributes: opinion  $x$ , personal parameter  $\kappa$ , and an iterative map to update her own opinion differently as her interlocutors. This kind of agent becomes a fundamental piece of a more heterogeneous artificial society.

The presented model, also, considers pairwise interactions among agents and uses the confidence bound  $\epsilon$  like Hegselmann & Krause and Deffuant & Weisbuch classical models to set a limit for dissimilar agents opinion case and random absolute weights to describe the subjective trust given to agents' opinions, defining an artificial social web.

The main interest of this work was to study consensus arising in this new artificial society; two classes of consensus were considered: a strong one which is the convergence of the opinions to a fixed point and a weak one which is the convergence of the opinions to a subset of the opinion space. Theorem 3 provides the necessary and sufficient conditions for the arising of a strong consensus in this artificial heterogeneous society.

Finally two sets of simulations were performed; in each set, a different iterative map and three different confidence bounds were used. In each simulation, were used either positive different personal parameters or mixed (positive and negative) personal parameters, random absolute weights,

or random initial opinions, but the same iterative map for all agents. However, simulations show practically the same behaviors and convergence times as found in [8]; some of them show the emergence of strong consensus or the existence of weak consensus regions.

As perspectives of future research work, the model could be used to study the opinion dynamic of the electoral preferences regarding three political parties when a charismatic political actor (a very persuasive agent) is present. It is also possible to generalize the model to opinion spaces with four or more options, spheres of two or more dimensions. These latter models would be useful to study the situation when there are four or more political parties.

## Appendix

### A. On the Role of the Personal Parameter

From a mathematical point of view, iterative maps present a vast range of behaviors; some of them can be visualized in the corresponding bifurcation diagrams; see Marotto [13]. Some of these mathematical behaviors are used to model how agents update their own opinion: with certainty, if the opinion converges without oscillating; with doubt, if the opinion converges oscillating.

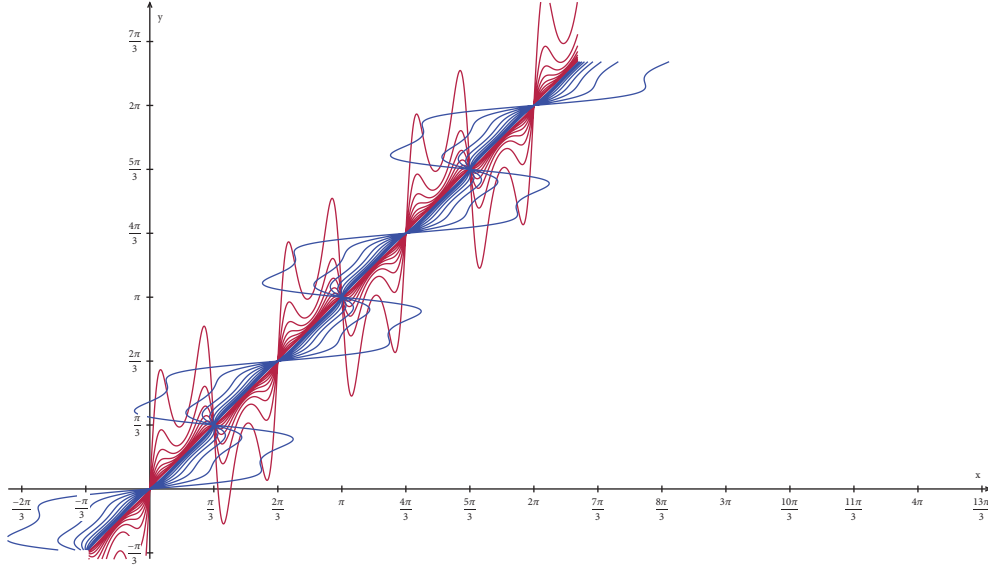


FIGURE 6: The figure shows a parametric plot of families of curves for system (9) for  $\Xi_{(x)} = x - \kappa_x g_1(\sin(3x)) \sin(3x)$ ,  $\kappa_x = 0.66$ , and different relative weights  $\alpha = 0.1, 0.2, \dots, 0.9$  (red lines),  $\Xi_{(y)} = y - \kappa_y g_2(\sin(3y)) \sin(3y)$ ,  $\kappa_y = 0.4$  and different relative weights  $\delta = 0.1, 0.2, \dots, 0.9$  (blue lines). The intersections correspond to different fixed points of different pairs of equations. Notice that only those fixed points of the form  $(p, p)$  are common to all equations in system (7). Other fixed points depend on parameters' values.

The iterative map  $x_{n+1} = \Xi(x_n, \kappa)$  converges to one of the fixed points  $p = s\pi/3$  without oscillation if

$$0 < \left. \frac{d\Xi(x, \kappa)}{dx} \right|_p < 1; \quad (\text{A.1})$$

this happens for  $0 < \kappa < 1/3$  and  $s = 0, 2, 4$  or  $-1/3 < \kappa < 0$  and  $s = 1, 3, 5$ .

The iterative map  $x_{n+1} = \Xi(x_n, \kappa)$  converges to one of the fixed points  $p = s\pi/3$  with oscillation if

$$0 < \left. \frac{d\Xi(x, \kappa)}{dx} \right|_p < 1; \quad (\text{A.2})$$

this happens for  $1/3 \leq \kappa \leq 2/3$  and  $s = 0, 2, 4$  or  $-2/3 \leq \kappa \leq -1/3$  and  $s = 1, 3, 5$ .

The above fixed points bifurcate in a 2-cycle for  $|\kappa| = 2/3$ ; for greater values of  $|\kappa|$ , other bifurcations occur, finally leading to a chaotic behavior; see Figures 4 and 5. In Medina *et al.* [9],  $n$ -cycles are used to model different possible doubt processes, in which agents opinions jump among  $n$ -different postures; in particular, a 2-cycle is interpreted as a dilemma. The chaotic behavior models the behavior of an agent, who changes her opinion in an erratic way.

## B. Fixed Points of the Updating Rules

Fixed points  $(p_s, q_s)$  for  $s = 1, \dots, M$  of system (9) can be found solving the system

$$\begin{aligned} p &= \alpha \Xi_{(x)}(p, \kappa_x) + \beta q, \\ q &= \gamma p + \delta \Xi_{(y)}(q, \kappa_y). \end{aligned} \quad (\text{B.1})$$

However, due to the nonlinear nature of the system, it is difficult to obtain solutions in the explicit form:  $p = p(\kappa_x, \kappa_y, \alpha, \delta)$ ,  $q = q(\kappa_x, \kappa_y, \alpha, \delta)$ . Nevertheless, it is always possible to find them graphically. For example, in Figure 6, the special case is considered when two different mappings are used  $\Xi_{(x)}(x, \kappa_x) = x - \kappa_x \sin(3x) \cos(\sin(3y))^4$  (red lines) and  $\Xi_{(y)}(y, \kappa_y) = y - \kappa_y \sin(3y) \exp(-\sin(3y)^2)$  (blue lines) in system (B.1) with  $\kappa_x = 0.66$  and  $\kappa_y = 0.4$ ;  $\alpha = 0.1, \dots, 0.9$  and  $\delta = 0.1, \dots, 0.9$ , respectively. In Figure 7, the same situation is considered but now using  $\kappa_x = -0.66$  and  $\kappa_y = 0.66$ . Notice that the corresponding fixed points of a concrete pair of equations correspond to intersections of only one red curve with one blue curve. Nevertheless, there are fixed points common to all equations pairs, those of the form  $(p, p)$ . Since, in general, in each temporal step, different pairs of agents interact, so that different pairs of equations are used each time, consequently, the only permanent fixed points are those of Theorem 1.

## Data Availability

The manuscript uses data from computational experiments.

## Conflicts of Interest

The authors declare that they have no conflicts of interest.

## Acknowledgments

This work was supported by Universidad de Guadalajara. The authors thank the reviewers for their valuable observations and the editor who handled the work.

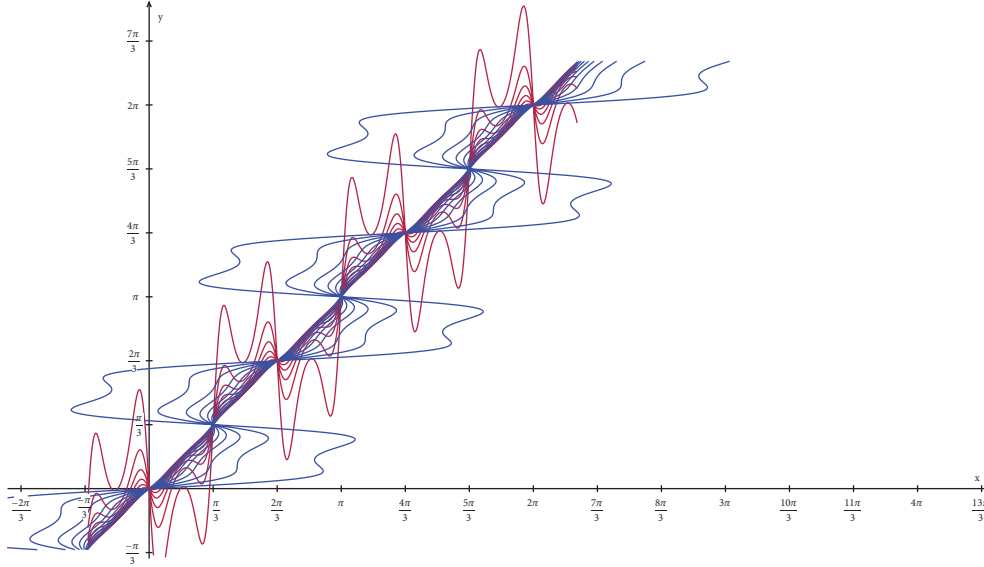


FIGURE 7: The figure shows a parametric plot of families of curves for system (9) for  $\Xi_{(x)} = x - \kappa_x g_1(\sin(3x))\sin(3x)$ ,  $\kappa_x = -0.66$ , and different relative weights  $\alpha = 0.1, 0.2, \dots, 0.9$  (red lines),  $\Xi_{(y)} = y - \kappa_y g_2(\sin(3y))\sin(3y)$ ,  $\kappa_y = 0.66$  and different relative weights  $\delta = 0.1, 0.2, \dots, 0.9$  (blue lines). The intersections correspond to different fixed points of different pairs of equations. Notice that only those fixed points of the form  $(p, p)$  are common to all equations in system (7); however, they are unstable. Other fixed points depend on parameters' values.

## References

- [1] Y. Ding and L. Mo, "Improved finite time in eliminating disagreement of opinion dynamics via noise," *Advances in Mathematical Physics*, vol. 2017, Article ID 1098169, 6 pages, 2017.
- [2] X. Chen, X. Zhang, Y. Xie, and W. Li, "Opinion dynamics of social-similarity-based Hegselmann-Krause model," *Complexity*, vol. 2017, Article ID 1820257, 12 pages, 2017.
- [3] G. D'Aniello, M. Gaeta, S. Tomasiello, and L. Rarità, "A fuzzy consensus approach for Group Decision Making with variable importance of experts," in *Proceedings of the 2016 IEEE International Conference on Fuzzy Systems (FUZZ-IEEE '16)*, pp. 1693–1700, Vancouver, Canada, 2016.
- [4] A. Lu, C. Sun, and Y. Liu, "The Impact of Community Structure on the Convergence Time of Opinion Dynamics," *Discrete Dynamics in Nature and Society*, vol. 2017, Article ID 9396824, 7 pages, 2017.
- [5] Y. Dong, M. Zhan, G. Kou, Z. Ding, and H. Liang, "A survey on the fusion process in opinion dynamics," *Information Fusion*, vol. 43, pp. 57–65, 2018.
- [6] G. Marcjasz and K. Sznajd-Weron, "Phase transitions in the kinetic ising model on the temporal directed random regular graph," *Frontiers in Physics*, vol. 5, p. 24, 2017.
- [7] A. L. Vilela and H. E. Stanley, "Effect of strong opinions on the dynamics of the majority-vote model," *Scientific Reports*, vol. 8, no. 1, p. 8709, 2018.
- [8] M. G. Medina-Guevara, J. E. Macías-Díaz, J. E. Gallegos et al., "On SI as an alternative continuous opinion space in a three-party regime," *Journal of Computational and Applied Mathematics*, vol. 318, pp. 230–241, 2017.
- [9] M. G. Medina-Guevara, J. E. Macías-Díaz, A. Gallegos, and H. Vargas-Rodríguez, "Consensus formation simulation in a social network modeling controversial opinion dynamics with pairwise interactions," *International Journal of Modern Physics C*, vol. 28, no. 5, 2017.
- [10] G. Deffuant, D. Neau, F. Amblard, and G. Weisbuch, "Mixing beliefs among interacting agents," *Advances in Complex Systems (ACS)*, vol. 3, pp. 87–98, 2000.
- [11] G. Deffuant, F. Amblard, G. Weisbuch, and T. Faure, "How can extremism prevail? A study based on the relative agreement interaction model," *Journal of Artificial Societies and Social Simulation*, vol. 5, no. 4, p. 1, 2002.
- [12] R. Hegselmann and U. Krause, "Opinion dynamics and bounded confidence: models, analysis and simulation," *Journal of Artificial Societies and Social Simulation*, vol. 5, p. 1, 2002.
- [13] F. R. Marotto, *Introduction to Mathematical Modeling Using Discrete Dynamical Systems*, Thomson Brooks/Cole, London, UK, 2006.
- [14] T. S. Shores, *Applied Linear Algebra and Matrix Analysis*, Springer, 2018.



## Research Article

# Positive Periodic Solutions for an Generalized SIS Epidemic Model with Time-Varying Coefficients and Delays

Zhiwen Long 

College of Mathematics and Finance, Hunan University of Humanities, Science and Technology, Loudi, Hunan 417000, China

Correspondence should be addressed to Zhiwen Long; longzw2005@126.com

Received 28 April 2018; Revised 30 July 2018; Accepted 9 September 2018; Published 11 October 2018

Guest Editor: Stefania Tomasiello

Copyright © 2018 Zhiwen Long. This is an open access article distributed under the Creative Commons Attribution License, which permits unrestricted use, distribution, and reproduction in any medium, provided the original work is properly cited.

This paper mainly explores a generalized SIS epidemic model with time-varying coefficients and delays. By employing Lyapunov function method and differential inequality approach, a sufficient criterion to guarantee the existence and exponential stability of positive periodic solutions for the addressed model is obtained, which complements the earlier publications. Particularly, an example and its numerical simulations are given to demonstrate our theoretical results.

## 1. Introduction

In the study of infectious dynamics, under the assumption that there is no mortality due to illness, A. Iggridr, K. Niri b, and E. Ould Moulay Ely [1] proposed the following delayed SIS epidemic model:

$$\begin{aligned} i'(t) &= \beta [1 - i(t)] i(t) - \beta [1 - i(t - \omega)] i(t - \omega) e^{-d\omega} \\ &\quad - d i(t), \end{aligned} \quad (1)$$

where  $i(t) = I(t)/N(t)$ ,  $N(t) = S(t) + I(t)$ ,  $S(t)$ ,  $I(t)$ , and  $N(t)$  denote the susceptible numbers, infective numbers, and total numbers at time  $t$ , respectively. Here  $\beta$  is the transmission rate,  $\omega > 0$  designates the average latent period of the disease, and  $d$  represents the natural death rate. A more detailed description of the model can be found in [2]. Recently, some criteria ensuring the global attractivity of the endemic equilibrium of (1) have been established in [3]. On the one hand, any biological or environmental parameters are naturally subject to fluctuation in time and it is more realistic to consider the model with time-varying coefficients and delays. One can easily find that (1) can be extended to the case with time-varying delay and time-varying coefficients when  $d(t)$  has a special form. On the other hand, in the real world, the model coefficients are usually assumed to be periodic because the correlation coefficients are susceptible to the change of climate and other factors. In fact, periodic phenomena are found in the spread of many infectious diseases

such as influenza and chickenpox. Therefore it is worthwhile to investigate how periodic solutions arise and the stability of periodic solutions in an epidemiological model (see, for instance, [4–7]). However, to the best of our knowledge, there are no existing papers on positive periodic solutions of (1). According to the previous analysis, in this paper, our goal is to study the existence and the exponential stability of positive periodic solutions of the following generalized SIS model with time-varying delays and coefficients:

$$\begin{aligned} i'(t) &= \beta(t) [1 - i(t)] i(t) \\ &\quad - \beta(t) [1 - i(t - \omega(t))] i(t - \omega(t)) e^{-d(t)\omega(t)} \\ &\quad - d(t) i(t), \end{aligned} \quad (2)$$

where  $\beta(t)$ ,  $\omega(t)$ ,  $d(t)$  are nonnegative bounded and continuous  $T$ -periodic functions.

For convenience, we introduce the following notations.

$$\begin{aligned} g^+ &= \sup_{t \in \mathbb{R}} |g(t)|, \\ g^- &= \inf_{t \in \mathbb{R}} |g(t)|, \\ C &= C([- \omega^+, 0], \mathbb{R}), \\ C_+ &= C([- \omega^+, 0], \mathbb{R}_+), \\ i_t(\theta) &= i(t + \theta). \end{aligned} \quad (3)$$

By virtue of the biological interpretation of model (2), one can find that all solutions of (2) should remain in the interval  $[0, 1]$ . Then, we introduce the initial value conditions of (2) as follows:

$$i_{t_0} = \varphi, \quad \varphi \in C([- \omega^+, 0], [0, 1]) \subset C_+ \text{ and } i(0) > 0. \quad (4)$$

In addition, define a continuous map  $f: \mathbb{R} \times C_+ \rightarrow \mathbb{R}$  by

$$\begin{aligned} f(t, \varphi) &= \beta(t) \varphi(0) (1 - \varphi(0)) \\ &\quad - \beta(t) \varphi(-\omega(t)) (1 - \varphi(-\omega(t))) e^{-d(t)\omega(t)} \\ &\quad - d(t) \varphi(0). \end{aligned} \quad (5)$$

Clearly, the existence and uniqueness of the solution of (2) with the initial condition (4) are guaranteed by which  $f$  is a locally Lipschitz map with respect to  $\varphi \in C_+$ . Let  $i(t; t_0, \varphi)$  be a solution of the initial value problem (2) and (4) and  $[t_0, \eta(\varphi))$  be the maximal right-interval of the existence of  $i(t; t_0, \varphi)$ .

Let  $\theta(t) = \beta(t)((1 - e^{-d(t)\omega(t)})/d(t))$ ,  $g(t, x) = \beta(t)[(1 - x) - (1/4x)e^{-d(t)\omega(t)}]/d(t) - 1$ ,  $t \in \mathbb{R}$ . In the following, we always

assume that  $\theta(t) > 2$ , for all  $t \in \mathbb{R}$ . Fix  $t \in \mathbb{R}$ ; it is not difficult to verify that  $g(t, x)$  is increasing on  $(0, (1/2)e^{-d(t)\omega(t)/2})$  and decreasing on  $((1/2)e^{-d(t)\omega(t)/2}, +\infty)$  about the variable  $x$ . Note that

$$\begin{aligned} g\left(t, \frac{1}{2}e^{-d(t)\omega(t)/2}\right) &\geq g\left(t, \frac{1}{2}\right) \\ &= \frac{\beta(t)(1 - e^{-d(t)\omega(t)})}{2d(t)} - 1 \\ &= \frac{\theta(t)}{2} - 1 > 0, \quad \forall t \in \mathbb{R}. \end{aligned} \quad (6)$$

And

$$\begin{aligned} g(t, x) &\rightarrow -\infty \quad \text{as } x \rightarrow 0^+; \\ g(t, x) &\rightarrow -\infty \quad \text{as } x \rightarrow +\infty. \end{aligned} \quad (7)$$

For fixed  $t \in \mathbb{R}$ , we denote the unique zero solution of  $g(t, x)$  on  $(0, (1/2)e^{-d(t)\omega(t)/2})$  by  $\kappa(t)$ . For any  $\kappa \in (\kappa^+, 1/2)$ , denote  $M = 1 - \kappa$ ,  $C^\kappa = \{\varphi \in C \mid \varphi(\theta) \in (\kappa, M) \text{ for all } \theta \in [-\omega^+, 0]\}$ . Furthermore, it is not hard to see that

$$g(t, \kappa) > 0, \quad \forall t \in \mathbb{R}. \quad (8)$$

## 2. Preliminary Results

The following lemmas are helpful to prove our main results in Section 3.

**Lemma 1.** Assume that  $d^- > 0$ ,  $\omega^- > 0$ , and

$$2d(t) < \beta(t)(1 - e^{-d(t)\omega(t)}) < \frac{d(t)}{\kappa} \quad \text{for all } t \in \mathbb{R}. \quad (9)$$

Then, for  $\varphi \in C^\kappa$ ,

$$\begin{aligned} \eta(\varphi) &= \infty \text{ and} \\ i(t; t_0, \varphi) &\in C^\kappa \quad \text{for } t \geq t_0. \end{aligned} \quad (10)$$

*Proof.* For the sake of simplicity of notations, let  $i(t) = i(t; t_0, \varphi)$  for all  $t \in [t_0 - \omega^+, \eta(\varphi))$ . We first show that

$$i(t) > \kappa \quad \text{for all } t \in [t_0, \eta(\varphi)). \quad (11)$$

Arguing by contradiction, if this is not true, then there must exist  $T_1 \in (t_0, \eta(\varphi))$  such that

$$\begin{aligned} i(T_1) &= \kappa, \\ i(t) &> \kappa \quad \text{for all } t \in (t_0 - \omega^+, T_1), \end{aligned} \quad (12)$$

which, with the help of (8), (9), and (12), entails that

$$\begin{aligned} i'(T_1) &= \beta(T_1)[1 - i(T_1)]i(T_1) - \beta(T_1) \\ &\quad \cdot [1 - i(T_1 - \omega(T_1))]i(T_1 - \omega(T_1))e^{-d(T_1)\omega(T_1)} \\ &\quad - d(T_1)i(T_1) \geq \beta(T_1)(1 - \kappa)\kappa - \frac{\beta(T_1)}{4} \\ &\quad \cdot e^{-d(T_1)\omega(T_1)} - d(T_1)\kappa = d(T_1) \\ &\quad \cdot \kappa \left\{ \frac{\beta(T_1)[(1 - \kappa) - (1/4\kappa)e^{-d(T_1)\omega(T_1)}]}{d(T_1)} - 1 \right\} \\ &> 0, \end{aligned} \quad (13)$$

which is contrary to the fact that  $i'(T_1) \leq 0$ . Hence (11) holds. Next, we demonstrate that

$$i(t) < M \quad \text{for } t \in [t_0, \eta(\varphi)). \quad (14)$$

If not, there must exist  $T_2 \in (t_0, \eta(\varphi))$  such that

$$\begin{aligned} i(T_2) &= M, \\ i(t) &< M \quad \text{for all } t \in (t_0 - \omega^+, T_2), \end{aligned} \quad (15)$$

which, together with (9) and (15), suggests that

$$\begin{aligned} i'(T_2) &= \beta(T_2)[1 - i(T_2)]i(T_2) - \beta(T_2) \\ &\quad \cdot [1 - i(T_2 - \omega(T_2))]i(T_2 - \omega(T_2))e^{-d(T_2)\omega(T_2)} \\ &\quad - d(T_2)i(T_2) \leq \beta(T_2)(1 - M)M - \beta(T_2) \\ &\quad \cdot (1 - M)Me^{-d(T_2)\omega(T_2)} - d(T_2)M \\ &= M[\beta(T_2)(1 - M)(1 - e^{-d(T_2)\omega(T_2)}) - d(T_2)] \\ &< 0, \end{aligned} \quad (16)$$

which is a contradiction with  $i'(T_2) \geq 0$  and hence (14) is true. In view of (9), (11), and (14), we can show that

$$\kappa < i(t) < M \quad \text{for all } t \in [t_0 - \omega^+, \eta(\varphi)). \quad (17)$$

From Theorem 2.3.1 in [8], we can easily obtain  $\eta(\varphi) = +\infty$ . This completes the proof.  $\square$

**Lemma 2.** Assuming that the conditions of Lemma 1 are established, we further assume that

$$d(t) > \beta(t)(1 - 2\kappa) \left(1 + e^{-d(t)\omega(t)}\right) \quad \text{for } t \in \mathbb{R}. \quad (18)$$

Then there exists a positive  $\lambda$  such that

$$|i(t; t_0, \varphi) - i(t; t_0, \varphi^*)| \leq K_{\varphi, \varphi^*} e^{-\lambda t} \quad (19)$$

for  $\varphi, \varphi^* \in C^\kappa$  and  $t \geq t_0$ ,

where  $K_{\varphi, \varphi^*} = e^{\lambda t_0} (\max_{\theta \in [-\omega^+, 0]} |\varphi(\theta) - \varphi^*(\theta)| + 1)$ .

*Proof.* Consider  $\Gamma : [0, 1] \rightarrow \mathbb{R}$  defined by

$$\Gamma(u) = \sup_{t \in \mathbb{R}} \left\{ - \left[ d(t) - (1 - 2\kappa) \beta(t) \left(1 + e^{-d(t)\omega(t)} e^{u\omega^+} \right) - u \right] \right\}, \quad (20)$$

for  $u \in [0, 1]$ .

Clearly,  $\Gamma$  is continuous. Note that  $\Gamma(0) = \sup_{t \in \mathbb{R}} \{-[d(t) - (1 - 2\kappa)\beta(t)(1 + e^{-d(t)\omega(t)})]\} < 0$ , which follows from the continuity and periodicity of  $d(t)$ ,  $\omega(t)$ , and  $\beta(t)$ , then there are  $\eta > 0$  and  $1 > \lambda > 0$  such that  $\Gamma(\lambda) < -\eta$  or

$$- \left[ d(t) - (1 - 2\kappa) \beta(t) \left(1 + e^{-d(t)\omega(t)} e^{\lambda\omega^+} \right) - \lambda \right] < -\eta \quad (21)$$

$< 0 \quad \text{for } t \in \mathbb{R}.$

Let  $\varphi, \varphi^* \in C^\kappa$ . For simplicity, denote  $i(t; t_0, \varphi)$  and  $i(t; t_0, \varphi^*)$  by  $i(t)$  and  $i^*(t)$ , respectively. From Lemma 1, we have

$$\begin{aligned} \kappa &< i(t), \\ i^*(t) &< M \end{aligned} \quad (22)$$

for all  $t \in [t_0 - \omega^+, \infty)$ .

Let  $y(t) = i(t) - i^*(t)$  for  $t \in [t_0 - \omega^+, \infty)$ . Then, for  $t \geq t_0$ ,

$$\begin{aligned} y'(t) &= -[\beta(t)(i(t) + i^*(t) - 1) + d(t)] y(t) + \beta(t) \\ &\quad \cdot e^{-d(t)\omega(t)} [i(t - \omega(t)) + i^*(t - \omega(t)) - 1] \\ &\quad \cdot y(t - \omega(t)). \end{aligned} \quad (23)$$

Consider the Lyapunov functional

$$V(t) = |y(t)| e^{\lambda t} \quad \text{for } t \geq t_0. \quad (24)$$

We claim that  $V(t) \leq K_{\varphi, \varphi^*}$  for  $t \geq t_0$ . Otherwise, there exists  $t_* > t_0$  such that

$$\begin{aligned} V(t_*) &= K_{\varphi, \varphi^*} \text{ and} \\ V(t) &< K_{\varphi, \varphi^*} \end{aligned} \quad (25)$$

for all  $t \in [t_0 - \omega^+, t_*)$ .

Then

$$\begin{aligned} 0 &\leq D^-(V(t_*)) \leq -[\beta(t_*)(i(t_*) + i^*(t_*) - 1) \\ &\quad + d(t_*)] |y(t_*)| e^{\lambda t_*} + \beta(t_*) e^{-d(t_*)\omega(t_*)} |i(t_* \\ &\quad - \omega(t_*)) + i^*(t_* - \omega(t_*)) - 1| |y(t_* - \omega(t_*))| \\ &\quad \cdot e^{\lambda t_*} + \lambda |y(t_*)| e^{\lambda t_*} = -[\beta(t_*)(i(t_*) + i^*(t_*) \\ &\quad - 1) + d(t_*) - \lambda] |y(t_*)| e^{\lambda t_*} + \beta(t_*) \\ &\quad \cdot e^{-d(t_*)\omega(t_*)} |i(t_* - \omega(t_*)) + i^*(t_* - \omega(t_*)) - 1| \\ &\quad \cdot |y(t_* - \omega(t_*))| e^{\lambda(t_* - \omega(t_*))} e^{\lambda\omega(t_*)} \leq -[\beta(t_*)(2\kappa \\ &\quad - 1) + d(t_*) - \lambda] |y(t_*)| e^{\lambda t_*} + (2M - 1) \beta(t_*) \\ &\quad \cdot e^{-d(t_*)\omega(t_*)} |y(t_* - \omega(t_*))| e^{\lambda(t_* - \omega(t_*))} e^{\lambda\omega(t_*)} \\ &\leq \left\{ -[d(t_*) + \beta(t_*)(2\kappa - 1) - \lambda] + (1 - 2\kappa) \right. \\ &\quad \cdot \beta(t_*) e^{-d(t_*)\omega(t_*)} e^{\lambda\omega^+} \left. \right\} K_{\varphi, \varphi^*} \leq \left\{ -[d(t_*) \right. \\ &\quad - \beta(t_*)(1 - 2\kappa) \left(1 + e^{-d(t_*)\omega(t_*)} e^{\lambda\omega^+} \right) - \lambda] \left. \right\} K_{\varphi, \varphi^*} \\ &< -\eta K_{\varphi, \varphi^*} < 0, \end{aligned} \quad (26)$$

a contradiction. Consequently, we infer that (19) holds. The proof is completed.  $\square$

### 3. Main Results

Combined with Lemmas 1 and 2, we have the following theorem.

**Theorem 3.** Under the assumptions of Lemma 2, then system (2) has exactly one positive  $T$ -periodic solution which is exponentially stable.

*Proof.* Fix a  $\varphi \in C^\kappa$ ; let  $i(t) = i(t; t_0, \varphi)$  be a solution of system (2) and (4). According to Lemma 1, we have

$$\kappa < i(t; t_0, \varphi) < M \quad \text{for all } t \geq t_0 - \omega^+. \quad (27)$$

From the periodicity of coefficients and delays for system (2), for any nonnegative integer  $h$ , we get

$$\begin{aligned} i'(t + hT) &= \beta(t + hT) [1 - i(t + hT)] i(t + hT) \\ &\quad - \beta(t + hT) [1 - i(t + hT - \omega(t + hT))] \\ &\quad \cdot i(t + hT - \omega(t + hT)) e^{-d(t+hT)\omega(t+hT)} \\ &\quad - d(t + hT) i(t + hT) = \beta(t) [1 - i(t + hT)] \\ &\quad \cdot i(t + hT) - \beta(t) [1 - i(t + hT - \omega(t))] \\ &\quad \cdot i(t + hT - \omega(t)) e^{-d(t)\omega(t)} - d(t) i(t + hT) \end{aligned} \quad (28)$$

which implies that  $i(t + hT; t_0, \varphi)$  is also a solution to system (2) on  $[t_0 - \omega^+ - hT, \infty)$ . Denote  $\psi = i(t + T; t_0, \varphi)$ . In view of

Lemma 2, for any nonnegative integer  $h$  and  $t + hT \geq t_0$ , we obtain

$$\begin{aligned} & |i(t + (h+1)T; t_0, \varphi) - i(t + hT; t_0, \varphi)| \\ &= |i(t + hT; t_0, \psi) - i(t + hT; t_0, \varphi)| \\ &\leq K_{\varphi, \psi} e^{-\lambda(t+hT)}, \end{aligned} \quad (29)$$

where  $K_{\varphi, \psi} = e^{\lambda t_0} (\max_{\theta \in [-\omega^+, 0]} |\varphi(\theta) - \psi(\theta)| + 1)$ .

Now, we claim that  $i(t + qT; t_0, \varphi)$  is convergent on any compact interval as  $q \rightarrow \infty$ . For an arbitrary subset  $[a, b] \subset \mathbb{R}$ , we can pick a nonnegative integer  $q_0$  satisfying  $t + q_0T \geq t_0$  for  $t \in [a, b]$ . Then for  $t \in [a, b]$  and  $q > q_0$ , one can see that

$$\begin{aligned} i(t + qT) &= i(t + q_0T) \\ &+ \sum_{h=q_0}^{q-1} [i(t + (h+1)T) - i(t + hT)] \end{aligned} \quad (30)$$

which implies that  $\{i(t + qT)\}_q$  converges uniformly to a continuous function  $i^*(t)$ . Due to the arbitrariness of  $[a, b]$ , one can easily find that  $i(t + qT) \rightarrow i^*(t)$  as  $q \rightarrow \infty$  for  $t \in \mathbb{R}$ . Moreover, we get

$$\kappa \leq i^*(t) \leq M \quad \text{for all } t \in \mathbb{R}. \quad (31)$$

Next we show that  $i^*$  is a  $T$ -periodic solution of (2). The periodicity can be obtained immediately from the fact

$$\begin{aligned} i^*(t + T) &= \lim_{q \rightarrow \infty} i((t + T) + qT) \\ &= \lim_{q+1 \rightarrow \infty} i(t + (q+1)T) = i^*(t) \end{aligned} \quad (32)$$

for all  $t \in \mathbb{R}$ . Noting that  $i(t + qT)$  is a solution to (2),

$$\begin{aligned} i(t + qT) - i(t_0 + qT) &= \int_{t_0}^t \{\beta(s) [1 - i(s + qT)] \\ &\cdot i(s + qT) - \beta(s) [1 - i(s + qT - \omega(s))] \\ &\cdot i(s + qT - \omega(s)) e^{-d(s)\omega(s)} - d(s) i(s + qT)\} ds \end{aligned} \quad (33)$$

for  $t \geq t_0$ . Letting  $q \rightarrow \infty$  gives us

$$\begin{aligned} i^*(t) - i^*(t_0) &= \int_{t_0}^t \{\beta(s) [1 - i^*(s)] i^*(s) \\ &- \beta(s) [1 - i^*(s - \omega(s))] i^*(s - \omega(s)) e^{-d(s)\omega(s)} \\ &- d(s) i^*(s)\} ds \end{aligned} \quad (34)$$

for  $t \geq t_0$ ; namely,  $i^*$  is a solution to (2) on  $[t_0 - \omega^+, \infty)$ . Finally, by the same method as that in the proof of Lemma 2, we can show that  $i^*(t)$  is exponentially stable. This finishes the proof.  $\square$

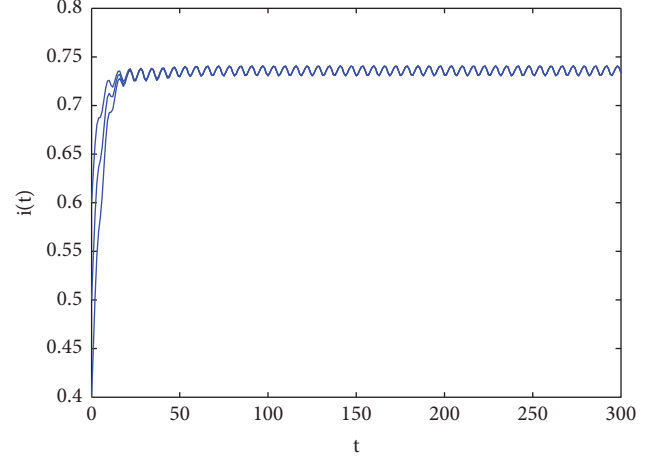


FIGURE 1: Numerical solutions  $i(t)$  of model (35) for initial value  $\varphi(t) = 0.4, 0.5, 0.6$ ,  $t \in [-50, 0]$ .

#### 4. An Example

*Example 1.* Regard the following generalized SIS epidemic model with time-varying delays and coefficients:

$$\begin{aligned} i'(t) &= (0.32 + 0.08 \sin t) [1 - i(t)] i(t) \\ &- (0.32 + 0.08 \sin t) [1 - i(t - (40 + 10 \sin t))] \\ &i(t - (40 + 10 \sin t)) e^{-(0.08 + 0.02 \sin t)(40 + 10 \sin t)} \\ &- (0.08 + 0.02 \sin t) i(t). \end{aligned} \quad (35)$$

Then

$$e^{-4} \leq e^{-d(t)\omega(t)} \leq e^{-1.8} \approx 0.1653, \quad \text{for all } t \in \mathbb{R}, \quad (36)$$

and  $\kappa^+ \approx 0.23025$ . Choose  $\kappa = 1/3$ , then  $1/4 < \kappa$ . By a simple computation, we can easily check that all the conditions of Theorem 3 are satisfied. Therefore, system (35) with initial values in  $\varphi \in C^\kappa$  has a unique positive  $2\pi$ -periodic solution  $i^*(t)$  which is exponentially stable. The numerical simulations in Figure 1 strongly support the conclusion.

*Remark 5.* To the author's knowledge, it is the first time to focus attention on the exponential stability of positive periodic solutions for (2), which is the generalization of (1). By constructing invariant sets ingeniously, under appropriate conditions, we represent that all solutions of the addressed model converge exponentially to the positive periodic solution. In addition, one can find that all the results in [1, 3–6] cannot be applicable to show the global exponential stability on the positive periodic solution of (35), which implies that the results of this paper are new and complement of previously known results. In future, we will consider the properties of almost periodic solutions and pseudo almost periodic solutions of the model.

#### Data Availability

No data were used to support this study.

## Conflicts of Interest

The author declares that there are no conflicts of interest.

## Acknowledgments

This work was supported by the Natural Scientific Research Fund of Hunan Province of China (grant no. 2018JJ2194).

## References

- [1] A. Iggidr, K. Niri, and E. O. M. Ely, "Fluctuations in a SIS epidemic model with variable size population," *Applied Mathematics and Computation*, vol. 217, no. 1, pp. 55–64, 2010.
- [2] H. W. Hethcote and P. van den Driessche, "An SIS epidemic model with variable population size and a delay," *Journal of Mathematical Biology*, vol. 34, no. 2, pp. 177–194, 1995.
- [3] B. Liu, "Convergence of an SIS epidemic model with a constant delay," *Applied Mathematics Letters*, vol. 49, pp. 113–118, 2015.
- [4] Z. Bai and Y. Zhou, "Existence of two periodic solutions for a non-autonomous SIR epidemic model," *Applied Mathematical Modelling: Simulation and Computation for Engineering and Environmental Systems*, vol. 35, no. 1, pp. 382–391, 2011.
- [5] L. Li, Y. Bai, and Z. Jin, "Periodic solutions of an epidemic model with saturated treatment," *Nonlinear Dynamics*, vol. 76, no. 2, pp. 1099–1108, 2014.
- [6] L. Liu and Y. Ye, "Existence and uniqueness of periodic solution for a discrete-time SIR epidemic model with time delays and impulses," *International Journal of Computational and Mathematical Sciences*, vol. 5, no. 4, pp. 229–235, 2011.
- [7] B. Liu, "Global exponential stability of positive periodic solutions for an epidemic model with saturated treatment," *Annales Polonici Mathematici*, vol. 116, no. 2, pp. 155–171, 2016.
- [8] J. K. Hale and S. M. Verduyn Lunel, *Introduction to Functional-Differential Equations*, Springer, Berlin, Germany, 1993.

## Research Article

# Uniqueness and Novel Finite-Time Stability of Solutions for a Class of Nonlinear Fractional Delay Difference Systems

Danfeng Luo and Zhiguo Luo 

Department of Mathematics, Hunan Normal University, Changsha, Hunan 410081, China

Correspondence should be addressed to Zhiguo Luo; [luozgl956@163.com](mailto:luozgl956@163.com)

Received 5 July 2018; Revised 28 August 2018; Accepted 16 September 2018; Published 30 September 2018

Guest Editor: Ahmed S. Hendy

Copyright © 2018 Danfeng Luo and Zhiguo Luo. This is an open access article distributed under the Creative Commons Attribution License, which permits unrestricted use, distribution, and reproduction in any medium, provided the original work is properly cited.

This paper focuses on the uniqueness and novel finite-time stability of solutions for a kind of fractional-order nonlinear difference equations with time-varying delays. Under some new criteria and by applying the generalized Gronwall inequality, the new constructive results have been established in the literature. As an application, two typical examples are delineated to demonstrate the effectiveness of our theoretical results.

## 1. Introduction

The time difference of fractional order was firstly studied by Kuttner [1] in 1957; since then, various kinds of definitions of fractional difference were studied by many authors. We know fractional difference equations play an important role in promoting modern mathematics development and have been widely applied, especially in physics, dynamic mechanics, medicines, and communications. There is a growing tendency nowadays that many experts show their great enthusiasm for fractional difference equations, and in the past few years, a lot of achievements have been done. For an extensive collection of such results, we recommend the readers to monograph [2] and papers [3–16].

The study about uniqueness of discrete solutions for fractional difference equations is one of the most interesting and valuable topics. Recently, Abdeljawad et al. [3] studied the following nonlinear fractional difference system

$$\begin{aligned}({}^{CFR}_a \nabla^\alpha y)(t) &= f(t, y(t)), \quad t \in \mathbb{N}_{a,b}, \\ y(a) &= c.\end{aligned}\quad (1)$$

Let  $f(t, y)$  satisfy Lipschitz condition: there exists a constant  $A > 0$  such that

$$|f(t, y_1) - f(t, y_2)| \leq A |y_1 - y_2|, \quad (2)$$

and  $f : \mathbb{N}_{a,b} \times \mathbb{R} \rightarrow \mathbb{R}$  and  $y : \mathbb{N}_{a,b} \rightarrow \mathbb{R}$ . By Banach Contraction Principle, authors obtained that system (1) had a unique solution  $x \in X$ ,  $X = \{x : \max_{t \in \mathbb{N}_{a,b}} |x(t)| < \infty\}$ , if

$$\frac{A}{B(\alpha - 1)} \left( (2 - \alpha)(b - a) + \frac{(\alpha - 1)(b - a)^2}{2} \right) < 1, \quad (3)$$

where  $B(\alpha)$  is a normalization positive constant depending on  $\alpha$  satisfying  $B(0) = B(1) = 1$ , and  ${}^{CFR}_a \nabla^\alpha$  is a fractional operator defined as in Definition 4 of paper [3].

In [4], Abdeljawad and M. Al-Mdallal considered the fractional difference system

$$\begin{aligned}({}^{ABC}_a \nabla^\alpha y)(t) &= f(t, y(t)), \quad t \in \mathbb{N}_{a,b}, \\ y(a) &= c,\end{aligned}\quad (4)$$

such that  $b \equiv a \pmod{1}$ ,  $f(a, y(a)) = 0$ . Let  $f$  admit the Lipschitz condition,  $A$  be a Lipschitz constant, and  $y : \mathbb{N}_{a,b} \rightarrow \mathbb{R}$ . Then system (4) had a unique solution provided that

$$A \left( \frac{1 - \alpha}{B(\alpha)} + \frac{(b - a)^{\bar{\alpha}}}{\Gamma(\alpha) B(\alpha)} \right) < 1, \quad (5)$$

where  ${}^{ABC}_a \nabla^\alpha$  is a fractional operator, and we can see it in Definition 4 of paper [4].



What will happen if the nonlinear equations (1) and (4) subjecting the initial value condition extend into fractional delay difference equation? We are particularly interested in fractional difference equation involving time-varying delays.

On the other hand, stability analysis is also one of the most crucial themes for fractional nonlinear systems, such as [17, 18] researching stability in nondelay fractional systems and [14, 19–22] in delay fractional difference systems. Specifically, in [17, 18], using Lyapunov's direct method, the stability of discrete nonautonomous systems with the nabla Caputo fractional difference was studied. In [19], the authors studied a class of linear fractional difference equations with impulse effects, and they provided the generalized Mittag-Leffler stability by numerical illustration. In papers [20, 22], asymptotic stability of a fractional discrete system was discussed and the theorem for a discrete fractional Lyapunov direct method was proved. In [21], the researchers investigated the stability of the equilibrium solution of a linear fractional difference equation with the initial condition, and to achieve this target, the well-known unilateral  $z$ -transform was successfully employed. In paper [14], the researchers considered the following linear fractional difference equations with a constant delay

$${}^C\Delta_a^\nu x(t) = A_0 x(t + \nu) + A_1 x(t + \nu - k), \quad 0 < \nu < 1, \quad (6)$$

where  $x(t) \in \mathbb{R}^l$ ,  $k$  is a fixed positive integer, and  ${}^C\Delta_a^\nu x(t)$  denotes the Caputo delta fractional difference of  $x(t)$  on the discrete time. The finite-time stable conclusions are presented in the addressed paper.

Deeply inspired by [3, 4, 14] and other mentioned papers, in this paper, we are concerned with the uniqueness and finite-time stability of solutions for the following fractional discrete equation with time-varying delays

$$\begin{aligned} {}^C\Delta_a^\nu x(t) &= Ax(t) + Bx(t - h(t)) + Dw(t) \\ &\quad + f(t, x(t), x(t - h(t)), w(t)), \end{aligned} \quad (7)$$

$$t \in J_1,$$

$$x(t) = \phi(t), \quad t \in J_2,$$

where  ${}^C\Delta_a^\nu$  denotes the Caputo fractional difference operator with  $\nu \in (0, 1]$ , and  $J_1 = \{t \in \mathbb{Z} \mid a + 1 - \nu \leq t \leq a + M\}$ , and  $J_2 = \{t \in \mathbb{Z} \mid a + 1 - \nu - h \leq t \leq a + 1 - \nu\}$ ,  $a \in \mathbb{R}$ ,  $M$  is a positive integer;  $x(t) \in \mathbb{R}^n$  is the state vector,  $w(t) \in \mathbb{R}^m$  is the disturbance vector,  $h(t)$  is a function satisfying  $0 \leq h(t) \leq h$ , and  $\phi(t) \in \mathbb{R}^n$  is the given function;  $A \in \mathbb{R}^{n \times n}$ ,  $B \in \mathbb{R}^{n \times n}$ ,  $D \in \mathbb{R}^{n \times m}$  are constant matrices, and  $f: J_1 \times \mathbb{R}^n \times \mathbb{R}^n \times \mathbb{R}^m \rightarrow \mathbb{R}^n$ .

Compared with some recent results in the literatures, such as [14, 17, 19–22], the chief contributions of this study contain at least the following three:

- (1) In [14, 17, 19–22], the literatures investigated the stability of fractional difference equations with constant delays, but the delay term we studied in system (7) is a bounded function with respect to the variable  $t$ . This is a significant breakthrough in dealing with fractional difference system with time-varying delays.
- (2) The model we are concerned with is more generalized, some ones in the articles are the special cases of it.

In [19, 22], the coefficients of the fractional discrete system researched by authors are one-dimensional real numbers which are too simple to describe the mathematical model well, and we adopt constant matrices as coefficients in (7). Therefore, the generalized models are originally discussed in the present paper. Furthermore, our conclusions can also be applied to the equations with function matrices, and you can see it by the following Corollaries 10 and 13.

- (3) An innovative method based on the generalized Gronwall inequality is exploited to discuss the uniqueness and finite-time stability of the solutions for the fractional-order difference equation with time-varying delays. The results established are essentially new.

The following article is organized as follows: in Section 2, we will recall some known results for our considerations. Some lemmas and definitions are useful to our work. Section 3 is devoted to researching the uniqueness of solutions for the fractional-order difference equation with time delay. Subsequently, we investigate the finite-time stability of the addressed equation, and then we will come up with the main theorem. To explain the results clearly, we finally provide two examples in Section 4.

## 2. Preliminaries

In this section, we plan to introduce some basic definitions and lemmas which are used throughout this paper.

*Definition 1* ([23, 24]). We define

$$t^\nu := \frac{\Gamma(t+1)}{\Gamma(t+1-\nu)}, \quad (8)$$

as for any  $t$  and  $\nu$  for which the right-hand side is defined. Here and in what follows  $\Gamma$  denotes the gamma function. We also appeal to the common convention that if  $t+1-\nu$  is a pole of the gamma function and  $t+1$  is not a pole, then  $t^\nu = 0$ .

*Definition 2* ([24]). The  $\nu$ -th fractional sum of a function  $f$ , for  $\nu > 0$ , is defined to be

$$\Delta_a^{-\nu} f(t) = \Delta_a^{-\nu} f(t; a) := \frac{1}{\Gamma(\nu)} \sum_{s=a}^{t-\nu} (t-s-1)^{\nu-1} f(s), \quad (9)$$

where  $t \in \{a + \nu, a + \nu + 1, \dots\} =: \mathbb{N}_{a+\nu}$ . We also define the  $\nu$ -th fractional difference, where  $\nu > 0$  and  $0 \leq N-1 < \nu \leq N$  with  $N \in \mathbb{N}$ , to be  $\Delta^\nu f(t) := \Delta^N \Delta^{N-\nu} f(t)$ , where  $t \in \mathbb{N}_{a+\nu}$ .

**Lemma 3** ([15]). Assume that  $\mu > 0$  and  $f$  is defined on  $\mathbb{N}_a$ . Then

$$\begin{aligned} \Delta^{-\mu} \Delta^\mu f(t) &= f(t) - \sum_{k=0}^{n-1} \frac{(t-a)^{(k)}}{k!} \Delta^k f(a) \\ &= f(t) + c_0 + c_1 t + \dots + c_{n-1} t^{(n-1)}, \end{aligned} \quad (10)$$

where  $n$  is the smallest integer greater than or equal to  $\mu$ ,  $c_i \in \mathbb{R}$ ,  $i = 1, 2, \dots, n-1$ .



**Lemma 4** ([10]). Let  $v \in \mathbb{R}$  and  $t, s \in \mathbb{R}$  such that  $(t-s)^{\underline{\nu}}$  is well defined, then  $\Delta_s(t-s)^{\underline{\nu}} = -v(t-s-1)^{\underline{\nu-1}}$ .

**Definition 5** ([14]). Given positive numbers  $c_1, c_2$  satisfying  $c_1 < c_2$ , system (7) is finite-time stable if and only if

$$\|\phi\| \leq c_1 \implies \|x(t)\| \leq c_2, \quad \forall t \in J_1 \cup J_2, \quad (11)$$

$$x(t) = \begin{cases} x(a) + \frac{1}{\Gamma(\nu)} \sum_{s=a}^{t-\nu} (t-s-1)^{\underline{\nu-1}} [Ax(s) + Bx(s-h(s)) + Dw(s) + f(s, x(s), x(s-h(s)), w(s))], & t \in J_1, \\ \phi(t), & t \in J_2. \end{cases} \quad (13)$$

**Lemma 7** (generalized Gronwall inequality). Let  $\alpha > 0$ , and  $u(t), v(t)$  be nonnegative functions and  $w(t)$  be nonnegative, nondecreasing function for  $t \in \mathbb{N}_a$  such that  $w(t) \leq M$ , where  $M$  is a constant. If

$$u(t) \leq v(t) + w(t) \Gamma(\alpha) \Delta_a^{-\alpha} u(t), \quad (14)$$

then

$$u(t) \leq v(t) + \sum_{k=1}^{\infty} (w(t) \Gamma(\alpha))^k \Delta_a^{-k\alpha} v(t). \quad (15)$$

*Proof.* Define operator

$$B\phi(t) = w(t) \sum_{s=a}^{t-\alpha} (t-s-1)^{\underline{\alpha-1}} \phi(s), \quad (16)$$

then from (14), we know

$$u(t) \leq v(t) + Bu(t), \quad (17)$$

which implies that  $u(t) \leq \sum_{k=0}^{n-1} B^k v(t) + B^n u(t)$ . The following proof process is similar to the relevant conclusion, and we can refer to Theorem 3.2 in [14].  $\square$

### 3. Main Results

Let  $\lambda(A)$  be the set of all eigenvalues of  $A$  and  $\lambda_{\max}(A) = \max\{\operatorname{Re}(\lambda) : \lambda \in \lambda(A)\}$ . Assume that  $\|A\|$  denotes the spectral norm defined by  $\sqrt{\lambda_{\max}(A^T A)}$ , and let  $\|x\|$  be the norm of  $x(t) = (x_1(t), x_2(t), \dots, x_n(t))^T \in \mathbb{R}^n$  defined by  $\|x\| = \max_{t \in J_1 \cup J_2} (\sum_{i=1}^n x_i^2)^{1/2}$ . Suppose that  $\mathcal{B}^+(J_1)$  denotes the set of all nonnegative bounded functions on  $J_1$ . Assume that the nonlinear function  $f : J_1 \times \mathbb{R}^n \times \mathbb{R}^n \times \mathbb{R}^m \rightarrow \mathbb{R}^n$  satisfies the condition  $(H_1)$ : there exists a positive constant  $l(t) \in \mathcal{B}^+(J_1)$  such that

$$\begin{aligned} & \|f(t, x_1, y_1, w_1) - f(t, x_2, y_2, w_2)\| \\ & \leq l(t) (\|x_1 - x_2\| + \|y_1 - y_2\| + \|w_1 - w_2\|), \end{aligned} \quad (18)$$

where  $f(t, 0, 0, 0) = 0$ . In this section, we always assume that

$$\|A\| = \bar{a},$$

$$\|B\| = \bar{b},$$

for all disturbances  $w(t)$  satisfying the following condition:

$$\exists \eta > 0 : w^T(t) w(t) \leq \eta^2. \quad (12)$$

**Definition 6.** A function  $x(t)$  is called the solution of (7) if  $x(t)$  satisfies

$$\begin{aligned} \|D\| &= \bar{d}, \\ \sup_{s \in [a, t-\nu]} l(s) &= \bar{L}. \end{aligned} \quad (19)$$

**Theorem 8.** Assume that  $0 \leq (\bar{a} + \bar{b} + 2\bar{L})/\Gamma(\nu) < 1$ , then system (7) has a unique solution on  $J_1 \cup J_2$  if the condition  $(H_1)$  holds.

*Proof.* Let  $x(t)$  and  $\tilde{x}(t)$  be any two different solutions to system (7), then  $x(t)$  and  $\tilde{x}(t)$  both satisfy (13). Let  $z(t) = x(t) - \tilde{x}(t)$ .

We can easily obtain  $z(t) = 0$  for  $t \in J_2$ . That is to say, system (7) has a unique solution as  $t \in J_2$ .

When  $t \in J_1 = J_{11} \cup J_{12}$ , and  $J_{11} = \{t \in \mathbb{Z} \mid a+1-\nu \leq t \leq a+\nu\}$ ,  $J_{12} = \{t \in \mathbb{Z} \mid a+\nu \leq t \leq a+M\}$ , we get

$$\begin{aligned} z(t) &= \frac{1}{\Gamma(\nu)} \sum_{s=a}^{t-\nu} (t-s-1)^{\underline{\nu-1}} [Az(s) + Bz(s-h(s)) \\ &+ f(s, x(s), x(s-h(s)), w(s)) \\ &- f(s, \tilde{x}(s), \tilde{x}(s-h(s)), w(s))]. \end{aligned} \quad (20)$$

If  $t \in J_{11}$ , then

$$\begin{aligned} z(t) &= \frac{1}{\Gamma(\nu)} \sum_{s=a}^{t-\nu} (t-s-1)^{\underline{\nu-1}} [Az(s) \\ &+ f(s, x(s), x(s-h(s)), w(s)) \\ &- f(s, \tilde{x}(s), \tilde{x}(s-h(s)), w(s))]. \end{aligned} \quad (21)$$

Now applying the norm  $\|\cdot\|$  on both sides of (21), we get

$$\begin{aligned} \|z(t)\| &\leq \frac{1}{\Gamma(\nu)} \sum_{s=a}^{t-\nu} (t-s-1)^{\underline{\nu-1}} [\|A\| \|z(s)\| \\ &+ \|f(s, x(s), x(s-h(s)), w(s)) \\ &- f(s, \tilde{x}(s), \tilde{x}(s-h(s)), w(s))\|] \leq \frac{1}{\Gamma(\nu)} \sum_{s=a}^{t-\nu} (t-s \\ &- 1)^{\underline{\nu-1}} [(\|A\| + l(s)) \|z(s)\|] \leq \frac{\bar{a} + \bar{L}}{\Gamma(\nu)} \sum_{s=a}^{t-\nu} (t-s \\ &- 1)^{\underline{\nu-1}} \|z(s)\|. \end{aligned} \quad (22)$$

Applying the Generalized Gronwall Inequality in Lemma 7, we have

$$\|z(t)\| \leq 0. \quad (23)$$

Namely,  $x(t) = \tilde{x}(t)$  for  $t \in J_{11}$ .

If  $t \in J_{12}$ , then applying the norm  $\|\cdot\|$  on both sides of (20), it follows that

$$\begin{aligned} \|z(t)\| &\leq \frac{1}{\Gamma(\nu)} \sum_{s=a}^{t-\nu} (t-s-1)^{\nu-1} \\ &\cdot [(\bar{a} + l(s)) \|z(s)\| + (\bar{b} + l(s)) \|z(s-h(s))\|] \\ &\leq \frac{\bar{a} + \bar{L}}{\Gamma(\nu)} \sum_{s=a}^{t-\nu} (t-s-1)^{\nu-1} \|z(s)\| + \frac{\bar{b} + \bar{L}}{\Gamma(\nu)} \\ &\cdot \sum_{s=a+\nu+1}^{t-\nu} (t-s-1)^{\nu-1} \times \|z(s-h(s))\|. \end{aligned} \quad (24)$$

Let  $z^*(t) = \sup_{\theta \in [-h, 0]} \|z(t+\theta)\|$ ,  $t \in J_{12}$ , then we have

$$z^*(t) \leq \frac{\bar{a} + \bar{b} + 2\bar{L}}{\Gamma(\nu)} \sum_{s=a}^{t-\nu} (t-s-1)^{\nu-1} z^*(s). \quad (25)$$

Similarly, applying the generalized Gronwall inequality in Lemma 7, it follows that

$$\|z(t)\| \leq z^*(t) < 0. \quad (26)$$

Hence we can obtain  $x(t) = \tilde{x}(t)$ . This completes the proof.  $\square$

*Remark 9.* When we demonstrate the uniqueness of solutions for the fractional discrete system with time delay, we find that the conditions we needed have nothing to do with the disturbance vector  $w(t)$ . That is to say, disturbance vector does not affect the uniqueness of solution for the system.

One can extend the constant matrices in (7) to the function form as follows:

$$\begin{aligned} {}^C\Delta_a^\nu x(t) &= A(t)x(t) + B(t)x(t-h(t)) \\ &+ D(t)w(t) \\ &+ f(t, x(t), x(t-h(t)), w(t)), \end{aligned} \quad (27)$$

$$t \in J_1,$$

$$x(t) = \phi(t), \quad t \in J_2.$$

Our conclusion (Theorem 8) can also be applied to (27) if  $f(\cdot)$  satisfies the condition  $(H_1)$ . In the case, let  $\|A(t)\| = \bar{a}$ ,  $\|B(t)\| = \bar{b}$ ,  $\|D(t)\| = \bar{d}$  in the same proof.

**Corollary 10.** Assume that  $0 \leq (\bar{a} + \bar{b} + 2\bar{L})/\Gamma(\nu) < 1$ , then system (27) has a unique solution on  $J_1 \cup J_2$  if the condition  $(H_1)$  holds.

**Theorem 11.** Suppose that  $(H_1)$  holds, and  $0 \leq (\bar{a} + \bar{b} + 2\bar{L})/\Gamma(\nu) < 1$ , and there exist positive numbers  $c_1 < c_2$ , and  $\|\phi\| \leq c_1$ , then system (7) is finite-time stable on  $J_1 \cup J_2$  if

$$\begin{aligned} &\left( c_1 + \frac{\eta(\bar{d} + \bar{L})M^\nu}{\Gamma(\nu+1)} \right) \\ &\cdot \left( 1 + \sum_{k=1}^{\infty} (\bar{a} + \bar{b} + 2\bar{L})^k \cdot \frac{M^{k\nu}}{\Gamma(k\nu+1)} \right) \leq c_2. \end{aligned} \quad (28)$$

*Proof.* Let  $u(t) = \sup_{\theta \in [a+1-\nu-h, t]} \|x(\theta)\|$ , for  $t \in J_1$ . We have  $\|x(s)\| \leq u(s)$ , and  $\|x(s-h(s))\| \leq u(s)$ ,  $\forall s \in [0, t]$ . According to (12) and (13), one can obtain

$$\begin{aligned} \|x(t)\| &\leq \|x(a)\| + \frac{1}{\Gamma(\nu)} \sum_{s=a}^{t-\nu} (t-s-1)^{\nu-1} [\|A\| \|x(s)\| \\ &+ \|B\| \|x(s-h(s))\| + \|D\| \|w(s)\| \\ &+ \|f(s, x(s), x(s-h(s)), w(s))\|] \leq \|\phi\| \\ &+ \frac{\bar{a} + \bar{b} + 2\bar{L}}{\Gamma(\nu)} \sum_{s=a}^{t-\nu} (t-s-1)^{\nu-1} u(s) + \frac{\eta(\bar{d} + \bar{L})}{\Gamma(\nu)} \\ &\cdot \frac{(t-a)^\nu}{\nu} \leq \|\phi\| + \frac{\eta(\bar{d} + \bar{L})M^\nu}{\Gamma(\nu+1)} + \frac{\bar{a} + \bar{b} + 2\bar{L}}{\Gamma(\nu)} \\ &\cdot \sum_{s=a}^{t-\nu} (t-s-1)^{\nu-1} u(s). \end{aligned} \quad (29)$$

As for all  $\theta \in [a+1-\nu, t]$ , we have

$$\begin{aligned} \|x(\theta)\| &\leq \|\phi\| + \frac{\eta(\bar{d} + \bar{L})M^\nu}{\Gamma(\nu+1)} \\ &+ \frac{\bar{a} + \bar{b} + 2\bar{L}}{\Gamma(\nu)} \sum_{s=a}^{\theta-\nu} (\theta-s-1)^{\nu-1} u(s) \\ &\leq \|\phi\| + \frac{\eta(\bar{d} + \bar{L})M^\nu}{\Gamma(\nu+1)} \\ &+ \frac{\bar{a} + \bar{b} + 2\bar{L}}{\Gamma(\nu)} \sum_{s=a}^{t-\nu} (t-s-1)^{\nu-1} u(s). \end{aligned} \quad (30)$$

Therefore, we have

$$\begin{aligned} u(t) &= \sup_{\theta \in [a+1-\nu-h, t]} \|x(\theta)\| \\ &\leq \max \left\{ \sup_{\theta \in [a+1-\nu-h, a+1-\nu]} \|x(\theta)\|, \sup_{\theta \in [a+1-\nu, t]} \|x(\theta)\| \right\} \\ &\leq \max \left\{ \|\phi\|, \|\phi\| + \frac{\eta(\bar{d} + \bar{L})M^\nu}{\Gamma(\nu+1)} \right. \\ &+ \left. \frac{\bar{a} + \bar{b} + 2\bar{L}}{\Gamma(\nu)} \sum_{s=a}^{t-\nu} (t-s-1)^{\nu-1} u(s) \right\} = \|\phi\| \\ &+ \frac{\eta(\bar{d} + \bar{L})M^\nu}{\Gamma(\nu+1)} + \frac{\bar{a} + \bar{b} + 2\bar{L}}{\Gamma(\nu)} \sum_{s=a}^{t-\nu} (t-s-1)^{\nu-1} u(s). \end{aligned} \quad (31)$$

According to Lemma 7, we can get

$$\begin{aligned}
 u(t) &\leq \|\phi\| + \frac{\eta(\bar{a} + \bar{L})M^\nu}{\Gamma(\nu + 1)} + \sum_{k=1}^{\infty} (\bar{a} + \bar{b} + 2\bar{L})^k \\
 &\quad \cdot \frac{1}{\Gamma(k\nu)} \sum_{s=a}^{t-k\nu} (t-s-1)^{k\nu-1} \\
 &\quad \times \left( \|\phi\| + \frac{\eta(\bar{a} + \bar{L})M^\nu}{\Gamma(\nu + 1)} \right) \\
 &\leq \left( \|\phi\| + \frac{\eta(\bar{a} + \bar{L})M^\nu}{\Gamma(\nu + 1)} \right) \\
 &\quad \cdot \left( 1 + \sum_{k=1}^{\infty} (\bar{a} + \bar{b} + 2\bar{L})^k \cdot \frac{M^{k\nu}}{\Gamma(k\nu + 1)} \right).
 \end{aligned} \tag{32}$$

Hence,

$$\begin{aligned}
 \|x(t)\| &\leq u(t) \leq \left( c_1 + \frac{\eta(\bar{a} + \bar{L})M^\nu}{\Gamma(\nu + 1)} \right) \\
 &\quad \cdot \left( 1 + \sum_{k=1}^{\infty} (\bar{a} + \bar{b} + 2\bar{L})^k \cdot \frac{M^{k\nu}}{\Gamma(k\nu + 1)} \right) \leq c_2.
 \end{aligned} \tag{33}$$

As for  $t \in J_2$ , obviously, system (7) has finite-time stability. According to Definition 5, we can obtain that system (7) is finite-time stable. This completes the proof of Theorem 11.  $\square$

**Remark 12.** Different from the research in uniqueness of solutions, the disturbance vector  $w(t)$  plays a key role in studying the finite-time stability. It can be easily analyzed by (33).

When  $A, B, D$  are function matrices instead of constant ones, our conclusion about the finite-time stability (Theorem 11) also can be applied to system (27). In this case, we assume that  $\|A(t)\| = \bar{a}$ ,  $\|B(t)\| = \bar{b}$ ,  $\|D(t)\| = \bar{d}$  in the same proof.

**Corollary 13.** Given positive numbers  $c_1, c_2, M$ , such that  $c_1 < c_2$ , then system (27) is finite-time stable on  $J_1 \cup J_2$  if all the conditions in Theorem 11 hold.

#### 4. Example

In this section, we will present the following two examples to illustrate our main results.

**Example 14.** Suppose that  $\nu = 1/20$ , and  $f(\cdot) = 0.1 \sin x(t) + 0.1 \cos x(t - h(t))$  with  $x = (x_1(t), x_2(t))^T$ . Consider system (7), where

$$A = \begin{pmatrix} 1 & 0 \\ 0 & 2 \end{pmatrix}, \tag{34}$$

$$B = \begin{pmatrix} 2 & 3 \\ 0 & 0 \end{pmatrix}. \tag{35}$$

We have  $\|A\| = \bar{a} = 4$ ,  $\|B\| = \bar{b} = 13$ , and  $\bar{L} = 0.1$ ,  $\Gamma(\nu) \approx 19.47$ , which imply that the condition  $0 < (\bar{a} + \bar{b} + 2\bar{L})/\Gamma(\nu) < 1$  referred to in Theorem 8 holds. Therefore, the specific system (7) has a unique solution.

**Remark 15.** Since there are few papers researching the uniqueness of solutions for the nonlinear fractional-order difference equation with time-varying delay, one can see that all the results in [23, 25–28] can not directly be applicable to Example 14 to obtain the uniqueness of the solution. This implies that the results in this paper are essentially new.

**Example 16.** Suppose that

$$f(\cdot) = 0.1 \begin{pmatrix} \sqrt{x_1^2(t) + x_1^2(t-h)} + \sin x_1 \\ \sqrt{x_2^2(t) + x_2^2(t-h)} + \sin x_2 \end{pmatrix}, \tag{36}$$

and let

$$A = \begin{pmatrix} 0.2 & 0 \\ 0 & 0.3 \end{pmatrix}, \tag{37}$$

$$B = \begin{pmatrix} 0 & 0 \\ 0.4 & 0.2 \end{pmatrix}, \tag{38}$$

$$D = \begin{pmatrix} 1 \\ 0 \end{pmatrix}. \tag{39}$$

Let  $M = 10$ ,  $w(t) = \sqrt{2}$ ,  $h = 1$ ,  $\nu = 0.03$ ,  $\Gamma(\nu) \approx 32.79$ ,  $\Gamma(\nu + 1) \approx 0.98$ ,  $a = 1$ ,  $\eta = 1.42$ ,  $\phi(t) = (0.8, 0.8)^T$ . We have  $\bar{a} = 0.3$ ,  $\bar{b} = 0.45$ ,  $\bar{d} = 1$ ,  $\bar{L} = 0.1$ . One can assume that  $c_1 = 1.14$ ,  $c_2 \geq 463.26$ ,  $0 < (\bar{a} + \bar{b} + 2\bar{L})/\Gamma(\nu) \approx 0.97 < 1$ . By Mathematica software, we can get

$$\begin{aligned}
 &\left( c_1 + \frac{\eta(\bar{a} + \bar{L})M^\nu}{\Gamma(\nu + 1)} \right) \\
 &\quad \cdot \left( 1 + \sum_{k=1}^{\infty} (\bar{a} + \bar{b} + 2\bar{L})^k \cdot \frac{M^{k\nu}}{\Gamma(k\nu + 1)} \right) \approx 463.26 \\
 &\leq c_2,
 \end{aligned} \tag{40}$$

which implies that inequality (28) holds, and we conclude that all conditions in Theorem 11 are satisfied. Therefore, the specific system (7) is finite-time stable.

#### 5. Conclusion

In this paper, we are concerned with a nonlinear fractional-order difference equation. The addressed equation has time delay terms, which are quite different from the related references discussed in the literature [18, 23, 24, 28, 29]. The nonlinear fractional-order difference system studied in the present paper is more generalized and more practical. By applying the generalized Gronwall inequality and the definition of the finite-time stability, we employ a novel argument and the easily verifiable sufficient conditions have

been provided to determine the uniqueness and finite-time stability of the solutions for the considered equation. Finally, two typical examples have been presented at the end of this paper to illustrate the effectiveness and feasibility of the proposed criterion. Consequently, this paper shows theoretically and numerically that some related references known in the literature can be enriched and complemented.

## Data Availability

The data in this study were mainly collected via discussion during our class. Readers wishing to access these data can do so by contacting the corresponding author.

## Conflicts of Interest

The authors declare that they have no conflicts of interest.

## Acknowledgments

This work was supported by the National Natural Science Foundation of China (Grant No. 11471109).

## References

- [1] B. Kuttner, "On differences of fractional order," *Proceedings of the London Mathematical Society. Third Series*, vol. 7, pp. 453–466, 1957.
- [2] C. Goodrich and A. C. Peterson, *Discrete Fractional Calculus*, Springer International, New York, NY, USA, 2015.
- [3] T. Abdeljawad, Q. M. Al-Mdallal, and M. . Hajji, "Arbitrary order fractional difference operators with discrete exponential kernels and applications," *Discrete Dynamics in Nature and Society*, Art. ID 4149320, 8 pages, 2017.
- [4] T. Abdeljawad and Q. M. Al-Mdallal, "Discrete Mittag-Leffler kernel type fractional difference initial value problems and Gronwall's inequality," *Journal of Computational and Applied Mathematics*, vol. 339, pp. 218–230, 2018.
- [5] Y. Sun and G. Li, "Finite-time stability and stabilization of networked control systems with bounded Markovian packet dropout," *Discrete Dynamics in Nature and Society*, Art. ID 176919, 6 pages, 2014.
- [6] X. Mo, H. Niu, and Q. Lan, "Finite-time stabilization for a class of nonlinear differential-algebraic systems subject to disturbance," *Discrete Dynamics in Nature and Society*, Art. ID 9730312, 14 pages, 2017.
- [7] Y. Xu, J. Zhang, W. Zhou, and D. Tong, "Finite-time bounded synchronization of the growing complex network with nonde-layed and delayed coupling," *Discrete Dynamics in Nature and Society*, Art. ID 6501583, 7 pages, 2017.
- [8] C. Lizama and M. Murillo-Arcila, "Maximal regularity in  $l^p$  spaces for discrete time fractional shifted equations," *Journal of Differential Equations*, vol. 263, no. 6, pp. 3175–3196, 2017.
- [9] T. Yu, Y. Zhong, T. Chen, and C. Chen, "Finite-time stabilization of uncertain switched positive linear systems with time-varying delays," *Discrete Dynamics in Nature and Society*, vol. 2015, Article ID 954782, 9 pages, 2015.
- [10] T. Abdeljawad and B. Abdalla, "Monotonicity results for delta and nabla caputo and riemann fractional differences via dual identities," *Filomat*, vol. 31, no. 12, pp. 3671–3683, 2017.
- [11] T. Abdeljawad and D. F. M. Torres, "Symmetric duality for left and right Riemann-Liouville and Caputo fractional differences," *Arab Journal of Mathematical Sciences*, vol. 23, pp. 157–172, 2017.
- [12] I. K. Dassios and D. I. Baleanu, "Duality of singular linear systems of fractional nabla difference equations," *Applied Mathematical Modelling*, vol. 39, no. 14, pp. 4180–4195, 2015.
- [13] F. M. Atıcı and P. W. Eloe, "Two-point boundary value problems for finite fractional difference equations," *Journal of Difference Equations and Applications*, vol. 17, no. 4, pp. 445–456, 2011.
- [14] G.-C. Wu, D. Baleanu, and S.-D. Zeng, "Finite-time stability of discrete fractional delay systems: Gronwall inequality and stability criterion," *Communications in Nonlinear Science and Numerical Simulation*, vol. 57, pp. 299–308, 2018.
- [15] T. Abdeljawad, "On Riemann and Caputo fractional differences," *Computers & Mathematics with Applications*, vol. 62, no. 3, pp. 1602–1611, 2011.
- [16] T. Abdeljawad, J. Alzabut, and D. Baleanu, "A generalized  $q$ -fractional Gronwall inequality and its applications to nonlinear delay  $q$ -fractional difference systems," *Journal of Inequalities and Applications*, Paper No. 240, 13 pages, 2016.
- [17] M. Wyrwas, D. Mozyrska, and E. Girejko, "Stability of discrete fractional-order nonlinear systems with the nabla Caputo difference," *IFAC Proceedings Volumes*, vol. 46, no. 1, pp. 167–171, 2013.
- [18] G.-C. Wu, D. Baleanu, and W.-H. Luo, "Lyapunov functions for Riemann-Liouville-like fractional difference equations," *Applied Mathematics and Computation*, vol. 314, pp. 228–236, 2017.
- [19] G.-C. Wu, D. Baleanu, and L.-L. Huang, "Novel Mittag-Leffler stability of linear fractional delay difference equations with impulse," *Applied Mathematics Letters*, vol. 82, pp. 71–78, 2018.
- [20] Fulai Chen and Zhigang Liu, "Asymptotic Stability Results for Nonlinear Fractional Difference Equations," *Journal of Applied Mathematics*, vol. 2012, Article ID 879657, 14 pages, 2012.
- [21] R. Abu-Saris and Q. Al-Mdallal, "On the asymptotic stability of linear system of fractional-order difference equations," *Fractional Calculus and Applied Analysis*, vol. 16, no. 3, pp. 613–629, 2013.
- [22] D. Baleanu, G.-C. Wu, Y.-R. Bai, and F.-L. Chen, "Stability analysis of Caputo-like discrete fractional systems," *Communications in Nonlinear Science and Numerical Simulation*, vol. 48, pp. 520–530, 2017.
- [23] C. S. Goodrich, "Existence and uniqueness of solutions to a fractional difference equation with nonlocal conditions," *Computers & Mathematics with Applications*, vol. 61, no. 2, pp. 191–202, 2011.
- [24] C. S. Goodrich, "Continuity of solutions to discrete fractional initial value problems," *Computers & Mathematics with Applications*, vol. 59, no. 11, pp. 3489–3499, 2010.
- [25] L. Plociniczak and M. Switala, "Existence and uniqueness results for a time-fractional nonlinear diffusion equation," *Journal of Mathematical Analysis and Applications*, vol. 462, no. 2, pp. 1425–1434, 2018.
- [26] Y. Zou and G. He, "On the uniqueness of solutions for a class of fractional differential equations," *Applied Mathematics Letters*, vol. 74, pp. 68–73, 2017.
- [27] C. S. Goodrich, "On positive solutions to nonlocal fractional and integer-order difference equations," *Applicable Analysis and Discrete Mathematics*, vol. 5, no. 1, pp. 122–132, 2011.

- [28] F. L. Chen and Y. Zhou, "Existence and Ulam stability of solutions for discrete fractional boundary value problem," *Discrete Dynamics in Nature and Society*, vol. 2013, Article ID 459161, 7 pages, 2013.
- [29] C. S. Goodrich, "A convexity result for fractional differences," *Applied Mathematics Letters*, vol. 35, no. 1, pp. 58–62, 2014.

## Research Article

# A Hybrid Ant Colony Optimization for Dynamic Multidepot Vehicle Routing Problem

Haitao Xu , Pan Pu , and Feng Duan

*School of Computer Science and Technology, Hangzhou Dianzi University, Hangzhou, China*

Correspondence should be addressed to Haitao Xu; xuhaitao@hdu.edu.cn

Received 19 July 2018; Accepted 10 September 2018; Published 25 September 2018

Guest Editor: Ahmed S. Hendy

Copyright © 2018 Haitao Xu et al. This is an open access article distributed under the Creative Commons Attribution License, which permits unrestricted use, distribution, and reproduction in any medium, provided the original work is properly cited.

In the real world, the vehicle routing problem (VRP) is dynamic and variable, so dynamic vehicle routing problem (DVRP) has obtained more and more attentions among researchers. Meanwhile, due to actual constraints of service hours and service distances, logistics companies usually build multiple depots to serve a great number of dispersed customers. Thus, the research of dynamic multidepot vehicle routing problem (DMDVRP) is significant and essential. However, it has not attracted much attention. In this paper, firstly, a clustering approach based on the nearest distance is proposed to allocate all customers to the depots. Then a hybrid ant colony optimization (HACO) with mutation operation and local interchange is introduced to optimize vehicle routes. In addition, in order to deal with dynamic problem of DMDVRP quickly, a real-time addition and optimization approach is designed to handle the new customer requests. Finally, the *t*-test is applied to evaluate the proposed algorithm; meanwhile the relations between degrees of dynamism (*dod*) and HACO are discussed minutely. Experimental results show that the HACO algorithm is feasible and efficient to solve DMDVRP.

## 1. Introduction

In the history of VRP, the most original and famous routing problem is Traveling Salesman Problem (TSP) [1]. By transforming the TSP, a great number of different kinds of VRP are designed. Generally, VRP has been classified to the following several variants: Capacitated VRP (CVRP), VRP with time windows (VRPTW), VRP with Pickup and Delivery (VRPPD), multidepot VRP (MDVRP), and so on [2–6]. Most particularly, considering that many logistics companies are desirous to improve service quality and save time, the MDVRP receives more and more attentions.

In VRP models, most of the researchers usually define some basic information concerning customers' locations and demands, available vehicles, etc., which are entirely known before carrying out service. However, VRP is dynamic in most of the actual situations; in other words, the arrangements of customers are changing gradually over time, although a part of customer requests may be known in advance. In recent years, due to the development of new technologies, such as Global Position System, Communication Technology, Information Technology, some researchers have

studied DVRP. However, few researchers focus on DVRP with multiple depots, so this paper will study dynamic multidepot vehicle routing problem (DMDVRP) [7].

Comparatively, the number of research projects on the DMDVRP is fewer. T. C. Su introduced a dynamic vehicle control and scheduling of a multidepot physical distribution system in 1999 [8]. For solving dynamic multidepot pickup and delivery problem, T. Huth and D. C. Mattfeld proposed a framework to anticipate dynamic events by model adaptation in 2006 [9]. In 2008, A. Hadjar and F. Soumis introduced multidepot vehicle scheduling problem with time windows, which is a dynamic window reduction. Y. Kuo and C. C. Wang proposed an insertion heuristic to solve dynamic multidepot vehicle routing problem where the pick-up and delivery requests are both considered in 2014 [10]. Liu Y et al. proposed a method with three steps to solve the multiperiod and multidepot dynamic vehicle routing problem with time windows in 2016 [7].

In general, DMDVRP is a NP-hard problem [11], so some exact algorithms (branch and bound algorithm, linear programming, cutting plane algorithm, etc.) are almost impossible to solve it in finite time. However, modern



heuristic algorithms, such as ant colony optimization (ACO) [12, 13], genetic algorithm (GA) [14–16], and particle swarm optimization (PSO) [17], have the ability to generate high quality solutions, although they may not search the best solution. In these approaches, ACO is widely applied to solve different types of VRP.

The original ACO was put forward by Dorigo in his Ph.D. Thesis [18], which is called ant system. However, it is nonconvergent and easy to fall into local optimization. To improve its weaknesses, many researchers have formed several variants of the ant system, such as the ant colony system, the elite ant system, and the largest ant system [19]. In addition, some new mechanisms are proposed to optimize the algorithm, such as enlarging the degree of random search [13], N-Opt local random search, and designing distributed control [20]. For DMDVRP, the objective of the algorithm is not only to search the optimal solution, but also to track the optimal solution through the information of the previous search space over time. Based on this consideration, a hybrid ACO is proposed to solve DMDVRP.

There are two main contributions in this paper. The first contribution of this paper is to use hybrid ACO algorithm to solve DMDVRP, and the method strives to improve the randomization and avoids falling into local search prematurely. In order to improve ACO, the following modifications of ACO are implemented:

- (1) Dividing region by the nearest distance cluster
- (2) Optimizing vehicle routes with mutation operation
- (3) Improving the solutions with local interchange operation

Hybrid ACO has shown its advantages through a large number of comparative experiments based on data sets of different scales.

The second contribution is that a real-time addition and optimization approach is designed to add new real-time customers to known routes and immediately optimize vehicle routes. The process of dynamic optimization can be accelerated.

The remainder of this paper is organized as follows. In Section 2, we describe DMDVRP model and define the problem. In Section 3, the details of hybrid ACO are shown. A real-time addition and optimization approach is introduced in Section 4. Experimental results are discussed in Section 5. Some conclusions are provided in Section 6.

## 2. Dynamic Multidepot Vehicle Routing Problem

**2.1. The Description of DMDVRP.** In the real world, MDVRP is affected by the dynamic environment. With the wide application of information technology and Global Positioning System (GPS) technology, the process of logistics service can be tracked and adjusted in real time. Due to the development of these new technologies, the service mode of plan-execute is replaced by the dynamic execution task [21].

Generally speaking, the dynamic nature of DMVRP mainly reflects the uncertainty of customer requests in the

service process. Specifically, the type of request includes the uncertain quantity of goods [21–23] and the uncertain service time [24, 25]. This paper focuses on the change of service time and processing orders dynamically according to customer request time. A DMDVRP example is shown in Figure 1. In Figure 1(a), three different depots (red square) are responsible to serve the customers (black dots) which are allocated to them, and black and red lines represent initial routes. In Figure 1(b), some new customers (blue triangle) are added to system, and some new routes will be generated in time.

**2.2. The Formulation of DMDVRP.** The DMDVRP can be formalized as follows. An undirected graph  $G = (V, E)$  is established to describe mathematical model. In this model,  $V = \{V_C, V_D\}$  represents the vertex set and  $E = \{(v_i, v_j) \mid v_i, v_j \in V, i < j\}$  is the edge set.  $V_C = \{v_1, v_2, \dots, v_n\}$  is the set of customers and  $V_D = \{v_{n+1}, v_{n+2}, \dots, v_{n+m}\}$  is the set of depots. In  $E$ , we get distance matrix  $C = (c_{ij})$  by calculating the Euclidean distance of customers  $v_i$  and  $v_j$ . Every customer  $v_i$  has a demand  $q_i$  and needs to be visited once by only one vehicle. There is also a fleet of  $K$  identical vehicles, each with capacity  $Q$ .

In the mathematical formulation that follows, binary variable  $x_{ijk}$  is equal to 1 when vehicle  $k$  visits node  $j$  immediately after node  $i$ .

$$\text{Minimize} \quad \sum_{i=1}^{n+m} \sum_{j=1}^{n+m} \sum_{k=1}^K c_{ij} x_{ijk}, \quad (1)$$

subject to

$$\sum_{i=1}^{n+m} \sum_{k=1}^K x_{ijk} = 1 \quad (j = 1, 2, \dots, n); \quad (2)$$

$$\sum_{j=1}^{n+m} \sum_{k=1}^K x_{ijk} = 1 \quad (i = 1, 2, \dots, n); \quad (3)$$

$$\sum_{i=1}^{n+m} \sum_{j=1}^{n+m} q_i x_{ijk} \leq Q \quad (k = 1, 2, \dots, K); \quad (4)$$

$$\sum_{i=n+1}^{n+m} \sum_{j=1}^n x_{ijk} \leq 1 \quad (k = 1, 2, \dots, K); \quad (5)$$

$$\sum_{j=n+1}^{n+m} \sum_{i=1}^n x_{ijk} \leq 1 \quad (k = 1, 2, \dots, K). \quad (6)$$

The objective (1) minimizes the total cost. Constraints (2) and (3) guarantee that each customer is served by exactly one vehicle. Vehicle capacity constraint is found in (4). Finally, constraints (5) and (6) check vehicle availability.

**2.3. Measuring Dynamism.** In most papers, three popular metrics of *degree of dynamism* [16], *effective degree of dynamism*, and *effective degree of dynamism with TW* [22] are introduced to describe dynamism concretely. In this paper, the metric of *degree of dynamism (dod)* is selected



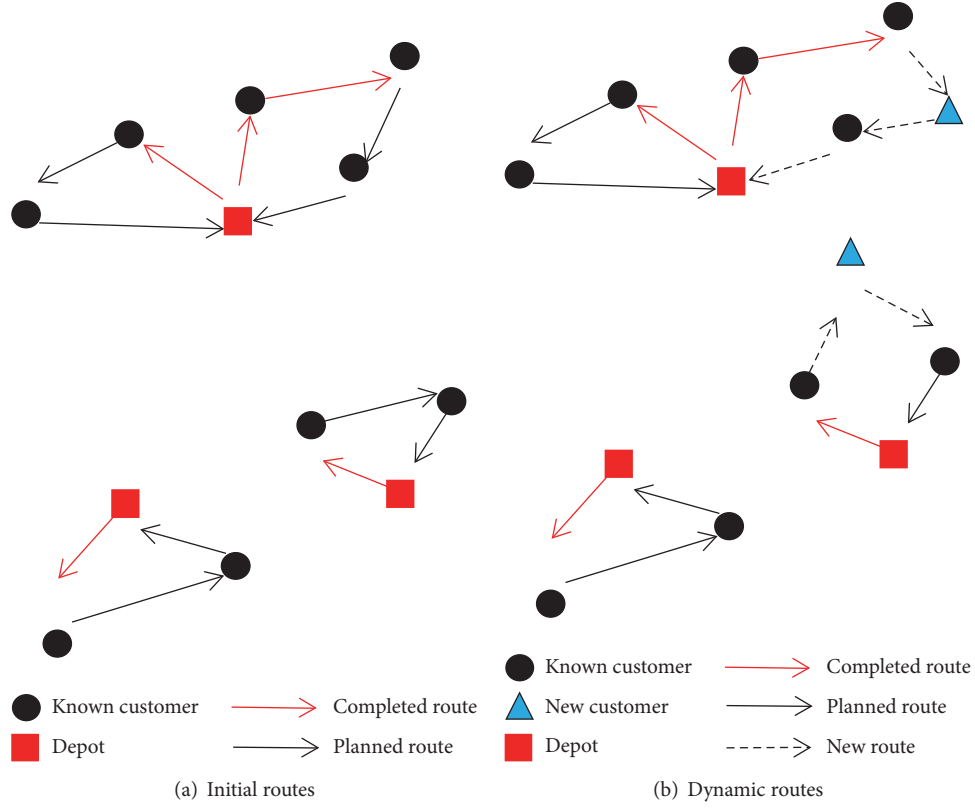


FIGURE 1: An example of DMDVRP with three depots.

to characterize the dynamical degree of DMDVRP, and the following is the calculation formula of *dod*. The range of *dod* is from 0 to 1 [16].

$$dod = \frac{\text{count of customers (known in advance)}}{\text{all customers}} \quad (7)$$

### 3. A Hybrid Ant Colony Algorithm for DMDVRP

**3.1. Hybrid Ant Colony Optimization.** By reviewing previous algorithms about solving VRP, we find that ant colony algorithm (ACO) is a common and effective algorithm. In this paper, the ant colony algorithm is improved by the nearest distance clustering, mutation operation, and 2-Opt algorithm to obtain better solutions. The flowchart of hybrid ant colony optimization (HACO) for the DMDVRP is shown in Figure 2. The details of HACO will be introduced in the following sections.

**3.2. The Nearest Distance Cluster Algorithm.** Generally, in order to serve customers preferably, the depots are usually placed at the locations which are as close to customers as possible. Therefore, the nearest distance cluster algorithm is proposed to exactly allocate each customer to its nearest depot. By the nearest distance cluster algorithm, a whole DMDVRP is divided into several little DVRPs; meanwhile the whole service area is divided into a set of little regions.

An example of the nearest distance cluster algorithm is in Figure 3; as shown, the black triangles are depots, and the different color points represent that customers are allocated to the nearest depot.

**3.3. Generate Initial Solutions.** In ACO, each ant represents a vehicle and visits all customers once. The complete routes that ants have passed are initial solutions. The ants will decide to select the next customer by formula (8).

$$p_{ij}(k) = \begin{cases} \frac{(\tau_{(i,j)})^\alpha \times (\eta_{(i,j)})^\beta}{\sum_{I \notin \text{tabu}} (\tau_{(i,I)})^\alpha \times (\eta_{(i,I)})^\beta} & j \notin \text{tabu}_k \\ 0 & \text{otherwise} \end{cases} \quad (8)$$

In formula (8),  $p_{ij}(k)$  is the probability of selecting  $j$  as the next customer of  $i$ .  $\tau_{(i,j)}$  and  $\alpha$  are the pheromone density of edge  $(i, j)$  and the relative influence of the pheromone trails, respectively.  $\eta_{(i,j)}$  and  $\beta$  are the visibility of edge  $(i, j)$  and the relative influence of the visibility values, respectively.  $\text{tabu}_k$  is a list, which stores the unvisited nodes for the  $k$ th ant [12].

#### 3.4. Optimization Operation

**3.4.1. Mutation Operation.** Mutation operation is derived from genetic algorithms (GA) primitively [23, 24], but it can be applied to fusing other optimization algorithms. For example, the optimization operation can help ACO

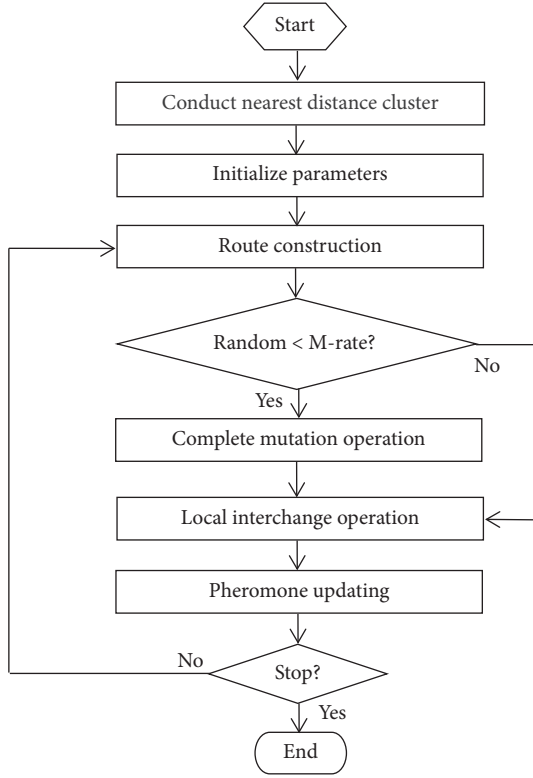


FIGURE 2: The flowchart of HACO.

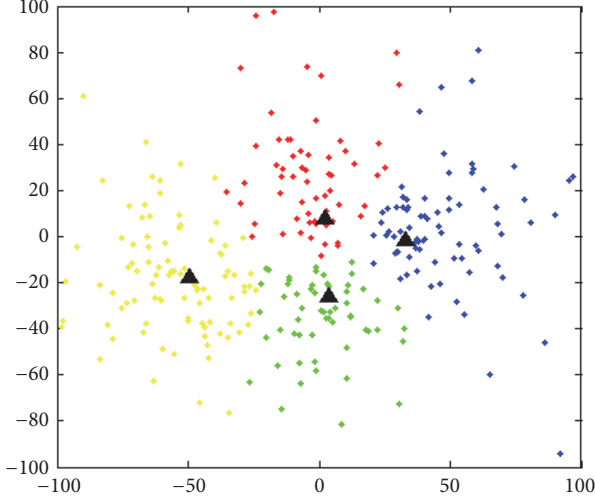


FIGURE 3: An example of the nearest distance cluster algorithm.

get further solutions in the period of searching. The most important step of mutation operation is to randomly select a solution and exchange customers by mutation probability  $P_m$ . Therefore, the operational process may produce new solutions and increase the likelihood of searching a better solution.

Generally,  $P_m$  has influence on the performance in the mutation. If  $P_m$  is so small it is not easy to produce the new individual. If  $P_m$  is so large the algorithm becomes a purely random search algorithm. Therefore, the adaptive method is

applied to change the mutation probability with the fitness. At the same time, considering the mutation coefficient  $k$ , it can also affect the performance of mutation.  $P_m$  and  $k$  can be determined according to the following formulas.

$$P_m = \begin{cases} P_{m1} - \frac{P_{m2}(f_m - f_{avg})}{f_{max} - f_{avg}}, & f_m \geq f_{avg} \\ P_{m1}, & f_m < f_{avg} \end{cases} \quad (9)$$

$$k = \begin{cases} k_1 + \frac{k_2(f_m - f_{avg})}{f_{max} - f_{avg}}, & f_m \geq f_{avg} \\ k_1 + k_2, & f_m < f_{avg} \end{cases} \quad (10)$$

where  $f_{max}$  is the largest fitness value,  $f_{avg}$  is average in groups, and  $f_m$  is the fit value for mutation.  $P_{m1}$ ,  $P_{m2}$ ,  $k_1$ , and  $k_2$  are initial variables [25].

In most GA, considering that biological gene mutation is a small probability event, the mutation rate is less than 0.1. However, in view of the aim of exploring greater search space, a mutation operation with a larger mutation rate is introduced to optimize route. Figure 4 is a demo of mutation operation process. The red line route and the black line route are serviced by two different vehicles. By exchanging 4 and 6, two new routes (1-3-2-6-1 and 1-4-5-1) are generated and have more appropriate arrangements.

**3.4.2. Local Interchange Operation.** In all local optimization algorithms, 2-Opt is a common and classical heuristic proposed by Croes [26] in 1958. The main idea is to try to choose a route and exchange two adjacent locations and calculate the results of new route. This operation may avoid local optimization and obtain a better route.

In this paper, the 2-Opt optimization is applied to improve the route. First, swapping the locations of all possible adjacent customers generates some new potential routes. Then we test each new route to see if this pair of exchanges can improve the quality of the route [27]. Finally, the best route will be selected to replace previous old route. Figure 5 is a demo of 2-Opt operation: (a) is the original route and (b) is the new route of implementing the operation of exchanging 2 and 7.

**3.5. Update of Pheromone Information.** In ACO, the most important step is the update of ant pheromones, which is key to obtain high quality solution. In order to ensure that each link has the same advantages, the following formula will be implemented to update pheromones:

$$\tau_{ij}^{new} = \rho \times \tau_{ij}^{old} + \sum_k \Delta \tau_{ij}^k \quad \rho \in (0, 1) \quad (11)$$

In formula (11),  $\tau_{ij}^{new}$  and  $\tau_{ij}^{old}$  are the new and initial pheromone concentration of link  $(i, j)$ , respectively,  $\rho$  is a constant and regulates the rate of evaporation,  $k$  is the number of all routes,  $K$  is the number of the routes in specific solution, and  $\Delta \tau_{ij}^k$  is the increased pheromone of link  $(i, j)$  in route  $k$ .

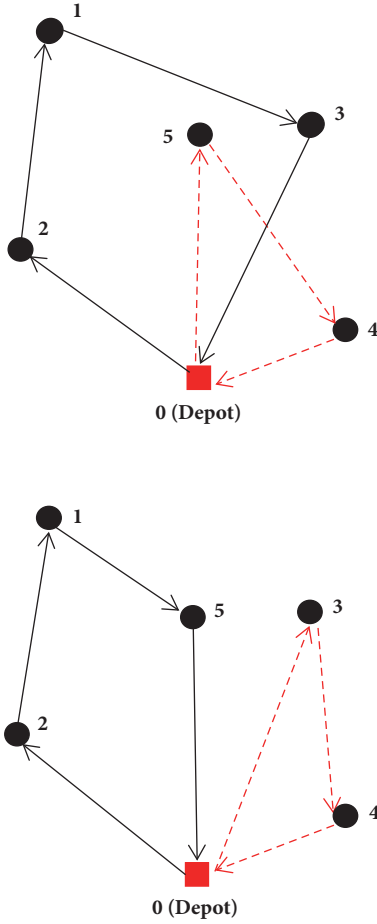


FIGURE 4: The example of mutation operation.

#### 4. A Real-Time Addition and Optimization Approach

In this section, a new real-time addition and optimization approach is applied to dynamically add new customer to known routes; meanwhile it can optimize the new generated route. The procedure of this approach is shown in Figure 6.

##### 4.1. The Strategy of Adding New Customers to Known Routes.

In the strategy of adding new customers to known routes, a working day is split into 24 same length time slices, and the customer requests are occurring in each time slice. The distances between each new customer and the serving customers or just finished serving customers are computed and compared, and the new customer will be added to the route which is the nearest to the new customer. If the new customer demands exceed the vehicle capacity, they will be handled by arranging another vehicle, and an extra route will be formed.

An example of this strategy is shown in Figure 7; as shown, some customers (black dots) have been known in advance. Red lines and black lines represent initial designed routes to serve known customers. As time goes on, new customers (blue triangle N1, N2, N3) are added to system,

and the distances between N1 and the serving or just finished serving customers (black dots 3, 5, 8) will be computed, respectively; then new customer (N1) is added to the nearest route (0-7-8-N1-9-0). Similarly, the new customers (N2, N3) are added to routes (0-1-2-3-N2-0, 0-4-5-N3-6-0), respectively. Although the new generated routes are not the best, the optimized operations will be conducted in the next section.

**4.2. Reoptimize Routes Dynamically.** Due to adding some new customers to initial routes, the routes need to be reoptimized dynamically. Each new route is divided into two subroutes, and the first subroute which has been served remains unchanged; meanwhile, the remaining part is optimized by mutation and 2-Opt in Section 3.4.

### 5. Experimental Results and Discussions

In this section, the performance of HACO algorithm solving for DMVVRP is evaluated strictly and completely. Through a series of experiments based on different data sets, the HACO will be analyzed by solution quality, running time, degrees of dynamism, and so on. The data sets are completely open and can be available at <http://neo.lcc.uma.es/vrp/vrp-instances/multiple-depot-vrp-instances/>. The detailed information of data sets is shown in Table 1. In this table, the numbers of depots, the numbers of customers, and the capacity are explained.

Table 2 shows that the parameters are used in HACO. The number of ants is 30; weight of pheromone is 2; weight of visibility is 1; evaporation rate of pheromone is 0.8; initial mutation rate is 0.8; number of iterations is 100. The algorithm implementation is based on the MATLAB (2010b) language, and the computer configuration is an Intel(R) Core (TM) i5-6500 3.19 GHz, 8 GB RAM running Windows 10(x64). All the results are averaged over 10 runs.

**5.1. Comparisons Based on Four Different ACO.** The comparisons of the solution quality in terms of the route length and running time among four proposed ACO algorithms are implemented in this section, and the four algorithms are ACO, MACO, LACO, and HACO, respectively. The ACO is from Montemanni et al. [28]; MACO and LACO are basic ACO fusing mutation operation and 2-Opt, respectively; modifying ACO with mutation operation and 2-Opt forms the final HACO. In addition, the scale of experimental data sets is between 80 and 288, and the degree of dynamism is 0.3. Table 3 gives the route length and running time of four algorithms. In this paper, the best solutions are in bold entries. From the comparisons, MACO, LACO, and HACO are 3.25%, 0.73%, and 10.9% less than the ACO, respectively. The results indicate that the mutation operation and 2-Opt can improve ACO effectively, and HACO is effective algorithm for solving DMVVRP.

This result may be attributed to the fact that the introduction of 2-Opt algorithm and mutation operation can improve the randomization and avoid falling into local search prematurely, and make HACO obtain better solutions.

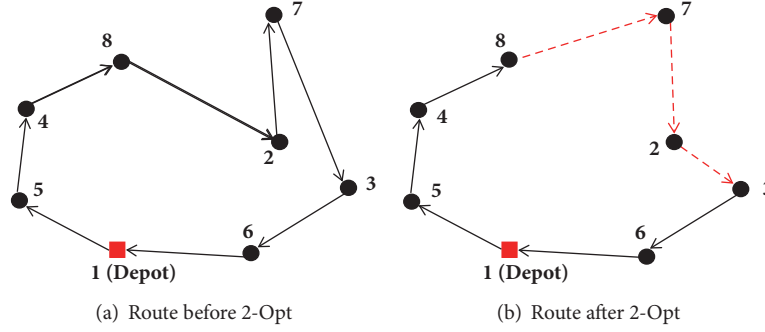


FIGURE 5: The demo of 2-Opt operation.

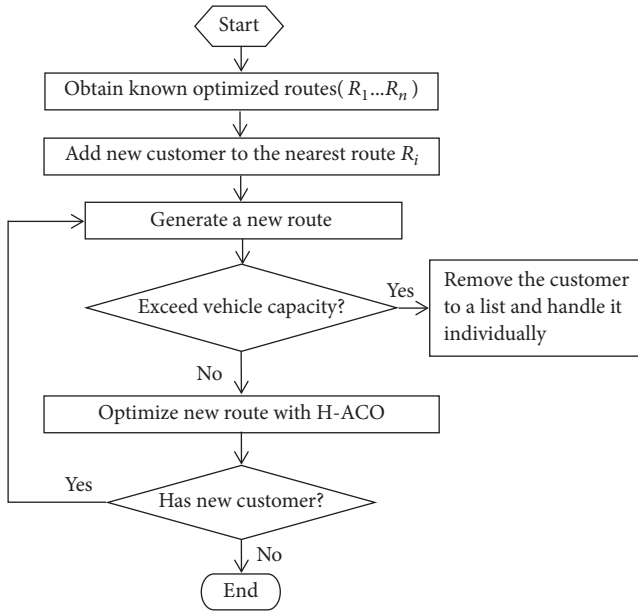


FIGURE 6: The flowchart of real-time addition and optimization approach.

TABLE 1: The detailed information of data sets.

Problem	Depots	Customers	Capacity
01	4	50	80
02	4	50	160
03	5	75	140
04	2	100	100
05	2	100	200
06	3	100	100
07	4	100	100
08	2	249	500
09	3	249	500
10	4	249	500
11	5	249	500
12	2	80	60
13	4	160	60
14	4	48	200
15	4	96	195
16	4	144	190
17	4	192	185
18	4	240	180
19	4	288	175

TABLE 2: HACO parameters settings.

Parameter	Description	Value
M	The number of Ants	30
$\alpha$	Weight of pheromone	2
$\beta$	Weight of visibility	1
$\rho$	Evaporation rate of pheromone	0.8
t	Initial Mutation rate	0.1
N	Number of iterations	100

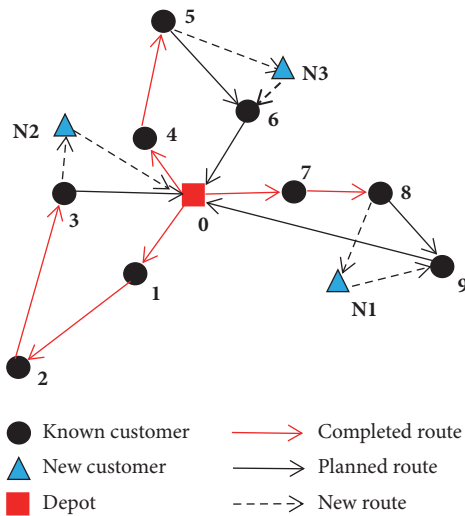


FIGURE 7: An example of the strategy of adding new customers to known routes.

In addition, a paired  $t$ -test is performed to investigate whether there are statistically significant differences between HACO and other improved ACO algorithms. Since it is expected that the solution quality of HACO is better than other ACO, a one-sided alternative hypothesis  $H_1$  is given below:

$$H_1 : \mu_{H-ACO} - \mu_{CA} < 0 \quad (12)$$

TABLE 3: Comparisons based on four different ACO.

Problem	ACO		MACO		LACO		HACO	
	Length	Time	Length	Time	Length	Time	Length	Time
01	833.06	35.27	839.46	52.27	932.75	46.47	<b>811.72</b>	60.45
02	716.17	26.55	718.64	42.57	729.37	26.83	<b>599.60</b>	46.62
03	1061.86	40.24	1105.81	77.84	1062.03	43.17	<b>1033.07</b>	89.86
04	1490.26	81.59	1570.71	154.06	1541.79	78.66	<b>1482.00</b>	158.92
05	1267.82	52.54	1323.36	115.64	1240.11	54.99	<b>1255.38</b>	130.16
06	1313.02	79.38	1279.35	124.45	1318.54	63.79	<b>1274.60</b>	137.51
07	1377.80	60.93	1328.30	109.80	1322.94	60.17	<b>1292.97</b>	123.60
08	8737.04	147.12	8264.29	525.99	8014.18	165.17	<b>7873.47</b>	599.77
09	6723.11	162.60	6616.01	416.62	6820.88	168.08	<b>6279.87</b>	453.87
10	6357.03	138.60	6344.92	343.92	6103.97	137.69	<b>6076.75</b>	384.96
11	6410.59	146.39	6262.12	343.00	6202.83	142.02	<b>6101.29</b>	366.24
12	1539.51	68.24	1533.00	120.76	1541.37	69.29	<b>1524.62</b>	106.05
13	3118.52	137.43	2979.31	242.30	3124.21	142.99	<b>3100.88</b>	214.50
14	1561.51	23.01	1399.14	35.12	1445.15	23.61	<b>1443.02</b>	39.38
15	2383.12	45.73	2109.31	85.79	2436.77	44.54	<b>2003.30</b>	98.77
16	3173.39	77.47	3295.31	148.20	3469.17	75.40	<b>3236.13</b>	165.18
17	3603.98	105.81	3724.63	237.49	3604.21	115.32	<b>3368.47</b>	242.12
18	4035.92	154.08	6493.59	246.79	6398.13	121.50	<b>3803.42</b>	357.06
19	8541.46	156.46	4972.95	446.51	6468.04	176.03	<b>4652.53</b>	449.91
Average	3381.32	91.55	3271.59	203.64	3356.65	92.40	<b>3011.21</b>	222.36
Increased by	0		3.25%		0.73%		10.9%%	

TABLE 4: Results of paired  $t$ -test based on route length.

Problem	HACO vs ACO	HACO vs MACO	HACO vs LACO
Mean Difference	-370.11	-260.37	-345.44
$p$ value	0.083	0.077	0.041

where  $\mu_{H-ACO}$  and  $\mu_{CA}$  are population mean for HACO and CA, respectively. CA refers to algorithm, which is compared with HACO. For example, if HACO is compared with MACO, the CA will refer to MACO.

Table 4 shows pairs, mean differences for instances, and  $p$  value at statistical level of  $\alpha = 0.1$ . The mean differences of HACO vs ACO, MACO, and LACO are -370.11, -260.37, and -345.44 with  $p$  value of 0.083, 0.077, and 0.041, respectively. This indicates that HACO is statistically significantly different from other ACO; meanwhile HACO fusing mutation and 2-Opt can explore more possibilities and search better solutions.

**5.2. Comparisons Based on Different Degrees of Dynamism.** In order to investigate the relation of degrees of dynamism ( $dod$ ) and HACO, the experiment based on different  $dod$  (0.3, 0.5, 0.7) is performed in this section. Table 5 gives the detailed routes length and running time of comparisons. In addition, we count the average value, number, and proportion of different  $dod$  in terms of the routes length and running time. When  $dod$  are 0.3, 0.5, and 0.7, the proportions of the best length are 78.95%, 5.26%, and 15.79%, respectively, and the proportions of the best time are 15.79%, 52.63%, and 31.58%, respectively. By the statistical data, the results reveal

that  $dod$  is directly proportional to routes length. However, the running time of  $dod$  (0.5 and 0.7) is less than that of  $dod$  (0.3). This illustrates that the proposed real-time addition and optimization approach can reduce algorithm running time, along with the increase of  $dod$ .

**5.3. The Analyses of Real-Time Addition and Optimization Approach.** In Table 6, the analyses of real-time addition and optimization approach are conducted, and the results are based on  $dod$  (0.3) in this section. In this table, the second, fourth, and fifth columns are the results of static routes length, additional extra routes length, and dynamic routes length, respectively; the third and sixth columns are static and dynamic running time; the seventh and eighth columns are the whole length and running time.

From the analyses of results based on average value, the average dynamic routes length is 2618.7, and it is 23.64% more than the average static routes length. Meanwhile, the average dynamic running time is 24.9 seconds, and it just accounts for 11.20% of the whole running time. These results reveal that the real-time addition and optimization approach can solve the DMDVRP efficiently. The strategy of adding new customers to the nearest known routes is feasible and efficient to solve dynamic problem.

TABLE 5: Comparisons based on different degrees of dynamism.

Problem	<i>dod</i> = 0.3		<i>dod</i> = 0.5		<i>dod</i> = 0.7	
	Length	Time	Length	Time	Length	Time
01	811.72	60.45	802.57	<b>49.81</b>	<b>783.52</b>	62.96
02	<b>599.60</b>	46.62	846.88	36.83	834.74	<b>27.80</b>
03	1033.07	89.86	1038.82	<b>67.68</b>	<b>1018.35</b>	78.12
04	<b>1482.00</b>	158.92	1523.84	149.00	1541.10	<b>95.22</b>
05	<b>1255.38</b>	130.16	1338.78	<b>100.67</b>	1718.58	183.34
06	<b>1274.60</b>	137.51	1378.00	<b>106.24</b>	1419.99	137.65
07	<b>1292.97</b>	123.60	1377.39	245.13	1467.39	<b>105.61</b>
08	7873.47	599.77	7251.37	300.56	<b>7090.63</b>	<b>145.94</b>
09	<b>6279.87</b>	453.87	6738.20	326.09	7358.75	<b>298.08</b>
10	<b>6076.75</b>	384.96	6713.71	<b>311.21</b>	7158.48	331.20
11	<b>6101.29</b>	366.24	6525.99	<b>329.49</b>	7711.66	417.96
12	1524.62	<b>106.05</b>	<b>1511.59</b>	128.06	1709.70	131.95
13	<b>3100.88</b>	<b>214.50</b>	3115.21	250.86	3407.92	270.14
14	<b>1443.02</b>	39.38	1487.92	27.40	2013.60	<b>25.92</b>
15	<b>2003.30</b>	98.77	2774.69	<b>73.84</b>	2640.64	86.81
16	<b>3236.13</b>	165.18	3576.19	<b>140.96</b>	3927.35	159.61
17	<b>3368.47</b>	<b>242.12</b>	4118.43	260.63	4419.52	290.03
18	<b>3803.42</b>	357.06	4457.53	<b>312.86</b>	5063.65	426.19
19	<b>4652.53</b>	449.91	5117.38	<b>425.45</b>	6069.40	619.00
Average	<b>3011.24</b>	220.78	3247.08	<b>191.72</b>	3545.00	204.92
Count	15	3	1	<b>10</b>	3	6
Proportion	<b>78.95%</b>	15.79%	5.26%	<b>52.63%</b>	15.79%	31.58%

TABLE 6: Results of real-time addition and optimization approach.

Problem	Len-S	Time-S	Len-E	Len-D	Time-D	All-Length	All-Time
01	530.36	50.96	152.18	659.54	9.49	811.72	60.45
02	402.51	40.93	67.48	532.11	5.69	599.60	46.62
03	1787.62	77.01	160.15	872.92	12.85	1033.07	89.86
04	1018.21	128.09	340.43	1141.57	30.82	1482.00	158.92
05	788.61	102.83	288.92	966.46	27.33	1255.38	130.16
06	880.39	117.87	249.77	1024.83	19.64	1274.60	137.51
07	846.64	108.18	230.12	1062.85	15.41	1292.97	123.60
08	5471.76	578.84	731.18	7142.29	20.93	7873.47	599.77
09	4161.98	425.35	964.16	5315.71	28.51	6279.87	453.87
10	3971.37	367.37	535.12	5541.63	17.59	6076.75	384.96
11	3914.98	335.17	883.43	5217.86	31.07	6101.29	366.24
12	1101.56	71.93	336.47	1188.15	34.12	1524.62	106.05
13	2193.00	145.49	654.49	2446.39	69.01	3100.88	214.50
14	627.68	34.95	204.10	1238.92	4.43	1443.02	39.38
15	1288.89	93.90	118.85	1884.45	4.87	2003.30	98.77
16	1726.21	150.22	251.35	2984.78	14.97	3236.13	165.18
17	2043.77	218.86	266.67	3101.80	23.26	3368.47	242.12
18	2470.63	299.59	818.56	2984.85	57.47	3803.42	357.06
19	2765.14	404.28	204.28	4448.24	45.64	4652.53	449.91
Average	1999.54	197.46	392.51	2618.70	24.90	3011.21	222.36



TABLE 7: Comparisons based on other two algorithms.

Problem	GA		PSO		HACO	
	Length	Time	Length	Time	Length	Time
01	<b>736.39</b>	61.11	788.56	68.51	811.72	60.45
02	<b>569.69</b>	56.96	598.73	60.50	599.60	46.62
03	931.87	97.18	<b>911.40</b>	101.09	1033.07	89.86
04	<b>1374.53</b>	126.36	1411.22	132.62	1482.00	158.92
05	1396.97	139.64	<b>1226.40</b>	144.05	1255.38	130.16
06	1544.30	126.95	1444.62	147.58	<b>1274.60</b>	137.51
07	1497.30	126.87	1475.88	146.60	<b>1292.97</b>	123.60
08	9253.53	447.36	7987.20	511.32	<b>7873.47</b>	599.77
09	8633.74	349.46	6940.90	387.90	<b>6279.87</b>	453.87
10	7088.22	348.61	6541.11	389.81	<b>6076.75</b>	384.96
11	6684.20	353.06	6686.50	382.13	<b>6101.29</b>	366.24
12	1616.50	134.80	<b>1493.42</b>	129.90	1524.62	106.05
13	4549.78	144.42	3720.01	146.55	<b>3100.88</b>	214.50
14	<b>1124.46</b>	35.76	1244.96	41.97	1443.02	39.38
15	2305.61	104.37	2107.53	111.19	<b>2003.30</b>	98.77
16	3549.58	151.35	3398.40	175.16	<b>3236.13</b>	165.18
17	3876.65	255.01	3651.31	274.10	<b>3368.47</b>	242.12
18	4270.49	371.66	4058.70	402.31	<b>3803.42</b>	357.06
19	5268.36	364.75	5486.40	396.60	<b>4652.53</b>	449.91
Average	3488.01	199.77	3219.64	218.42	<b>3011.21</b>	222.36
Count	4		3		<b>12</b>	
Proportion	21.05%		15.79%		<b>63.16%</b>	

**5.4. Comparisons Based on Other Two Algorithms.** In order to better evaluate the performance of the proposed HACO in terms of solution quality in minimizing travel distance, HACO is compared with previously published algorithms. These algorithms are Wang et al.'s [29] genetic algorithm (GA) and Yao et al.'s [30] particle swarm optimization (PSO), respectively.

Table 7 gives the best solution length and running time of this comparison and counts the number and proportion of the best length of each algorithm. From Table 6, the proposed HACO based on DMDVRP finds 12 new best solutions in the 19 problems, accounting for 63.16% of the best, while GA and PSO reach 4 and 3 best possible solutions, accounting for 21.05% and 15.79%, respectively. The results indicate that the HACO is effective algorithm for solving DMDVRP.

## 6. Conclusions

In the past few decades, few researchers focused on dynamic multidepot vehicle routing problem (DMDVRP). However, DMDVRP has wide application scenarios, so we have a research on DMDVRP. In order to improve the efficiency of ACO, we proposed a hybrid ant colony optimization algorithm (HACO) to solve DMDVRP. The HACO is based on fusion of ACO and the nearest distance cluster, meanwhile using mutation and 2-Opt to optimize routes further. In addition, a real-time addition and optimization approach is proposed to add customers and optimize routes dynamically.

In the experiments, the ACO, MACO, LACO, and HACO are compared directly. In order to demonstrate the efficiency of proposed algorithm, the *t*-test is applied to perform statistical analysis. But beyond that, the relations of HACO and degree of dynamism (*dod*) are analyzed by a number of tests based on different *dod*. With the aim of testing the performance of real-time addition and optimization approach, the comparisons of static routes quality and dynamic routes quality are conducted. Experimental results show that the HACO algorithm is feasible and efficient to solve DMDVRP.

## Data Availability

The initial data used to support the findings of this study have been deposited in the NEO repository (<http://neo.lcc.uma.es/vrp/vrp-instances/>). The data sets are valid and can be accessed.

## Conflicts of Interest

The authors declare that they have no conflicts of interest.

## Acknowledgments

This work was supported by Chinese National Natural Science Foundation (61572165) and Public Projects of Zhejiang Province (LGF18F030006).



## References

- [1] S. Lin and B. W. Kernighan, "An effective heuristic algorithm for the traveling-salesman problem," *Operations Research*, vol. 21, pp. 498–516, 1973.
- [2] J. W. Ohlmann and B. W. Thomas, "A compressed-annealing heuristic for the traveling salesman problem with time windows," *INFORMS Journal on Computing*, vol. 19, no. 1, pp. 80–90, 2007.
- [3] Z. Wang and C. Zhou, "A Three-Stage Saving-Based Heuristic for Vehicle Routing Problem with Time Windows and Stochastic Travel Times," *Discrete Dynamics in Nature and Society*, vol. 2016, Article ID 7841297, 2016.
- [4] M. A. Cruz-Chávez and A. Martínez-Oropeza, "Feasible Initial Population with Genetic Diversity for a Population-Based Algorithm Applied to the Vehicle Routing Problem with Time Windows," *Mathematical Problems in Engineering*, vol. 2016, Article ID 3851520, 11 pages, 2016.
- [5] C. Prodhon and C. Prins, *Metaheuristics for Vehicle Routing Problems*, Springer International Publishing, 2016.
- [6] J. Caceres-Cruz, P. Arias, D. Guimaran, D. Riera, and A. A. Juan, "Rich vehicle routing problem: Survey," *ACM Computing Surveys*, vol. 47, no. 2, article no. 32, 2014.
- [7] Y. Liu, I. H. Khalifa, and A. E. Kamel, "The multi-period and multi-depot dynamic vehicle routing problem with time windows," in *Proceedings of the 3rd IEEE International Conference on Logistics Operations Management, GOL 2016*, pp. 1–6, May 2016.
- [8] C.-T. Su, "Dynamic vehicle control and scheduling of a multi-depot physical distribution system," *Integrated Manufacturing Systems*, vol. 10, no. 1, pp. 56–65, 1999.
- [9] T. Huth and D. C. Mattfeld, "Dynamics of the Multi-Depot Pickup and Delivery Problem," 2007.
- [10] Y. Kuo and C. C. Wang, "Using Insertion Heuristic to Solve Dynamic Multi-Depot Vehicle Routing Problem," *Journal of Algorithms & Optimization*, 2014.
- [11] P. Toth and D. Vigo, *An Overview of Vehicle Routing Problems*, Society for Industrial and Applied Mathematics, 2002.
- [12] B. Yu, Z. Yang, and B. Yao, "An improved ant colony optimization for vehicle routing problem," *European Journal of Operational Research*, vol. 196, no. 1, pp. 171–176, 2009.
- [13] C.-H. Chen and C.-J. Ting, "An improved ant colony system algorithm for the vehicle routing problem," *Journal of the Chinese Institute of Engineers*, vol. 23, no. 2, pp. 115–126, 2006.
- [14] F. T. Hanshar and B. M. Ombuki-Berman, "Dynamic vehicle routing using genetic algorithms," *Applied Intelligence*, vol. 27, no. 1, pp. 89–99, 2007.
- [15] A. Cheng and D. Yu, "Genetic algorithm for vehicle routing problem," in *Proceedings of the 4th International Conference on Transportation Engineering, ICTE 2013*, pp. 2876–2881, Chengdu, China, October 2013.
- [16] A. M. F. M. AbdAllah, D. L. Essam, and R. A. Sarker, "On solving periodic re-optimization dynamic vehicle routing problems," *Applied Soft Computing*, vol. 55, pp. 1–12, 2017.
- [17] M. Okulewicz and J. Mandziuk, "Application of Particle Swarm Optimization Algorithm to Dynamic Vehicle Routing Problem," in *International Conference on Artificial Intelligence and Soft Computing*, pp. 547–558, 2013.
- [18] M. Dorigo, V. Maniezzo, and A. Coloni, "Ant system: optimization by a colony of cooperating agents," *IEEE Transactions on Systems, Man, and Cybernetics, Part B: Cybernetics*, vol. 26, no. 1, pp. 29–41, 1996.
- [19] M. Dorigo and C. Blum, "Ant colony optimization theory: a survey," *Theoretical Computer Science*, vol. 344, no. 2–3, pp. 243–278, 2005.
- [20] E. Bonabeau, M. Dorigo, and G. Theraulaz, "Inspiration for optimization from social insect behaviour," *Nature*, vol. 406, no. 6791, pp. 39–42, 2000.
- [21] V. Pillac, M. Gendreau, C. Guéret, and A. L. Medaglia, "A review of dynamic vehicle routing problems," *European Journal of Operational Research*, vol. 225, no. 1, pp. 1–11, 2013.
- [22] A. Larsen, *The Dynamic Vehicle Routing Problem*, Technical University of Denmark, 2001.
- [23] A. Attanasio, J.-F. Cordeau, G. Ghiani, and G. Laporte, "Parallel Tabu search heuristics for the dynamic multi-vehicle dial-a-ride problem," *Parallel Computing*, vol. 30, no. 3, pp. 377–387, 2004.
- [24] A. Goel and V. Gruhn, "A general vehicle routing problem," *European Journal of Operational Research*, vol. 191, no. 3, pp. 650–660, 2008.
- [25] C.-Y. Liu, "An improved adaptive genetic algorithm for the multi-depot vehicle routing problem with time window," *Journal of Networks*, vol. 8, no. 5, pp. 1035–1042, 2013.
- [26] G. A. Croes, "A method for solving traveling-salesman problems," *Operations Research*, vol. 6, pp. 791–812, 1958.
- [27] T. Vidal, M. Battarra, A. Subramanian, and G. Erdoğan, "Hybrid metaheuristics for the Clustered Vehicle Routing Problem," *Computers & Operations Research*, vol. 58, pp. 87–99, 2015.
- [28] R. Montemanni, L. M. Gambardella, A. E. Rizzoli, and A. V. Donati, "A new algorithm for a Dynamic Vehicle Routing Problem based on Ant Colony System," in *Proceedings of the Second International Workshop on Freight Transportation Logistics*, pp. 27–30, 2003.
- [29] S. Wang, Z. Lu, L. Wei, G. Ji, and J. Yang, "Fitness-scaling adaptive genetic algorithm with local search for solving the Multiple Depot Vehicle Routing Problem," *Simulation*, vol. 92, no. 7, pp. 601–616, 2016.
- [30] B. Z. Yao, B. Yu, J. J. Gao, and M. H. Zhang, "An improved particle swarm optimization for carton heterogeneous vehicle routing problem with a collection depot," *Annals of Operations Research*, vol. 242, pp. 303–320, 2016.

## Research Article

# Laplace Transform Method for Pricing American CEV Strangles Option with Two Free Boundaries

Zhiqiang Zhou  and Hongying Wu

*School of Mathematics and Finance, Xiangnan University, Chenzhou 423000, China*

Correspondence should be addressed to Zhiqiang Zhou; [zqzhou@2014.swufe.edu.cn](mailto:zqzhou@2014.swufe.edu.cn)

Received 24 March 2018; Accepted 13 August 2018; Published 4 September 2018

Academic Editor: Jorge E. Macias-Diaz

Copyright © 2018 Zhiqiang Zhou and Hongying Wu. This is an open access article distributed under the Creative Commons Attribution License, which permits unrestricted use, distribution, and reproduction in any medium, provided the original work is properly cited.

Laplace transform method (LTM) has a lot of applications in the evaluation of European-style options and exotic options without early exercise features. However the Laplace transform methods for pricing American options have unsatisfactory accuracy and suffer from the instability. The aim of this paper is to develop a Laplace transform method for pricing American Strangles options with the underlying asset price following the constant elasticity volatility (CEV) models. By approximating the free boundaries, the Laplace transform is taken on a fixed space region to replace the moving boundaries space. After solving the linear system in Laplace space, Gaver-Stehfest formula (GSF) and hyperbola contour integral method (HCIM) are applied to compute the Laplace inversion. Numerical results show that the LTM-HCIM outperform the LTM-GSF in regard to the accuracy and stability for the option values.

## 1. Introduction

The Laplace transform methods for option pricing originate from the idea of randomizing the maturity in [1]. The Laplace transform methods are applied in the pricing options without early exercise features: Pelsser [2] for pricing double barrier options, Davydov and Linetsky [3] for pricing and hedging path dependent options under constant elasticity of variance (CEV) models, Sepp [4] for pricing double barrier options under double-exponential jump diffusion models, Cai and Kou [5] for pricing European options under mixed-exponential jump diffusion models, and Cai and Kou [6] for pricing Asian options under hyperexponential jump diffusion models.

This technique is known to work well for options without early exercise features, but, for American-style options, one difficulty has been perceived that the Black-Scholes-Merton PDE only holds where it is optimal to retain the option. Mallier and Alobaidi [7] develop a partial Laplace transform method for pricing American options in which the location of the free boundary for all values of the transform variable has to be determined by solving nonlinear integral equations. The approach is only conceptually appealing but practically ineffective in numerical implementations as for each transform

variable one has to solve the nonlinear integral equations. In fact Mallier and Alobaidi [7] do not give the numerical computations.

A simple framework for Laplace transform methods is introduced by Zhu [8] for pricing American options under GBM models. This framework is later developed for evaluation of finite-lived Russian options by Kimura [9], pricing American options under CEV models by Wong and Zhao [10] and by Pun and Wong [11], pricing American options under hyperexponential jump-diffusion model by Leippold and Vasiljević [12], pricing stock loan (essentially an American option with time-dependent strike) by Lu and Putri [13], and pricing American options with regime switching by Ma et al. [14]. But this framework suffers from a drawback that numerical Laplace inversion such as Gaver-Stehfest (GS) and Gaver-Wynn-Rho (GWR) algorithm are not stable. Pun and Wong [11] explain the complex calculation of special functions as one of the possible reasons causing instability.

Zhou et al. [15] develop a new Laplace transform method for solving the free-boundary fractional diffusion equations arising in the American option pricing. By approximating the free boundary, the Laplace transform is taken on a fixed space region to replace the moving boundaries space. Then the

hyperbola contour integral method is exploited to restore the option values. The coefficient matrix has theoretically proven to be sectorial. Therefore, the highly accurate approximation and computational stability of the fast Laplace transform method are guaranteed.

In this paper, we develop the new Laplace transform method for solving American Strangles option pricing under CEV model. The Black-Scholes-Merton PDE of Strangles option is defined on the moving region  $[S_p(\tau), S_c(\tau)]$ , where  $S_p(\tau)$  is put side and  $S_c(\tau)$  is call side. The idea of the new method is modifying PDE into a new form on certain fixed region  $[\underline{S}_p, \bar{S}_c]$ . Then performing the Laplace transform leads to a ODE which involves the inverse functions  $\tau_p(S)$  and  $\tau_c(S)$  of  $S_p(\tau)$  and  $S_c(\tau)$ , respectively. Using the finite difference method combined with the approximation of functions  $\tau_p(S)$  and  $\tau_c(S)$ , where the optimal parameters of the approximation are obtained by minimizing the prescribed residual error, we obtain the numerical solution of the ODE in the Laplace space. In the final step, both the inversion Laplace Gaver-Stehfest formula (GSF) and the hyperbola contour integral method (HCIM) are used to recover the option value and the free boundary.

Numerical examples show the inverse Laplace GSF is unstable if the number of discrete integral nodes is great than 20, so HCIM is an effective algorithm for computing Laplace inversion. However, the technics of spectral analysis in [15] cannot be applied over here, because the coefficients of PDEs arising from CEV Strangles option are not constant. This paper gives a convergence theorem by analysing the so-called Laplace transform iteration algorithm.

The remaining parts of this paper are arranged as follows: In Section 2, we develop the Laplace transform method for pricing American CEV Strangles option; in Section 3, we discuss the hyperbola contour integral method to compute inverse Laplace and give some stable conditions for HCIM. In Section 4, some examples are taken to conform the theoretical results of HCIM. Conclusions are given in the final section.

## 2. Evaluation of American Strangles under CEV Model

Assume that the underlying asset price is governed by CEV (see, e.g., [16]):

$$dS_t = (r - q) S_t dt + \delta S_t^{\beta+1} dW_t, \quad (1)$$

where  $r > 0$  is the risk-free interest rate,  $q \geq 0$  is the dividend yield, and  $W_t$  is standard Brownian motion.  $\sigma(S) = \delta S^\beta$  represents the local volatility function and  $\beta$  can be interpreted as the elasticity of  $\sigma(S)$ .  $\delta$  is the scale parameter fixing the initial instantaneous volatility at time  $t = 0$ , i.e.,  $\delta = \sigma(S_0)/S_0^\beta := \sigma_0/S_0^\beta$ . If  $\beta = 0$ , the SDE (1) becomes the standard log-normal diffusion model or so-called geometric Brownian motion models (GBM). If  $\beta = -1/2$ , the SDE (1) nests the Cox-Ingersoll-Ross (CIR) model.

Let

$$f(S, t) = \sup_{\tau \in \mathcal{T}_{0,T}} E \left[ e^{-r(\tau-t)} \Pi(S_\tau) \mid S_t = S \right] \quad (2)$$

be the price of an American Strangles position written on an underlying asset with price  $S$  at time  $t$  and the payoff

$$\Pi(S_\tau) = \max(K_1 - S_\tau, 0) + \max(S_\tau - K_2, 0). \quad (3)$$

This position is formed using a long put with strike  $K_1$  and a long call with strike  $K_2$ . Note that  $K_1 < K_2$ . Let  $\tau = T - t$ ,  $v(S, \tau) = f(S, T - t)$ , and the early exercise boundary on the put side be denoted by  $S_p(\tau)$ , and the early exercise boundary on the call side be denoted by  $S_c(\tau)$ . It is known that  $v(S, \tau)$  satisfies the Black-Scholes PDE:

$$\frac{\partial v}{\partial \tau} = \frac{1}{2} \delta^2 S^{2\beta+2} \frac{\partial^2 v}{\partial S^2} + (r - q) S \frac{\partial v}{\partial S} - r v, \quad (4)$$

$$S_p(\tau) < S < S_c(\tau)$$

with initial condition

$$v(S, 0) = \max(K_1 - S, 0) + \max(S - K_2, 0), \quad (5)$$

$$S_p(0) < S < S_c(0)$$

and free boundary conditions

$$v(S, \tau) = K_1 - S, \quad (6)$$

$$\frac{\partial}{\partial S} v(S, \tau) = -1,$$

$$S \geq S_p(\tau),$$

$$v(S, \tau) = S - K_2, \quad (7)$$

$$\frac{\partial}{\partial S} v(S, \tau) = 1,$$

$$S \leq S_c(\tau).$$

Chiarella and Ziogas [17] apply Fourier transform technique to derive a coupled integral equation system for the Strangles free boundaries, and then a numerical algorithm is provided to solve this system.

To establish the new Laplace transform method proposed by Zhou et al. [15], we first note some properties of early exercise boundary for American Strangle option under the CEV model (1). It is known from [18–20] that the free-boundary functions  $S_p(\tau)$  and  $S_c(\tau)$  of American Strangles are continuously differentiable on the interval  $[0, +\infty)$ . We call the fact that  $S_p(\tau)$  is a decreasing function of variable  $\tau$ , while  $S_c(\tau)$  is an increasing function of variable  $\tau$ . Denote

$$\begin{aligned} \underline{S}_p &= S_p(\infty), \\ \bar{S}_p &= S_p(0), \\ \underline{S}_c &= S_c(0), \\ \bar{S}_c &= S_c(\infty), \end{aligned} \quad (8)$$

Then we know

$$\begin{aligned} \bar{S}_p &= \min \left( K_1, \frac{r}{q} K_1 \right), \\ \underline{S}_c &= \max \left( K_2, \frac{r}{q} K_2 \right), \end{aligned} \quad (9)$$

```

1: Step 1. Let  $L_1 = 1, H_1 = j_1, L_2 = j_2, H_2 = N - 1$ .
2: Step 2. Do the following loop:
3: while  $L_1 < H_1 - 1$  or  $L_2 < H_2 - 1$  do
4:   Let  $k_1 = \text{floor}[0.5 * (L_1 + H_1)]$  and  $k_2 = \text{floor}[0.5 * (L_2 + H_2)]$ .
5:   Solve linear system (13) with boundary  $v_{k_1} = K_1 - S_{k_1}$  and  $v_{k_2} = S_{k_2} - K_2$ .
6:   % Finite difference approximation (6).
7:   if  $\frac{v_{k_1+1} - v_{k_1}}{\Delta S} < -1$  then
8:      $L_1 = k_1$ ;
9:   else
10:     $H_1 = k_1$ ;
11:   end if
12:   % Finite difference approximation (7).
13:   if  $\frac{v_{k_2} - v_{k_2-1}}{\Delta S} < 1$  then
14:      $L_2 = k_2$ ;
15:   else
16:     $H_2 = k_2$ .
17:   end if
18: end while
19: Step 3. Output  $\underline{S}_p = S_{k_1}$  and  $\bar{S}_c = S_{k_2}$ .

```

ALGORITHM 1: Algorithm for solving  $\underline{S}_p$  and  $\bar{S}_c$ .

$\underline{S}_p > 0, \bar{S}_c < \infty$  and  $v^\infty(S) = v(S, \infty)$  satisfy the following ODE (similar to perpetual American option):

$$\frac{1}{2} \delta^2 S^{2\beta+2} \frac{d^2 v^\infty}{dS^2} + (r - q) S \frac{dv^\infty}{dS} - r v^\infty = 0, \quad (10)$$

$$\underline{S}_p < S < \bar{S}_c,$$

$$\begin{aligned} v^\infty(\underline{S}_p) &= K_1 - \underline{S}_p, \\ \frac{d}{dS} v^\infty(\underline{S}_p) &= -1, \\ v^\infty(\bar{S}_c) &= \bar{S}_c - K_2, \\ \frac{d}{dS} v^\infty(\bar{S}_c) &= 1. \end{aligned} \quad (11)$$

$$(12)$$

The values of  $\underline{S}_p$  and  $\bar{S}_c$  could be computed by secant method. Define uniform mesh  $S_j = j\Delta S$ ,  $j = 0, 1, \dots, N$  and take larger enough number  $S_{max} = S_N$  such that  $S_{max} > \bar{S}_c$ . The discrete form of (10) is as follows:

$$\begin{aligned} \left( \frac{\delta^2 S_j^{2\beta+2}}{2(\Delta S)^2} - \frac{(r-q)S_j}{2\Delta S} \right) v_{j-1} - \left( \frac{\delta^2 S_j^{2\beta+2}}{(\Delta S)^2} + r \right) v_j \\ + \left( \frac{\delta^2 S_j^{2\beta+2}}{2(\Delta S)^2} + \frac{(r-q)S_j}{2\Delta S} \right) v_{j+1} = 0. \end{aligned} \quad (13)$$

for  $j = 1, 2, \dots, N-1$  with  $v_j = v^\infty(S_j)$ . Assuming  $\bar{S}_p = S_{j_1}$  and  $\underline{S}_c = S_{j_2}$ , we have the pseudocode as Algorithm 1.

**Theorem 1.** With the same initial condition (5) and boundary conditions (6)-(7), the PDE (4) is equivalent to the following PDE:

$$\begin{aligned} \frac{\partial v}{\partial \tau} = \frac{1}{2} \delta^2 S^{2\beta+2} \frac{\partial^2 v}{\partial S^2} + (r-q) S \frac{\partial v}{\partial S} - r v \\ + (rK_1 - qS) \mathbf{1}_{\{S \leq \underline{S}_p(\tau)\}} - (rK_2 - qS) \mathbf{1}_{\{S \geq \bar{S}_c(\tau)\}}. \end{aligned} \quad (14)$$

for  $\tau \in (0, +\infty)$  and  $S \in (\underline{S}_p, \bar{S}_c)$ , where  $\mathbf{1}_{\{\cdot\}}$  is the indicator function.

*Proof.* (i) On the region  $\tau \in (0, \infty)$ ,  $S \in (0, \underline{S}_p(\tau))$ , we know from the boundary condition (6) that  $v(S, \tau) = K_1 - S$ . Direct calculation shows that  $v(S, \tau) = K_1 - S$  satisfies (14). (ii) On the region  $\tau \in (0, \infty)$ ,  $S \in (\underline{S}_p(\tau), \bar{S}_c(\tau))$ , both (4) and (14) have the same forms. (iii) On the region  $\tau \in (0, \infty)$ ,  $S \in (\bar{S}_c(\tau), \infty)$ , we know from the boundary condition (7) that  $v(S, \tau) = S - K_2$ . Direct calculation shows that  $v(S, \tau) = S - K_2$  satisfies (14). Combining (i), (ii), and (iii), we get this theorem.  $\square$

Let  $\tau_p(S)$  and  $\tau_c(S)$  be the inverse functions of  $S_p(\tau)$  and  $S_c(\tau)$ , respectively. Taking Laplace transform

$$[\mathcal{L}v(\tau)](z) := \int_0^\infty e^{-z\tau} v(\tau) d\tau, \quad (15)$$

$$\begin{aligned} \mathcal{L}[\mathbf{1}_{\{S \leq \underline{S}_p(\tau)\}}] &= \int_0^{+\infty} e^{-z\tau} \mathbf{1}_{\{S \leq \underline{S}_p(\tau)\}} d\tau \\ &= \int_0^{+\infty} e^{-z\tau} \mathbf{1}_{\{\tau \leq \tau_p(S)\}} d\tau = \int_0^{\tau_p(S)} e^{-z\tau} d\tau \quad (16) \\ &= -\frac{1}{z} e^{-z\tau} \Big|_0^{\tau_p(S)} = \frac{1}{z} (1 - e^{-z\tau_p(S)}), \end{aligned}$$

and

$$\mathcal{L} \left[ \mathbf{1}_{\{S \geq S_c(\tau)\}} \right] = \frac{1}{z} \left( 1 - e^{-z\tau_c(S)} \right), \quad (17)$$

to the both sides of (14), we get

$$\begin{aligned} z\hat{v} &= \frac{1}{2} \delta^2 S^{2\beta+2} \frac{\partial^2 \hat{v}}{\partial S^2} + (r-q) S \frac{\partial \hat{v}}{\partial S} - r\hat{v} \\ &\quad + \max(K_1 - S, 0) + \max(S - K_2, 0) \\ &\quad + (rK_1 - qS) \frac{1}{z} \left( 1 - e^{-z\tau_p(S)} \right) \\ &\quad - (rK_2 - qS) \frac{1}{z} \left( 1 - e^{-z\tau_c(S)} \right) \end{aligned} \quad (18)$$

on fixed space region  $S \in (\underline{S}_p, \bar{S}_c)$ . The initial free boundary conditions (6) and (7) become the following forms:

$$\hat{v}(\underline{S}_p, z) = \frac{1}{z} (K_1 - \underline{S}_p), \quad (19)$$

$$\frac{\partial}{\partial S} \hat{v}(\underline{S}_p, z) = -\frac{1}{z},$$

$$\hat{v}(\bar{S}_c, z) = \frac{1}{z} (\bar{S}_c - K_2), \quad (20)$$

$$\frac{\partial}{\partial S} \hat{v}(\bar{S}_c, z) = \frac{1}{z}.$$

Now, the free boundaries  $\tau_p(S)$  and  $\tau_c(S)$  can be approximated. To this end, we give the fit functions with unknown parameters  $p_i, \alpha_i$  for  $i = 1, 2$ :

$$\begin{aligned} \tau_p(S) &\approx \tau_p(S; p_1, \alpha_1) \\ &= \begin{cases} 0, & S \geq \bar{S}_p, \\ p_1 \left( -\log \frac{S - \underline{S}_p}{\bar{S}_p - \underline{S}_p} \right)^{\alpha_1}, & \underline{S}_p < S < \bar{S}_p, \\ +\infty, & S = \underline{S}_p, \end{cases} \end{aligned} \quad (21)$$

$$\begin{aligned} \tau_c(S) &\approx \tau_c(S; p_2, \alpha_2) \\ &= \begin{cases} +\infty, & S \geq \bar{S}_c, \\ p_2 \left( -\log \frac{\bar{S}_c - S}{\bar{S}_c - \underline{S}_c} \right)^{\alpha_2}, & \underline{S}_c < S < \bar{S}_c, \\ 0, & S = \underline{S}_c. \end{cases} \end{aligned} \quad (22)$$

Redefine uniform mesh  $S_j = \underline{S}_p + j\Delta S$ ,  $j = 0, 1, \dots, n+1$  with  $\Delta S = (\bar{S}_c - \underline{S}_p)/(n+1)$ . Equations (18) can be discretized as follows:

$$(z\mathbf{I} - \mathbf{A}) \hat{\mathbf{v}}^n(z) = \mathbf{g}(z), \quad (23)$$

with index  $n$  representing the number of space mesh partition. Matrix  $\mathbf{A}$ , solution vector  $\hat{\mathbf{v}}^n(z)$ , and RHS vector  $\mathbf{g}(z)$  are defined as

$$\mathbf{A}(z) = \begin{bmatrix} b_1 & c_1 & 0 & \cdots & 0 & 0 \\ a_2 & b_2 & c_2 & \cdots & 0 & 0 \\ 0 & a_3 & b_3 & \ddots & 0 & 0 \\ \vdots & \ddots & \ddots & \ddots & \ddots & \vdots \\ 0 & 0 & 0 & \ddots & b_{n-1} & c_{n-1} \\ 0 & 0 & 0 & \cdots & a_n & b_n \end{bmatrix}_{n \times n}, \quad (24)$$

$$\begin{aligned} a_j &= \frac{\delta^2 S_j^{2\beta+2}}{2(\Delta S)^2} - \frac{(r-q)S_j}{2\Delta S}, \\ b_j &= -\frac{\delta^2 S_j^{2\beta+2}}{(\Delta S)^2} - r, \end{aligned} \quad (25)$$

$$c_j = \frac{\delta^2 S_j^{2\beta+2}}{2(\Delta S)^2} + \frac{(r-q)S_j}{2\Delta S}, \quad (26)$$

$$\hat{\mathbf{v}}^n(z) = [\hat{v}^n(S_1, z), \hat{v}^n(S_2, z), \dots, \hat{v}^n(S_n, z)]^T, \quad (27)$$

$$\mathbf{g}(z; p_1, p_2, \alpha_1, \alpha_2) = [g_1, \dots, g_n]^T, \quad (28)$$

where

$$g_1 = a_1 (K_1 - \underline{S}_p), \quad (29)$$

$$\begin{aligned} g_j &= \max(K_1 - S_j, 0) + \max(S_j - K_2, 0) \\ &\quad + \frac{1}{z} (rK_1 - qS_j) \left( 1 - e^{-z\tau_p(S_j; p_1, \alpha_1)} \right) \\ &\quad - \frac{1}{z} (rK_2 - qS_j) \left( 1 - e^{-z\tau_c(S_j; p_2, \alpha_2)} \right), \end{aligned} \quad (j = 2, \dots, n-1)$$

$$g_n = c_n (\bar{S}_c - K_2). \quad (30)$$

Denote  $\mathbf{a}_1(z)$  and  $\mathbf{a}_n(z)$  to be the first row and the  $n^{th}$  row of  $(z\mathbf{I} - \mathbf{A})^{-1}(z)$ , respectively.  $\mathbf{a}_1(z)$  and  $\mathbf{a}_n(z)$  can be obtained by solving linear equation:

$$\mathbf{a}_1(z) (z\mathbf{I} - \mathbf{A}) = [1, 0, 0, \dots, 0], \quad (31)$$

$$\mathbf{a}_n(z) (z\mathbf{I} - \mathbf{A}) = [0, 0, \dots, 0, 1]. \quad (32)$$

Then, we reach the expressions

$$\begin{aligned} \hat{v}(S_1, z) &= \mathbf{a}_1(z) \mathbf{g}(z; p_1, p_2, \alpha_1, \alpha_2), \\ \hat{v}(S_n, z) &= \mathbf{a}_n(z) \mathbf{g}(z; p_1, p_2, \alpha_1, \alpha_2). \end{aligned} \quad (33)$$

We find the parameters  $p_i, \alpha_i$  ( $i = 1, 2$ ) such that conditions (19) and (20) hold for all real values of  $z > 0$ . A practicable way is to consider a positive sequence  $\{z_1, z_2, \dots, z_m\}$  which are used for numerical Laplace inversion and find the values



**Step 1.** Use Algorithm 1 to compute  $\underline{S}_p$  and  $\bar{S}_c$ .  
**Step 2.** Compute  $\tau_p(S)$  and  $\tau_c(S)$  by optimizing (34).  
**Step 3.** Solve the linear system (23) to get  $\hat{\mathbf{v}}^n(z)$ .  
**Step 4.** Apply Laplace inversion GSF or HCIM to restore American Strangles option value  $\mathbf{v}^n(\tau)$ .

ALGORITHM 2: NLTM algorithm for pricing American Strangles.

of unknown  $p_i$  and  $\alpha_i$  that optimizing the following objective function:

$$\begin{aligned} \min_{p_1, p_2, \alpha_1, \alpha_2 \geq 0} F(p_1, p_2, \alpha_1, \alpha_2) \\ = \sum_{i=1}^m E_1(i; p_1, p_2, \alpha_1, \alpha_2) + \sum_{i=1}^m E_2(i; p_1, p_2, \alpha_1, \alpha_2) \end{aligned} \quad (34)$$

with

$$\begin{aligned} E_1(i; p_1, p_2, \alpha_1, \alpha_2) &= \left( \frac{\hat{v}(S_1, z_i) - \hat{v}(S_0, z_i)}{\Delta S} \right. \\ &\quad \left. - \frac{\partial}{\partial S} \hat{v}(S_0, z_i) \right)^2 \\ &= \left[ \frac{\mathbf{a}_1(z_i) \mathbf{g}(z_i; p_1, p_2, \alpha_1, \alpha_2) - (1/z_i)(K_1 - \underline{S}_p)}{\Delta S} \right. \\ &\quad \left. + \frac{1}{z_i} \right]^2, \end{aligned} \quad (35)$$

$$\begin{aligned} E_2(i; p_1, p_2, \alpha_1, \alpha_2) &= \left( \frac{\hat{v}(S_{n+1}, z_i) - \hat{v}(S_n, z_i)}{\Delta S} \right. \\ &\quad \left. - \frac{\partial}{\partial S} \hat{v}(S_{n+1}, z_i) \right)^2 \\ &= \left[ \frac{(1/z_i)(\bar{S}_c - K_2) - \mathbf{a}_n(z_i) \mathbf{g}(z_i; p_1, p_2, \alpha_1, \alpha_2)}{\Delta S} \right. \\ &\quad \left. - \frac{1}{z_i} \right]^2. \end{aligned} \quad (36)$$

After determining  $\tau_p(S)$  and  $\tau_c(S)$  we can compute  $\hat{\mathbf{v}}^n(z)$  by solving linear system (23), and the value of American Strangles can be expressed in terms of the inverse Laplace transforms

$$\mathbf{v}^n(S_j, \tau) = \mathcal{L}^{-1}[\hat{\mathbf{v}}^n(S_j, z)], \quad j = 1, 2, \dots, n. \quad (37)$$

Applying polynomial interpolations, we can obtain the option value  $\mathbf{v}(S, \tau)$  for any values  $S \in (0, \infty)$ . Moreover, the vector version of inverse Laplace can be formulated as

$$\mathbf{v}^n(\tau) = \mathcal{L}^{-1}[\hat{\mathbf{v}}^n(z)]. \quad (38)$$

One of the classical numerical Laplace inversion is the Gaver-Stehfest formula (GSF) (see [21, 22]):

$$\mathbf{v}^n(\tau) \approx \mathbf{v}^{n,L}(\tau) = \frac{\ln 2}{\tau} \sum_{k=1}^L C_k^{(L)} \hat{\mathbf{v}}^n\left(\frac{k \ln 2}{\tau}\right), \quad (39)$$

where

$$C_k^{(L)} = (-1)^{k+L/2} \cdot \sum_{j=\lceil (k+1)/2 \rceil}^{\min[k, L/2]} \frac{j^{L/2} (2j)!}{(L/2 - j)! j! (j-1)! (k-j)! (2j-k)!} \quad (40)$$

with  $L$  being taken as an even positive integer. Another effective numerical scheme for inverse Laplace transform is the so-called hyperbolic contour integral method (HCIM). We discuss HCIM in next section and give some examples, in Section 4, to illustrate the advantages of HCIM compared with GSF.

We finally summarize the Laplace transform method (NLTM) for pricing American Strangles as Algorithm 2.

### 3. Hyperbolic Contour Integral Method for Laplace Inversion

Many computational experiences show that the Gaver-Stehfest inverse Laplace formula (39) is unstable when  $L \geq 20$  (see [21, 22]; also see Example 1 in this paper). So, it is very important to develop an appropriate numerical algorithm for restoring the option values. In this section, we discuss how to apply the Hyperbolic contour integral method to compute  $\mathbf{v}^n(\tau)$  from  $\hat{\mathbf{v}}^n(\tau)$ .

The inversion of Laplace transform is based on numerical integration of the Bromwich complex contour integral:

$$\mathbf{v}(S, \tau) = \frac{1}{2\pi i} \int_{\eta - i\infty}^{\eta + i\infty} e^{z\tau} \hat{\mathbf{v}}(S, z) dz, \quad \eta > \eta_0, \quad (41)$$

where  $i = \sqrt{-1}$  and  $\eta_0$  is the convergence abscissa. This means that all the singularities of  $\hat{\mathbf{v}}(S, z)$  (with respect to  $z$ ) lie in the open half-plane  $\text{Re}(z) \leq \eta_0$ . The integral (41) is not well-suited for numerical integration. First, the exponential factor is highly oscillatory on the Bromwich line,  $z = \eta + iy$ ,  $-\infty < y < +\infty$ . Second, the transform  $\hat{\mathbf{v}}(S, z)$  typically decays slowly as  $|y| \rightarrow \infty$ . One strategy for circumventing the slow decay is due to Talbot [23], who suggests that the Bromwich line be deformed into a contour  $\Gamma$  that begins and ends in the left half-plane, such that  $\text{Re}(z) \rightarrow -\infty$  at each end. On such a



contour, the exponential factor in (41) forces a rapid decay of the integrand as  $\text{Re}(z) \rightarrow -\infty$ . This makes the integral well suited for approximation by the trapezoidal or midpoint rules. Owing to Cauchy's theorem, such a deformation of contour is permissible as long as no singularities are traversed in the process, provided that  $\hat{v}(S, z) \rightarrow 0$  uniformly in  $\text{Re}(z) \leq \eta_0$  as  $|z| \rightarrow \infty$ .

Because the coefficient matrix  $\mathbf{A}$  in (23) is not Toeplitz matrix, the technics of spectral analysis in [15] cannot be

applied over here. To apply the idea of Talbot [23] and Zhou [15], we rewrite the linear system (23) as follows:

$$(z\mathbf{I} - \tilde{\mathbf{A}}) \hat{\mathbf{v}}^n(z) = \mathbf{C} \hat{\mathbf{v}}^n(z) + \mathbf{g}(z), \quad (42)$$

where  $\mathbf{I}$  is the identity matrix,

$$\tilde{\mathbf{A}} = \mathbf{D}\mathbf{B}, \quad (43)$$

$$\mathbf{B} = \frac{1}{(\Delta S)^2} \begin{bmatrix} -1 & \frac{1}{2} & 0 & \cdots & 0 & 0 \\ \frac{1}{2} & -1 & \frac{1}{2} & \cdots & 0 & 0 \\ 0 & \frac{1}{2} & -1 & \ddots & 0 & 0 \\ \vdots & \ddots & \ddots & \ddots & \ddots & \vdots \\ 0 & 0 & \ddots & \frac{1}{2} & -1 & \frac{1}{2} \\ 0 & 0 & \cdots & 0 & \frac{1}{2} & -1 \end{bmatrix}, \quad (44)$$

$$\mathbf{D} = \begin{bmatrix} \delta S_1^{2\beta+2} & & & & & \\ & \delta S_2^{2\beta+2} & & & & \\ & & \ddots & & & \\ & & & \delta S_n^{2\beta+2} & & \end{bmatrix},$$

$$\mathbf{C} = \begin{bmatrix} -r & \frac{(r-q)S_1}{2\Delta S} & 0 & \cdots & 0 & 0 \\ -\frac{(r-q)S_2}{2\Delta S} & -r & \frac{(r-q)S_2}{2\Delta S} & \cdots & 0 & 0 \\ 0 & -\frac{(r-q)S_2}{2\Delta S} & -r & \ddots & 0 & 0 \\ \vdots & \ddots & \ddots & \ddots & \ddots & \vdots \\ 0 & 0 & \ddots & -\frac{(r-q)S_{n-1}}{2\Delta S} & -r & \frac{(r-q)S_{n-1}}{2\Delta S} \\ 0 & 0 & \cdots & 0 & -\frac{(r-q)S_n}{2\Delta S} & -r \end{bmatrix} \quad (45)$$

and  $\mathbf{g}(z)$  is defined by (27). Note that  $\mathbf{B}$  is a Toeplitz matrix. The linear system (42) can be solved by the following iteration algorithm:

$$[\hat{\mathbf{v}}^n(z)]^{(\ell+1)} = (z\mathbf{I} - \tilde{\mathbf{A}})^{-1} (\mathbf{C} [\hat{\mathbf{v}}^n(z)]^{(\ell)} + \mathbf{g}(z)), \quad (46)$$

$$\ell = 0, 1, \dots$$

with  $[\hat{\mathbf{v}}^n(z)]^{(0)} = \mathbf{0}$ .

Let  $\mathbf{D}^{-1}$ -inner product and the corresponding vector norm be defined by

$$(\mathbf{v}, \mathbf{v})_{\mathbf{D}^{-1}} = \mathbf{v}^* \mathbf{D}^{-1} \mathbf{v},$$

$$\|\mathbf{v}\|_{\mathbf{D}^{-1}} = \sqrt{(\mathbf{v}, \mathbf{v})_{\mathbf{D}^{-1}}}, \quad (47)$$

$$\forall \mathbf{v} \in \mathbb{C},$$

with  $\mathbf{D}$  being defined by (44). Matrix  $\mathbf{D}^{-1}$ -norm is induced by the vector  $\mathbf{D}^{-1}$ -norm, i.e.,

$$\|\mathbf{A}\|_{\mathbf{D}^{-1}} = \max_{\mathbf{v} \neq \mathbf{0}} \frac{\|\mathbf{A}\mathbf{v}\|_{\mathbf{D}^{-1}}}{\|\mathbf{v}\|_{\mathbf{D}^{-1}}}, \quad \forall \mathbf{A} \in \mathbb{C}^{n \times n}. \quad (48)$$

The theorem below shows that the iteration algorithm (46) is convergent if  $z$  falls outside of a sectorial region.

**Theorem 2.** (i) The spectrum  $\Lambda(\tilde{\mathbf{A}})$  of  $\tilde{\mathbf{A}}$  defined by (43) lies in the sectorial region  $\Sigma_\epsilon$  for any values of  $\epsilon \in (0, \pi/2)$ , i.e.,

$$\Lambda(\tilde{\mathbf{A}}) \subseteq \Sigma_\epsilon = \{z \in \mathbb{C} : |\arg(-z)| \leq \epsilon\}. \quad (49)$$

(ii) For  $\tilde{\mathbf{A}}$  defined by (43), we have

$$\|(z\mathbf{I} - \tilde{\mathbf{A}})^{-1}\|_{\mathbf{D}^{-1}} \leq \frac{1}{1 + \text{dist}(z, \Sigma_\epsilon)}, \quad z \notin \Sigma_\epsilon, \quad (50)$$

with  $\Sigma_\epsilon$  being defined by (49) and  $\text{dist}(z, \Sigma_\epsilon) = \inf\{|z - \xi| : \xi \in \Sigma_\epsilon\}$ .

(iii) Let  $\|\mathbf{C}\|_{\mathbf{D}^{-1}} \leq \gamma_0$  with  $\mathbf{C}$  being defined by (45) and assume  $\text{dist}(z, \Sigma_\epsilon) \geq \gamma$  such that  $0 < \gamma_0 < 1 + \gamma$ . Assuming  $\hat{\mathbf{v}}^n(z)$  solve (42), we have

$$\|[\hat{\mathbf{v}}^n(z)]^{(\ell+1)} - \hat{\mathbf{v}}^n(z)\|_{\mathbf{D}^{-1}} = \left(\frac{\gamma_0}{1 + \gamma}\right)^{\ell+1} \|\hat{\mathbf{v}}^n(z)\|_{\mathbf{D}^{-1}}. \quad (51)$$

Therefore,  $[\hat{\mathbf{v}}^n(z)]^{(\ell+1)}$  is convergent to  $\hat{\mathbf{v}}^n(z)$  according to  $\|\cdot\|_{\mathbf{D}^{-1}}$ -norm.

(iv) Under the assumptions of (iii), we have

$$\|\hat{\mathbf{v}}^n(z)\|_{\mathbf{D}^{-1}} \leq \frac{1}{1 + \gamma - \gamma_0} \|\mathbf{g}(z)\|_{\mathbf{D}^{-1}}. \quad (52)$$

*Proof.* (i) Matrix  $\mathbf{B}$  defined by (44) is a Toeplitz matrix and the generating function  $f(\eta)$  of  $\mathbf{B}$  is

$$\begin{aligned} f(\eta) &= \frac{1}{(\Delta S)^2} \left( \frac{1}{2} e^{i\eta} - e^{-0i\eta} + \frac{1}{2} e^{-i\eta} \right) \\ &= \frac{1}{(\Delta S)^2} (\cos \eta - 1), \quad \eta \in (-\pi, \pi). \end{aligned} \quad (53)$$

From the above generating function  $f(\eta)$  and the discussion of Pang and Sun [24], we know the spectrum  $\Lambda(\mathbf{B})$  lies the sectorial region  $\Sigma_\epsilon$  for any values of  $\epsilon \in (0, \pi/2)$ . Since  $\mathbf{D}$  is positive definite, the spectrum  $\Lambda(\tilde{\mathbf{A}}) = \Lambda(\mathbf{D}\mathbf{B})$  also lies in the same sectorial region  $\Sigma_\epsilon$  (see [24, Lemma 3.5]).

(ii) The inequality (50) is proven in [24, Theorem 3.3].

(iii) From linear system (42) and iteration algorithm (46), we have

$$\begin{aligned} &\|[\hat{\mathbf{v}}^n(z)]^{(\ell+1)} - \hat{\mathbf{v}}^n(z)\|_{\mathbf{D}^{-1}} \\ &\leq \|(z\mathbf{I} - \tilde{\mathbf{A}})^{-1} \mathbf{C}\|_{\mathbf{D}^{-1}} \|[\hat{\mathbf{v}}^n(z)]^{(\ell)} - \hat{\mathbf{v}}^n(z)\|_{\mathbf{D}^{-1}} \\ &\leq \|(z\mathbf{I} - \tilde{\mathbf{A}})^{-1}\|_{\mathbf{D}^{-1}} \|\mathbf{C}\|_{\mathbf{D}^{-1}} \|[\hat{\mathbf{v}}^n(z)]^{(\ell)} - \hat{\mathbf{v}}^n(z)\|_{\mathbf{D}^{-1}} \\ &\leq \frac{1}{1 + \text{dist}(z, \Sigma_\epsilon)} \|\mathbf{C}\|_{\mathbf{D}^{-1}} \|[\hat{\mathbf{v}}^n(z)]^{(\ell)} - \hat{\mathbf{v}}^n(z)\|_{\mathbf{D}^{-1}} \\ &\leq \frac{\gamma_0}{1 + \gamma} \|[\hat{\mathbf{v}}^n(z)]^{(\ell)} - \hat{\mathbf{v}}^n(z)\|_{\mathbf{D}^{-1}}, \end{aligned} \quad (54)$$

for  $\ell = 0, 1, 2, \dots$

Therefore,

$$\begin{aligned} &\|[\hat{\mathbf{v}}^n(z)]^{(\ell+1)} - \hat{\mathbf{v}}^n(z)\|_{\mathbf{D}^{-1}} \\ &\leq \frac{\gamma_0}{1 + \gamma} \|[\hat{\mathbf{v}}^n(z)]^{(\ell)} - \hat{\mathbf{v}}^n(z)\|_{\mathbf{D}^{-1}} \\ &\leq \left(\frac{\gamma_0}{1 + \gamma}\right)^{\ell+1} \|[\hat{\mathbf{v}}^n(z)]^{(0)} - \hat{\mathbf{v}}^n(z)\|_{\mathbf{D}^{-1}} \\ &= \left(\frac{\gamma_0}{1 + \gamma}\right)^{\ell+1} \|\hat{\mathbf{v}}^n(z)\|_{\mathbf{D}^{-1}}, \end{aligned} \quad (55)$$

and

$$\lim_{\ell \rightarrow \infty} \|[\hat{\mathbf{v}}^n(z)]^{(\ell+1)} - \hat{\mathbf{v}}^n(z)\|_{\mathbf{D}^{-1}} = 0, \quad (56)$$

which means  $[\hat{\mathbf{v}}^n(z)]^{(\ell+1)}$  is convergent to  $\hat{\mathbf{v}}^n(z)$  according to  $\|\cdot\|_{\mathbf{D}^{-1}}$ -norm.

(iv) From linear equation (42) we have

$$\begin{aligned} \|\hat{\mathbf{v}}^n(z)\|_{\mathbf{D}^{-1}} &\leq \|(z\mathbf{I} - \tilde{\mathbf{A}})^{-1}\|_{\mathbf{D}^{-1}} \|\mathbf{C}\|_{\mathbf{D}^{-1}} \|\hat{\mathbf{v}}^n(z)\|_{\mathbf{D}^{-1}} \\ &\quad + \|(z\mathbf{I} - \tilde{\mathbf{A}})^{-1}\|_{\mathbf{D}^{-1}} \|\mathbf{g}\|_{\mathbf{D}^{-1}} \\ &\leq \frac{\gamma_0}{1 + \gamma} \|\hat{\mathbf{v}}^n(z)\|_{\mathbf{D}^{-1}} + \frac{1}{1 + \gamma} \|\mathbf{g}\|_{\mathbf{D}^{-1}}. \end{aligned} \quad (57)$$

Consequently,

$$\|\hat{\mathbf{v}}^n(z)\|_{\mathbf{D}^{-1}} \leq \frac{1}{1 + \gamma - \gamma_0} \|\mathbf{g}(z)\|_{\mathbf{D}^{-1}}, \quad (58)$$

which ends the proof.  $\square$

From Theorem 2, we see the iteration sequence  $\{[\hat{\mathbf{v}}^n(z)]^{(\ell)}, \ell = 0, 1, 2, \dots\}$  and the limit  $\hat{\mathbf{v}}^n(z)$  are analytical if  $z$  lies out the sectorial region  $\Sigma_\epsilon$  defined by (49). Therefore, the convergence of iteration algorithm (46) requires that  $z$  is far away from the sectorial region  $\Sigma_\epsilon$  such that  $\|(z\mathbf{I} - \tilde{\mathbf{A}})^{-1}\|_{\mathbf{D}^{-1}} \|\mathbf{C}\|_{\mathbf{D}^{-1}} < 1$ . This condition could be satisfied in next discussion.

The Laplace inversion of  $\hat{\mathbf{v}}^n(z)$  with respect to  $z$  can be expressed as

$$\mathbf{v}^n(\tau) = \frac{1}{2\pi i} \int_{\Gamma} e^{z\tau} \hat{\mathbf{v}}^n(z) dz. \quad (59)$$

This is the vector version of Laplace inversion (41). Weideman et al. [25] (also see Pang and Sun [24]) suggest to select the hyperbolic contour  $\Gamma$ , which can be parameterized by

$$\Gamma : z(\zeta) = \mu [1 + \sin(i\zeta - \theta)], \quad -\infty < \zeta < \infty, \quad (60)$$

where parameters  $\mu > 0$  and  $\theta$  set the width and the asymptotic angle of the hyperbolic contour, respectively. Then substituting the contour (60) into (59) gives

$$\begin{aligned} \mathbf{v}^n(\tau) &= \frac{1}{2\pi i} \int_{\Gamma} e^{z\tau} \hat{\mathbf{v}}^n(z) dz \\ &= \frac{1}{2\pi i} \int_{-\infty}^{+\infty} e^{z(\zeta)\tau} z'(\zeta) \hat{\mathbf{v}}^n(z(\zeta)) d\zeta. \end{aligned} \quad (61)$$

Discretization of this integral with uniform node spacing  $h$  yields

$$\mathbf{v}^n(\tau) = \frac{h}{2\pi i} \sum_{k=-\infty}^{+\infty} e^{z(\zeta_k)\tau} z'(\zeta_k) \widehat{\mathbf{v}}^n(z(\zeta_k)) + DE_+(h) + DE_-(h) \quad (62)$$

$$= \frac{h}{2\pi i} \sum_{k=-L}^L e^{z(\zeta_k)\tau} z'(\zeta_k) \widehat{\mathbf{v}}^n(z(\zeta_k)) + DE_+(h) + DE_-(h) + TE(hL) \quad (63)$$

$$:= \mathbf{v}^{n,L}(\tau) + DE_+(h) + DE_-(h) + TE(hL), \quad (64)$$

where  $\zeta_k = kh$  for the trapezoidal rule and  $\zeta_k = (k + 1/2)h$  for the midpoint rule,  $L$  is the number of quadrature nodes,  $DE_{\pm}(h)$  are the discretization errors, and  $TE(hL)$  is the truncation error. Define

$$g_{\tau}(\zeta) = \frac{1}{2\pi i} e^{z(\zeta)\tau} z'(\zeta) \widehat{\mathbf{v}}^n(z(\zeta)) \quad (65)$$

and assume the function  $g_{\tau}(\zeta + id)$  to be analytic in the strip  $d \in (d_-, d_+)$  with  $d_+ > 0$  and  $d_- < 0$ , then the discretization errors are bounded as

$$\begin{aligned} \|DE_+(h)\| &= \frac{M(d_+)}{e^{2\pi d_+/h} - 1}, \\ \|DE_-(h)\| &= \frac{M(d_-)}{e^{-2\pi d_-/h} - 1}, \end{aligned} \quad (66)$$

where

$$M(d) = \int_{-\infty}^{+\infty} \|g_{\tau}(\zeta + id)\| d\zeta, \quad d = d_+ \text{ (or } d_-) \quad (67)$$

and  $\|\cdot\|$  is some vector norm. The truncation error  $TE(hL)$  can be approximated by the magnitude of the last term retained, i.e.,

$$\|TE(hL)\| = \mathcal{O}(\|g_{\tau}(hL)\|), \quad L \rightarrow \infty. \quad (68)$$

We note that the estimates in (66) and (68) are extended in a straightforward manner, from the case  $g_{\tau}(\zeta)$  being scalar functions (see [24–26]) to the case when  $g_{\tau}(\zeta)$  takes value in a complex vector space.

To make all the singularities of the integrand in (61) to fall into the sectorial region  $\Sigma_{\epsilon}$  defined by (49) for a given  $\epsilon > 0$ , the expressions of optimal parameters  $h$ ,  $\mu$ , and  $\theta$  must be chosen appropriately. By asymptotically matching  $\|DE_{\pm}(h)\|$  and  $\|TE(hL)\|$ ,  $h$  and  $\mu$  are derived as follows:

$$\begin{aligned} h &= \frac{\rho(\theta)}{L}, \\ \mu &= \frac{4\pi\theta - \pi^2 + 2\pi\epsilon}{\rho(\theta)} \frac{L}{\tau}, \\ \rho(\theta) &= \cosh^{-1} \left( \frac{2\theta}{(4\theta - \pi + 2\epsilon) \sin \theta} \right) \end{aligned} \quad (69)$$

and  $\theta$  is a free parameter satisfying  $\theta < \pi/2 - \epsilon$ . With this choice the predicted convergence rate is given by

$$\|\mathbf{v}^{n,L}(\tau) - \mathbf{v}^n(\tau)\| \leq \mathcal{O}(e^{-R(\theta)L}), \quad (70)$$

where

$$R(\theta) = \frac{\pi^2 - 2\pi\theta - 2\pi\epsilon}{\rho(\theta)}. \quad (71)$$

According to (70), we see that once the semiangle  $\epsilon$  of the sectorial region (49) is given, then one can find the optimal  $\theta$  by maximizing the function  $R(\theta)$ . Consequently, the optimal parameters  $h$  and  $\mu$  can be obtained from formulas (69).

Denoting  $z_k = z(\zeta_k)$  and  $z'_k = z'(\zeta_k)$ , we have

$$\begin{aligned} \mathbf{v}^{n,L}(\tau) &= \frac{h}{2\pi i} \sum_{k=-L}^L e^{z_k\tau} z'_k(\zeta_k) \widehat{\mathbf{v}}^n(z_k) \approx \mathbf{v}^{n,L,L}(\tau) \\ &:= \frac{h}{2\pi i} \sum_{k=-L}^L e^{z_k\tau} z'_k(\zeta_k) [\widehat{\mathbf{v}}^n(z_k)]^{(\ell)}. \end{aligned} \quad (72)$$

Now, we give the convergence condition of the iteration algorithm (46). From [27, Theorem 3.3], the distance between  $\Sigma_{\epsilon}$  and  $\Gamma$  is given by

$$\text{dist}(\Sigma_{\epsilon}, \Gamma) := \min_{P_1 \in \Sigma_{\epsilon}, P_2 \in \Gamma} |P_1 - P_2| = \mu(1 - \sin \theta). \quad (73)$$

Inserting the above equation and the expression  $\mu = ((4\pi\theta - \pi^2 + 2\pi\epsilon)/\rho(\theta))(L/\tau)$  into following inequality

$$\|(z\mathbf{I} - \widetilde{\mathbf{A}})^{-1}\|_{\mathbf{D}^{-1}} \leq \frac{1}{1 + \text{dist}(\Sigma_{\epsilon}, \Gamma)} \quad (74)$$

we get

$$\begin{aligned} &\|(z\mathbf{I} - \widetilde{\mathbf{A}})^{-1}\|_{\mathbf{D}^{-1}} \\ &\leq \frac{1}{1 + ((4\pi\theta - \pi^2 + 2\pi\epsilon)(1 - \sin \theta)/\rho(\theta))(L/\tau)}. \end{aligned} \quad (75)$$

Denote  $\gamma = \mu(1 - \sin \theta) = \text{dist}(\Sigma_{\epsilon}, \Gamma)$ . If we take  $L$  such that

$$\frac{L}{\tau} > \frac{\rho(\theta)(\gamma_0 - 1)}{(4\pi\theta - \pi^2 + 2\pi\epsilon)(1 - \sin \theta)}, \quad (76)$$

then  $1 + \gamma > \gamma_0$  and the iteration algorithm (46) is convergent according to norm  $\|\cdot\|_{\mathbf{D}^{-1}}$ . Inequality (76) requires that  $L$  is large enough such that the hyperbolic contour  $\Gamma$  is far away from the sectorial region  $\Sigma_{\epsilon}$ .

In following Theorem, we give an estimation for  $\|\mathbf{C}\|_{\mathbf{D}^{-1}}$  and then give the minimum estimation for  $L$ .

**Theorem 3.** For matrix  $\mathbf{C}$  being defined by (45), we have the following estimation:

$$\begin{aligned} \|\mathbf{C}\|_{\mathbf{D}^{-1}} &\leq \gamma_0 := \frac{M(\underline{S}_p, \overline{S}_c)}{2\Delta S} \\ &\cdot \sqrt{(8r^2 - 4r(r - q))(\Delta S)^2 + 3(r - q)^2 \underline{S}_p^2}, \end{aligned} \quad (77)$$

where  $\bar{S}_c$  and  $\underline{S}_p$  are defined by (8) in Section 2 and

$$M(\underline{S}_p, \bar{S}_c) = \frac{\bar{S}_c}{\underline{S}_p} \frac{\max_j S_j^{\beta+1}}{\min_j S_j^{\beta+1}} = \begin{cases} \left(\frac{\bar{S}_c}{\underline{S}_p}\right)^{\beta+2}, & \beta \geq -1, \\ \left(\frac{\bar{S}_c}{\underline{S}_p}\right)^{\beta}, & \beta < -1. \end{cases} \quad (78)$$

If  $\Delta S$  is small enough, then

$$\|C\|_{D^{-1}} \leq \gamma_0 := \frac{\sqrt{3}|r-q|\underline{S}_p M(\underline{S}_p, \bar{S}_c)}{2\Delta S} = \mathcal{O}\left(\frac{1}{\Delta S}\right), \quad (79)$$

$\Delta S \rightarrow 0.$

*Proof.* Firstly, we verified the inequality

$$\|C\|_{D^{-1}} \leq \frac{\max_j S_j^{\beta+1}}{\min_j S_j^{\beta+1}} \|C\|, \quad (80)$$

where  $\|\cdot\|$  represents the vector  $\ell_2$ -norm. Indeed,

$$\begin{aligned} \|C\|_{D^{-1}} &= \max_{v \neq 0} \frac{\|Cv\|_{D^{-1}}}{\|v\|_{D^{-1}}} = \max_{v \neq 0} \frac{\sqrt{(Cv)^* D^{-1} Cv}}{\sqrt{v^* D^{-1} v}} \\ &\leq \max_{v \neq 0} \frac{\sqrt{(1/\min_j \delta S_j^{2\beta+2})(Cv)^* Cv}}{\sqrt{(1/\max_j \delta S_j^{2\beta+2})v^* v}} \\ &= \frac{\sqrt{\max_j S_j^{2\beta+2}}}{\sqrt{\min_j S_j^{2\beta+2}}} \max_{v \neq 0} \frac{\|Cv\|}{\|v\|} = \frac{\max_j S_j^{\beta+1}}{\min_j S_j^{\beta+1}} \|C\|. \end{aligned} \quad (81)$$

From definition (45), we have  $C = (1/2\Delta S)D_1 C_1$  with

$$C_1 = \begin{bmatrix} -\frac{2r\Delta S}{S_1} & (r-q) & 0 & \cdots & 0 & 0 \\ -(r-q) & -\frac{2r\Delta S}{S_2} & (r-q) & \cdots & 0 & 0 \\ 0 & -(r-q) & -\frac{2r\Delta S}{S_3} & \ddots & 0 & 0 \\ \vdots & \ddots & \ddots & \ddots & \ddots & \ddots \\ 0 & 0 & \ddots & -(r-q) & -\frac{2r\Delta S}{S_{n-1}} & (r-q) \\ 0 & 0 & \cdots & 0 & -(r-q) & -\frac{2r\Delta S}{S_n} \end{bmatrix} \quad (82)$$

and  $D_1 = \text{Diag}[S_1, S_2, \dots, S_n]$ . By carefully calculating, we have

$$C_1^T C_1 = [c_{jk}]_{n \times n} \quad (83)$$

where

$$\begin{aligned} c_{jj} &= \frac{4r^2 (\Delta S)^2}{S_j^2} + (r-q)^2, \quad j = 1, n, \\ c_{jj} &= \frac{8r^2 (\Delta S)^2}{S_j^2} + (r-q)^2, \quad j = 2, 3, \dots, n-1, \end{aligned} \quad (84)$$

$$c_{j,j-1} = c_{j,j+1} = \frac{2r(r-q)(\Delta S)^2}{S_j S_{j+1}}, \quad j = 1, 2, \dots, n,$$

$$c_{j,j-2} = c_{j,j+2} = -(r-q)^2, \quad j = 1, 2, \dots, n,$$

and  $c_{jk} = 0$  for  $j = 1, 2, \dots, n$ ,  $k < j-2$  and  $k > j+2$ . By the Gershgorin circle theorem, each eigenvalue  $\lambda(C_1^T C_1)$  of  $C_1^T C_1$  falls into a certain Gerschgorin disk  $\mathcal{G}_j$ , i.e.,

$$\lambda(C_1^T C_1) \in \mathcal{G}_j := \left\{ z : |z - c_{jj}| \leq \sum_{k=j-2, k \neq j}^{j+2} c_{jk} \right\} \quad (85)$$

for some index  $j$ . Incorporating (84) and (85), we get

$$\begin{aligned} \lambda(C_1^T C_1) &\leq \max_j \left\{ \frac{8r^2 (\Delta S)^2}{S_j^2} + \frac{4r(r-q)(\Delta S)^2}{S_j S_{j+1}} \right. \\ &\quad \left. + 3(r-q)^2 \right\} \leq \frac{1}{\min_j S_j^2} \left\{ (8r^2 - 4r(r-q))(\Delta S)^2 \right. \\ &\quad \left. + 3(r-q)^2 \min_j S_j^2 \right\}. \end{aligned} \quad (86)$$

Therefore,

$$\begin{aligned} \|C_1\| &\leq \sqrt{\lambda(C_1^T C_1)} \leq \frac{1}{\min_j S_j} \\ &\quad \cdot \sqrt{(8r^2 - 4r(r-q))(\Delta S)^2 + 3(r-q)^2 \min_j S_j^2}. \end{aligned} \quad (87)$$

Incorporating (80) and (87), we have

$$\begin{aligned} \|C\|_{D^{-1}} &\leq \frac{\max_j S_j^{\beta+1}}{\min_j S_j^{\beta+1}} \|C\| = \frac{1}{2\Delta S} \frac{\max_j S_j^{\beta+1}}{\min_j S_j^{\beta+1}} \|D_1 C_1\| \\ &\leq \frac{1}{2\Delta S} \frac{\max_j S_j^{\beta+1}}{\min_j S_j^{\beta+1}} \|D_1\| \|C_1\| \leq \frac{1}{2\Delta S} \frac{\max_j S_j^{\beta+1}}{\min_j S_j^{\beta+1}} \\ &\quad \cdot \frac{\max_j S_j}{\min_j S_j} \\ &\quad \cdot \sqrt{(8r^2 - 4r(r-q))(\Delta S)^2 + 3(r-q)^2 \min_j S_j^2} \end{aligned} \quad (88)$$

Let  $\max_j S_j = \bar{S}_c$ ,  $\min_j S_j = \underline{S}_p$  and  $M(\underline{S}_p, \bar{S}_c) = (\bar{S}_c / \underline{S}_p)(\max_j S_j^{\beta+1} / \min_j S_j^{\beta+1})$ ; we finally obtain the estimate expression (77).

Finally, we give two remarks as follows.  $\square$

TABLE 1: Values of American Strangles at time  $t = 0$  (i.e.,  $\tau = T$ ) with  $K_1 = 1$ ,  $K_2 = 1.5$ ,  $r = 0.05$ ,  $q = 0.1$ ,  $S_0 = 1.5$ ,  $\sigma_0 = 0.4$ , different values of  $\beta$ , and different values of  $L$ . The CPU time is about 20s, 22s, and 680s for LTM-GSF, LTM-HCIM, and FDM, respectively.

$\beta$	$L = 10$		$L = 20$		$L = 26$		FDM
	LTM-GSF	LTM-HCIM	LTM-GSF	LTM-HCIM	LTM-GSF	LTM-HCIM	
-0.50	0.260862	0.260864	0.297905	0.260864	18.447801	0.260864	0.258805
-0.25	0.253815	0.253800	0.284163	0.253800	22.070192	0.253800	0.251154
0	0.247986	0.247964	0.261926	0.247964	24.667532	0.247964	0.244310
0.25	0.245120	0.245090	0.239312	0.245090	-0.098661	0.245090	0.238169
0.50	0.236749	0.236703	0.217691	0.236724	-9.087067	0.236724	0.232615

*Remark 4.* (i) For the fixed hyperbolic contour parameters  $\theta$  and  $\epsilon$ , Theorem 3 and iteration convergence condition (76) show that we must take  $L = \mathcal{O}(1/\Delta S)$ . (ii) For inverse Laplace formula  $\mathbf{v}^{n,L}(\tau)$  in (72), we solve  $\hat{\mathbf{v}}^n(z)$  by directly computing linear equations  $\hat{\mathbf{v}}^n(z) = (\mathbf{I} - \mathbf{A})^{-1} \mathbf{g}(z)$  (i.e., expression (23) in Section 2) if  $L$  satisfies inequality (76) with  $\gamma_0$  being defined by (77).

*Remark 5.* From the upper estimate (52) for  $\|\hat{\mathbf{v}}^n(z)\|_{\mathbf{D}^{-1}}$ , we see the convergence of inverse Laplace depends on the norm  $\|\mathbf{g}(z)\|_{\mathbf{D}^{-1}}$ . Moreover, observing the expression of  $\mathbf{g}(z)$  defined by (27) and (29), the exponential terms  $e^{-z\tau_p(S_j; p_1, \alpha_1)}$  and  $e^{-z\tau_c(S_j; p_2, \alpha_2)}$  play important roles. Following the strategy of Zhou et al. [15], we split  $g_j(z)$  into two parts  $g_j(z) = g_{1j}(z) + g_{2j}(z)$  with

$$\begin{aligned}
 g_{1j} &= \max(K_1 - S_j, 0) + \max(S_j - K_2, 0) \\
 &\quad + \frac{1}{z} (rK_1 - qS_j) - \frac{1}{z} (rK_2 - qS_j) \\
 &\quad - \frac{1}{z} (rK_1 - qS_j) e^{-z\tau_c(S_j)} \mathbf{1}_{\{\tau > \tau_c(S_j)\}} \\
 &\quad + \frac{1}{z} (rK_2 - qS_j) e^{-z\tau_c(S_j)} \mathbf{1}_{\{\tau > \tau_p(S_j)\}} \\
 g_{2j} &= -\frac{1}{z} (rK_1 - qS_j) e^{-z\tau_c(S_j)} \mathbf{1}_{\{\tau < \tau_c(S_j)\}} \\
 &\quad + \frac{1}{z} (rK_2 - qS_j) e^{-z\tau_c(S_j)} \mathbf{1}_{\{\tau < \tau_p(S_j)\}}
 \end{aligned} \tag{89}$$

for  $j = 1, 2, \dots, n$ . Therefore, we have splitting expression  $\mathbf{g}(z) = \mathbf{g}_1(z) + \mathbf{g}_2(z)$ .  $e^{z\tau} \mathbf{g}_1(z)$  rapidly decays as  $\text{Re}(z) \rightarrow -\infty$  if  $z$  falls on the hyperbola contour  $\Gamma$  defined by (60). To make the Laplace transform method convergent, we define an other hyperbola contour  $\tilde{\Gamma}$ :

$$\tilde{\Gamma} : z(\zeta) = \mu [1 + \sin(i\zeta + \theta)], \quad -\infty < \zeta < \infty, \tag{90}$$

which begins and ends in the right half-plane, such that  $\text{Re}(z) \rightarrow +\infty$  at each end. We select the same parameters  $\epsilon$ ,  $\mu$ , and  $\theta$  as those of  $\Gamma$ . Obviously,  $e^{z\tau} \mathbf{g}_2(z)$  rapidly decays as  $\text{Re}(z) \rightarrow +\infty$  if  $z$  falls on the hyperbola contour  $\tilde{\Gamma}$  defined by (90). The inverse Laplace of  $\hat{\mathbf{v}}^n(z)$  with respect to  $z$  can be expressed as

$$\begin{aligned}
 \mathbf{v}^n(\tau) &= \frac{1}{2\pi i} \int_{\Gamma} e^{z\tau} \hat{\mathbf{v}}^n(z) dz \\
 &= \frac{1}{2\pi i} \int_{\Gamma} e^{z\tau} (z\mathbf{I} - \mathbf{A})^{-1} (\mathbf{g}_1(z) + \mathbf{g}_2(z)) dz \\
 &= \frac{1}{2\pi i} \int_{\Gamma} e^{z\tau} (z\mathbf{I} - \mathbf{A})^{-1} \mathbf{g}_1(z) dz \\
 &\quad + \frac{1}{2\pi i} \int_{\tilde{\Gamma}} e^{z\tau} (z\mathbf{I} - \mathbf{A})^{-1} \mathbf{g}_2(z) dz \approx \mathbf{v}_1^{n,L}(\tau) \\
 &\quad + \mathbf{v}_2^{n,L}(\tau),
 \end{aligned} \tag{91}$$

where  $\mathbf{v}_1^{n,L}(\tau)$  and  $\mathbf{v}_2^{n,L}(\tau)$  have the predicted convergence rate  $R(\theta)$  defined by formula (70).

#### 4. Numerical Examples

In this subsection, we list some Strangles option values computed by the Laplace transform method and hyperbola contour integral method (labeled by “LTM-HCIM”). These results are compared with those obtained by LTM using inverse Laplace GSF (labeled by “LTM-GSF”) and FDM. The parameters in model (4)-(7) are taken as  $T = 1(\text{year})$ ,  $r = 0.05(1/\text{year})$ ,  $q = 0.1(\$)$ ,  $K_1 = 1(\$)$ ,  $K_2 = 1.5(\$)$ ,  $S_0 = 1.5$ ,  $\delta = \sigma_0/S_0^\beta$  and  $S_{\max} = 4K_2$ . The values of parameters in HCIM are taken as  $\theta = 0.8$  and  $\epsilon = 0.4$ . We take the number of space partition  $N = 3000$  to compute  $\underline{S}_p$  and  $\bar{S}_c$  and take  $n = 3000$  to optimise  $\tau_p(S)$  and  $\tau_c(S)$ . The positive values  $z_i = 1 + 3i/m$  with  $m = 6$  in expressions (35) and (36). The size of space mesh and the time mesh is set as  $N = 2000$ ,  $\Delta t = T/2000$  for FDM.

*Example 1.* Table 1 lists the American Strangles option prices with  $\sigma_0 = 0.4$ , different values of  $\beta$  and different values of  $L$ . From the table, we see LTM-GSF is unstable when  $L > 20$ , while the values of LTM-HCIM is very close to ones of FDM for  $L = 10, 20, 26$ . So, LTM-HCIM outperforms the LTM-GSF formula in regard to the accuracy and stability for the option values.

*Example 2.* This example illustrates the convergence rate of LTM-HCIM for the number  $n$  of space mesh and the number  $L$  for HCIM. Table 2 lists the space convergence rate with  $L = 20$  and fixed  $N = 3000$ . The column labeled “Value” shows the option values at stock price  $S_0 = 1.5$ ; the column labeled “Err” is defined by

TABLE 2: Values of American Strangles at time  $t = 0$  (i.e.,  $\tau = T$ ) with  $K_1 = 1$ ,  $K_2 = 1.5$ ,  $r = 0.05$ ,  $q = 0.1$ ,  $S_0 = 1.5$ ,  $L = 20$ , different values of  $\sigma_0$ , different values of  $\beta$ , and different space partition  $n$ .

$n$	$\sigma_0 = 0.2, \beta = 0.5$			$\sigma_0 = 0.4, \beta = -0.5$		
	Value	Err	Rate	Value	Err	Rate
24	0.150660	3.3277e-003	0.6061	0.262272	2.7302e-003	1.5515
49	0.149394	2.1862e-003	0.5367	0.260271	9.3141e-004	0.9603
99	0.149262	1.5070e-003	0.5154	0.260335	4.7871e-004	1.0611
199	0.149211	1.0543e-003	0.5076	0.260319	2.2943e-004	0.9601
399	0.149187	7.4158e-004	0.5037	0.260274	1.1793e-004	0.9812
799	0.149191	5.2302e-004	0.5018	0.260276	5.9737e-005	0.9920
1599	0.149189	3.6937e-004	—	0.260275	3.0034e-005	—
3199	0.149189	—	—	0.260275	—	—

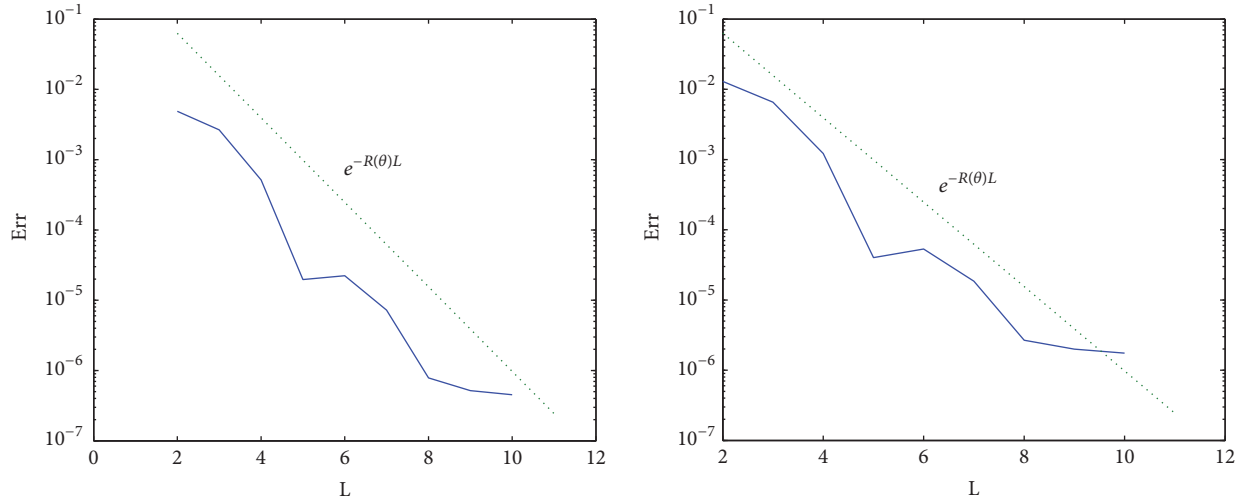


FIGURE 1: LTM-HCIM errors in log-scale v.s.  $L$  for American CEV Strangles option at  $\tau = 1$ . Left: log scale errors with  $\sigma_0 = 0.2, \beta = 0.5$ ; Right: log scale errors with  $\sigma_0 = 0.4, \beta = -0.5$ .

$$\text{Err}(n) = \sqrt{\Delta S(n)} \left\| \mathbf{v}^{n,L}(\tau) - \mathcal{I}[\mathbf{v}^{2n,L}(\tau)] \right\|, \quad (92)$$

where  $\mathcal{I}[\mathbf{v}^{2n,L}(\tau)]$  is the linear interpolation of  $\mathbf{v}^{2n,L}(\tau)$  from  $2n$ -mesh to  $n$ -mesh,  $\|\cdot\|$  is the  $\ell_2$  vector norm and  $\Delta S(n) = (\bar{S}_c - \underline{S}_p)/(n+1)$ , and the convergence rate is defined by

$$\text{Rate}(n) = \log_2 \frac{\text{Err}(n)}{\text{Err}(2n)}. \quad (93)$$

From Table 2, we see the convergence rate of LTM-HCIM is 0.5 and 1.0 for  $\beta = 0.5$  and  $\beta = -0.5$ , respectively. It is very interesting to investigate the relationship between the convergence rates and the values of  $\beta$  and we leave this topic to the future.

We regard the computational solution  $\mathbf{v}^{n,L}(\tau)$  with  $n = 1599, L = 30$  as the reference option prices, i.e.,  $\mathbf{v}^n(\tau) \approx \mathbf{v}^{1599,30}(\tau)$ , and the LTM-HCIM time-errors are defined by

$$\text{Err}(L) = \sqrt{\Delta S(1600)} \left\| \mathbf{v}^{1599,L}(\tau) - \mathbf{v}^{1599,30}(\tau) \right\|, \quad (94)$$

for different values of  $L$ . Figure 1 plots the LTM-HCIM errors in log-scale v.s.  $L$ . From this Figure we see the numerical convergence rates are consistent with the predicted rates

$$\left\| \mathbf{v}^{n,L}(\tau) - \mathbf{v}^n(\tau) \right\| \leq \mathcal{O}\left(e^{-R(\theta)L}\right), \quad (95)$$

for moderate values of  $L$ .

## 5. Conclusions

An efficient Laplace transform method was developed for pricing American Strangles option under CEV diffusion. Numerical examples show LTM is a fast algorithm to solve PDEs with free boundaries and the hyperbola contour integral method has higher numerical accuracy and good stability for numerical Laplace inversion. The method developed here can be extended to the pricing of other American options, such as American options with regime switching and with jump-diffusion process.

## Data Availability

All Matlab codes supporting the results of this study are available from the corresponding author on request.

## Conflicts of Interest

The authors declare that they have no conflicts of interest.

## Authors' Contributions

Hongying Wu carried out the experiments in Section 4 and Zhiqiang Zhou made the main contributions to the



other sections. All authors read and approved the final manuscript.

## Acknowledgments

The work was supported by Natural Science Foundation of Hunan Province of China (no. 2017JJ2113).

## References

- [1] P. Carr, "Randomization and the American put," *Review of Financial Studies*, vol. 11, no. 3, pp. 597–626, 1998.
- [2] A. Pelsser, "Pricing double barrier options using Laplace transforms," *Finance and Stochastics*, vol. 4, no. 1, pp. 95–104, 2000.
- [3] D. Davydov and V. Linetsky, "Pricing and hedging path-dependent options under the CEV process," *Management Science*, vol. 47, no. 7, pp. 949–965, 2001.
- [4] A. Sepp, "Analytical pricing of double-barrier options under a double-exponential jump diffusion process: applications of Laplace transform," *International Journal of Theoretical and Applied Finance*, vol. 7, no. 2, pp. 151–175, 2004.
- [5] N. Cai and S. G. Kou, "Option pricing under a mixed-exponential jump diffusion model," *Management Science*, vol. 57, no. 11, pp. 2067–2081, 2011.
- [6] N. Cai and S. Kou, "Pricing Asian options under a hyper-exponential jump diffusion model," *Operations Research*, vol. 60, no. 1, pp. 64–77, 2012.
- [7] R. Mallier and G. Alobaidi, "Laplace transforms and American options," *Applied Mathematical Finance*, vol. 7, no. 4, pp. 241–256, 2000.
- [8] S.-P. Zhu, "A new analytical approximation formula for the optimal exercise boundary of American put options," *International Journal of Theoretical and Applied Finance*, vol. 9, no. 7, pp. 1141–1177, 2006.
- [9] T. Kimura, "Valuing finite-lived Russian options," *European Journal of Operational Research*, vol. 189, no. 2, pp. 363–374, 2008.
- [10] H. Y. Wong and J. Zhao, "Valuing American options under the CEV model by Laplace-Carson transforms," *Operations Research Letters*, vol. 38, no. 5, pp. 474–481, 2010.
- [11] C. S. Pun and H. Y. Wong, "CEV asymptotics of American options," *Journal of Mathematical Analysis and Applications*, vol. 403, no. 2, pp. 451–463, 2013.
- [12] M. Leippold and N. Vasiljevic, "Pricing and Disentanglement of American Puts in the Hyper-Exponential Jump-Diffusion Model," *SSRN Electronic Journal*, 2015, <http://ssrn.com/abstract=2571208>.
- [13] X. Lu and E. R. Putri, "Finite maturity margin call stock loans," *Operations Research Letters*, vol. 44, no. 1, pp. 12–18, 2016.
- [14] J. Ma, Z. Zhou, and Z. Cui, "Hybrid Laplace transform and finite difference methods for pricing American options under complex models," *Computers and Mathematics with Applications*, vol. 74, no. 3, pp. 369–384, 2017.
- [15] Z. Zhou, J. Ma, and H.-w. Sun, "Fast Laplace transform methods for free-boundary problems of fractional diffusion equations," *Journal of Scientific Computing*, vol. 74, no. 1, pp. 49–69, 2018.
- [16] J. C. Cox, "The constant elasticity of variance option pricing model," *The Journal of Portfolio Management*, vol. 22, pp. 16–17, 1996.
- [17] C. Chiarella and A. Ziogas, "Evaluation of American strangles," *Journal of Economic Dynamics and Control*, vol. 29, no. 1–2, pp. 31–62, 2005.
- [18] X. Chen and J. Chadam, "A mathematical analysis of the optimal exercise boundary for American put options," *SIAM Journal on Mathematical Analysis*, vol. 38, no. 5, pp. 1613–1641, 2006/07.
- [19] Y. K. Kwok, *Mathematical Models of Financial Derivatives*, Springer Verlag, Singapore, Singapore, 1998.
- [20] M. Xu and C. Knessl, "On a free boundary problem for an American put option under the CEV process," *Applied Mathematics Letters*, vol. 24, no. 7, pp. 1191–1198, 2011.
- [21] H. Stehfest, "Numerical inversion of Laplace transforms," *Communications of the ACM*, vol. 13, no. 1, pp. 47–49, 1970.
- [22] P. P. Valkó and J. Abate, "Comparison of sequence accelerators for the Gaver method of numerical Laplace transform inversion," *Computers & Mathematics with Applications*, vol. 48, no. 3–4, pp. 629–636, 2004.
- [23] A. Talbot, "The accurate numerical inversion of Laplace transforms," *Journal of the Institute of Mathematics and Its Applications*, vol. 23, no. 1, pp. 97–120, 1979.
- [24] H.-K. Pang and H.-W. Sun, "Fast numerical contour integral method for fractional diffusion equations," *Journal of Scientific Computing*, vol. 66, no. 1, pp. 41–66, 2016.
- [25] J. A. Weideman and L. N. Trefethen, "Parabolic and hyperbolic contours for computing the Bromwich integral," *Mathematics of Computation*, vol. 76, no. 259, pp. 1341–1356, 2007.
- [26] J. A. Weideman, "Improved contour integral methods for parabolic PDEs," *IMA Journal of Numerical Analysis (IMAJNA)*, vol. 30, no. 1, pp. 334–350, 2010.
- [27] J. Ma and Z. Zhou, "Convergence analysis of iterative Laplace transform methods for the coupled PDEs from regime-switching option pricing," *Journal of Scientific Computing*, vol. 75, no. 3, pp. 1656–1674, 2018.

## Research Article

# A Solvable Time-Inconsistent Principal-Agent Problem

Chao Li  and Zhijian Qiu

*School of Economic Mathematics, Southwestern University of Finance and Economics, Chengdu, China*

Correspondence should be addressed to Chao Li; [1160202z1004@2016.swufe.edu.cn](mailto:1160202z1004@2016.swufe.edu.cn)

Received 8 March 2018; Accepted 10 June 2018; Published 1 August 2018

Academic Editor: Jorge E. Macias-Diaz

Copyright © 2018 Chao Li and Zhijian Qiu. This is an open access article distributed under the Creative Commons Attribution License, which permits unrestricted use, distribution, and reproduction in any medium, provided the original work is properly cited.

We consider the dynamic contract model with time inconsistency preference of principal-agent problem to study the influence of the time inconsistency preference on the optimal effort and the optimal reward mechanism. We show that when both the principal and the agent are time-consistent, the optimal effort and the optimal reward are the decreasing functions of the uncertain factor. And when the agent is time-inconsistent, the impatience of the agent has a negative impact on the optimal contract. The higher the discount rate of the agent is, the lower the efforts provided; agents tend to the timely enjoyment. In addition, when both the principal and the agent are time-inconsistent, in a special case, their impatience can offset the impact of uncertainty factor on the optimal contract, but, in turn, their impatience will affect the contract.

## 1. Introduction

The principal-agent problem is a classic issue of the optimal contract and is widely used in financial and economical fields. The principal and the agent, as two parties of the contract, interact with each other. Under the constraints of the contract, the agent creates profits for the principal and the principal pays the salary for the agent as incentives. In this paper, we introduce an optimal contract where both the principal and the agent are time-inconsistent to solve the principal-agent problem under moral hazard in a dynamic environment. In general, the agent is regarded as risk-neutral and the principal is risk aversion.

In solving the optimal contract with the time-inconsistent principal-agent problem, there are three problems we need to face. The first is the solution to the principal-agent's problem in the continuous-time. A continuous-time model where the agent controls the Brownian motion drift rate over the time interval is studied by [1]. Later, [2, 3] uses martingale methods to develop the first-order approach of principal-agent problems under moral hazard with exponential utility. Reference [4] shows that the first best sharing rule is also linear in output in the continuous-time principal-agent model with exponential utility. Reference [5, 6] uses the stochastic maximum principle to extended Holmstrom's model, and

discuss the optimal solution of the agent with private information in the continuous-time model. Reference [7, 8] uses the forward-backward stochastic differential equations to consider the optimal contract under moral hazard. Reference [9] systematically expands the problem of continuous-time principal-agent. However, the above methods solved the principal-agent problem in a continuous period of time under the time-consistent preference, which is simplistic for the actual situation. Therefore, it is natural to consider the time inconsistency in the principal-agent model.

The second problem is how to find the optimal strategy when the time preference is inconsistent. Reference [10] proposes the optimal contracts for the principal who contracted with the dynamically inconsistent agents in a discrete case. Their study includes exploitative contracts that applied for naive agents to better explain the true contractual arrangements. Based that, [11, 12] takes the neutral agent as a benchmark to study the possibility that the principal manipulates the naive agent. The result shows that the innocence of the agent does not bring benefits to the principal, and the maximum effectiveness of the principal is the same in front of the neutral agent and naive agent. Besides, the definition of naive and neutral agent was firstly mentioned in [13]. Reference [14] takes the discount of the quasi-hyperbolic  $\beta\delta$  as the agent's discount function, then discuss the optimal contract and the

profit level of the principal when the agent is neutral or naive. The above mainly deals with the problem of time-inconsistent agents in discrete time. However, less attention is paid in continuous-time because it is complicated to solve the closed-loop solution under nonconstant discounting. Reference [15] proposes the optimal contract models based on the Pontryagin maximum principle for forward-backward stochastic differential equations to study a general continuous-time principal-agent problem in which the utility function is time-inconsistent.

The third question is how to find the exact solution of the Hamilton-Jacobi-Bellman (HJB) equation. Using the stochastic control to solve the HJB equation is a complex mathematical process, especially in the case of increasing the control variables, which will be more complex nonlinear partial differential equations. By the Legendre transform, the problem can be transformed into a dual problem that is convenient for analysis, so as to solve some model solving problems. Reference [16] studies the portfolio problem under the general utility function, and prove the effectiveness of using the Legendre dual method to solve the HJB equation. Reference [17] uses Legendre transform-dual theory to solve the optimal investment problem based on hyperbolic absolute risk aversion (HARA) preference under constant elastic variance model. References [18, 19] study the investment-consumption of HARA utility by Legendre method.

In this paper, we study the optimal incentive contract under moral hazard in the framework of the principal-agent problem with time inconsistency in continuous-time. Assume both the principal and the agent are time-inconsistent, where the principal is risk-averse with an exponential utility function and the agent is risk-neutral with a linear utility function. To describe the time inconsistency of participants, we assume that the discount rate of participants is a function of time (not a constant) but still takes the form of exponential discounting because the principal's utility function is the exponential utility function. According to the property of the exponential function, we can divide the discount function into two parts: one part is the traditional discount function (discount rate is constant) and the other part is the uncertainty. Under the moral hazard, the principal can observe the process of output but cannot observe the agent's efforts and random perturbations. Thus the principal considers a part of the discount function as an unknown factor that affects the output. Reference [20] puts forward that the principal can constantly learn and update his belief from the unknown factor (the uncertain part of the discount function) through the existing information and historical information in the production process. Therefore, we transform the time-inconsistent principal into a principal who has the consistent time and learning process. For time-inconsistent agents, we can employ the Markov subgame perfect Nash equilibrium method [21] to get its time consistency strategy.

Through the above assumption, we solve the optimal contract in two cases where the principal is time-consistent and time-inconsistent. When the principal is time consistency, we use the stochastic optimal control method to derive the nonlinear partial differential equation (HJB equation) for the optimal value function of the principal. This partial

differential equation is hard to solve for an exact closed-loop solution; however, the original problem can transfer to a dual problem by applying the Legendre transform in some cases. To obtain the exact solution of the optimal contract (closed-loop solution), we use the Legendre transform-dual theory to obtain the explicit solution of the optimal solution and the optimal contract. When the principal is time-inconsistent, we obtain a value function which takes the time, the agent's personal information, and the utility of agent as variables, so as to derive a three-dimensional nonlinear second-order HJB equation. In this situation, we solve the HJB equation by guess solution.

The general structure of this paper is as follows. Section 2 presents the model. The incentive compatibility conditions and the given proof are provided in Section 3. Section 4 studies the optimal contract of a time-consistent and time-inconsistent principal. Section 5 provides numerical simulation of optimal strategy. Finally, we made the conclusion in Section 6.

## 2. The Model

**2.1. The Agent.** Suppose a principal made the contract with a time-inconsistent agent to manage a production process (or invest a risk project) and the initial time of contracting period is recorded as 0. Consider an infinite horizon stochastic environment; let  $\{W_t^0\}$  be a standard Brownian motion on the probability space  $(\Omega, \mathcal{F}, \mathbb{P}^0)$ . The risk process that pays a cumulative process  $Y_t$  evolved on period  $[0, T]$  as follows:

$$dY_t = (e_t - c_t) dt + \sigma dW_t^0 \quad (1)$$

assumes that  $A \in \mathbb{R}$  is a compact set and  $e_t \in A$  is the agent's effort choice.  $c_t \in \mathbb{R}$  is the salary of the agent (or his consumption).  $\sigma$  is the project's volatility (constant) where  $\sigma > 0$ . The path of  $Y_t$  is observable both from the principal and the agent, but the path of  $\{W_t^0\}$  is observable only from the agent, and the effort choice  $e_t$  is unobservable from the principal.

At the initial moment time 0, the principal provides the agent with a contract (pay the salary according to the contract). Assume that the salary is composed of two parts, a continuous payment  $c_t$  and a terminal payment  $C_T$ . Moreover, we assume that the agent is risk-neutral,  $u$  and  $v$  (we will give the explicit functional forms for  $u$  and  $v$  in the specific question (see (26) and (27))) are utility functions, and  $u$  and  $v$  are concave and twice continuously differentiable. And the agent has a discount function  $h$ , where  $h(t) = e^{-\int_0^t \rho(s) ds}$  (in this paper, for convenience, sometimes  $h(t)$  is written as  $h_t$ ) is a general discount function; see [22]; then the agent will be time-inconsistent if  $\rho(s)$  is time dependence.

The agent's preferences as of time 0 read

$$J_A(0; e) = \mathbb{E} \left[ \int_0^T h(t) u(c_t, e_t) dt + h(T) v(C_T) \right] \quad (2)$$

**2.2. The Principal.** In this paper, we assume that the principal is partially naive type ([23] in a discrete time-inconsistent model, disaggregate participants into mature type, naive type, and partially naive type based on the cognitive differences of

participants about their own future preference), which means that the principal knows he is time-inconsistent (his discount function is time-variant), but his current perception of the future discount rate is biased against the true value of the future discount rate (at time  $t$ , he cannot be sure the value of discount rate  $\delta(\tau)$  (we can further assume that  $\rho(t), \delta(t) : [0, T] \rightarrow [0, 1]$ ) when  $0 \leq t < \tau \leq T$ ). Therefore, the principal will continuously update his belief in the future discount rate based on the past information. The detailed analysis is as follows.

The principal's preferences as of time 0 will be

$$J_P(0; e, c) = \mathbb{E} \left[ \int_0^T k(t) U(e_t - c_t) dt + k(T) L(-C_T) \right] \quad (3)$$

where  $U$  and  $L$  are utility functions by the principle and  $k(t) = e^{-\int_0^t \delta(s) ds}$  is the discount function. Assume that the utility function  $U(e_t - c_t) = -e^{-\lambda(e_t - c_t)}$  over salary (consumption) and effort and  $L(-C_T) = -e^{-\lambda(-C_T)}$ , where  $\lambda$  is an absolute risk aversion coefficient. Hence, we rewrite (3) as follows:

$$\begin{aligned} J_P(0; e, c) &= \mathbb{E} \left[ \int_0^T e^{-\int_0^t \delta(s) ds} \cdot (-e^{-\lambda(e_t - c_t)}) dt \right. \\ &\quad \left. + e^{-\int_0^T \delta(s) ds} \cdot (-e^{-\lambda(-C_T)}) \right] \\ &= \mathbb{E} \left[ \int_0^T e^{-\bar{\delta}t} (-e^{-\lambda(e_t - c_t + K_t)}) dt \right. \\ &\quad \left. + e^{-\bar{\delta}T} (-e^{-\lambda(-C_T + K_T)}) \right] \end{aligned} \quad (4)$$

where  $K_t = (\int_0^t \delta(s) ds - \bar{\delta}t)/\lambda$  that  $t \in [0, T]$ .

From (4), we can split the principal's discount factor  $\delta$  into two parts under the condition of the exponential utility function: one part is a constant discount rate  $\bar{\delta}$  and another part is  $K_t$ . The purpose of the above operation is that the principal estimates a suitable constant discount rate  $\bar{\delta}$  instead of a time-varying discount rate  $\delta(t)$ , and the principal does not know the exact value of this constant. Therefore, the principal will constantly update the recognition of  $\bar{\delta}$  based on past information.  $c_t$  is the subjective choice of the principal, but  $K_t$  indicates an objective reality, reflects the type of principal (time-inconsistent or time-consistent), and does not depend on the subjective choice of the principal. So we can set  $K_t$  as a part of the output (investment) process. In this way, we can turn the principal's time inconsistency problem into an unknown constant discount rate problem. If the principal is time-consistent, namely, the principal's discount rate is a constant  $\delta_0$ , he can choose  $\delta_0$  as a constant discount rate  $\bar{\delta}$ ; hence  $\delta_0 = \bar{\delta}$  (or  $K_t = 0$ ). Under the probability measure  $\mathbb{P}$  of the principal, we can regard that  $K_t$  is an intrinsic influence of the risk item and is not subject to the control of the principal but must be considered. Hence the risk process (1) becomes

$$dY_t = (e_t - c_t + K_t) dt + \sigma dW_t^{\mathbb{P}} \quad (5)$$

As discussed above, we know that the process  $Y_t$  and the path of  $W_t^0$  are observable from the agent; therefore the measure for the agent is  $\mathbb{P}^0$ , which means that the agent does not learn in secretly, so the agent's beliefs will not be a hidden-state variable ([24]) (this does not mean that the agent cannot mislead the principal by choosing an effort, just that such actions do not cause persistent hidden states according to the agent's beliefs). From (1) we have

$$dY_t = (e_t - c_t) dt + \sigma dW_t^{\mathbb{P}^0} \quad (6)$$

Equation (5) expresses the principal's beliefs about the project and (6) expresses the agent's beliefs. The disagreement between the principal and the agent is caused by principal's nonindex discount.

At time  $t$ , the principal knows the exact value of  $\int_0^t \delta(s) ds$ , because  $\delta(s)$  is his discount rate, but he does not know the exact value of  $\bar{\delta}$ ; therefore we use a sided Bayesian learning model after signed contract, and we assume that the prior about  $K$  at time 0 is normally distributed with mean 0 and variance  $\theta_0$ . The agent does not update his beliefs because he has perfect information. If the agent follows the recommended effort choice  $e$ , the principal's posterior beliefs about  $K_t$  depend on  $Y_t$  and on cumulative effort  $E_t = \int_0^t e_s ds$ .

According to the Kalman-Bucy filter, see [25]. The conditional expectation  $\widehat{K}_t = \mathbb{E}[K_t | Y_t, E_t] = \sigma^{-2}(Y_t - E_t)/\theta_t$  and the precision of filtering  $\theta_t = \mathbb{E}[(K_t - \widehat{K}_t)^{-2}]$  satisfy the system of equations

$$d\widehat{K}_t = \frac{1}{\sigma\theta_t} [dY_t - (e_t - c_t + \widehat{K}_t) dt] \quad (7)$$

$$\theta_t = \theta_0 + \sigma^{-2}t$$

where  $\widehat{K}_0 = 0$  and  $\theta_0 = 0$  and  $Z_t$  is a standard Brownian motion under the measure induced by the effort sequence  $\{e_s : 0 \leq s \leq t\}$  as

$$dZ_t \triangleq \frac{dY_t - (e_t - c_t + \widehat{K}_t) dt}{\sigma} \quad (8)$$

### 3. Incentive Compatible Conditions

In this section, we focus on the agent's problem. Since the agent's objective function relies on the consumption process  $\{c_t\}$ , that is, it relies on the history of the whole output, so it is non-Markov (the specific proof see [6]). Thus, the agent optimization problem cannot be solved by the standard dynamic programming principle. We will employ the stochastic maximum principle of the solution to the weak situation of the agent problem. The main idea is to apply random variational methods; the relative papers [8, 20, 26] used the similar approach.



Define the agent's continuation value (promised utility)  $q_t$  as the expected discounted utility for remaining in the contract from date  $t$  forward

$$q_t = \max_{e \in \mathbf{A}} \mathbb{E} \left[ \int_t^T e^{-\int_t^s \rho(\tau) d\tau} u(c(s, \bar{Y}_s), e_s) ds + e^{-\int_t^T \rho(\tau) d\tau} v(C_T) \mid \mathcal{F}_t^e \right] \quad (9)$$

where  $\bar{Y}_s \triangleq \{Y_t : 0 \leq t \leq s\}$  is the output history. We use  $\Gamma$  to relate the expectation operator  $\mathbb{E}_e[\cdot]$  under the measure  $\mathbb{Q}_e$  (because the agent's objective function depends on the consumption process  $c_t$ , which is non-Markovian since it depends on the whole output path  $\bar{Y}_t$ ; hence the optimization problem (9) cannot be analyzed with standard methods. So we use a martingale approach. Given a contract  $(c, e^*)$ , the agent controls the distribution of salary through his choice of effort. For the specific technical treatment see Appendix A). The agent's objective function can be recast as

$$J_A(0; e, \bar{c}) = \mathbb{E}_e \left[ \int_0^T h(s) u(c(s, \bar{Y}), e_s) ds + h(T) v(C_T) \right] = \mathbb{E} \left[ \int_0^T \Gamma_{t,s} h(s) u(c(s, \bar{Y}), e_s) ds + \Gamma_{t,T} h(T) v(C_T) \right] \quad (10)$$

where  $\bar{c} = c(s, \bar{Y})$  represents the salary paid by the principal based on output history.

After the change of measure, the time-inconsistent agent's problem only has one control. We apply a stochastic maximum principle to characterize the agent's optimality condition, and we also use the dynamic programming equation derive a stochastic maximum principle with general time-inconsistent.

The agent's problem is to find an admissible control to maximize the expected reward  $J_A(0; e, \bar{c})$ . In other words, the agent needs to solve the problem

$$\sup_{e \in \mathbf{A}} J_A(0; e, \bar{c}) \quad (11)$$

Given  $\bar{c}$ , for all  $0 \leq t \leq T$ , subject to

$$d\Gamma_t = \Gamma_t \sigma^{-1} [e_t - c(t, \bar{Y}) + \widehat{K}_t] dZ_t^0 \quad (12)$$

next we define the optimal effort for the time-inconsistent agent. Let  $\varepsilon > 0$  and  $\mathbf{E}_\varepsilon \subseteq [0, T]$  be a measurable set whose Lebesgue measure is  $|\mathbf{E}_\varepsilon| = \varepsilon$ . Let  $e_t \in \mathbf{A}$  be an arbitrary effort choice. We define the following:

$$e_t^\varepsilon = \begin{cases} e_t^*, & t \in [0, T] \setminus \mathbf{E}_\varepsilon, \\ e_t, & t \in \mathbf{E}_\varepsilon. \end{cases} \quad (13)$$

with  $\mathbf{E}_\varepsilon = [0, \varepsilon]$ , and it is clear that  $e_t^\varepsilon \in \mathbf{A}$ . We refer  $e_t^\varepsilon$  as a needle variation of the effort choice  $e_t^*$ . Then, we have following definition.

**Definition 1.** An effort choice  $e_t^*$  is an optimal effort choice for the time-inconsistent agent, for  $t \in (0, T]$ , if

$$\lim_{\varepsilon \rightarrow 0} \frac{J_A(0; e^*, \bar{c}) - J_A(0; e^\varepsilon, \bar{c})}{\varepsilon} \geq 0 \quad (14)$$

The optimal density process  $\{\Gamma^*(t)\}_{t \in [0, T]}$  is a solution of the stochastic differential equation.

$$d\Gamma_t^* = \Gamma_t^* \sigma^{-1} [e_t^* - c(t, \bar{Y}_t) + \widehat{K}(t, Y_t, E_t^*)] dZ_t^0 \quad (15)$$

Through the above technical processing, we convert the time-inconsistent strategy into time consistency optimal strategy of the agent.

Next, we analyze the conditions for the implementation of incentive contract. According to the previous analysis, the agent will control the distribution of salary by choosing his effort. The idea of using the distribution of salary as control to solve principal-agent problem goes back to [27] is and expanded by [5, 20]. The learning process of the principal complicates our problem, as the past effort affects not only current salary but also future expectations of the agent and the principal. Therefore, we have to deal with a principal-agent problem with time inconsistency and learning process. In Appendix B, we show how this difficulty can be handled through an extension of the proof by [8, 20]. And the conclusion presents the following.

**Proposition 2.** The agent's continuation value can be uniquely represented by the following differential form:

$$\begin{aligned} dq_t &= [\rho(t) q_t - u(c_t, e_t^*)] dt + \gamma_t \sigma dZ_t \\ q_T &= v(C_T) \end{aligned} \quad (16)$$

where  $\gamma_t$  is a square integrable predictable process.

The necessary and sufficient conditions for  $e_t^*$  is the optimal effort choice reads:

(i) If  $e_t^*$  is the optimal effort choice, then for every  $t \in [0, T]$  there exists a solution  $\{q_t, \gamma_t\}_{t \in [0, T]}$  of (16) which satisfies (in this paper,  $\partial_e u$  and  $\partial_{ee} u$  represent function  $u$  taking the first-order partial derivative and second-order partial derivative of  $e$ , respectively)

$$\gamma_t + \frac{\sigma^{-2}}{\theta_t} p_t + \partial_e u(c_t, e_t^*) = 0 \quad (17)$$

where

$$p_t \triangleq \theta_t \cdot \mathbb{E} \left[ - \int_t^T e^{-\int_t^s \rho(\tau) d\tau} \gamma_s \theta_s^{-1} ds \mid \mathcal{F}_t^e \right] \quad (18)$$

(ii) For almost all  $t$ , if the following inequality holds

$$-2h(t) \partial_{ee} u(c_t, e_t) \geq \sigma^2 \xi_t \theta_t \quad (19)$$

where  $\xi$  is the predictable process defined by

$$\begin{aligned} & \mathbb{E} \left[ - \int_0^T e^{-\int_0^s \rho(\tau) d\tau} \gamma_s \frac{\sigma^{-2}}{\theta_s} ds \mid \mathcal{F}_t^{e^*} \right] \\ & - \mathbb{E} \left[ - \int_0^T e^{-\int_0^s \rho(\tau) d\tau} \gamma_s \frac{\sigma^{-2}}{\theta_s} ds \mid \mathcal{F}_0^{e^*} \right] \quad (20) \\ & = \int_0^t \xi_s \sigma dZ_s \end{aligned}$$

then  $e_t^*$  is the optimal effort choice.

According to (18), we say that  $p_t$  is a stochastic process capturing the value of private information and then obtain the solution

$$p_t = \mathbb{E} \left[ \int_t^T h(s-t) \partial_e u(c_s, e_s) ds \mid \mathcal{F}_t^e \right] \quad (21)$$

for all  $s \in [t, T]$ .

In the following, at any time  $e_s^* > 0$ , the process for  $p$  reads

$$\begin{aligned} dp_t &= [\rho_t p_t - \partial_e u(c_t, e_t)] dt + \vartheta_t \sigma dZ_t \\ p_T &= 0. \end{aligned} \quad (22)$$

the coefficients  $\vartheta$  is chosen by the principal to maximize his expected utility (the proof is given by [20])

According to (19), the process  $\xi_t$  is the random fluctuation in the discounted sum of marginal utilities evaluated from time 0. Based on the stochastic differential equation of  $p_t$ , we can obtain that  $\xi_t = e^{-\int_0^t \rho(s) ds} \sigma \theta_t$ . Besides that,  $c_t$ ,  $e_t$ ,  $\gamma_t$ , and  $\xi_t$  are endogenous, which implies that we need to get a contract to satisfy the necessary conditions and then prove that it also meets the sufficient conditions. If the contract has no explicit solution, it will be difficult to prove that the contract also satisfies the sufficient condition. In this paper, the utility function for the principal is exponential function and the utility function for the agent is linear function. In the next section we will employ the exponential utility function to get the closed-loop solution of the contract.

#### 4. The Optimal Contract

This section detailedly explains how to solve the principal's problem and derive the optimal contract in closed form when the principal's utility is exponential.

**Eliminating  $\widehat{K}$  from the list states.** For a given contract  $(c, e^*)$ , the principal expected utility form data  $t$  forward reads

$$\begin{aligned} \Pi_t(c, e^*) &\triangleq \mathbb{E} \left[ \int_t^T e^{-\bar{\delta}(s-t)} \left( -e^{-\lambda(e_s - c_s + \widehat{K}_s)} \right) ds \right. \\ &\quad \left. + e^{-\bar{\delta}(T-t)} \cdot \left( -e^{-\lambda(-C_T + \widehat{K}_T)} \right) \mid \mathcal{F}_t^Y \right] \end{aligned} \quad (23)$$

and defines

$$\begin{aligned} J_P(t, c, e^*) &\triangleq \mathbb{E} \left[ \int_t^T e^{-\bar{\delta}(s-t)} \cdot \left( -e^{-\lambda(e_s - c_s)} \right) ds \right. \\ &\quad \left. + e^{-\bar{\delta}(T-t)} \cdot \left( -e^{-\lambda(-C_T)} \right) \mid \mathcal{F}_t^Y \right] \end{aligned} \quad (24)$$

and we have the following result.

**Proposition 3.**

$$\max_{c, e} \Pi_t(c, e^*) \iff \max_{c, e} J_P(t, c, e^*) \quad (25)$$

*Proof in Appendix C.*

Assume that Propositions 2 and 3 hold, so that the necessary condition is also sufficient. The principal's problem consists of solving for  $J_P(t, c, e)$  subject to the two promise-keeping constraints (9) and (18) and also to the incentive constraint (17). Given that the posterior mean  $\widehat{K}$  does not enter directly into any of the constraints, it can be dispensed as a state, only leaving the precision as a belief state. Furthermore, since  $\theta_t$  is deterministic, we may index the precision by  $t$ . The fact is that the expected value of  $K_t$  is immaterial to the principal's objective and illustrates that incentives are designed to reward effort, not to ability.

**The Agent's utility function.** To obtain the solution of optimal contract, according to our assumption in Section 2.1, the agent is risk-neutral and the utility functions of the agent are linear, i.e.,

$$u(c, e) = c - \frac{e^2}{2}; \quad (26)$$

moreover, we make a particular assumption about the terminal utility for the agent, setting

$$v(C_T) = a + \ln C_T \quad (27)$$

where  $a$  is a constant. This assumption implies a situation in which an infinitely lived agent retires at the termination date  $T$  of the contract and, after retirement, he can consume a permanent annuity derived from  $C_T$ . We always concentrate on problems where the contracting horizon goes to infinity  $T \rightarrow \infty$ , so this particular assumption  $v$  is not critical.

**Incentive providing contracts.** Restore the principal's optimization problem as

$$V_t \triangleq \max_{c, \gamma, \vartheta} \mathbb{E} \left[ \int_t^T e^{-\bar{\delta}(s-t)} \cdot \left( -e^{-\lambda(e_s - c_s)} \right) ds + e^{-\bar{\delta}(T-t)} \cdot \left( -e^{-\lambda(-C_T)} \right) \mid \mathcal{F}_t^Y \right] \quad (28)$$



subject to

$$dq_t = [\rho_t q_t - u(c_t, e_t)] dt + \gamma_t \sigma dZ_t, \quad q_T = v(C_T) \quad (29)$$

$$dp_t = [\rho_t p_t - \partial_e u(c_t, e_t)] dt + \vartheta \sigma dZ_t, \quad p_T = 0 \quad (30)$$

$$\gamma_t = -\partial_e u(c_t, e_t) - \frac{\sigma^{-2}}{\theta_t} p_t \quad (31)$$

Since the state variables  $q_t$  and  $p_t$  are Markovian processes, we can use the HJB equation to analyze the principal's optimal control problem. Take  $V(t, q, p)$  as the principal's value function; this value function satisfies the HJB equation for  $0 < t < T$ :

$$\begin{aligned} \bar{\delta}V - \partial_t V = \max_{c, e, \gamma, \vartheta} & \left\{ -e^{-\lambda(e-c)} + \partial_q V \cdot [\rho_t q - u(c, e)] \right. \\ & + \partial_p V \cdot [\rho_t p - \partial_e u(c, e)] + \frac{1}{2} \sigma^2 [\partial_{qq} V \cdot \gamma(p, c, e)^2 \\ & \left. + \partial_{pp} V \cdot \vartheta^2 + 2\partial_{pq} V \cdot \vartheta \gamma(p, c, e)] \right\} \end{aligned} \quad (32)$$

#### 4.1. Second Best Contracts for the Time-Consistent Principal.

In this section, we mainly consider that the model with the time-consistent principal and setting hidden action means that the principal can observe the process  $Y_t$  but does not know the type of agent and also cannot observe the agent's effort  $e_t$ . For incentive contracts  $(e, c) : e_t > 0$ , for any  $t \geq 0$ , the necessary condition for incentive compatibility (17) becomes  $\gamma_t = -\partial_e u(c_t, e_t)$ . When the principal is time-consistent, it expresses that  $\delta_t = \bar{\delta}$  for all  $t \in [0, T]$ ; hence we say  $K = 0$ . There is no need to inquire  $K$  and there is no influence of belief manipulation, which indicates that the information value  $p$  is equal to zero.

**4.1.1. The HJB Equation.** When the time tends to infinity ( $T \rightarrow \infty$ ), the agent's continuous value function  $q$  is the only state variable for writing the principal's HJB equation as follows:

$$\begin{aligned} \bar{\delta}V - \partial_t V = \max_{c, e, \gamma} & \left\{ -e^{-\lambda(e-c)} + \partial_q V \right. \\ & \cdot \left[ \rho q - \left( c - \frac{e^2}{2} \right) \right] + \frac{1}{2} \sigma^2 \partial_{qq} V \cdot \gamma^2(c, e) \left. \right\} \end{aligned} \quad (33)$$

with the terminal condition  $V(T, q_T) = L(-C_T)$ , where  $q_T = v(C_T)$ . Taking the first-order conditions for  $(e, c)$ , we have

$$\begin{aligned} \lambda e^{-\lambda(e-c)} + \partial_q V \cdot e + \partial_{qq} V \cdot e \sigma^2 &= 0 \\ -\lambda e^{-\lambda(e-c)} - \partial_q V &= 0 \end{aligned} \quad (34)$$

Under full information, the principal can observe the agent's effort and consumption and there is no private information in this case. Hence, the principal can freely choose  $\gamma_t$  as parts of the contract; i.e.,  $\gamma$  is independent of  $c$  and  $e$ , and then we have the following proposition.

**Proposition 4.** *Under full information, the optimal effort for the principal is a constant  $e^* = 1$ . We say  $e^* = 1$  is the first best effort level.*

Under hidden action case, the optimal effort and consumption derived from (34) shows

$$\begin{aligned} e_t^* &= \frac{\partial_q V}{\partial_q V + \sigma^2 \partial_{qq} V}, \\ c_t^* &= \frac{\partial_q V}{\partial_q V + \sigma^2 \partial_{qq} V} + \frac{1}{\lambda} \ln \left( \frac{-\partial_q V}{\lambda} \right) \end{aligned} \quad (35)$$

Putting (35) into (33), the HJB equation (33) for the value function  $V(t, q)$  is rewritten as

$$\begin{aligned} \bar{\delta}V - \partial_t V &= \frac{\partial_q V}{\lambda} + \partial_q V \cdot \rho q - \partial_q V \\ &\cdot \left[ \frac{\partial_q V}{\partial_q V + \sigma^2 \partial_{qq} V} + \frac{1}{\lambda} \ln \left( \frac{-\partial_q V}{\lambda} \right) \right] \\ &+ \frac{\partial_q V}{2} \cdot \left( \frac{\partial_q V}{\partial_q V + \sigma^2 \partial_{qq} V} \right)^2 + \frac{1}{2} \sigma^2 \partial_{qq} V \\ &\cdot \left( \frac{\partial_q V}{\partial_q V + \sigma^2 \partial_{qq} V} \right)^2 \end{aligned} \quad (36)$$

Recalling the principal with the exponential utility function, the HJB equation is a complex nonlinear partial differential equation. It is difficult to take the classic separation of the variable method and solve it intuitively. In the next, we will employ the Legendre transform to turn the problem into a dual problem, by solving the dual problem to obtain the optimal solution for the original problem.

**4.1.2. Legendre Transform.** The dual function of  $V$  is defined by

$$\begin{aligned} \widehat{V}(t, z) &= \sup_{q>0} \{V(t, q) - qz\} \\ g(t, z) &= \inf_{q>0} \{q \mid V(t, q) \geq \widehat{V}(t, z) + qz\} \end{aligned} \quad (37)$$

where  $z < 0$  is the dual variable of  $q$ . The function  $g(t, z)$  is closely related to  $\widehat{V}(t, z)$  and can be used as a dual function of the function  $V(t, q)$ . In this paper,  $g(t, z)$  is defined as the dual function of  $V(t, q)$  and satisfies

$$g(t, z) = -\partial_z \widehat{V}(t, z) \quad (38)$$

According to the definition of the dual function, we have  $z = \partial_q V(t, q)$  and

$$\begin{aligned} g(t, z) &= q \\ \widehat{V}(t, z) &= V(t, q) - zg(t, z) \end{aligned} \quad (39)$$

Based on the conclusion in [28], the following transformation rules are obtained:

$$\begin{aligned}\partial_t V &= \partial_t \widehat{V}, \\ \partial_q V &= z, \\ \partial_{qq} V &= -\frac{1}{\partial_{zz} \widehat{V}}\end{aligned}\quad (40)$$

Define the dual function of the utility function as

$$\widehat{U}(t, z) = \sup_{x>0} \{U(t, x) - xz\} \quad (41)$$

$$G(t, z) = \inf_{x>0} \{x \mid U(t, x) \geq \widehat{U}(t, z) + xz\}$$

With the analysis from [29], the function  $U(x)$  and  $\widehat{U}(z)$  can be changed to pass the Legendre conversion

$$\widehat{U}(z) = \sup_{x>0} \{U(x) - xz\} \quad (42)$$

$$U(x) = \inf_{z>0} \{\widehat{U}(z) + xz\}$$

The relationship between the optimal values  $x^*$  and  $z^*$  is

$$\begin{aligned}z_t^* &= (\widehat{U}')^{-1}(-x_t^*), \\ x_t^* &= e^{\int_0^t \rho(s)ds} (U')^{-1}(z_t^*),\end{aligned}\quad (43)$$

$$Y_T^* - C_T^* = (L')^{-1}(z_T^*)$$

According to equation (39) and rules (40), the HJB equation for the dual problem is

$$\begin{aligned}\bar{\delta} \widehat{V} - \partial_t \widehat{V} &= \left( \frac{1}{\lambda} + \rho g - \bar{\delta} g \right) z - \frac{z}{\lambda} \ln \left( \frac{-z}{\lambda} \right) \\ &\quad - \frac{1}{2} \frac{z^2 \cdot \partial_{zz} \widehat{V}}{z \cdot \partial_{zz} \widehat{V} - \sigma^2}\end{aligned}\quad (44)$$

Taking the derivative of  $z$  and combining (35), we have

$$\begin{aligned}-\bar{\delta} g + \partial_t g &= -\bar{\delta} g - \bar{\delta} z \cdot \partial_z g + \rho g + \rho z \cdot \partial_z g \\ &\quad - \frac{1}{\lambda} \ln \left( \frac{-z}{\lambda} \right) - \frac{1}{2} + \frac{\sigma^2 (\sigma^2 - z^2 \cdot \partial_{zz} g)}{2 (z \cdot \partial_z g + \sigma^2)^2}\end{aligned}\quad (45)$$

**4.1.3. Solution of the HJB Equation.** According to the form of the principle's utility function, we have

$$G(T, z) = \frac{1}{\lambda} \ln \left( \frac{-z}{\lambda} \right) \quad (46)$$

We can assume that HJB equation (36) has the following form of solution:

$$g(t, z) = \frac{e^{\int_0^t \rho(s)ds}}{\lambda} \phi(t) \ln \left( \frac{-z}{\lambda} \right) + \varphi(t) \quad (47)$$

with  $\phi(T) = h(T)$ ,  $\varphi(T) = 0$ .

$$\begin{aligned}\partial_t g &= \frac{1}{\lambda} \left( \frac{\partial_t \phi \cdot h - \phi \cdot \partial_t h}{h^2} \right) \ln \left( \frac{-z}{\lambda} \right) + \partial_t \varphi \\ \partial_z g &= \frac{\phi}{\lambda h z}, \\ \partial_{zz} g &= -\frac{\phi}{\lambda h z^2}\end{aligned}\quad (48)$$

plug in (45) and separate the variables; then we have

$$\begin{aligned}0 &= -\frac{1}{\lambda h} \ln \left( \frac{z}{\lambda} \right) [\partial_t \phi + h] \\ &\quad + \frac{\phi}{\lambda h} \left[ \rho - \bar{\delta} - \frac{1}{2(\sigma^2 + \phi/\lambda h)} \right] + (\rho \varphi - \partial_t \varphi)\end{aligned}\quad (49)$$

Thus, the following two ordinary differential equations are established:

$$\begin{aligned}\partial_t \phi + h &= 0, \\ \phi(T) &= h(T)\end{aligned}\quad (50)$$

$$\begin{aligned}\partial_t \varphi - \rho \varphi + \frac{\phi}{\lambda h} \left[ \bar{\delta} - \rho(t) + \frac{1}{2(\sigma^2 + \phi/\lambda h)} \right] &= 0, \\ \varphi(T) &= 0\end{aligned}\quad (51)$$

**Proposition 5.** Assume that (i) the principal is time-consistent and the agent is time inconsistent, (ii)  $u(c, e)$  and  $v(C)$  are as defined in (26) and (27), and (iii)  $e_t^* > 0$  for all  $t$ , so that the incentive constraint (17) binds for almost all  $t \in [0, T]$ . Then recommended effort and the agent's consumption is given by

$$c_t^* = \frac{\phi/h}{\phi/h + \lambda \sigma^2} + \frac{h}{\phi} q - \frac{h}{\phi} \varphi \quad (52)$$

$$e_t^* = \frac{\phi/h}{\phi/h + \lambda \sigma^2}$$

where

$$\begin{aligned}\phi(t) &= h(T) + \int_t^T h(s) ds, \\ \varphi(t) &= \int_t^T \left[ e^{-\int_t^\tau \rho(s)ds} \frac{\phi}{\lambda h \rho} \left( \bar{\delta} - \rho + \frac{1}{2(\sigma^2 + \phi/\lambda h)} \right) \right] d\tau\end{aligned}\quad (53)$$

**4.2. Second Best Contracts for the Time-Inconsistent Principal.** In this section, we discuss the case when the principal is time-inconsistent, which means the discount rate  $\delta$  is not a constant. In this case, the principal still cannot observe the agent's efforts and consumption (moral hazard). Hence,

the value of private information is not zero. As described in Section 3, the HJB equation is as follows:

$$\begin{aligned} \bar{\delta}V - \partial_t V = \max_{c, e, \gamma, \vartheta} & \left\{ -e^{-\lambda(e-c)} + \partial_q V \cdot \left( \rho q - c + \frac{e^2}{2} \right) \right. \\ & + \partial_p V \cdot (\rho p + e) + \frac{1}{2} \sigma^2 \left[ \partial_{qq} V \cdot \left( e - \frac{\sigma^{-2}}{\theta} p \right)^2 \right. \\ & \left. \left. + \partial_{pp} V \cdot \vartheta^2 + 2\partial_{pq} V \cdot \vartheta \left( e - \frac{\sigma^{-2}}{\theta} p \right) \right] \right\} \end{aligned} \quad (54)$$

Now we need to solve this above equation by guessing the solution. Under the first-order conditions for  $(e, c, \vartheta)$ , we have

$$\begin{aligned} \lambda e^{-\lambda(e-c)} + \partial_p V & \\ + \left[ \partial_q V + \sigma^2 \frac{\partial_{pp} V \cdot \partial_{qq} V - (\partial_{pq} V)^2}{\partial_{pp} V} \right] \cdot e & \\ - \frac{\partial_{pp} V \cdot \partial_{qq} V - (\partial_{pq} V)^2}{\partial_{pp} V} \cdot \frac{p}{\theta} = 0 & \quad (55) \\ - \lambda e^{-\lambda(e-c)} - \partial_q V = 0 & \\ \vartheta = -\frac{\partial_{pq} V}{\partial_{pp} V} \gamma & \end{aligned}$$

Substituting (55) into (54), denoting that  $\tilde{V} = (\partial_{pp} V \cdot \partial_{qq} V - (\partial_{pq} V)^2)/\partial_{pp} V$ , we have

$$\begin{aligned} \partial_t V - \bar{\delta}V + \frac{\partial_q V}{\lambda} + \partial_q V \left[ \rho_t q - \frac{1}{\lambda} \ln \left( -\frac{\partial_q V}{\lambda} \right) \right] + \partial_p V & \\ \cdot \rho_t p - \frac{1}{2} \tilde{E} + \frac{\sigma^{-2} p^2}{2\theta^2} \tilde{V} = 0 & \quad (56) \end{aligned}$$

where  $\tilde{E} = ((p/\theta)\tilde{V} + \partial_q V - \partial_p V)^2/(\sigma^2 \tilde{V} + \partial_q V)$ .

In particular, we suppose the value function has the following form:

$$V(t, p, q) = -e^{\lambda[A(t)q + g(t, p)]} \quad (57)$$

with  $A(T) = 1$  and  $g(T, p) = 0$ .

Hence, for some functions  $A(t)$  and  $g(t, p)$ , the expressions of optimal effort and consumption are

$$\begin{aligned} e_t^* & \\ = \frac{\lambda A^2 \partial_{pp} g(p/\theta) + (A - \partial_p g) (\partial_{pp} g + \lambda (\partial_p g)^2)}{\lambda A^2 \partial_{pp} g \sigma^2 + A \partial_{pp} g + \lambda A (\partial_p g)^2} c_t^* & \quad (58) \\ = e_t^* + \frac{\ln A}{\lambda} + Aq + g & \end{aligned}$$

Substituting the optimal effort and consumption into (54), we deduce

$$\begin{aligned} \lambda [A_t + A\rho - A^2] q + \lambda \partial_t g - \bar{\delta} + A - A \ln A - \lambda A g & \\ + \rho \lambda p \partial_p g + \lambda A \left( \frac{\sigma^{-4}}{2\theta^2} p^2 - \frac{\sigma^{-2}}{\theta} p \right) & \quad (59) \\ + \frac{\lambda \sigma^{-2} \partial_p g}{\theta} p - \frac{\lambda}{2} \tilde{E} = 0 & \end{aligned}$$

where  $\tilde{E} = ((\partial_{pq} g + \lambda(\partial_p g)^2) \cdot ((p/\theta)\sigma^{-2} A + \partial_p g - A)^2)/(\lambda \sigma^2 A^2 \partial_{pq} g + A(\partial_{pp} g + \lambda(\partial_p g)^2))$ .

The following two differential equations can be obtained by eliminating the dependence on  $q$ :

$$\partial_t A + A\rho(t) - A^2 = 0, \quad A(T) = 1 \quad (60)$$

$$\begin{aligned} \partial_t g - \frac{1}{\lambda} (\bar{\delta} - A + A \ln A) - Ag + \rho p \partial_p g & \\ + A \left( \frac{\sigma^{-4}}{2\theta^2} p^2 - \frac{\sigma^{-2}}{\theta} p \right) + \frac{\sigma^{-2} \partial_p g}{\theta} p - \frac{1}{2} \tilde{E} = 0, & \quad (61) \\ g(T, p) = 0 & \end{aligned}$$

According to (60), we can obtain

$$A(t) = \frac{1}{e^{-\int_t^T \rho(s) ds} + \int_t^T e^{-\int_t^\tau \rho(s) ds} d\tau} \quad (62)$$

From the above analysis, we need to know the specific expressions of  $g(t, p)$  to get the explicit expression of effort  $e(t)$  and consumption  $c(t)$ .

Let us expand  $g(t, p)$  at  $p = 0$ ,

$$\begin{aligned} g(t, p) &= g(t, 0) + g_p(t, 0)p + \frac{g_{pp}(t, 0)}{2} p^2 + \dots \\ &+ \frac{g^{(n)}(t, 0)}{n!} p^n + \dots \quad (63) \\ &\triangleq \tilde{A}(t) + \tilde{B}(t)p + \tilde{C}(t)p^2 + \dots \end{aligned}$$

Here we consider a simple situation; according to the principal's utility function  $U = -e^{-\lambda(e-c)}$  and  $dp(t)/dt = \rho(t)p(t) + e(t)$ , suppose the structure of the solution of equation (61) is  $g(t, p) = \tilde{A}(t) + \tilde{B}(t)p$  with the terminal condition  $\tilde{A}(T) = 0$  and  $\tilde{B}(T) = \rho(T)$ .

**Lemma 6.** Suppose the structure of solution of (61) is  $g(t, p) = \tilde{A}(t) + \tilde{B}(t)p$ , with the terminal condition  $\tilde{A}(T) = 0$  and  $\tilde{B}(T) = 1$ , and then  $\tilde{A}(t)$  and  $\tilde{B}(t)$  are, respectively, the solutions of the following differential equations:

$$\tilde{A}(t) = - \int_t^T \left[ e^{-\int_t^\tau A(s) ds} \cdot D(\tau) \right] d\tau \quad (64)$$

$$\tilde{B}(t) = \rho(T) e^{\int_t^T [\rho(s) - A(s)] ds}$$

where  $D(\tau) = (1/\lambda)(\bar{\delta} - A(\tau) + A(\tau) \ln A(\tau)) + (A^2(\tau) + \bar{B}^2(\tau))/2A(\tau)$ .

It is proved as follows.

Substituting  $g(t, p) = \bar{A}(t) + \bar{B}(t)p$  into (61), we calculate to get

$$\left[ \partial_t \bar{A} - A\bar{A} - \frac{1}{\lambda} (\bar{\delta} - A + A \ln A) - \frac{A^2 + \bar{B}^2}{2A} \right] + [\partial_t \bar{B} - A\bar{B} + \rho \bar{B}] p = 0 \quad (65)$$

The following two differential equations can be obtained by eliminating the dependence on  $p$ :

$$\begin{aligned} \partial_t \bar{A} - A\bar{A} - \frac{1}{\lambda} (\bar{\delta} - A + A \ln A) - \frac{A^2 + \bar{B}^2}{2A} &= 0 \\ \partial_t \bar{B} - A\bar{B} + \rho \bar{B} &= 0 \end{aligned} \quad (66)$$

Lemma 6 conclusion can be provided by solving the above two differential equations.

**Proposition 7.** *When the principal is time-inconsistent, the expressions of optimal effort and consumption for the agent are*

$$\begin{aligned} e^*(t) &= 1 - \frac{\bar{B}(t)}{A(t)} \\ c^*(t) &= e^*(t) + \frac{\ln A(t)}{\lambda} + A(t)q(t) + \bar{A}(t) \\ &\quad + \bar{B}(t)p(t) \end{aligned} \quad (67)$$

where  $A(t)$ ,  $\bar{A}(t)$ , and  $\bar{B}(t)$  are given by (62) and (64), respectively.

It can be seen from the proposition that the second optimal effort is less than the first optimal effort. The optimal consumption is the linear function of the agent's promise value and private information.

## 5. Numerical Simulation

In this section, we provide a numerical simulation to characterize the dynamic behavior of the optimal portfolio strategy derived in the previous section. Firstly, an optimal effort numerical simulation is performed when the principal was time-consistent.

As shown in Figure 1, the discount rate of the agent is taken as the constant discount rate, namely,  $\rho(t) = \bar{\rho}$ . The optimal effort, under different volatility, is reduced with the increase of volatility. It also shows that the greater the uncertainty, the lower the efforts of the agent. In addition, the three curves are almost declining, indicating that effort is a decreasing function of time.

If we take the discount rate of the agent as  $dp(t)/dt = \bar{\rho} - \rho(t)$ , i.e.,  $\rho(t) = \bar{\rho} + e^{-t}$ , where  $\bar{\rho} = 0.1$  and  $\sigma = 0.1; 0.2; 0.5$ , respectively. The curves of effort variation are drawn in Figure 2.

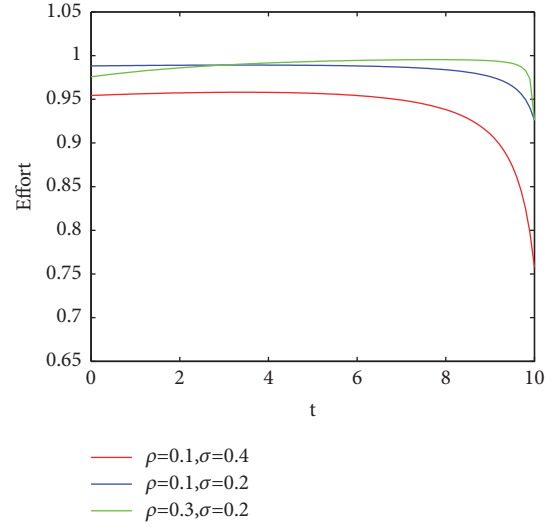


FIGURE 1: The efforts of constant discount rate for different uncertainty  $\sigma$ .

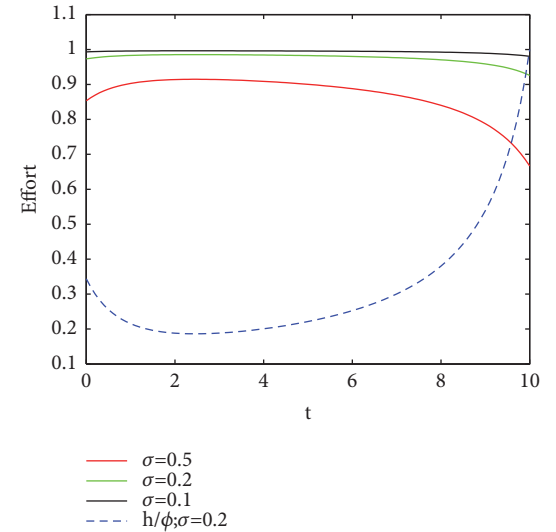


FIGURE 2: The efforts of variable discount rate for different uncertainty  $\sigma$ .

Analogy with Figure 1, although the discount function is different, we still can get the similar conclusion, which means that the greater the uncertainty for any type of agent is (whether he is time-consistent or time-inconsistent), the less effort he provides. The reason is that in the case of moral hazard, the principal cannot distinguish the influence of the agent's efforts and uncertainty on the risk project's return.

Next, we simulate the optimal consumption (salary) under the specific parameters. Let  $\rho(t) = \bar{\rho} = \bar{\delta}$ ,  $\lambda = \phi/h\rho$ , and  $\sigma^2 = 0.25$ . According to the expression of  $\varphi$ , we have

$$\varphi(t) = \frac{1 - e^{\rho(t-T)}}{2(\rho^2 + \sigma^2)} \quad (68)$$

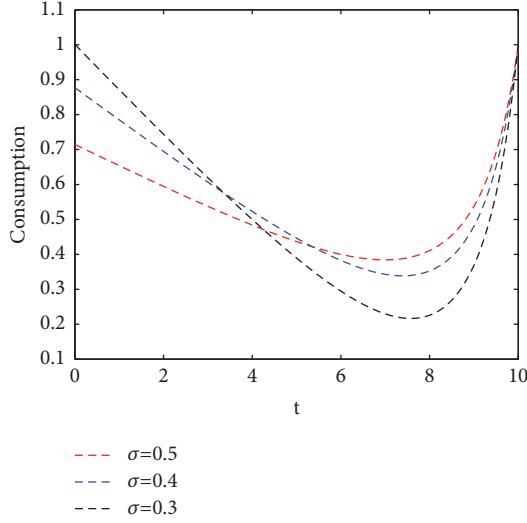


FIGURE 3: The consumption of constant discount rate for different uncertainty  $\sigma$ .

Since  $q$  is a stochastic process, the mathematical expectation of  $q$  can be expressed as

$$q(t) = e^{-\int_t^T (\rho - h(s)/\phi(s)) ds} \cdot v(C(T)) - \mathbb{E} \left[ \int_t^T e^{-\int_t^\tau (\rho - h(s)/\phi(s)) ds} \cdot \left[ e(\tau) - \frac{e(\tau)^2}{2} - \frac{h(\tau)}{\phi(\tau)} \varphi(\tau) \right] d\tau \right] \quad (69)$$

where  $q(T) = v(c(T)) \triangleq a + \ln c(T)$  within a constant  $a$ . Then we substitute the expressions of  $e$ ,  $q$  and  $\varphi$  into the above expression; the relationship between  $c(t)$  and time  $t$  can be simulated with the terminal condition  $c(T) = 1$ .

Consumption is initially diminishing because the effort is a function that decreases monotonically over time. After falling to a certain value, the bottoming out of consumption rose and this trend can be explained by the value of terminal condition of consumption setting. The overall consumption trend is shown in Figure 3.

As shown in Figure 3, in the period of time just after the contract has been performed (for example  $t \in [0, 5]$ ), the greater the volatility, the lower the consumption. The reason is that greater volatility leads to lower efforts. In the latter part of the contract, the situation is just the opposite.

Finally, we simulate the optimal effort trend when the principal is time-inconsistent. Assuming that the discount rate for the agent is the constant discount rate, then two different effort curves are both horizontal lines, as Figure 4 shows. This indicates that, under the established discount rate, the optimal effort does not change over time. The reason is that we hypothesize the value function of principal as an exponential function under private information. And also, the effort is a decreasing function of the agent discount rate, which means that if the agent pays more attention to the present value (timely enjoyment), the higher discount rate and the less effort provided.

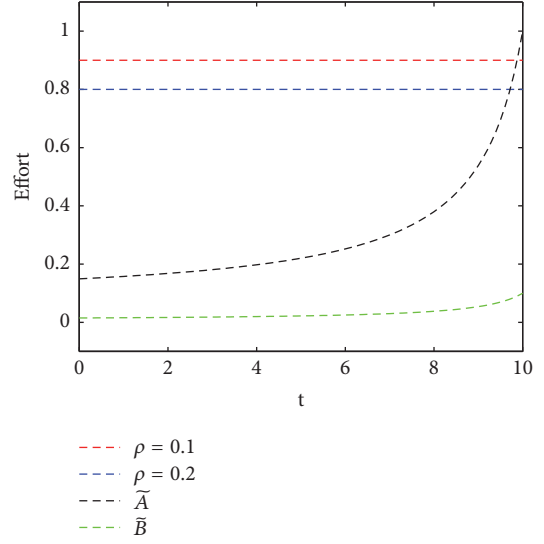


FIGURE 4: The efforts with time-inconsistent principle for different uncertainty  $\rho$ .

## 6. Conclusion

In this paper, we were interested in a time-inconsistent principal-agent problem under full information and moral hazard framework. In particular, the optimal contracts we discussed in details assume that the principal is risk aversion and the agent is risk-neutral. There are two main works we have done in the paper. First, we made the technical processing of the time-inconsistent principal and agent, respectively. We transformed the principal by the changing of the time-varying discount rate into the time-consistent. And we used the Markov subgame perfect Nash equilibrium method to get the time consistency strategy for the time-inconsistent agent. Second, we used the Legendre transform duality theory to transform the HJB equation into the dual equation. The solution of the original HJB equation was obtained smoothly, thus obtaining the explicit expression of the optimal effort and optimal consumption. Under moral hazard, we also obtained the exact solution of the original HJB equation by using the guessing solution. We found that the optimal consumption of agent is a linear function of promised value  $q$  and private information  $p$ . The optimal effort is the function of the agent discount rate. Eventually, we considered the contractual relationship between the principal and the agent in a special circumstances. The more general situations of time-inconsistent contracts should be considered in future research.

## Appendix

### A. Details of the Change of Measure

Consider the Brownian motion  $Z^0$  under a probability space with probability measure  $\mathbb{Q}$ . And let

$$dY_t = \sigma dZ_t^0 \quad (A.1)$$

so that  $Y_t$  is also a Brownian motion under  $\mathbb{Q}$ . Given a contract  $c(t, \bar{Y}_t)$ , we define the drift of output as

$$f(t, \bar{Y}, e_t) = e_t - c(t, \bar{Y}) + \widehat{K}_t \quad (\text{A.2})$$

Since expected output is linear in cumulative output, then we define a  $\mathcal{F}_t$ -predictable process with an effort  $e \in \mathbf{A}$ :

$$\begin{aligned} \Gamma_{0,t}(e) = \exp \left( \int_0^t \sigma^{-1} f(t, \bar{Y}, e_\tau) dZ_\tau^0 \right. \\ \left. - \frac{1}{2} \int_0^t \left| \sigma^{-1} f(t, \bar{Y}, e_\tau) \right|^2 d\tau \right) \end{aligned} \quad (\text{A.3})$$

for  $0 \leq t \leq T$ , and  $\Gamma_t$  is an  $\mathcal{F}_t$ -martingale with  $\mathbb{E}(\Gamma_T(e)) = 1$  for all  $e \in \mathbf{A}$ . By Girsanov theorem, the defined new measure  $\mathbb{Q}_e$  is as

$$\frac{d\mathbb{Q}_e}{d\mathbb{Q}} = \Gamma_T(e) \quad (\text{A.4})$$

and the process  $Z_t^e$  defined by

$$Z_t^e = Z_t^0 - \int_0^t \sigma^{-1} f(t, \bar{Y}, e_\tau) d\tau \quad (\text{A.5})$$

is a Brownian motion under  $\mathbb{Q}_e$ , and the triple  $(Y, Z^e, \mathbb{Q}_e)$  is a weak solution of the following SDE:

$$dY_t = f(t, \bar{Y}, e_t) dt + \sigma dZ_t^e \quad (\text{A.6})$$

Hence each effort choice  $e$  results in a different Brownian motion.  $\Gamma_t$  defined above satisfied  $\Gamma_t = \mathbb{E}(\Gamma_T \mid \mathcal{F}_t)$  which is the relative process for the change of measure.

## B. The Proof of Proposition 2

Consider the agent problem and suppose  $c(t, \bar{Y}_t)$  is given; in general we assume  $c = 0$  to ease the presentation. Let  $\{\Gamma_t^\varepsilon\}_{t \in [0, T]}$  be the density process corresponding to  $\{e_t^\varepsilon\}_{t \in [0, T]}$ , i.e.,

$$d\Gamma_t^\varepsilon = \Gamma_t^\varepsilon \sigma^{-1} \left[ e_t^\varepsilon + \widehat{K}(t, Y_t, E_t^\varepsilon) \right] dZ_t^0 \quad (\text{B.1})$$

Processes  $\{Y_t^\varepsilon\}_{t \in [0, T]}$  and  $\{Z_t^\varepsilon\}_{t \in [0, T]}$  are defined by the SDE

$$\begin{aligned} dY_t^\varepsilon = \sigma^{-1} \left\{ Y_t^\varepsilon \left[ e_t^\varepsilon + \widehat{K}(t, Y_t, E_t^\varepsilon) \right] \right. \\ \left. + \Gamma_t^* \left[ (e_t - e_t^*) + \left( \widehat{K}(t, Y_t, E_t) - \widehat{K}(t, Y_t, E_t^*) \right) \right] \right. \\ \left. \cdot \chi_{E_e}(t) \right\} dZ_t^0 \end{aligned} \quad (\text{B.2})$$

$$Y_0^\varepsilon = 0$$

and

$$\begin{aligned} dZ_t^\varepsilon = \sigma^{-1} \left\{ Z_t^\varepsilon \left[ e_t^\varepsilon + \widehat{K}(t, Y_t, E_t^\varepsilon) \right] \right. \\ \left. + Y_t^\varepsilon \left[ (e_t - e_t^*) + \left( \widehat{K}(t, Y_t, E_t) - \widehat{K}(t, Y_t, E_t^*) \right) \right] \right. \\ \left. \cdot \chi_{E_e}(t) \right\} dZ_t^0 \end{aligned} \quad (\text{B.3})$$

$$Z_0^\varepsilon = 0$$

can be regarded as the first-order and the second-order variation of the density process  $\{\Gamma_t^\varepsilon\}_{t \in [0, T]}$ .

From the reference of Theorem 4.4 in Chapter 3. in [30], the following expansion holds:

$$\begin{aligned} J_A(0; e_t^\varepsilon) - J_A(0; e_t^*) &= \mathbb{E} \left\{ v(C_T^*) (Y_T^\varepsilon + Z_T^\varepsilon) \right\} \\ &+ \mathbb{E} \int_0^T \left\{ h(t) (Y_t^\varepsilon + Z_t^\varepsilon) u(e_t) \right. \\ &\left. + h(t) \Gamma_t^* [u(e_t) - u(e_t^*)] \chi_{E_e}(t) \right\} dt + o(\varepsilon) \end{aligned} \quad (\text{B.4})$$

Define the adjoint variables  $\{M(t), N(t)\}_{t \in [0, T]}$  as follows:

$$\begin{aligned} dM(t) &= - \left[ N(t) \sigma^{-1} (e_t^* + \widehat{K}(t, Y_t, E_t^*)) \right. \\ &\left. + h(t) u(c_t, e_t^*) \right] dt + N(t) dZ_t \\ M(T) &= h(T) v(C_T) \end{aligned} \quad (\text{B.5})$$

Using adjoint processes  $\{M(t), N(t)\}_{t \in [0, T]}$  to partial integration, we can remove  $\{Y_t^\varepsilon\}_{t \in [0, T]}$ ,  $\{Z_t^\varepsilon\}_{t \in [0, T]}$  in the above equation.

Now we introduce the Hamiltonian function  $\mathcal{H}$  by

$$\begin{aligned} \mathcal{H}(t, \Gamma_t, u, M_t, N_t) &= \Gamma_t \cdot H(t, u, M_t, N_t) \\ &= \Gamma_t \left[ N_t \sigma^{-1} (e_t + \widehat{K}(t, Y_t, E_t)) + h(t) u(c_t, e_t) \right] \end{aligned} \quad (\text{B.6})$$

Since the control variable enters into the volatility of the density process, we have to introduce a second pair of adjoint processes  $\{P_t, Y_t\}_{t \in [0, T]}$  by

$$\begin{aligned} dP(t) &= - \left\{ P_t \sigma^{-2} \left[ e_s^* + \widehat{K}(s, Y_s, E_s^*) \right]^2 \right. \\ &+ 2Y_t \left[ e_s^* + \widehat{K}(s, Y_s, E_s^*) \right] \\ &\left. + h(t) \mathcal{H}_{\Gamma\Gamma}(t, \Gamma_t^*, u^*, M_t, N_t) \right\} dt + Y_t dZ_t \end{aligned} \quad (\text{B.7})$$

$$P_T = h(T) \partial_T v(C_T)$$

By using the Lemma 4.5 and Lemma 4.6 in Chapter 3 [30], we have

$$\begin{aligned} \lim_{\varepsilon \rightarrow 0} \frac{J_A(0; e_t^\varepsilon) - J_A(0; e_t^*)}{\varepsilon} \\ = \mathbb{E} \left\{ \left[ H(t, \Gamma_t^*, u^*, M_t, N_t) - H(t, \Gamma_t, u, M_t, N_t) \right] \right. \\ \left. - \frac{P_t}{2} (\Gamma_t \sigma^{-1})^2 \right. \\ \left. \cdot \left[ (e_t^* - e_t) + \left( \widehat{K}(t, Y_t, E_t^*) - \widehat{K}(t, Y_t, E_t) \right) \right]^2 \right\} \end{aligned} \quad (\text{B.8})$$

We claim that the process  $\{P_t\}_{t \in [0, T]}$  is nonpositive. As a matter of fact  $\mathcal{H}_{\Gamma\Gamma} = 0$ ; hence

$$dP(t) = - \left\{ P_t \sigma^{-2} \left[ e_s^* + \widehat{K}(s, Y_s, E_s^*) \right]^2 \right\} dt + Y_t d\widetilde{Z}_t \quad (\text{B.9})$$

$$P_T = 0$$



where

$$d\tilde{Z}_t = dZ_t + 2 \left[ e_t^* + \widehat{K}(s, Y_s, E_s^*) \right] dt \quad (\text{B.10})$$

Therefore a sufficient condition for  $e_t^*$  has to be an optimal effort strategy that

$$e_t^* = \operatorname{argmax}_{e \in \mathbf{A}} \mathcal{H}(t, \Gamma_t, u, M_t, N_t) \quad (\text{B.11})$$

Let  $e^{-\int_0^t \rho(s) ds} q_t = M_t$  and  $e^{-\int_0^t \rho(s) ds} \sigma \gamma_t = N_t$ ; we have

$$\begin{aligned} dq_t &= \rho(t) q_t \\ &\quad - \left[ \gamma_t (e_t^* + \widehat{K}(t, Y_t, E_t^*)) + u(c_t, e_t^*) \right] dt \\ &\quad + \gamma_t \sigma dZ_t = [\rho(t) q_t - u(c_t, e_t^*)] dt + \gamma_t \sigma dZ_t^e \\ q_T &= v(C_T) \end{aligned} \quad (\text{B.12})$$

Hence, (16) is satisfied.

There is no drift in  $\Gamma$ ; in addition, since  $\Gamma_t > 0$ , we can define the conditions on the Hamitonian  $H$  rather than  $\mathcal{H}$ . Hence, the first-order condition for  $e$  is

$$\begin{aligned} \partial_e H &= N_t \sigma^{-1} \left( 1 - \int_0^t \frac{\sigma^{-2}}{h_t} ds \right) + h(t) \cdot \partial_e u(c_t, e_t) \\ e^{\int_0^t \rho(s) ds} \cdot \partial_e H &= e^{\int_0^t \rho(s) ds} N_t \sigma^{-1} \left( 1 - \int_0^t \frac{\sigma^{-2}}{h_t} ds \right) \\ &\quad + u_e(c_t, e_t) = e^{\int_0^t \rho(s) ds} \left[ N_t \sigma^{-1} \right. \\ &\quad \left. - \int_t^T \left( N_s \sigma^{-1} \frac{\sigma^{-2}}{h_s} \right) ds \right] + \partial_e u(c_t, e_t) \\ &= e^{\int_0^t \rho(s) ds} \left[ e^{-\int_0^t \rho(s) ds} \gamma_t \right. \\ &\quad \left. - \int_t^T \left( e^{-\int_t^s \rho(\tau) d\tau} \gamma_s \frac{\sigma^{-2}}{h_s} \right) ds \right] + \partial_e u(c_t, e_t) = \left[ \gamma_t \right. \\ &\quad \left. - \int_t^T e^{-\int_t^s \rho(\tau) d\tau} \gamma_s \frac{\sigma^{-2}}{\theta_s} ds \right] + \partial_e u(c_t, e_t) \end{aligned} \quad (\text{B.13})$$

Finally, the necessary condition for  $e_t^*$  to be an optimal effort choice is  $\partial_e H = 0$ , namely,

$$\begin{aligned} &\left[ \gamma_t - \int_t^T e^{-\int_t^s \rho(\tau) d\tau} \gamma_s \frac{\sigma^{-2}}{\theta_s} ds \right] + \partial_e u(c_t, e_t^*) \\ &= \gamma_t + \frac{\sigma^{-2}}{\theta_t} p_t + \partial_e u(c_t, e_t^*) = 0 \end{aligned} \quad (\text{B.14})$$

On the other hand, from (9) the expected utility form  $e^*$  is given by  $J_A(0; e^*) = q_0^*$ ,

$$\begin{aligned} v(C_T) &= q_T \\ &= q_0^* - \int_0^T h(t) u(c_t, e_t^*) dt \\ &\quad + \int_0^T h(t) \gamma_t^* \sigma dZ_t^e \end{aligned} \quad (\text{B.15})$$

Then, for an arbitrary effort choice  $e \in \mathbf{A}$ , we define  $\omega_t = e_t - e_t^*$  and  $\Delta_t = \int_0^t \omega_s ds = E_t - E_t^*$ ; the following holds:

$$\begin{aligned} J_A(0; e) - J_A(0; e^*) &= \mathbb{E}_e \left[ \int_0^T h(t) [u(c_t, e_t) - u(c_t, e_t^*)] dt \right. \\ &\quad \left. + \int_0^T h(t) \gamma_t^* \sigma dZ_t^e \right] \\ &= \mathbb{E}_e \left[ \int_0^T h(t) [u(c_t, e_t) - u(c_t, e_t^*)] dt \right. \\ &\quad \left. + \int_0^T h(t) \gamma_t^* \sigma dZ_t^e \right. \\ &\quad \left. + \int_0^T h(t) \gamma_t^* \left[ \omega_t - \frac{\sigma^{-2}}{\theta_t} \Delta_t \right] dt \right] \end{aligned} \quad (\text{B.16})$$

The second term on the right hand side  $\mathbb{E}_e[\int_0^T h(t) \gamma_t^* \sigma dZ_t^e] = 0$  uses the fact that the stochastic integral is martingale. The last term on the right hand side can be written as

$$\begin{aligned} & - \int_0^T h(t) \gamma_t^* \frac{\sigma^{-2}}{\theta_t} \Delta_t dt \\ &= - \int_0^T h(t) \gamma_t^* \frac{\sigma^{-2}}{\theta_t} \left( \int_0^t \omega_s ds \right) dt \\ &= \int_0^T \omega_t \left( - \int_t^T h(s) \gamma_s^* \frac{\sigma^{-2}}{\theta_s} ds \right) dt \\ &= \int_0^T \omega_t \left( h(t) \frac{\sigma^{-2}}{\theta_t} p_t^* + \int_t^T \xi_s^* \sigma dZ_s^e \right) dt \end{aligned} \quad (\text{B.17})$$

where the last equality follows the form definition of  $p$  and  $\xi$ . Hence,

$$\begin{aligned} J_A(0; e) - J_A(0; e^*) &= \mathbb{E}_e \left[ \int_0^T h(t) \left[ u(c_t, e_t) \right. \right. \\ &\quad \left. \left. - u(c_t, e_t^*) + \omega_t \left( \gamma_t^* + \frac{\sigma^{-2}}{\theta_t} p_t^* \right) \right] dt \right] \\ &\quad + \mathbb{E}_e \left[ \int_0^T \omega_t \left( \int_t^T \xi_s^* \left( \omega_s - \frac{\sigma^{-2}}{\theta_s} \Delta_s \right) ds \right) dt \right] \\ &= \mathbb{E}_e \left[ \int_0^T h(t) \left[ u(c_t, e_t) - u(c_t, e_t^*) \right. \right. \end{aligned}$$

$$\begin{aligned}
& + \omega_t \left( \gamma_t^* + \frac{\sigma^{-2}}{\theta_t} p_t^* \right) \Big] dt \Big] \\
& + \mathbb{E}_e \left[ \int_0^T \xi_t^* \Delta_t \left( \omega_t - \frac{\sigma^{-2}}{\theta_t} \Delta_t \right) dt \right]
\end{aligned} \tag{B.18}$$

Similar to [20], we define a new function

$$\begin{aligned}
G(t, e, E, \gamma^*, \xi^*, p^*) \\
= u(c, e) + \left[ \gamma^* - h(t)^{-1} \xi^* (E^* - E) \right] e \\
- h(t)^{-1} \xi^* \frac{\sigma^{-2}}{\theta} E^2 + \frac{\sigma^{-2}}{\theta} p^* e
\end{aligned} \tag{B.19}$$

which says that  $G(\cdot)$  is a generalized Hamiltonian for the agent's problem with full information which means without private information (i.e.,  $\xi = 0$ ), we have  $h(t) \cdot G(t, \cdot) = H(t, \cdot)$ . Taking the first-order approximation on  $G(\cdot)$  around  $E^*$  yields

$$\begin{aligned}
& G(t, e_t, E_t) - G(t, e_t^*, E_t^*) - \partial_E G(t, e_t, E_t) \Big|_{e_t^*, E_t^*} \\
& \cdot (E_t - E_t^*) \\
& = u(c_t, e_t) - u(c_t, e_t^*) + \omega_t \left( \gamma_t^* + \frac{\sigma^{-2}}{\theta_t} p_t^* \right) \\
& + h(t)^{-1} \xi_t^* \Delta_t \left( \omega_t - \frac{\sigma^{-2}}{\theta_t} \Delta_t \right)
\end{aligned} \tag{B.20}$$

so that

$$\begin{aligned}
J_A(0; e) - J_A(0; e^*) & = \mathbb{E}_e \left[ \int_0^T h(t) \right. \\
& \cdot \left( G(t, e_t, E_t) - G(t, e_t^*, E_t^*) - \partial_E G(t, e_t, E_t) \Big|_{e_t^*, E_t^*} \right. \\
& \cdot (E_t - E_t^*) \Big) dt \Big]
\end{aligned} \tag{B.21}$$

is negative when  $G(\cdot)$  is concave. Concavity is considered by the Hessian matrix of  $G(\cdot)$ ,

$$\nabla G(t, e, A) = \begin{pmatrix} \partial_{ee} u(c_t, e_t) & h(t)^{-1} \xi_t \\ h(t)^{-1} \xi_t & -2h(t)^{-1} \xi_t \frac{\sigma^{-2}}{\theta_t} \end{pmatrix} \tag{B.22}$$

which is negative semidefinite when  $-2h(t)(\sigma^{-2}/\theta_t)\partial_{ee}u(c_t, e_t) \geq \xi_t$ . When the agent seeks to maximize expected utility,  $e_t^*$  is the optimal effort choice for the agent. All above completes the proof of Proposition 2.

### C. The Proof of Proposition 4

In front, we provide a significant lemma.

**Lemma C.1** (jessen inequality). *Let  $f(X)$  be a continuous convex function and  $X$  be a random variable with respect to*

$\mathcal{F}$  as  $\sigma$ -integrable; then  $f(X)$  is expected to exist with respect to  $\mathcal{F}$ ,

$$f(\mathbb{E}[X | \mathcal{F}]) \leq \mathbb{E}[f(X) | \mathcal{F}] \tag{C.1}$$

Then we prove Proposition 4; the belief  $\widehat{K}_t$  follows a martingale and it is  $\mathcal{F}_t^Y$ -predictable,

$$\begin{aligned}
\Pi_t(c, e^*) & = \mathbb{E} \left[ \int_t^T e^{-\bar{\delta}(s-t)} \cdot \left( -e^{-\lambda(e_s - c_s + \widehat{K}_s)} \right) ds \right. \\
& \left. + e^{-\bar{\delta}(T-t)} \cdot \left( -e^{-\lambda\beta(-C_T + \widehat{K}_T)} \right) \mid \mathcal{F}_t^Y \right] \\
& = \mathbb{E} \left[ \int_t^T e^{-\bar{\delta}(s-t)} \cdot \left( -e^{-\lambda(e_s - c_s + \widehat{K}_s)} \right) ds \mid \mathcal{F}_t^Y \right] \\
& + \mathbb{E} \left[ e^{-\bar{\delta}(T-t)} \cdot \left( -e^{-\lambda\beta(-C_T + \widehat{K}_T)} \right) \mid \mathcal{F}_t^Y \right]
\end{aligned} \tag{C.2}$$

Divide  $\Pi_t(c, e^*)$  into two parts: for the first part,

$$\begin{aligned}
& \mathbb{E} \left[ \int_t^T e^{-\bar{\delta}(s-t)} \cdot \left( -e^{-\lambda(e_s - c_s + \widehat{K}_s)} \right) ds \mid \mathcal{F}_t^Y \right] \\
& \leq \int_t^T \left\{ \mathbb{E} \left[ e^{-\bar{\delta}(s-t)} \cdot e^{-\lambda(e_s - c_s)} \mid \mathcal{F}_t^Y \right] \right. \\
& \cdot \mathbb{E} \left[ -e^{-\lambda\widehat{K}_s} \mid \mathcal{F}_t^Y \right] \Big\} ds \leq -e^{-\lambda\beta\widehat{K}_t} \\
& \cdot \int_t^T \left\{ \mathbb{E} \left[ e^{-\bar{\delta}(s-t)} \cdot e^{-\lambda(e_s - c_s)} \mid \mathcal{F}_t^Y \right] \right\} ds
\end{aligned} \tag{C.3}$$

and on the other hand,

$$\begin{aligned}
& - \left\{ \mathbb{E} \left[ \int_t^T e^{-\bar{\delta}(s-t)} \cdot \left( -e^{-\lambda(e_s - c_s + \widehat{K}_s)} \right) ds \mid \mathcal{F}_t^Y \right] \right\} \\
& \geq - \left\{ \int_t^T \left\{ \mathbb{E} \left[ e^{-\bar{\delta}(s-t)} \cdot e^{-\lambda(e_s - c_s)} \mid \mathcal{F}_t^Y \right] \right. \right. \\
& \cdot \mathbb{E} \left[ e^{-\lambda\widehat{K}_s} \mid \mathcal{F}_t^Y \right] \Big\} ds \Big\} \geq - \left\{ e^{-\lambda\beta\widehat{K}_t} \right. \\
& \cdot \int_t^T \left\{ \mathbb{E} \left[ e^{-\bar{\delta}(s-t)} \cdot e^{-\lambda(e_s - c_s)} \mid \mathcal{F}_t^Y \right] \right\} ds \Big\}
\end{aligned} \tag{C.4}$$

Combine the above two inequalities and then

$$\begin{aligned}
& \mathbb{E} \left[ \int_t^T e^{-\bar{\delta}(s-t)} \cdot \left( -e^{-\lambda(e_s - c_s + \widehat{K}_s)} \right) ds \mid \mathcal{F}_t^Y \right] \\
& = e^{-\lambda\beta\widehat{K}_t} \\
& \cdot \int_t^T \left\{ \mathbb{E} \left[ e^{-\bar{\delta}(s-t)} \cdot \left( -e^{-\lambda(e_s - c_s)} \right) \mid \mathcal{F}_t^Y \right] \right\} ds
\end{aligned} \tag{C.5}$$

For the second part,

$$\begin{aligned}
 & \mathbb{E} \left[ e^{-\bar{\delta}(T-t)} \cdot \left( -e^{-\lambda(-C_T + \bar{K}_T)} \right) \mid \mathcal{F}_t^Y \right] \\
 &= \mathbb{E} \left[ e^{-\bar{\delta}(T-t)} \cdot \left( -e^{-\lambda(-C_T)} \right) \mid \mathcal{F}_t^Y \right] \\
 & \quad \cdot \mathbb{E} \left[ -e^{-\lambda \bar{K}_T} \mid \mathcal{F}_t^Y \right] \\
 &\leq -e^{-\lambda \bar{K}_t} \cdot \mathbb{E} \left[ e^{-\bar{\delta}(T-t)} \cdot \left( -e^{-\lambda(-C_T)} \right) \mid \mathcal{F}_t^Y \right]
 \end{aligned} \tag{C.6}$$

And on the other hand,

$$\begin{aligned}
 & \mathbb{E} \left[ e^{-\bar{\delta}(T-t)} \cdot \left( -e^{-\lambda(-C_T + \bar{K}_T)} \right) \mid \mathcal{F}_t^Y \right] \\
 &= \mathbb{E} \left[ e^{-\bar{\delta}(T-t)} \cdot \left( -e^{-\lambda(-C_T)} \right) \mid \mathcal{F}_t^Y \right] \\
 & \quad \cdot \mathbb{E} \left[ e^{-\lambda \bar{K}_T} \mid \mathcal{F}_t^Y \right] \\
 &\geq e^{-\lambda \bar{K}_t} \cdot \mathbb{E} \left[ e^{-\bar{\delta}(T-t)} \cdot \left( -e^{-\lambda(-C_T)} \right) \mid \mathcal{F}_t^Y \right]
 \end{aligned} \tag{C.7}$$

Through the above two inequalities, we have

$$\begin{aligned}
 & \mathbb{E} \left[ e^{-\bar{\delta}(T-t)} \cdot \left( -e^{-\lambda(-C_T + \bar{K}_T)} \right) \mid \mathcal{F}_t^Y \right] \\
 &= e^{-\lambda \bar{K}_t} \cdot \mathbb{E} \left[ e^{-\bar{\delta}(T-t)} \cdot \left( -e^{-\lambda(-C_T)} \right) \mid \mathcal{F}_t^Y \right]
 \end{aligned} \tag{C.8}$$

Finally,

$$\begin{aligned}
 \Pi_t(c, e^*) &= e^{-\lambda \beta \bar{K}_t} \cdot \mathbb{E} \left[ \int_t^T e^{-\bar{\delta}(s-t)} \cdot \left( -e^{-\lambda(e_s - c_s)} \right) ds \right. \\
 & \quad \left. + e^{-\bar{\delta}(T-t)} \cdot \left( -e^{-\lambda(-C_T)} \right) \mid \mathcal{F}_t^Y \right] = e^{-\lambda \bar{K}_t} \\
 & \quad \cdot J_P(t, c, e^*).
 \end{aligned} \tag{C.9}$$

## Data Availability

No data were used to support this study.

## Conflicts of Interest

The authors declare that they have no conflicts of interest.

## References

- [1] B. Holmström and P. Milgrom, "Aggregation and linearity in the provision of intertemporal incentives," *Econometrica*, vol. 55, no. 2, pp. 303–328, 1987.
- [2] H. Schattler and J. Sung, "The first-order approach to the continuous-time principal-agent problem with exponential utility," *Journal of Economic Theory*, vol. 61, no. 2, pp. 331–371, 1993.
- [3] H. Schattler and J. Sung, "On optimal sharing rules in discrete- and continuous-time principal-agent problems with exponential utility," *Journal of Economic Dynamics and Control (JEDC)*, vol. 21, no. 2-3, pp. 551–574, 1997.
- [4] H. M. Müller, "The first-best sharing rule in the continuous-time principal-agent problem with exponential utility," *Journal of Economic Theory*, vol. 79, no. 2, pp. 276–280, 1998.
- [5] N. Williams, "Persistent private information," *Econometrica*, vol. 79, no. 4, pp. 1233–1275, 2011.
- [6] N. Williams, "A solvable continuous time dynamic principal-agent model," *Journal of Economic Theory*, vol. 159, no. part B, pp. 989–1015, 2015.
- [7] J. s. Cvitanic, X. Wan, and J. Zhang, "Optimal contracts in continuous-time models," *Journal of Applied Mathematics and Stochastic Analysis. JAMSA*, Art. ID 95203, 27 pages, 2006.
- [8] J. Cvitanic, X. Wan, and J. Zhang, "Optimal compensation with hidden action and lump-sum payment in a continuous-time model," *Applied Mathematics & Optimization*, vol. 59, no. 1, pp. 99–146, 2009.
- [9] J. s. Cvitanic and J. Zhang, *Contract Theory in Continuous-Time Models*, Springer-Verlag, New York, NY, USA, 2012.
- [10] K. Eliaz and R. Spiegler, "Contracting with diversely naive agents," *Review of Economic Studies*, vol. 73, no. 3, pp. 689–714, 2006.
- [11] M. Yilmaz, "Repeated moral hazard with a time-inconsistent agent," *Journal of Economic Behavior & Organization*, vol. 95, pp. 70–89, 2013.
- [12] M. Yilmaz, "Contracting with a naïve time-inconsistent agent: To exploit or not to exploit?" *Mathematical Social Sciences*, vol. 77, pp. 46–51, 2015.
- [13] D. Laibson, "Golden eggs and hyperbolic discounting," *The Quarterly Journal of Economics*, vol. 112, no. 2, pp. 443–478, 1997.
- [14] Z. Zou, S. Chen, Y. Yan, and Z. Honghao, "The optimization and decision-making of principal-agent problem based on time-inconsistency preference," *Chinese Journal of Management Science*, vol. 21, no. 4, pp. 27–34, 2013.
- [15] B. Djehiche and P. Helgesson, *The principal-agent problem with time inconsistent utility functions*, ArXiv preprint, arXiv, 1503.05416.
- [16] B. Bian and H. Zheng, "Turnpike property and convergence rate for an investment model with general utility functions," *Journal of Economic Dynamics & Control*, vol. 51, pp. 28–49, 2015.
- [17] E. J. Jung and J. H. Kim, "Optimal investment strategies for the HARA utility under the constant elasticity of variance model," *Insurance: Mathematics and Economics*, vol. 51, no. 3, pp. 667–673, 2012.
- [18] Hao Chang and Xi-min Rong, "Legendre Transform-Dual Solution for a Class of Investment and Consumption Problems with HARA Utility," *Mathematical Problems in Engineering*, vol. 2014, pp. 1–7, 2014.
- [19] H. Chang and K. Chang, "Optimal consumption investment strategy under the Vasicek model: HARA utility and Legendre transform," *Insurance: Mathematics & Economics*, vol. 72, pp. 215–227, 2017.
- [20] J. Prat and B. Jovanovic, "Dynamic contracts when the agent's quality is unknown," *Theoretical Economics*, vol. 9, no. 3, pp. 865–914, 2014.
- [21] I. Ekeland and A. Lazrak, *Being serious about non-commitment: subgame perfect equilibrium in continuous time*, Arxiv preprint math/0604264v1.
- [22] J.-m. Yong, "Deterministic time-inconsistent optimal control problems—an essentially cooperative approach," *Acta Mathematicae Applicatae Sinica*, vol. 28, no. 1, pp. 1–30, 2012.
- [23] T. O'Donoghue and M. Rabin, "Choice and procrastination," *The Quarterly Journal of Economics*, vol. 116, no. 1, pp. 121–160, 2001.

- [24] T. Adrian and M. M. Westerfield, "Disagreement and learning in a dynamic contracting model," *Review of Financial Studies*, vol. 22, no. 10, pp. 3873–3906, 2009.
- [25] R. S. S. A. N. Liptser, "Statistics of random processes, ii applications. no. 6 in applications of mathematics," *Stochastic Modelling and Applied Probability*.
- [26] Z. He, "Dynamic compensation contracts with private savings," *Review of Financial Studies*, vol. 25, no. 5, pp. 1494–1549, 2012.
- [27] J. Mirrlees, "Notes on welfare economics, information, and uncertainty," *Essays on economic behavior under uncertainty*, pp. 243–261, 1974.
- [28] J. W. Gao, "Stochastic optimal control of DC pension funds," *Insurance: Mathematics and Economics*, vol. 42, no. 3, pp. 1159–1164, 2008.
- [29] D. Kramkov and W. Schachermayer, "Necessary and sufficient conditions in the problem of optimal investment in incomplete markets," *The Annals of Applied Probability*, vol. 13, no. 4, pp. 1504–1516, 2003.
- [30] J. Yong and X. Y. Zhou, *Stochastic Controls: Hamiltonian Systems and HJB Equations*, vol. 43 of *Applications of Mathematics*, Springer, New York, NY, USA, 1999.

## Research Article

# Ising Model of User Behavior Decision in Network Rumor Propagation

Chengcheng Li, Fengming Liu , and Pu Li

*School of Management Science and Engineering, Shandong Normal University, Ji'nan 250014, China*

Correspondence should be addressed to Fengming Liu; [liufm@sdnu.edu.cn](mailto:liufm@sdnu.edu.cn)

Received 8 April 2018; Revised 27 June 2018; Accepted 12 July 2018; Published 1 August 2018

Academic Editor: Jorge E. Macias-Diaz

Copyright © 2018 Chengcheng Li et al. This is an open access article distributed under the Creative Commons Attribution License, which permits unrestricted use, distribution, and reproduction in any medium, provided the original work is properly cited.

The continuous breeding and rapid spread of rumors in social networks poses a severe challenge to the effective utilization and scientific management of social media. Therefore, it is of great theoretical significance and application value to study the decision-making behavior of users in rumors spread in social networks and to reveal the rumor transmission rules. Based on the Ising model, this paper constructs a social network rumor propagation dynamics model and then reveals the rumor transmission rules. In the model, the Monte Carlo method is used to simulate the interaction between the user's self-identity attribute (micropart), the user-user interaction (the middle part), and the social environment's influence (the macroscopic part) to study user decision behavior of rumor spread in a social network system. The results show that, in the rumor propagation system, von Neumann entropy can quantify well the phase transition of the system and is consistent with the phase transition information obtained by measuring the spontaneous magnetization and magnetic susceptibility of the system. In addition, the introduction of the self-identity characteristics of individual users into the Ising model has greatly changed the users' decision-making behavior of rumor spreading and changed the internal structure of the system, thus changing the type of phase transition. As the degree of self-identification increases, the need for lower temperatures can change the orderly state of the system, and user behavior changes more rapidly. For the rumor transmission system, the state of close order is conducive to the blocking of rumors, thus maintaining social stability.

## 1. Introduction

With the wide use of social networks and the convenience of the media, rumors permeate all aspects of social life. The importance, ambiguity, and potential dangers of rumors are often widely disseminated without confirmation [1, 2] which affects public attitudes, beliefs, and behaviors [3, 4]. In particular, the explosive development of online social networks such as Facebook, Twitter, and Microblog [5] make an increasingly rapid diffusion of rumors. A rumor can often bring a butterfly effect [6] and bring about huge social and network exchanges and normal social order. The negative impact can easily lead to serious social problems and even crisis social stability, economic development, and national security [7]. DiFonzo believes that Internet rumor has become an important issue that affects social stability.

The research on the rumors characteristics and propagation related to cyber rumor can effectively curb the negative effects caused by it [8]. The research [9–14] on identifying major depressive disorder (MDD) has also provided important ideas and methods for rumor identification and dissemination. Therefore, it is of great theoretical significance and practical value to study rumors spreading rules of social network and stop rumors immediately, which can effectively control rumors and maintain social stability.

The rumor spread in social media involves many factors such as information, users, and network environment. It not only embodies the network effect of information dissemination but also integrates the social psychological factors, the decision-making behaviors of human beings, and the interaction among users and the social environment influence. Rumor spread in social media will cause different

degrees of harm to people's lives and even the whole society. So the ultimate goal of rumor communication research is to suppress or even prevent rumors from spreading. Therefore, based on the user's attributes of the micropart, based on the interaction between the user parts of the micropart, and based on the environmental influence and positive and negative social reinforcement on the rumors of social media of the macropart has become an important research issue one.

In social media, the user's decision-making behavior is influenced by its factors and the influence of the neighborhood users on its impact and social environment. The dissemination users' intrinsic factors, specific purposes, and their authority, influence, and behavior characteristics determine the width and depth of rumor spread and the outbreak point of rumors. Scholars [15] have found that user differences can provide an important basis for rumor identification in the study of users' differences involved in the spread of rumors and nonrumors. Based on the Ising model, this paper combines the influence among users and the influence of social environment, that is, describing the decision-making behavior of users in the process of spreading rumors in the medium and macroaspects. At the same time, taking into account the user's attributes and introducing the individual identity characteristics (microcosmic part), the influence of the feature on the model is analyzed. Finally, the experiments show that the interaction of the user itself, interaction between a user and another, and the social environment in which the user is located can well maintain the orderly state of the cyberspace and provide the decision basis for decision-making of the network governance.

## 2. Related Works

In social media, the user's factors, the neighborhood users, and social environment influence the user's decision-making behavior. The study found that the spread of rumors is driven by many factors, including the internal factors that spread users, the influence of neighboring neighbors, social factors and environmental factors, and so on.

In the research of user decision behavior based on user's attributes, the internal factors of transmitting users (such as personality traits) and their specific purpose have influenced their behavior of spreading messages on social media. Chen et al. [16] have found that the Neuroticism and Openness in the user's personality have a significant impact on the spread of rumor news. In addition, the dissemination users' motivations for entertainment, socializing, and seeking status have also had a significant impact on the spread of rumor messages. In fact, whether users can spread rumors will be affected by a variety of factors, such as personal preference [17]. In recent years, many scholars have shifted their attention to the social attributes of human behavior [18].

In the research of user decision behavior based on the influence of neighbor nodes, since the nodes in social networks are users in real life, their propagation behavior is highly autonomous and independent. Therefore, it is necessary to evaluate the behavior decisions of individual nodes and their neighbor nodes. Simon et al. [19] found that, in

the case of infection, shopping, and social interaction, users' decision-making behavior is influenced by their neighbors or friends. People will make and modify their behavior decisions based on others' decisions. Jackson et al. [20] analyzed the game in social networks where each user would make a binary choice. And Lopez analyzes the influence of the neighbor nodes on the user's decision and gives the equation of the field average [21]. If a good reputation or influential person or a media participates in the spread of rumors, it will cause qualitative changes in rumors; that is to say, it will become quasi-news and make potential rumors and ballads increase significantly. Liao and Shi's [22] research on the contribution and influence of celebrities, certified users, mass media, organizations, websites, talent, and ordinary users in the process of rumor dissemination found that the users who played a major role in the dissemination process were dignitaries, celebrities, and the mass media. Considering that the decision-making in social networks is rational and autonomous, and the user's behavior decision-making is influenced by the neighbors' nodes. Many scholars use game theory to depict this kind of influence and regard the diffusion process of rumors in the network as the process of users choosing the best decision through the game and maximizing their interests.

In the analysis of user decision-making behavior based on the role of social environment, such as social strengthening mechanism, before an individual takes action, it will be affected by the superposition of multiple actions from his neighbors and even the society [23]. At present, some achievements have shown that external public opinion plays an important role in user communication [24]. But these studies only study the influence of positive or negative one of the social reinforcement mechanisms on the spread of rumors. However, in fact, due to the extremely vague nature of the rumors, people's life experience and education experience are different [25]. After the spread of rumors, it is easy to produce two opposing views at the same time, thus forming two powerful social reinforcing functions: positive and negative [26]. Most previous works focused on detecting rumors by shallow features of messages, including content and blogger features. Zhang et al. [27] also believe that shallow features cannot distinguish between rumors and nonrumors well in many situations. Therefore, they extracted four implicit features based on content: popularity orientation, internal and external consistency, emotional polarity, and comment point of view. The popularity orientation feature can obtain the correlation between the content of the message and a hot topic or event in the current society, and the feature value of popularity orientation can be obtained by calculating the Jaccard coefficient. In some cases, user's proximity to events physically or emotionally has a significant impact on whether they publish or forward messages [28–30]. When people have physical proximity to or are emotionally associated with people or places (such as friends, family, or former residences) that may be affected by the incident, they can spread more news and sometimes think of helping others by spreading the message. However, these messages may contain a large number of rumors and their forwarding expanded the spread of rumors.



### 3. Ising Model of the Decision-Making of Rumor Propagation

**3.1. Ising Model.** Ising model is an important model in statistical physics. It describes the phase transition of a matter by characterizing the interaction between particles and the effect of external environment on the particles; that is, magnetization disappears above certain critical temperature, while magnetization appears below certain critical temperature. In the Ising model, a ferromagnetic material consists of a stack of regularly arranged small magnetic pins, each of which has only two directions (spin) up and down. Adjacent small needles interact with each other through energy constraints. At the same time, the random magnetic transition (upside down or vice versa) occurs due to the interference of ambient thermal noise [31].

Assuming that the  $i$ th node is a small magnetic pin, each small magnetic pin has two states up and down. We use  $s_i$  to indicate this state and  $s_i = \begin{cases} +1 \\ -1 \end{cases}$  means the magnetic pin is up or down. The two adjacent small magnetic needles on the grid can interact.

In the Ising model, there is an interaction between each pair of adjacent spins, and the energy of the system is

$$E_{\{s_i\}} = -J \sum_{\langle i,j \rangle} s_i s_j - H \sum_i s_i, \quad (1)$$

where  $J$  is energy coupling constant and  $E_{\{s_i\}}$  represents the total energy of the system under state combination  $\{s_i\}$ . The summing subscript  $\langle i, j \rangle$  indicates the summation of all two adjacent small magnetic needles. We see that if  $s_i = s_j$ , the total energy is reduced by  $J$ .  $H$  represents the strength of the external magnetic field; the magnetic field up then  $H$  is positive and otherwise negative. If the direction of a small needle coincides with the field, the total energy is reduced by one unit.

**3.2. Ising Decision Model.** Based on the Ising model, this paper constructs a behavioral decision-making model of rumor propagation. Each small magnetic needle is compared to a user in a social network. The upper and lower states of the small magnetic needle are compared to the user's decision-making behavior, propagation, and nonpropagation. The interaction between adjacent small needles is analogous to the effect of behavioral decision-making among users. The temperature of the environment is analogous to the influence of the environment (the heat of the social network rumor topic and the appeal or influence of a rumor). In this way, the entire Ising model can express the dynamic evolution of rumors made by different users in social networks. In addition, this paper will also add the self-identity characteristics of individuals to the rumor communication behavior decision-making model and then analyze the characteristics of the impact of the model.

This paper calculates the revenue function of the behavior strategy adopted by the user through the rumor propagation user behavior decision-making model and obtains the equilibrium state of the system, that is, the time point when the rumor no longer propagates and the system reaches

the steady state. The Nash equilibrium is used to judge the decision-making distribution of each user when the social network is in a steady state. By measuring the von Neumann entropy, we study and analyze the phase transitions and critical phenomena of the user behavior decision-making system and get the critical information. Finally, the Monte Carlo simulation of the Ising model is carried out.

**3.3. Ising Model Construction.** The Ising model was originally used in phase change studies and later with the development of complexity science. Because of its simple mechanism and rich dynamic behavior [32], it can effectively simulate the evolution of binary opinion; it has been widely used in the study of viewpoint kinematics.

**3.3.1. User Decision Behavior Model.** Let  $Z^2$  be represented as a square lattice; the element  $i$  in the lattice is a pair of integers  $(i_1, i_2)$ , for any finite symmetric subset  $\Lambda \subset Z^2$ ; let  $\Omega_\Lambda = \{-1, 1\}^\Lambda$  denote the spin configuration on  $\Lambda$ ; the element of  $\Omega_\Lambda$  may be denoted as  $\sigma_\Lambda = \{\sigma_i : i \in \Lambda\}$ . Without being obfuscated, the subscript  $\Lambda$  in  $\sigma_\Lambda$  can be omitted. Considering the Ising model with the following Hamiltonian system, the energy of an Ising model system on a complex network over any  $\sigma \in \Omega_\Lambda$  is defined:

$$H_{\Lambda,h}(\sigma) = - \sum_{i,j \in \Lambda} J_{ij} \sigma_i \sigma_j - h \sum_{i \in \Lambda} \sigma_i, \quad (2)$$

where  $h$  is a real number, which represents the environmental influence of the microblog ( $h = \xi h_1 + (1 - \xi)h_2$ , where  $h_1$  represents the heat of the rumor topic,  $h_2$  represents the attraction or influence of the rumor, and  $\xi$  represents the environmental factor, the value of which depends on the real environment).  $J_{ij}$  is the interaction between users, the view of the individual  $i$  is updated by the nearest neighbors, and the direction selection similar to spin is subject to the local spin interaction

**3.3.2. Calculate the User's Local Environment.** Based on Simon's research, the user's neighbors or friends influence his or her decision-making behavior. People make and modify their own behavioral decisions based on others' decisions. Therefore, we can calculate the individual user's local environment. Assume that the users in the social network are at a point in the  $\Lambda$  grid ( $\Lambda$  is a subset of square grids  $Z^2$ ). At each point of time, the user decides whether to spread the rumor ( $\sigma_i = +1$ ) or not to spread the rumor ( $\sigma_i = -1$ ). The decision of each user  $i$  depends on the local environment  $I_i(t)$  at the time  $t$ , and its formula is

$$I_i(t) = \frac{1}{|\Lambda|} \sum_{j \in \Lambda} J_{ij}(t) \sigma_j(t) - h_i(t). \quad (3)$$

The first term in (3)  $(1/|\Lambda|) \sum_{j \in \Lambda} J_{ij}(t) \sigma_j(t)$  of  $I_i(t)$  denotes the influence of the behavior decision attitude of other users on the decision-making of user  $i$  at time  $t$ . Due to the interaction between users,  $J_{ij}(t)$  is time-varying and has the form  $J_{ij}(t) = a\xi(t) + b\eta_{ij}(t)$ ,  $a\xi(t)$ , which reflects the average effect of the entire society on the user  $i$  and  $b\eta_{ij}(t)$  reflects the influence of all users on user  $i$  decision.

The second term in (3)  $h_i(t) = c_i \sum_{i=1}^{i-1} \alpha x_i + d_i B(t)$  of  $I_i(t)$  represents the social environment,  $c_i \sum_{i=1}^{i-1} \alpha x_i$  represents the influence of the total return of behavior decision-making on the user  $i$  over a period,  $B(t)$  is the standard Brownian motion, which represents the external random information into society, and  $d_i B(t)$  reflects the impact of stochastic information on the behavior decisions of different users  $i$ .

**3.3.3. Calculate User's Behavior Decision Probability.** Users change their behavior decisions based on changes in the environment. At each moment  $t$ , the user changes his attitude with a certain probability, the probability of spreading the rumor is  $P$ , and the probability of not spreading the rumor is  $1 - P$ . Then the formula is as follows:

$$P = \frac{1}{1 + \exp[-2I_i(t)]}. \quad (4)$$

**3.3.4. Calculate the User's Revenue Function.** In social networks, users' behavioral decisions are influenced not only by their own interests, but also by their neighbors or friends. Everyone makes and modifies their behavioral decisions based on the decisions of others. Users choose the best decision through the game to maximize their own interests. Based on the game in social networks analyzed by Jackson et al., we can calculate the user's revenue function and find the equilibrium state threshold. Therefore, in the Ising model, user decisions are rational and autonomous, and users always choose to make their own decisions. An individual achieves an equilibrium state during the interaction, in which no individual can increase returns by unilaterally changing his or her behavior strategy. Therefore, the Nash equilibrium is used to judge the decision-making distribution of each user when the social network is in a steady state.

Suppose the social network group user  $i$  will choose to spread rumors with a probability of  $p$  and with a probability of  $1 - p$  choosing not to spread rumors. The user  $j$  will choose to spread rumors with a probability of  $q$ , with a probability of  $1 - q$  choosing not to spread rumors. Then the probability matrix of the user  $i$  and  $j$  selection behavior is  $P = p, 1 - p, Q = q, 1 - q$ , respectively; among them,  $0 \leq p \leq 1, 0 \leq q \leq 1$ . In addition,  $\beta_{ij}$  denotes the trust degree of the neighbor node,  $V_d$  denotes the proceeds of the choice of spreading the rumor,  $V_a$  denotes the proceeds of receiving the rumor, and  $C$  is the cost of spreading the rumor.

The expected utility function for user  $i$ 's choice of spreading rumor behavior is

$$U_i^s = q[\beta_{ij}(V_d + V_a) - C] + (1 - q)(\beta_{ij}V_d - C). \quad (5)$$

The expected utility function when choosing not to spread rumors is

$$U_i^{ns} = q\beta_{ij}V_a + 0(1 - q). \quad (6)$$

Get the user  $i$ 's overall expected utility function

$$\begin{aligned} U_i(p, 1 - p) \\ = p\{q[\beta_{ij}(V_d + V_a) - C] + (1 - q)(\beta_{ij}V_d - C)\} \\ + (1 - p)q\beta_{ij}V_a. \end{aligned} \quad (7)$$

Similarly, for the user  $j$ , its expected utility function is the same as  $i$ .

Differentiate the above-expected utility function to obtain the first-order condition:

$$\frac{\partial U_i}{\partial p} = \beta_{ij}V_d - C = 0, \quad \beta_{ij}V_d = C. \quad (8)$$

The user  $j$ 's hybrid strategy is  $(q, 1 - q)$ . If the user  $i$  chooses to propagate rumors, then the revenue is  $q\beta_{ij}V_a + \beta_{ij}V_d - C$ ; if user  $i$  chooses not to spread rumors, the revenue is  $q\beta_{ij}V_a$ . When  $\beta_{ij}V_d > C$ , the larger the value of  $p$ , the more the participants expected to spread the gains, at which point ( $p = 1$ ) represents the best strategy for  $i$ . When  $\beta_{ij}V_d < C$ , the user's expectation of the spread of earnings is inversely proportional to  $p$ . The smaller the  $p$  is, the less likely the user is to choose to spread the rumor. Do not spread rumors ( $p = 0$ ) to become the best strategy for  $i$ . When  $\beta_{ij}V_d = C$ , user  $i$  spreads that the benefits of nondissemination are the same. Therefore, every feasible  $p$  is the best strategy for user  $i$ . User  $j$  and user  $i$ 's analysis method are the same.

When  $\beta_{ij}V_d - C > 0$ , the game's mixed strategy Nash equilibrium is  $(1, 1)$ .

When  $\beta_{ij}V_d - C < 0$ , the game's mixed strategy Nash equilibrium is  $(0, 0)$ .

When  $\beta_{ij}V_d - C = 0$ , any feasible  $(p, q)$  is the mixed strategy Nash equilibrium of this game.

From this, we can conclude that the more the trustworthiness among users, the higher the rate of rumor propagation. If there is a massive spread of rumors and sensitive information on the Internet, the government and the media should timely release official messages to reduce the panic and anxiety in the society. The more important the rumor, the higher the spread rate. After the rumor incident, the public is easily influenced by herd mentality, and herd behavior can easily occur [33]. The common denominator of these events is the life, property, and economic interests of many people, even though the initial communicators are all very humble users. If the government clarifies the relevant laws and regulation to punish criminals who spread rumors, they can increase the risk of transmission of rumors, thus reducing the rate of spreading rumors.

**3.3.5. Calculate the Von Neumann Entropy.** In recent years, researchers have found that it is possible to quantify quantum phase transitions by measuring the entanglement of the quantum. The researchers found that von Neumann entropy shows finite-scale scaling behavior as a measure of quantum entanglement near the critical quantum point [34]. This method can effectively and directly obtain the quantum transition in the quantum model. By the predecessors, this paper uses the von Neumann entropy to study the Ising model and find out the transformation point and critical information of the rumor propagation system. The von Neumann's entropy formula is as follows:

$$\begin{aligned} S_p(T) &\equiv -\text{tr}_p \rho_p(T) \ln \rho_p(T) \\ &= 2 \ln 2 - \frac{1}{2} \left[ \gamma \ln \frac{1 + \gamma}{1 - \gamma} + \ln(1 - \gamma^2) \right]. \end{aligned} \quad (9)$$

Among them, the spin correlation is  $\gamma(T) = \langle \sigma_i \sigma_{i+1} \rangle$ . Where  $\rho_p(T)$  represents the reduced density matrix,  $\text{tr}_p \rho_p(T)$  represents the trace of the subsystem, and  $\gamma$  is a critical exponent.

#### 4. Monte Carlo Experimental Simulation

MC simulation refers to a calculation method that uses computer-generated pseudo-random numbers to deal with probability problems. In recent years, the MC method has become a standard method for scientific research and has been widely used in statistical physics and complex systems, nonlinear dynamic processes, chaos, and some chemical reactions and mathematical random processes.

The key to performing a Monte Carlo simulation is to first give the state transfer rate. First write the master equation

$$\frac{\partial P_s(t)}{\partial t} = \sum_{s \neq ns} (P_{ns} \Psi_{ns \rightarrow s} - P_s \Psi_{s \rightarrow ns}), \quad (10)$$

where  $P_s(t)$  represents the probability that the system is in the  $s$ -state at time  $t$ , and  $\Psi_{s \rightarrow ns}$  represents the transition rate from the state  $s$  to the state  $ns$ . When the system reaches equilibrium,  $\partial P_s(t)/\partial t = 0$ , so careful balance conditions can be written as follows:

$$P_{ns} \Psi_{ns \rightarrow s} = P_s \Psi_{s \rightarrow ns}. \quad (11)$$

In addition, the probability of balancing the temporal  $s$  can be given by the Boltzmann distribution:

$$P_s^{eq} = \frac{e^{-H_s/k_B T}}{Z}. \quad (12)$$

The denominator  $Z$  in the above formula is the distribution function of the system. In general, the partition function cannot be directly solved. For this reason, the method often used by people is to assume that the system evolution process is a Markov process, so that we can directly generate new states from the old state, and there is no time and other memory processes. The system transitions from one state to another, and its transition probability should satisfy the following formula:

$$\frac{\Psi_{s \rightarrow ns}}{\Psi_{ns \rightarrow s}} = \frac{P_{ns}^{eq}}{P_s^{eq}} = e^{-\Delta H/k_B T}, \quad \Delta H = H_{ns} - H_s. \quad (13)$$

Using the above method can avoid solving the complicated partition function. The ratio of the transition probability can be obtained by calculating the difference between the energy before and after the transition and the temperature. Only this one equation still cannot get the transition probability, so we introduce a fine balance condition to get another equation, for example, according to the rules of the Metropolis dynamics, you can write

$$\Psi_{ns \rightarrow s} = \begin{cases} \exp\left(-\frac{\Delta H}{k_B T}\right), & \Delta H > 0 \\ 1, & \Delta H < 0. \end{cases} \quad (14)$$

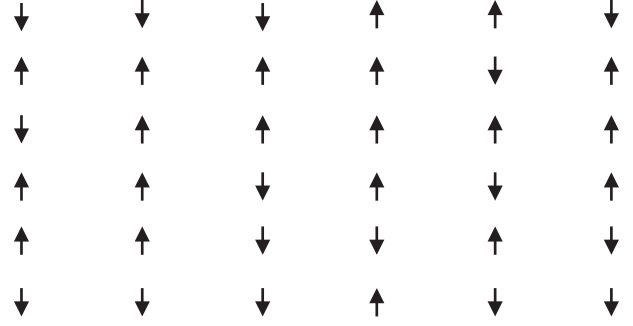


FIGURE 1: Ferromagnetic Ising model.

**4.1. Magnetization and Magnetic Susceptibility of Rumor Propagation Systems.** In order to prove the von Neumann entropy method to study the critical temperature  $T_c$  of the rumor propagation system and whether the phase transition type and some critical exponents the system experiences are effective and feasible. Therefore, the magnetization and magnetic susceptibility of the system are measured according to the traditional method. Magnetization is a physical quantity that describes the degree of magnetic properties of a macroscopic magnetic bod,  $\langle |m| \rangle = (1/N^2) \sum_{i=1}^{N^2} m_i$ ,  $m = (1/N^2) \sum_{i=1}^{N^2} \sigma_i$ . Magnetic susceptibility is a physical quantity that characterizes the properties of a magnetic medium,  $\chi/N^2 = (1/N^2)(\partial m/\partial T) = \langle (m - \langle |m| \rangle)^2 \rangle = \langle m^2 \rangle - \langle |m| \rangle^2$ . The “spontaneous magnetization” average  $m = (1/N^2) \sum_{i=1}^{N^2} \sigma_i$  as the order parameter [35]; among them  $\sigma_i \in \{+1, -1\}$ ;  $N \times N$  is the size of the network. Here, when  $\langle |m| \rangle$  is close to 1, the rumor propagation system is in an orderly state; when  $\langle |m| \rangle$  is 0, the system is in a completely disordered state. Therefore, we use Monte Carlo method to carry out numerical simulation, respectively, in the size of  $4 \times 4$ ,  $6 \times 6$ ,  $8 \times 8$ ,  $10 \times 10$ ,  $12 \times 12$ ,  $14 \times 14$ ,  $20 \times 20$ , and  $50 \times 50$  network to simulate; take the temperature interval  $\Delta T = 0.03$ ; the results are as shown in Figure 2.

It can be seen from Figure 2 that, as the scale  $N \times N$  of the system increases,  $T_c(N)$  will be close to the critical point  $T_c$  at which the true rumor propagation system intersects. Figure 1 shows us some change rules, but in order to obtain the exact critical point and the critical index, we assume that the critical index  $\nu = 1$  ( $\nu$  is expressed as a critical index in the rumor propagation system) fitted to the case, from which the critical point  $T_c = 2.3075, \pm 0.00852$  can be obtained.

**4.2. Von Neumann Entropy of Rumor Propagation System.** In order to study the critical temperature of the rumor propagation system and the types of phase transitions experienced by the system and some critical indices, we measured the von Neumann entropy of the system in a conventional way. von Neumann entropy formula is as follows:

$$\begin{aligned} S_p(T) &\equiv -\text{tr}_p \rho_p(T) \ln \rho_p(T) \\ &= 2 \ln 2 - \frac{1}{2} \left[ \gamma \ln \frac{1+\gamma}{1-\gamma} + \ln(1-\gamma^2) \right]. \end{aligned} \quad (15)$$

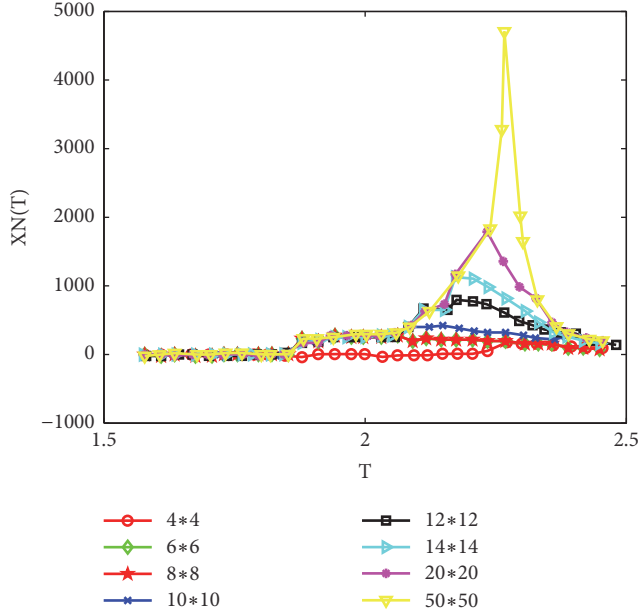


FIGURE 2: Functional images of magnetic susceptibility  $\chi_N(T)$  and temperature  $T$ .

Therefore, we performed simulations on  $15 \times 15$ ,  $20 \times 20$ ,  $30 \times 30$ ,  $35 \times 35$ ,  $50 \times 50$ ,  $80 \times 80$ , and  $100 \times 100$  networks, respectively; in the rumor propagation system, von Neumann entropy is measured, and the temperature interval of  $\Delta T = 0.03$ , according to finite-scale theory, and we got some information about the critical point; the results are shown in Figure 3.

From Figure 3, it can be easily found that the inflection point appears on the curve. This implies the existence of a critical point. Next, we observe the changes in these inflection points by deriving the curves.

From Figure 4, based on the finite-scale scale theory, we can determine that the critical temperature of the system is  $T_c = 2.30728$ .

**4.3. Comparison of Experimental Results.** Through the study of the Ising model of rumor propagation system from the aspects of measuring magnetization, magnetic susceptibility, and measuring von Neumann entropy, we get some conclusions, respectively.

(1) To study the magnetization and magnetic susceptibility, we obtain that the critical temperature of the system is  $T_c = 2.3075, \pm 0.00852$  and the critical length of the correlation length is  $\nu = 1$ .

(2) We study the von Neumann entropy of the rumor propagation system, and we obtain that the critical temperature of the system is  $T_c = 2.30728$  and the critical length of the correlation length is  $\nu = 1$ . The derivative of von Neumann entropy is logarithmically divergent at the critical point and reflects the secondary phase changing characteristics.

(3) Through comparative studies, von Neumann entropy of rumor propagation system can also be used to characterize the phase transition of user behavior decision in the system.

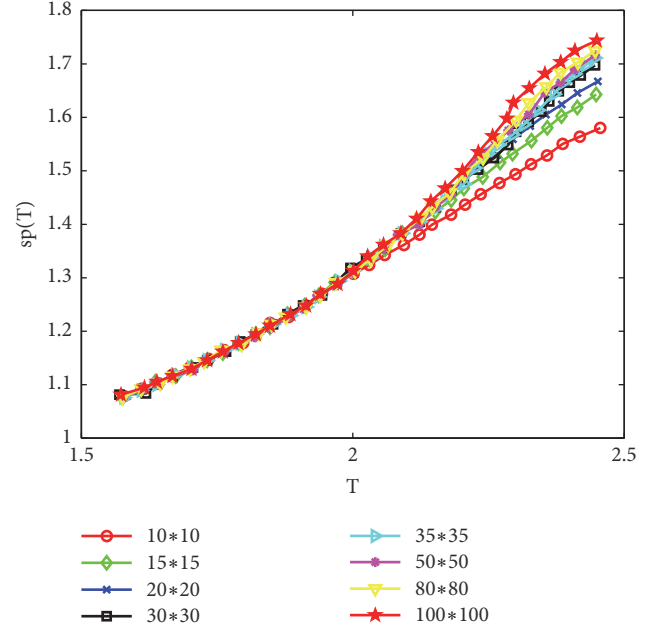


FIGURE 3: Variation of von Neumann entropy  $S_p(T)$  of different systems with temperature  $T$ .

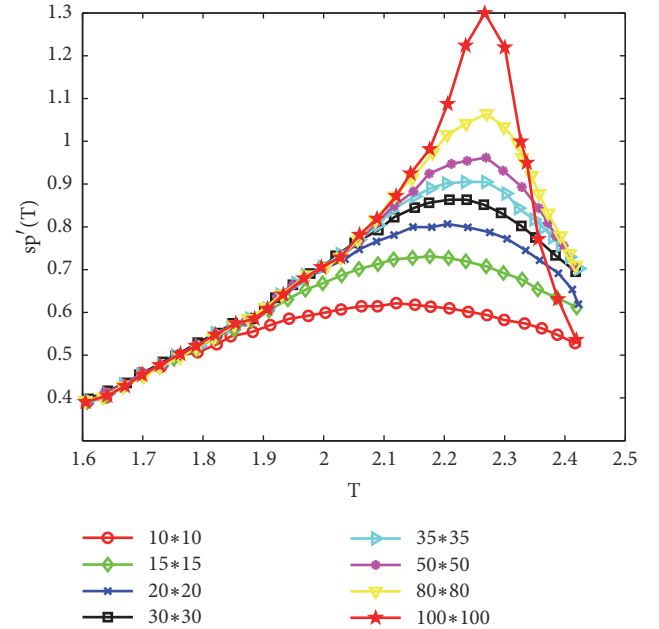


FIGURE 4: Variation of von Neumann entropy derivative  $S_p'(T)$  of different systems with temperature  $T$ .

## 5. Introducing Personal Self-Identity

The previous model ignores the individual differences in the system, such as differences in the self-identity characteristics of the population [36, 37]. Based on the Ising model, this paper introduces the self-identity into the rumor propagation dynamics. When this feature reaches a certain level of strength, the phase-shifting behavior of the user's rumor



decision in the rumor communication system changes from continuous to discontinuous.

**5.1. Construct Model.** In a homogeneous grid, each grid represents individual users in a social network, and each user has four neighbors individually. All user entities have one of two decision-making behaviors. Therefore, an individual's decision behavior can be described as one of two possible behaviors  $\sigma_i \in \{+1, -1\}$  at any moment. On the one hand, we introduce the function  $S(i) = 2\sigma_i \sum_{j=1}^4 \sigma_j$  to describe the relationship between the state of an individual  $i$  and the state of its companion  $j$  ( $j = 1, 2, 3, 4$ ). On the other hand, we use  $\varepsilon$  ( $0 < \varepsilon \leq 1$ ) to describe the individual's psychology of acceptance of the surrounding social environment, which allows the individual to follow the behavioral decisions of the majority of the neighbors. On the contrary,  $1 - \varepsilon$  describes the individual's self-identity psychology, which allows the individual to insist on his own behavior. The smaller the value of  $\varepsilon$  is, the more the individuals identifying with the self are, and the easier it is for individuals to adhere to their own behavioral decisions rather than following most of their neighbors' behavioral decisions.

Based on this, the following model is constructed as follows: when  $S(i) > 0$ ,  $\sigma_i$  is the same as most neighbors,  $\sigma_i$  changes its own behavior by the probability of  $\exp[-S(i)/T]$ , and  $T$  is a parameter of the class temperature associated with the internal fluctuation of the system; when  $S(i) < 0$ ,  $\sigma_i$  is contrary to the state of most neighbors, and  $\sigma_i$  changes its own state by the probability of  $\varepsilon$ ; when  $S(i) = 0$ , the number of states in the neighborhood is the same as and opposite to the state of the individual, so  $\sigma_i$  changes its own behavior decision according to its characteristics; that is,  $\sigma_i$  changes its own behavior decision with the probability of  $\varepsilon$ . From the dynamic evolution rules of the model, we find that, in the case of  $\varepsilon = 1$ , the model returns to the Ising model.

**5.2. Numerical Simulation Results.** Figure 5 shows that when the temperature is below the critical value, the final state of evolution of the rumor propagation system is ordered, and when the temperature is above the critical value, the final state of evolution of the system is disordered. As the degree of self-identity increases, the user behavior decision-making of the rumor communication system changes from an ordered state to an unordered state, from continuous phase change to discontinuous phase change, with  $\varepsilon_c$  being about 0.575. This shows that the individual's self-identity has greatly changed the dynamics of rumor transmission. As the level of self-identification increases, the need for lower temperatures will change the orderly status of the rumor transmission system and change more and more rapidly.

*Note.* In Figure 6(1), *a* is a graph of the probability density function of  $m$  in the case of  $\varepsilon = 0.8$ , where  $T$  is less than  $T_c$ . *b* is a graph of the probability density function of  $m$  in the case of  $\varepsilon = 0.8$ , where  $T$  is greater than  $T_c$ .

In Figure 6(2), *c* is a graph of the probability density function of  $m$  in the case of  $\varepsilon = 0.2$ , where  $T$  is less than  $T_c$ . *d*

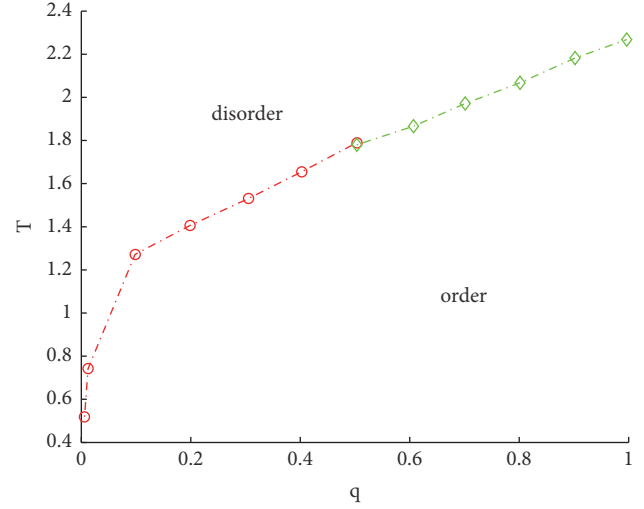


FIGURE 5: Phase diagram of model: discontinuous phase change occurs on the red representative system, and the continuous phase change occurs on the green representative system.  $q$  describes the individual's identity to the surrounding public opinion environment.

is a graph of the probability density function of  $m$  in the case of  $\varepsilon = 0.2$ , where  $T$  is greater than  $T_c$ .

In (1) and (2) of Figure 6, we show the variation of  $\langle |m| \rangle$  with temperature in the case of  $\varepsilon = 0.8$  and  $\varepsilon = 0.2$ , respectively. We find that the phase transitions at  $\varepsilon = 0.8$  are continuous and the phase transitions at  $\varepsilon = 0.2$  are discontinuous. The inset *a* and the inset *b* in Figure 6(1) are, respectively, the probability density functions of  $\langle |m| \rangle$  when less than  $T_c$  and greater than  $T_c$  in the case of  $\varepsilon = 0.8$ : when less than  $T_c$ , there are only two peaks on both sides of  $\langle |m| \rangle' = 0$ , but only one peak at  $\langle |m| \rangle' = 0$ . This is analogous to the continuous change of the ferromagnetic phase to the paramagnetic phase in a balanced phase transition. So when  $\varepsilon = 0.8$ , what happens to the rumor propagation system is a continuous phase change. The  $\langle |m| \rangle$  probability density function diagram in the case of illustration *c* and illustration *d* in Figure 6(2) in the case of  $\varepsilon = 0.2$  is less than  $T_c$  and greater than  $T_c$ , respectively: the most probable value of  $\langle |m| \rangle'$  in illustration *c* has two peaks of symmetry, and the most probable value of  $\langle |m| \rangle'$  in the illustration *d* has a peak. In the process of phase transition point  $T_c$ , the two peaks in the insertion of *c* become unstable, and, at  $T_c$ , the value of  $\langle |m| \rangle'$  rapidly changes to 0. Therefore, in the case of  $\varepsilon = 0.2$ , the system of rumor propagation is a discontinuous phase transition. Obviously, the characteristics of self-identity change the internal structure of rumor transmission system, which in turn changes the type of phase transition.

**5.3. Conclusion.** By introducing the self-identity of individuals into the nonequilibrium Ising model, the influence of individual self-identity on the dynamics of system rumor propagation is discussed. These studies have shown that the pervasive self-identity psychology of individuals in the social system has a significant impact on rumor propagation dynamics. The system presents a nonequilibrium phase transition from a state with a single public behavior decision

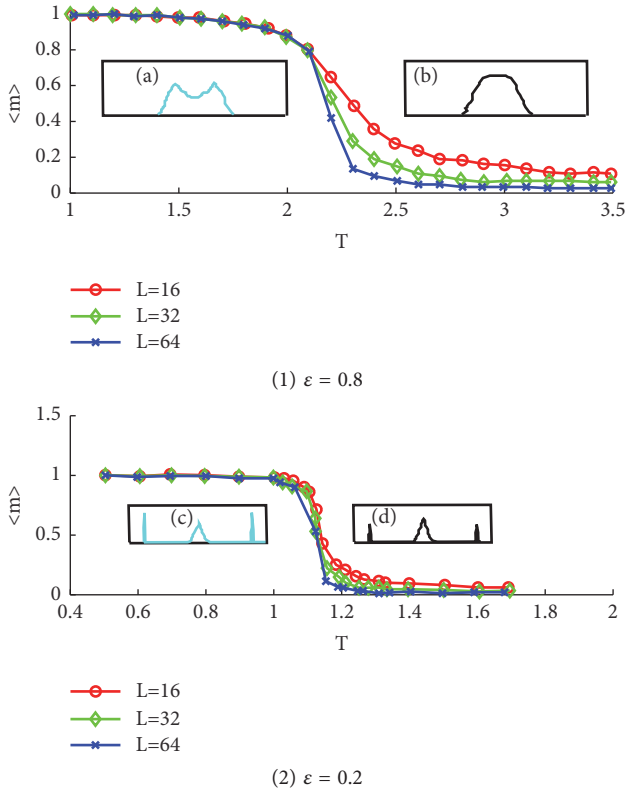


FIGURE 6: Order parameter changes with temperature (the illustration shows the distribution of probability density functions of order parameters).

to a state where a large number of behavioral decisions coexist. Moreover, with the strengthening of self-identity, the phase transition of the user decision in the rumor propagation system changes from the continuous phase to the discontinuous phase.

## 6. Conclusion and Outlook

**6.1. Conclusion.** Based on the Ising model, this paper combines the characteristics of the individual's self-identity (the micropart), the interaction between a user and another (the middle part), and the influence of the social environment (the macroscopic part) and then applies Monte Carlo simulation method to study the social network system rumor spreading user decision-making behavior, revealing that the law of rumor transmission has important theoretical significance and application value.

The results show that after the von Neumann entropy concept is used to study the phase transitions and the critical phenomena in the classical thermodynamic system, we use the Ising model to obtain the critical information of the rumor propagation system by measuring the von Neumann entropy of the system. The von Neumann entropy of the rumor propagation system can quantify well the phase transition of the system and is consistent with the phase change information obtained by measuring the spontaneous magnetization and the susceptibility of the system. The

successful application of von Neumann entropy in rumor propagation system proves that von Neumann entropy can indeed be used to quantify the phase transition of rumor propagation. This provides a good way to quantify the phase change of rumor communication. In addition, the study also shows that the introduction of self-identity characteristics of individual users into the Ising model has greatly changed the user decision-making behavior of rumor transmission and changed the internal structure of the system, thereby changing the type of phase transition. As the level of self-identification increases, the need for lower temperatures will change the orderly state of the system and the transition will change more rapidly. For the spread of rumors, the close order of the state is conducive to social stability.

**6.2. Outlook.** (1) Based on the Ising model, this paper only considers the feature of the user's personal self-identity but does not consider the positive and negative social reinforcement of the social environment. Double social enhancement plays a role in the spread of the rumor, and rumors vary in their attractiveness to users. The next step of research will be further combined with the differences in the ability of users to explore the impact of user influence on the spread of rumors. Through further analysis of rumors, we can find out its propagation rule, effectively reduce the final spread scale of rumors, weaken the biggest impact of rumors, and slow down the speed of rumor spreading and provide more time for relevant departments to take measures to control rumor spread.

(2) The user behavior decision model studied in this paper is individualized; that is, each node in the network represents each user, so it is not suitable for large-scale complex networks. In order to study the complex dynamic behavior of large-scale networks and their relationship with local structures, the next step is to use the theory and method of multiscale coarse-graining to look at multiple users as a node in the network. We merge nodes with similar strengths (i.e., user's friend nodes) into one coarse-grained node, because in weighted networks it is impractical to combine nodes of exactly the same strength. On the basis of modeling individual user behavior decision based on the Ising model, it is hoped that the coarse granulation method based on node strength merging can be proposed to make it suitable for large-scale complex networks. It is more widely used.

## Data Availability

The data used to support the findings of this study are included within the article.

## Conflicts of Interest

The authors declare that there are no conflicts of interest regarding the publication of this paper.

## Acknowledgments

This work was supported in part by the National Natural Science Foundation of China (nos. 61170038, 61472231, and



71701115), the National Social Science Foundation of China (no. 14BTQ049), the Shandong Natural Science Foundation (ZR2017MF058), and Special Project for Internet Development of Social Science Planning Special Program of Shandong Province (17CHLJ23).

## References

- [1] C. Zhang, "Research on the laws and laws of network rumor transmission under the new media era," *Application Research of Computers*, no. 33, article 188, 2017.
- [2] Y. Yang P. C. Fan J, J. Yang Z, and Y. Jin, "Rumor propagation model on multilayered interconnected complex networks based on official information driven," *Application Research of Computers*, no. 5, pp. 1–6, 2018.
- [3] S. y. Ding and Y. B. Zhou, "Governance and thinking of internet communication," *Modern Hospital Management*, vol. 15, no. 3, pp. 90–93, 2017.
- [4] D. Lu, J. L. Guo, and H. Y. He, "Research of WeChat rumors spread based on SIS2IR double S model," *Mathematics in Practice and Theory*, vol. 47, no. 16, pp. 157–163, 2017.
- [5] F. M. Liu, X. Q. Zhu, Y. X. Hu, L. H. Ren, and H. Johnson, "A cloud theory-based trust computing model in social networks," *Entropy*, vol. 19, no. 1, article 11, 2017.
- [6] L. Y. Cai and J. H. Zhang, "Butterfly effect: WeChat rumors spread mechanism," *New Media*, no. 6, pp. 72–75, 2015.
- [7] J. M. Lu, "Analysis on network rumor generation mechanism and its main harm," *Journal of News Research*, vol. 8, no. 17, pp. 27–28, 2017.
- [8] N. Difonzo, "Rumour research can douse digital wildfires," *Nature*, vol. 493, no. 7431, article 135, 2013.
- [9] C. L. Yu, B. T. Baune, K.-A. Fu, M.-L. Wong, and J. Licinio, "Genetic clustering of depressed patients and normal controls based on single-nucleotide variant proportion," *Journal of Affective Disorders*, vol. 227, pp. 450–454, 2017.
- [10] F. M. Liu, L. Wang, H. Johnson, and H. F. Zhao, "Analysis of network trust dynamics based on the evolutionary game," *Scientia Iranica, Transaction E: Industrial Engineering*, vol. 22, no. 6, pp. 2548–2557, 2015.
- [11] C. L. Yu, M. Arcos-Burgos, J. Licinio, and M.-L. Wong, "A latent genetic subtype of major depression identified by whole-exome genotyping data in a Mexican-American cohort," *Translational Psychiatry*, vol. 7, no. 5, Article ID e1134, 2017.
- [12] C. L. Yu, M. Deng, L. Zheng, R. L. He, J. Yang, and S. S.-T. Yau, "DFA7, a new method to distinguish between intron-containing and intronless genes," *PLoS ONE*, vol. 9, no. 7, Article ID e101363, 2014.
- [13] F. M. Liu, L. Wang, L. Gao, H. X. Li, H. F. Zhao, and S. K. Men, "A Web Service trust evaluation model based on small-world networks," *Knowledge-Based Systems*, vol. 57, pp. 161–167, 2014.
- [14] X. Q. Zhu and F. M. Liu, "Research on behavior model of rumor maker based on system dynamics," *Complexity*, vol. 2017, Article ID 5094218, 9 pages, 2017.
- [15] C. Castillo, M. Mendoza, and B. Poblete, "Information credibility on Twitter," in *Proceedings of the 20th International Conference Companion on World Wide Web*, pp. 675–684, Hyderabad, India, April 2011.
- [16] X. Chen, "The influences of personality and motivation on the sharing of misinformation on social media," in *Proceedings of the iConference 2016: Partnership with Society*, pp. 1–11, Philadelphia, Pa, USA, 2016.
- [17] L. H. Wang, "Study on the mechanism of rumor spreading based on agent social simulation," *Journal of Shangqiu Normal University*, vol. 33, no. 12, pp. 5–10, 2017.
- [18] H. P. Zhang, X. H. Guo, and N. Guo, "A study on factors influencing the behavior intention of recognizing internet rumors in emergency events," *Journal of Modern Information*, vol. 37, no. 7, pp. 60–65, 2017.
- [19] S. Simon and K. R. Apt, "Choosing products in social networks," in *Proceedings of the 8th WINE*, pp. 100–113, Liverpool, UK, 2012.
- [20] X. Dai, "Application of game theory in social networks," *Computer & Digital Engineering*, vol. 45, no. 6, pp. 1127–1132, 2017.
- [21] D. López-Pintado, "The spread of free-riding behavior in a social network," *Eastern Economic Journal*, vol. 34, no. 4, pp. 464–479, 2008.
- [22] Q. Liao and L. Shi, "She gets a sports car from our donation: rumor transmission in a Chinese microblogging community," in *Proceedings of the 2nd ACM Conference on Computer Supported Cooperative Work*, pp. 587–597, San Antonio, Tex, USA, February 2013.
- [23] Y. M. Zhang, C. S. Tang, and W. G. Li, "Research on interest attenuation and social reinforcement mechanism for rumor spreading in online social networks," *Journal of the China Society for Scientific and Technical Information*, no. 8, pp. 833–844, 2015.
- [24] Y.-J. Li, C. Yin, H. Yu, and Z. Liu, "Link prediction in microblog retweet network based on maximum entropy model," *Acta Physica Sinica*, vol. 65, no. 2, pp. 35–45, 2016.
- [25] K. Afassinou, "Analysis of the impact of education rate on the rumor spreading mechanism," *Physica A: Statistical Mechanics and its Applications*, vol. 414, pp. 43–52, 2014.
- [26] Y. M. Zhang, Y. Y. Su, and H. O. Liu, "Research of rumor spreading considering double social reinforcements in online social networks," *Journal of Chinese Computer Systems*, vol. 38, no. 4, pp. 705–711, 2017.
- [27] Q. Zhang, S. Zhang, J. Dong, J. Xiong, and X. Cheng, "Automatic detection of rumor on social network," in *Proceedings of the 4th CCF Conference on Natural Language Processing and Chinese Computing*, pp. 113–122, Nanchang, China, 2015.
- [28] W. Wang, X. W. Zhang, G. H. Ren, D. X. Qin, and L. L. Liu, "Predicting microblog user retweet behaviors based on energy optimization," *Acta Electronica Sinica*, vol. 45, no. 12, pp. 2987–2996, 2017.
- [29] C. Q. Zhou, Q. C. Zhao, and W. B. Lu, "Modeling of the forwarding behavior in microblogging with adaptive interest," *Journal of Tsinghua University (Science and Technology)*, vol. 55, no. 11, pp. 1163–1170, 2015.
- [30] Q. Liu, "User forwarding behavior predicting fusion of interests and behaviors," *Electronic Technology & Software Engineering*, no. 3, article 205, 2017.
- [31] Y. R. Chen, "Computational complexity of probabilistic inference in ising graphical model," *Computer Science*, no. 2, pp. 253–256, 288, 2013.
- [32] Z. Y. Guo, R. H. Xiao, and J. X. Fang, "Dynamics of quantum discord for Ising system with Dzialoshinskii-Moriya interaction," *Chinese Journal of Quantum Electronics*, vol. 29, no. 5, pp. 547–554, 2012.
- [33] S. B. Ye, "A study on discourse hegemony of key micro bloggers on micro blog," *Journal of Guangzhou University (Social Science Edition)*, vol. 16, no. 8, pp. 72–77, 2017.

- [34] X. Y. Zhai, Y. B. Li, and S. Y. Ma, “Partial entropy and quantum mutual entropy of anisotropic XY models in transverse fields,” *Journal of Nanjing Normal University (Natural Science Edition)*, no. 3, pp. 48–51, 2012.
- [35] L. Sabatelli and P. Richmond, “Non-monotonic spontaneous magnetization in a Sznajd-like consensus model,” *Physica A: Statistical Mechanics and its Applications*, vol. 334, no. 1-2, pp. 274–280, 2004.
- [36] X. Chen, “Self-identity and its risk in digital media,” *Cultural Studies*, no. 2, pp. 75–87, 2017.
- [37] H. J. Cui and T. X. Wang, “A literature review on consumers behavior strategy choice—in the context of self-identity threat,” *East China Economic Management*, vol. 31, no. 9, pp. 171–179, 2017.

## Research Article

# Spatial Dynamics for a Generalized Solow Growth Model

Yue Zhong  and Wenyi Huang 

*The School of Economic Mathematics, Southwestern University of Finance and Economics, Chengdu, Sichuan 611130, China*

Correspondence should be addressed to Yue Zhong; [zhongyue@2016.swufe.edu.cn](mailto:zhongyue@2016.swufe.edu.cn)

Received 10 May 2018; Revised 8 June 2018; Accepted 11 June 2018; Published 17 July 2018

Academic Editor: Jorge E. Macias-Diaz

Copyright © 2018 Yue Zhong and Wenyi Huang. This is an open access article distributed under the Creative Commons Attribution License, which permits unrestricted use, distribution, and reproduction in any medium, provided the original work is properly cited.

The existence of nontrivial equilibrium and poverty traps for a generalized Solow growth model with concave and nonconcave production functions is investigated. The explicit solutions of the growth model, which is expressed by a differential equation with corresponding boundary conditions, are employed to illustrate the spatial dynamics of the model in different economic regions. Numerical method is used to justify the validity of the theoretical analysis.

## 1. Introduction

The distribution over space of spatial economic activities has been investigated in many literatures, in which economic geographers study how and why people make their location choices, consider the reasons of production agglomeration, and find the formation of cities and migration flows. Early regional economic growth models focus on capital, labor, pollution flows, individuals' welfare, and the policymaker both in discrete and continuous cases. In recent years, the new economic geography emerges in economic analysis, where economic geographers employ a refined specification of whole market structures and several precise assumptions on the mobility of production factors. Fujita and Thisse [1] and Krugman [2] use a general equilibrium framework to explain production, consumption, and price formation in local and global economy. Mossay [3] studies that continuous space is not incompatible with regional divergence in different migration schemes which are decided by idiosyncrasies in location taste. Krugman [4] states that the economy always displays regional convergence and migration follows utility-level differentials.

Since the assumption of a continuous space structure in economic model fits better modern economies, several continuous space extensions of economic models have been discussed. Brito [5] has investigated spatial capital accumulation and capital mobility in the spatial Ramsey growth framework. In [5], production and capital accumulation are distributed in continuous space and capital differentials drive

the spatial capital dynamics. La Torre et al. [6] investigate the optimal dynamics of capital and pollution in a spatial economic growth model. Camacho and Barahona [7] analyze spatial optimal land use and environmental degradation. Boucekkine et al. [8] and Camacho et al. [9] illustrate how to choose optimal trajectories of capital and consumption by maximizing an objective function in a spatial Ramsey model with continuous space. Industrial dynamics and economic geography over time and space are considered in Capasso et al. [10]. The relationship between the growth process and stable spatially nonhomogenous distribution for per capital and income is described by Xepapadeas and Yannacopoulos [11]. Boucekkine et al. [12] prove the characterization of the optimal dynamics in a spatial AK model across as a circle and Fabbri [13] investigates the generalized model with AK production function in a generic geographic structure. For other studies of spatial economic growth model, the reader is referred to [14–18] and the references therein.

The classical Solow model describes the evolution in time of gross output which is based upon the input factors, labor, capital, and technology (see [19]). In the Solow model, there exist multiple steady states when production function is not concave for any level of capital. Kamihigashi and Soy [20] establish an optimal discrete time problem when an s-shaped production function is assumed. Ferrara et al. [21] discuss the stability of the classical Solow model with delay and nonconvex technology. Brianzoni et al. [22] investigate the dynamics of a discrete growth model with nonconcave production function in local and global economy. Camacho

and Zou [23] illustrate the long-run structure for the spatial distribution of the capital and the spatially homogeneous steady state when capital movement is modeled by local diffusion and spatial dynamics. Neto and Claeysen [24] consider the stability of a spatial Solow model with labor mobility and prove that capital induced labor migration is a necessary condition for the spatiotemporal dynamics of the model. Capasso et al. [25] prove the steady state of the classical Solow model with a nonconcave production function and analyze the convergence of a spatial Solow model with technological diffusion. In our paper, we generalize the classical Solow model in [25] and obtain the steady states of the generalized Solow model in a geographic structure. In open regions, we prove the existence and uniqueness of solution for a partial differential equation with corresponding boundary conditions, which is different from convergence analysis in [25].

Precisely, the aim of this paper is to investigate the steady states of a generalized Solow model with both concave and nonconcave production functions and obtain the asymptotic properties of solutions for the model in continuous space and bounded time. Using the monotonic property of functions, we choose a function to show the steady state of the generalized Solow model with a concave production function. When production function is not concave, we introduce a nonconcave production function into the generalized Solow model to get the existence of nontrivial equilibrium and poverty traps. Our main contribution is to obtain the explicit solution of an ordinary differential equation which expresses the generalized Solow model in close regions and prove the existence and uniqueness of solution for a partial differential equation in open economy. The obtained result in our work shows the asymptotic capital distribution across space. This is different from those in [23], where solution of a spatial Solow model is given in global economy. On the proof of existence and uniqueness of solution for the generalized Solow model in open economy, we apply an approach used in Boucekkine et al. [8], in which a generalized Ramsey growth model is investigated in global economy.

This paper is organized as follows. Section 2 states a generalized Solow model with concave and nonconcave production functions. We prove the existence of nontrivial equilibrium and poverty traps when several conditions are satisfied and get the time path of capital per effective worker in close economic regions. Section 3 presents the generalized Solow model in open economy and we obtain the existence and uniqueness of the solution for the model. In Section 4, we use numerical method to analyze the solution of the corresponding partial differential equation with boundary conditions by discretizing the space variable. Our conclusions are presented in Section 5.

## 2. A Generalized Solow Model in Autarkic Regions

*2.1. Steady States of the Model with Concave and Nonconcave Production Functions.* Assume that there is only one final good signed to be consumed or invested in one economy market. The generalized Solow model describes the evolution

in time for gross output  $Y(x, t)$  which depends upon the input factors, labor  $L(x, t)$ , capital  $K(x, t)$ , and technology  $A(x, t)$  at work in location  $x \in \Omega$ . The typical mathematical expression linking the input variable is

$$Y(x, t) = A(x, t) F(K(x, t), L(x, t)), \quad (1)$$

where  $F$  is a production function which is continuous and twice differentiable. The usual production function satisfies constant returns to scale or linear homogeneity, which means that the marginal products depend only on the ratio  $K/L$ . All inputs satisfy

$$F(0, L) = F(K, 0) = 0. \quad (2)$$

The evolution of the physical capital over time is described by the following differential equation:

$$\frac{\partial}{\partial t} K(x, t) = Y(x, t) - C(x, t) - \eta K(x, t), \quad (3)$$

where the change of capital stock  $(\partial/\partial t)K(x, t)$  is related to the saved quantity after consumption  $C(x, t)$  and depreciation  $\eta K(x, t)$ . If a traction of the output is saved, we have

$$Y(x, t) - C(x, t) = sY(x, t). \quad (4)$$

We rewrite (3) in the form

$$\frac{\partial}{\partial t} K(x, t) = sA(x, t) F(K(x, t), L(x, t)) - \eta K(x, t). \quad (5)$$

Using a new variable  $k(x, t) = K(x, t)/L(x, t)$ , we obtain

$$\frac{1}{L(x, t)} F(K(x, t), L(x, t)) = F(k(x, t), 1) \quad (6)$$

and

$$\begin{aligned} \frac{\partial}{\partial t} k(x, t) &= \frac{\partial}{\partial t} \left( \frac{K(x, t)}{L(x, t)} \right) \\ &= \frac{L(x, t) (\partial/\partial t) K(x, t) - K(x, t) (\partial/\partial t) L(x, t)}{L^2(x, t)} \\ &= \frac{1}{L(x, t)} \frac{\partial}{\partial t} K(x, t) - n(x, t) \frac{K(x, t)}{L(x, t)}, \end{aligned} \quad (7)$$

where  $n(x, t) = (1/L(x, t))(\partial/\partial t)L(x, t)$  denotes the constant growth rate of the labor input. From (5) and (7), we have the following generalized Solow model:

$$\frac{\partial}{\partial t} k(x, t) = sA(x, t) f(k(x, t)) - (\eta + n)k(x, t), \quad (8)$$

where  $f(k(x, t)) \equiv F(k(x, t), 1)$ ,  $n(x, t) = n$  and  $k(x, t)$  denotes the capital stock held by the representative household located at  $x$  and  $t, x \in \Omega \subset \mathbb{R}, t \geq 0$ .

The hypothesis of a concave production function has played a crucial role in many economic growth models based on intertemporal allocation. It describes the maximum output for all possible combinations of input factors and determines the way that the economic model evolves in time. Usually, a production function  $f(k)$  fulfills the so-called Inada conditions (see [26]), if  $f(k)$  satisfies the following assumptions:

- (A<sub>1</sub>)  $f(k)$  is nonnegative, increasing, and concave;  
 (A<sub>2</sub>)  $\lim_{k \rightarrow 0} f'(k) = +\infty$ ,  $\lim_{k \rightarrow \infty} f'(k) = 0$ ,  $f(0) = 0$ .

Condition (A<sub>2</sub>) implies that the marginal productivity of capital is only related to the distribution of the per capital stock of capital. It is possible to get high returns when one invests only a small amount of money. Obviously, this is not realistic. Even if a basic structure is established for production, one might still get small returns when the returns increase to the point where the law of diminishing returns takes effect. This fact is known as poverty traps (see [27]).

By the change of capital per worker, or to be more precise, one conclusion of (8) shows that the capital per worker can reach its steady state described in the following proposition.

**Proposition 1.** Assume that  $A(x, t) = 1$  and  $f(k)$  is a concave production function. At location  $x_0 \in \Omega$ , if  $\eta + n \in (0, 1)$  and  $s \in (0, 1)$ , (8) has a unique steady state  $\bar{k}$  which is given by

$$\bar{k} = \varphi^{-1} \left( \frac{\eta + n}{s} \right), \quad (9)$$

where  $\varphi(k) = f(k)/k$ .

*Proof.* Equation (8) reaches its steady state if and only if

$$0 = sf(k) - (\eta + n)k. \quad (10)$$

Let

$$\varphi(k) = \frac{f(k)}{k} = \frac{\eta + n}{s}. \quad (11)$$

The function  $\varphi$  gives the output-to-capital ratio in the economy. Since  $f$  is continuous, decreasing, and satisfies the Inada conditions, we have

$$\varphi'(k) = \frac{f'(k)k - f(k)}{k^2} = -\frac{F_L}{k^2} \quad (12)$$

and

$$\begin{aligned} \varphi(0) &= f'(0) = +\infty, \\ \varphi(\infty) &= f'(\infty) = 0. \end{aligned} \quad (13)$$

Since  $\varphi'(k) < 0$ , the function  $\varphi(k) \equiv f(k)/k$  is a decreasing function, which means that (11) has a solution and the solution is unique. Therefore, the steady state of the economy is unique and given by

$$\bar{k} = \varphi^{-1} \left( \frac{\eta + n}{s} \right). \quad (14)$$

□

**Remark 2.** The steady state of the economy in Proposition 1 can be described in other words. That is to say, if there is no technological progress and exponential labor growth, the rate of capital per worker is determined by three variables: saving rate  $s$ , depreciation rate  $\eta$ , and growth rate of labor input  $n$ . Moreover, the capital per worker increases whenever  $sf(k) > (\eta + n)k$  and decreases otherwise.

If  $f(\cdot)$  is a Cobb-Douglas production function, that is,  $f(k) = k^\alpha$ , the economy always converges to the so-called steady state where the capital per capita is constant. Namely, there is just enough money saved to cover the population growth and the amount of capital lost through depreciation. Thus, in the short term, the economy grows faster and both the output per capita and the capital per capita increase. In the long term, the economy tends to a new steady state and the economic growth rate eventually is  $n$  again. Moreover, the saving rate has no effect on the growth rate of the economy. Therefore, the main consequence of the spatial Solow model is that the only way to obtain enduring economic growth is to assume a nonconstant technological progress.

When  $f(\cdot)$  is not concave for any level of capital, the economy is history-dependent and the poverty traps exist in the long-run structure. Using the similar method in [25], we consider a nonconcave production function

$$f(k) = \frac{k^p}{\gamma_1 + \gamma_2 k^p}, \quad (15)$$

where all involved parameters are nonnegative and  $p \geq 2$ .

We focus on the existence of a poverty trap for (8) at location  $x_0 \in \Omega$ . For simplicity, we assume  $A = 1$ ,  $s \in (0, 1)$ , and  $\eta + n = \delta \in (0, 1)$ . If  $sf(k^*) - \delta k^* = 0$ , we have a nontrivial equilibrium  $k^*$ , with  $k^* \neq 0$ . That is,

$$\frac{s(k^*)^p}{\gamma_1 + \gamma_2 (k^*)^p} - \delta k^* = 0. \quad (16)$$

The following proposition states the existence of a poverty trap if

$$\delta < \bar{\delta} = \frac{s[\gamma_1(p-1)/\gamma_2]^{(p-1)/p}}{\gamma_1 p}. \quad (17)$$

**Proposition 3.** At location  $x_0 \in \Omega$ , if  $\delta < s[\gamma_1(p-1)/\gamma_2]^{(p-1)/p}/\gamma_1 p$ , (8) shows two nontrivial equilibria  $k_1^*$  and  $k_2^*$ , with  $k_1^* < k_2^*$ . The economy is unstable at  $k_1^*$  while it is stable at  $k_2^*$ .

*Proof.* From (16), we have

$$\delta = \frac{s(k^*)^{p-1}}{\gamma_1 + \gamma_2 (k^*)^p}. \quad (18)$$

Let  $\varphi(k) = s(k)^{p-1}/(\gamma_1 + \gamma_2(k)^p)$ . Using the basic notions of calculus, when  $\varphi'(\bar{k}^*) = 0$ , we obtain the maximum of the function  $\varphi(k)$  at point  $\bar{k}^* = [\gamma_1(p-1)/\gamma_2]^{1/p}$ . Then the optimal value is

$$\bar{\delta} = \varphi(\bar{k}^*) = \frac{s[\gamma_1(p-1)/\gamma_2]^{(p-1)/p}}{\gamma_1 p}. \quad (19)$$

If  $\delta < \bar{\delta}$ , there exist two equilibria  $k_1^*$  and  $k_2^*$ , with  $k_1^* < [\gamma_1(p-1)/\gamma_2]^{1/p} < k_2^*$ . We come back to (16). Let

$$g(k) := \frac{sk^p}{\gamma_1 + \gamma_2 k^p} - \delta k. \quad (20)$$



We have the first derivative of  $g$ , which is given by

$$g'(k) = \frac{\gamma_1 p s k^{p-1}}{(\gamma_1 + \gamma_2 k^p)^2} - \delta. \quad (21)$$

We verify that  $g'(k_1^*) > 0$  and  $g'(k_2^*) < 0$ , which means that the economy is unstable at  $k_1^*$  while it is stable at  $k_2^*$ .  $\square$

**Remark 4.** Proposition 3 shows that when the level of physical capital surpasses the threshold  $k_1^*$ , it converges certainly to a nontrivial steady state  $k_2^*$ , which is similar to those of the classical Solow model in [25].

**2.2. Asymptotic Analysis.** Assume that all regions are closed and there is no capital flows among the regions, which means that real transfers of goods between regions cannot be financed and there is no trade between regions. Furthermore, a mathematical representation of the assumption is that all locations have access to goods in modern economy (see [1]). Since there are no arbitrage opportunities in an autarkic region (see [5]), we write the regional balance equation as

$$\int_{\Omega} \left\{ \frac{\partial k(x, t)}{\partial t} - s A(x, t) f(k(x, t)) + \eta k(x, t) \right\} dx = 0, \quad \forall (x, t) \in \Omega \times [0, T], \quad (22)$$

where we assume  $L(x, t) = L$  for all  $t$ , which implies  $n = 0$  and the capital stock depreciates at a fixed rate  $\eta$ . We set  $s = 1$  for simplicity. The production function and the technology affect the economic growth. According to the regional balance equation, the instantaneous budget constraint of household at  $x \in \Omega$  is written in the form

$$\frac{\partial k(x, t)}{\partial t} = A(x, t) f(k(x, t)) - \eta k(x, t), \quad (23)$$

$$\forall (x, t) \in \Omega \times [0, T].$$

In addition to (23), we assume that the initial capital distribution  $k(x, 0)$  is known and that there is no capital flow through the boundary  $\partial\Omega$ . Since there is no capital flow if the location is far away from the origin, we have

$$\lim_{x \rightarrow +\infty} \frac{\partial k(x, t)}{\partial x} = 0. \quad (24)$$

We write the initial problem of (23) in the form

$$\frac{\partial k(x, t)}{\partial t} = A(x, t) f(k(x, t)) - \eta k(x, t), \quad (25)$$

$$(x, t) \in \Omega \times [0, T],$$

$$k(x, 0) = k_0(x), \quad x \in \Omega.$$

In order to present the solution of problem (25), we denote  $k(t)(x) \equiv k(x, t)$ . Then, we have

$$k_t(t) = A(x, t) f(k(t)) - \eta k(t), \quad (26)$$

$$(x, t) \in \Omega \times [0, T],$$

$$k(0) = k_0, \quad x \in \Omega,$$

where  $k_t(t) = dk(t)/dt$ . Therefore, problem (26) is equivalent to the standard one-dimensional Solow model.

**Theorem 5.** Suppose that  $A$  is a positive constant. If  $f(k(t)) = k^\alpha(t)$  is a Cobb-Douglas production function, there exists the time path of capital per effective worker to (26).

*Proof.* By a change of variables  $w(t) = k^{1-\alpha}(t)$ , we transform (26) into the following linear differential equation:

$$w_t(t) + (1 - \alpha) \eta w(t) = (1 - \alpha) A. \quad (27)$$

Using the knowledge of ordinary differential equation, we get the mild solution (see [12]) of (27), which is given by

$$\begin{aligned} w(t) &= e^{(\alpha-1)\eta t} w(0) + \int_0^t e^{(t-s)(\alpha-1)\eta} (1 - \alpha) A ds \\ &= e^{(\alpha-1)\eta t} w(0) + (1 - \alpha) A e^{(\alpha-1)\eta t} \int_0^t e^{(1-\alpha)\eta s} ds \\ &= e^{(\alpha-1)\eta t} w(0) + \frac{A}{\eta} e^{(\alpha-1)\eta t} [e^{(1-\alpha)\eta t} - 1] \\ &= e^{(\alpha-1)\eta t} \left( w(0) - \frac{A}{\eta} \right) + \frac{A}{\eta}. \end{aligned} \quad (28)$$

Combining the initialization  $w(0) = k^{1-\alpha}(0)$  into (28), we obtain

$$k(t) = \left[ \left( k^{1-\alpha}(0) - \frac{A}{\eta} \right) e^{(\alpha-1)\eta t} + \frac{A}{\eta} \right]^{1/(1-\alpha)}, \quad (29)$$

which shows the time path of capital per effective worker in autarkic regions.  $\square$

**Remark 6.** Assume that  $r$  is an exogenous interest rate with  $\lambda = r + \eta$ . We get the lifetime budget constraint expressed in present discounted value form for agent if (23) is multiplied by  $e^{-rt}$ . Assume that all debts are required to be paid off. Integrating over  $t$  from  $t = 0$  to  $\infty$ , we obtain a reformulation of the instantaneous budget constraint in the static form

$$\int_0^\infty e^{-rt} \{k_0 + A(x, t) f(k(x, t)) - \lambda k(x, t)\} dt = 0. \quad (30)$$

**Remark 7.** Equation (30) shows an investment optimization problem which is required to characterize the spatial structure of the capital stock. When there exists quadratic adjustment cost denoted by  $(\alpha/2)[\partial k(x, t)/\partial t]^2$  and  $A(x, t) = 1$ , Brock et al. [28] investigates the following investment optimization problem:

$$\begin{aligned} \max_{k'(x, \cdot)} \int_0^\infty e^{-rt} \left\{ f(k(x, t), k^e(x, t)) - \lambda k(x, t) \right. \\ \left. - \frac{\alpha}{2} \left[ \frac{\partial k(x, t)}{\partial t} \right]^2 \right\} dt, \quad \forall x \in \Omega, \end{aligned} \quad (31)$$

where  $k^e(x, t)$  denotes the geographical spillovers.



### 3. A Generalized Solow Growth Model in Open Regions

When capital and goods flow among open regions and there are no (intertemporal) adjustment costs, the aggregate balance equation for region  $\Omega$  becomes

$$\int_{\Omega} \left\{ \frac{\partial k(x, t)}{\partial t} - A(x, t) f(k(x, t)) + \eta k(x, t) + i(x, t) \right\} dx = 0, \quad (32)$$

where  $i(x, t) \neq 0$  is the household's net trade balance of household  $x$  at time  $t$ . The trade is matched by reallocations of capital among regions in a centralized economy. When a decentralized equilibrium is set, we assume that there exists an interspatial capital market where stocks are traded. From (32), for a region  $\Omega$ , the budget constraint follows

$$\frac{\partial k(x, t)}{\partial t} = A(x, t) f(k(x, t)) - \eta k(x, t) - i(x, t), \quad (33)$$

$$(x, t) \in \Omega \times [0, T].$$

In order to eliminate interregional arbitrage opportunities, we consider that capital always flows from regions with low marginal productivity of capital to regions with high marginal productivity of capital. Since  $i(x, t)$  is symmetry of capital account balance, when there are no institutional barriers to capital flows and the regions are internally homogeneous, the current account balance  $i(x, t)$  is measured by the symmetry of the difference of capital intensities with the adjacent regions

$$\begin{aligned} \int_{\Omega} i(x, t) dx &= - \left[ \frac{\partial k(x_i + \Delta x_i, t)}{\partial x} - \frac{\partial k(x_i, t)}{\partial x} \right] \\ &= - \int_{x_i}^{x_i + \Delta x_i} \frac{d}{dx} \left( \frac{\partial k}{\partial x} \right) dx \end{aligned} \quad (34)$$

See [8], that is,

$$\begin{aligned} i(x, t) &= - \frac{d}{dx} \left( \frac{\partial k}{\partial x} \right) \\ &= - \lim_{\Delta x \rightarrow 0} \frac{k_x(x + \Delta x, t) - k_x(x, t)}{\Delta x} \\ &= - \frac{\partial^2 k(x, t)}{\partial x^2}. \end{aligned} \quad (35)$$

Substituting (35) into (32), we have

$$\int_{\Omega} \left\{ \frac{\partial k(x, t)}{\partial t} - \frac{\partial^2 k(x, t)}{\partial x^2} - A(x, t) f(k(x, t)) + \eta k(x, t) \right\} dx = 0 \quad (36)$$

for  $\forall t \geq 0$ .

If we assume that the space interval is sufficiently large and there is no capital flow, we have the following Neumann boundary condition:

$$\frac{\partial k}{\partial x}(x, t) = 0, \quad \partial\Omega \times [0, T]. \quad (37)$$

Then, the budget constraint (36) is written in the form

$$\begin{aligned} \frac{\partial k(x, t)}{\partial t} - \frac{\partial^2 k(x, t)}{\partial x^2} &= A(x, t) f(k(x, t)) \\ &\quad - \eta k(x, t), \quad \Omega \times [0, T], \\ \frac{\partial k}{\partial x} &= 0, \quad \partial\Omega \times [0, T], \\ k(x, 0) &= k_0(x) > 0, \quad x \in \Omega. \end{aligned} \quad (38)$$

System (38) describes the distribution of capital for the generalized Solow model in open economic regions. In recent economic analysis, Boucekine et al. [8] consider the solutions of a generalized Ramsey growth model in global economy. Following the method of [8], we investigate the existence and uniqueness of solution for system (38) in the next theorem.

**Theorem 8.** Suppose  $(A_1)$  and  $(A_2)$  hold. For any given finite  $T$ , if there exist positive constants  $a$  and  $b$  with  $0 < k_0(x) < ae^{b|x^2|}$ , then, problem (38) has a unique solution  $k(x, t) \in C^{2,1}(\Omega \times [0, T])$ , which is given by

$$\begin{aligned} k(x, t) &= \int_{\Omega} k_0(\xi) G(x, \xi, t) d\xi \\ &\quad + \int_0^t \int_{\Omega} (A f(k(\xi, \tau)) - \eta k(\xi, \tau)) \\ &\quad \cdot G(x, \xi, t - \tau) d\xi d\tau, \end{aligned} \quad (39)$$

where

$$G(x, \xi, t) = \begin{cases} \frac{1}{2\sqrt{\pi t}} \exp\left[-\frac{(x - \xi)^2}{4t}\right], & t > 0, \\ 0, & t \leq 0. \end{cases} \quad (40)$$

*Proof.* Defining a sequence  $\{k^{(n)}\}$ ,  $n \geq 1$ , we have the following iteration process:

$$\begin{aligned} \Delta k^{(n)} &= k_t^{(n)} - k_{xx}^{(n)} \\ &= A f(k^{(n-1)}(x, t)) - \eta k^{(n-1)}(x, t), \\ &\quad (x, t) \in \Omega \times [0, T], \end{aligned} \quad (41)$$

$$k^{(n)}(x, 0) = k_0(x), \quad x \in \Omega,$$

where  $k^{(0)}(x, t) = k_0(x)$ . According to Theorem 7.1.1 in [29], we get a unique solution sequence  $\{k^{(n)}\} \in C^{2,1}(R \times [0, T])$ , which is given by

$$k^{(n)}(x, t) = \int_0^t \int_{\Omega} \left( A f(k^{(n-1)}(\xi, t)) - \eta k^{(n-1)}(\xi, t) \right) \cdot G(x, \xi, t - \tau) d\xi d\tau + \int_{\Omega} k_0(\xi) G(x, \xi, t) d\xi, \quad (42)$$

where  $G(x, \xi, t)$  is the fundamental solution to the parabolic operator  $\Lambda$  and given by

$$G(x, \xi, t) = \begin{cases} \frac{1}{2\sqrt{\pi t}} \exp\left[-\frac{(x - \xi)^2}{4t}\right], & t > 0, \\ 0, & t \leq 0. \end{cases} \quad (43)$$

Moreover, for each  $n$ , the solution satisfies the following growth condition:

$$|k^{(n)}| \leq M e^{\beta|x|^2}, \quad x \longrightarrow \pm\infty, \quad (44)$$

where  $M$  and  $\beta$  are positive constants (see [30]). Since the sequence starts from  $k_0$  and  $M$  does not depend on  $n$ , we obtain an estimate of the solution

$$|k^{(n)}| \leq M_1 e^{\beta_1|x|^2}, \quad (x, t) \in \Omega \times [0, T] \quad (45)$$

for positive constants  $M_1$  and  $\beta_1$ . Then, there is a subsequence  $k^{(n_j)}$  which converges to a function  $\tilde{k} \in C^{2,1}(\Omega \times [0, T])$  and satisfies

$$|\tilde{k}| \leq M_2 e^{\beta_2|x|^2}, \quad (x, t) \in \Omega \times [0, T], \quad (46)$$

where  $M_2$  and  $\beta_2$  are positive constants. Following the uniqueness of the solution to the linear equation, we know that the whole sequence converges to the function  $\tilde{k}$ . In (42), when  $n \longrightarrow \infty$ , taking the limit on both sides, we obtain that

$$\begin{aligned} \tilde{k}(x, t) &= \int_{\Omega} k_0(\xi) G(x, \xi, t) d\xi \\ &+ \int_0^t \int_{\Omega} \left( A f(\tilde{k}(\xi, t)) - \eta \tilde{k}(\xi, t) \right) \cdot G(x, \xi, t - \tau) d\xi d\tau \end{aligned} \quad (47)$$

is the solution of problem (38) for  $(x, t) \in \Omega \times [0, T]$ .  $\square$

#### 4. Numerical Method

In this section, numerical method is used to analyze problem (38). Following the idea of Capasso et al. [25], we make problem (38) dimensionless by choosing a characteristic time  $\tilde{t}$  and a characteristic space  $\tilde{x}$  with  $\tilde{t} = t/\tau$  and  $\tilde{x} = x/\chi$ . Considering our model on the interval  $[0, L]$  with  $\chi = L$  as the characteristic space quantity, we get  $\tilde{x} \in [0, 1]$ . Similarly, we assume  $\tau = \eta^{-1}$  on the time interval  $[0, T]$ , where the

end point  $T$  is a characteristic time. Introducing  $\tilde{t}$  and  $\tilde{x}$  into problem (38), we get

$$\begin{aligned} \eta \frac{\partial u}{\partial \tilde{t}}(\tilde{x}, \tilde{t}) - \frac{1}{L^2} \frac{\partial^2 u}{\partial \tilde{x}^2}(\tilde{x}, \tilde{t}) \\ = A(\tilde{x}, \tilde{t}) f(u(\tilde{x}, \tilde{t})) - \eta u(\tilde{x}, \tilde{t}), \end{aligned} \quad (48)$$

where  $u(\tilde{x}, \tilde{t}) = k(\tilde{x}, \tilde{t})$ . For convenience, we rename the characteristic dimensions  $\tilde{x}$  and  $\tilde{t}$  as  $x$  and  $t$ . Then, (48) becomes

$$\begin{aligned} \frac{\partial u(x, t)}{\partial t} - \frac{1}{\eta L^2} \frac{\partial^2 u(x, t)}{\partial x^2} \\ = \frac{A(x, t)}{\eta} f(u(x, t)) - u(x, t). \end{aligned} \quad (49)$$

We introduce an equidistant grid on the region  $\Omega = [0, 1]$  to discretize the space variable (see [31]), that is,

$$0 = x_0 < x_1 < \dots < x_N = 1 \quad (50)$$

with  $x_j = jh$ , for  $h = 1/N$ , and  $j = 0, \dots, N$ .

Using classical difference quotient, we replace the second order space derivative by the following form:

$$\frac{\partial^2 u_j}{\partial x^2}(t) \approx \frac{1}{h^2} [u_{j+1}(t) - 2u_j(t) + u_{j-1}(t)]. \quad (51)$$

From (49), we get the semidiscrete form of (38) in the form

$$\begin{aligned} \frac{\partial u_j}{\partial t}(t) - \frac{1}{h^2 \eta L^2} [(u_{j+1}(t) - 2u_j(t) + u_{j-1}(t))] \\ = \frac{A_j(t)}{\eta} f(u_j(t)) - u_j(t), \end{aligned} \quad (52)$$

for  $j = 1, \dots, N-1$ , where  $u_j(t) \approx u(x_j, t)$ ,  $A_j(t) \approx A(x_j, t)$ . We approximate the boundary condition of (38) by

$$\begin{aligned} \frac{u_1(t) - u_0(t)}{h} &= 0, \\ \frac{u_N(t) - u_{N-1}(t)}{h} &= 0. \end{aligned} \quad (53)$$

Then, we have

$$\begin{aligned} u_1(t) &= u_0(t), \\ u_N(t) &= u_{N-1}(t). \end{aligned} \quad (54)$$

Defining the matrix  $B \in R^{(N+1) \times (N+1)}$

$$B = \frac{1}{h^2} \times \begin{bmatrix} -2 & 1 & & & \\ 1 & -2 & 1 & & 0 \\ & 1 & -2 & 1 & \\ & & \ddots & \ddots & \ddots \\ & & & 1 & -2 & 1 \\ 0 & & & & 1 & -2 & 1 \\ & & & & & 1 & -2 \end{bmatrix} \quad (55)$$

and the vectors

$$\begin{aligned} U_h(t) &= (u_j(t)), \\ F_h(U_h(t)) &= f(u_j(t)), \\ j &= 0, \dots, N, \end{aligned} \quad (56)$$

we rewrite (52) in the form

$$\frac{dU_h}{dt}(t) - \frac{1}{\eta L^2} B U_h(t) = \frac{A(t)}{\eta} F_h(U_h(t)) - U_h(t). \quad (57)$$

In order to obtain the time discretization, we choose a grid on the interval  $[0, T]$  by  $t_k = \tau k$ , where  $\tau = T/m$  and  $k = 0, \dots, m$ , and denote the values by approximating  $U_h(t)$  at the discrete point of time. Using a backward difference quotient, we approximate the time derivative in the form

$$\frac{dU_{h,\tau}}{dt}(t_k) \approx \frac{1}{\tau} (U_{h,\tau}(t_k) - U_{h,\tau}(t_{k-1})). \quad (58)$$

Then, we obtain

$$\begin{aligned} [U_{h,\tau}(t_k) - U_{h,\tau}(t_{k-1})] - \frac{\tau}{\eta L^2} B U_{h,\tau}(t_k) \\ = \frac{\tau A_j(t_k)}{\eta} F_h(U_{h,\tau}(t_k)) - \tau U_{h,\tau}(t_k), \end{aligned} \quad (59)$$

that is,

$$\begin{aligned} U_{h,\tau}(t_k) + \tau U_{h,\tau}(t_k) - \frac{\tau}{\eta L^2} B U_{h,\tau}(t_k) \\ = \frac{\tau A_j(t_k)}{\eta} F_h(U_{h,\tau}(t_k)) + U_{h,\tau}(t_{k-1}). \end{aligned} \quad (60)$$

Defining

$$F'_h(U_{h,\tau}(t_k)) = \text{diag}\left(\frac{df}{du}(u_j(t_k))\right), \quad (61)$$

where

$$\begin{aligned} f(u_j(t_k)) &\approx f(u_j(t_{k-1})) \\ &+ \frac{df}{du}(u_j(t_{k-1}))(u_j(t_k) - u_j(t_{k-1})) \end{aligned} \quad (62)$$

for all  $j = 0, \dots, N$  and  $k = 1, \dots, m$ , we write (60) in the form

$$\begin{aligned} \left[ I + \tau I - \frac{\tau}{\eta L^2} B - \frac{\tau A_j(t_k)}{\eta} F'_h(U_{h,\tau}(t_{k-1})) \right] U_{h,\tau}(t_k) \\ = \frac{\tau A_j(t_k)}{\eta} [F_h(U_{h,\tau}(t_{k-1})) \\ - F'_h(U_{h,\tau}(t_{k-1})) U_{h,\tau}(t_{k-1})] + U_{h,\tau}(t_{k-1}), \end{aligned} \quad (63)$$

where  $I \in R^{N+1 \times N+1}$  is the identity matrix. From (63), we obtain

$$U_{h,\tau}(t_k) = \bar{B}^{-1} D, \quad (64)$$

where

$$\bar{B} = I + \tau I - \frac{\tau}{\eta L^2} B - \frac{\tau A_j(t_k)}{\eta} F'_h(U_{h,\tau}(t_{k-1})) \quad (65)$$

and

$$\begin{aligned} D = \frac{\tau A_j(t_k)}{\eta} [F_h(U_{h,\tau}(t_{k-1})) \\ - F'_h(U_{h,\tau}(t_{k-1})) U_{h,\tau}(t_{k-1})] + U_{h,\tau}(t_{k-1}). \end{aligned} \quad (66)$$

## 5. Conclusions

In this paper, we have investigated a generalized Solow model with continuous space and bounded time. Introducing concave and nonconcave production functions into the generalized Solow model in close regions, we get the steady states of the model when several conditions are satisfied. The asymptotic properties of solutions for the generalized Solow model are proved. We obtain the explicit time path of capital per effective worker by solving an ordinary differential equation in close regions and prove the existence and uniqueness of the solution for the generalized Solow model in open regions. The obtained results show the asymptotic capital distribution across space. Discretizing the space variable, we employ numerical method for the system of partial differential equation to justify the validity of the theoretical analysis.

## Data Availability

No data were used to support this study.

## Conflicts of Interest

The authors declare that they have no conflicts of interest.

## Authors' Contributions

The article is a joint work of two authors who contributed equally to the final version of the paper. All authors read and approved the final manuscript.

## Acknowledgments

This work is supported by the Fundamental Research Funds for the Central Universities (JBK120504).

## References

- [1] M. Fujita and J. F. Thisse, *Economics of Agglomeration*, Cambridge University Press, 2002.
- [2] P. Krugman, "Increasing returns and economic geography," *Journal of Political Economy*, vol. 99, no. 3, pp. 483–499, 1991.

- [3] P. Mossay, "Increasing returns and heterogeneity in a spatial economy," *Regional Science & Urban Economics*, vol. 33, no. 4, pp. 419–444, 2003.
- [4] P. Krugman, *The Self-Organizing Economy, Appendix: A Central Place Model*, Blackwell, Cambridge, MA, USA, 1996.
- [5] P. Brito, *The Dynamics of Growth And Distribution in A Spatially Heterogeneous World*, Working Paper, Department of Economics, ISEG, University of Lisbon, 2004.
- [6] D. La Torre, D. Liuzzi, and S. Marsiglio, "Pollution diffusion and abatement activities across space and over time," *Mathematical Social Sciences*, vol. 78, pp. 48–63, 2015.
- [7] C. Camacho and A. P. Barahona, "Land use dynamics and the environment," *Journal of Economic Dynamics & Control*, vol. 52, pp. 96–118, 2015.
- [8] R. Boucekkine, C. Camacho, and B. Zou, "Bridging the gap between growth theory and the new economic geography: The spatial Ramsey model," *Macroeconomic Dynamics*, vol. 13, no. 1, pp. 20–45, 2009.
- [9] C. Camacho, B. Zou, and M. Briani, "On the dynamics of capital accumulation across space," *European Journal of Operational Research*, vol. 186, no. 2, pp. 451–465, 2008.
- [10] M. Capasso, E. Stam, and E. Cefis, "Industrial dynamics and economic geography," *Regional Studies*, vol. 49, no. 1, pp. 5–9, 2015.
- [11] A. Xepapadeas and A. N. Yannacopoulos, "Spatial growth with exogenous saving rates," *Journal of Mathematical Economics*, vol. 67, pp. 125–137, 2016.
- [12] R. Boucekkine, C. Camacho, and G. Fabbri, "Spatial dynamics and convergence: the spatial AK model," *Journal of Economic Theory*, vol. 148, no. 6, pp. 2719–2736, 2013.
- [13] G. Fabbri, "Geographical structure and convergence: a note on geometry in spatial growth models," *Journal of Economic Theory*, vol. 162, pp. 114–136, 2016.
- [14] R. Boucekkine, G. Fabbri, and P. A. Pintus, "Short-run pain, long-run gain: the conditional welfare gains from international financial integration," *Economic Theory*, vol. 65, no. 2, pp. 329–360, 2018.
- [15] S. Marsiglio and M. Tolotti, "Endogenous growth and technological progress with innovation driven by social interactions," *Economic Theory*, vol. 65, no. 2, pp. 293–328, 2018.
- [16] G. Fabbri, S. Faggian, and G. Freni, *Spatial Resource Wars: A Two Region Example*, Working Paper, Department of Economics Ca' Foscari University of Venice, 2018.
- [17] S. Anita, V. Capasso, H. Kunze, and D. La Torre, "Optimal control and long-run dynamics for a spatial economic growth model with physical capital accumulation and pollution diffusion," *Applied Mathematics Letters*, vol. 26, no. 8, pp. 908–912, 2013.
- [18] W. A. Brock, A. Xepapadeas, and A. N. Yannacopoulos, "Spatial externalities and agglomeration in a competitive industry," *Journal of Economic Dynamics & Control*, vol. 42, pp. 143–174, 2014.
- [19] R. Solow, "A contribution to the theory of economic growth," *The Quarterly Journal of Economics*, vol. 70, pp. 65–94, 1956.
- [20] T. Kamihigashi and S. Roy, "Dynamic optimization with a non-smooth, nonconvex technology: the case of a linear objective function," *Economic Theory*, vol. 29, no. 2, pp. 325–340, 2006.
- [21] M. Ferrara, L. Guerrini, and M. Sodini, "Nonlinear dynamics in a Solow model with delay and non-convex technology," *Applied Mathematics and Computation*, vol. 228, pp. 1–12, 2014.
- [22] S. Brianzoni, C. Mammanna, and E. Michetti, "Local and global dynamics in a discrete time growth model with nonconcave production function," *Discrete Dynamics in Nature and Society*, vol. 2012, Article ID 536570, 22 pages, 2012.
- [23] C. Camacho and B. Zou, "The spatial Solow model," *Economics Bulletin*, vol. 18, pp. 1–11, 2004.
- [24] J. P. J. Neto and J. C. R. Claeysen, "Capital-induced labor migration in a spatial solow model," *Journal of Economy*, vol. 115, pp. 25–47, 2015.
- [25] V. Capasso, R. Engbers, and D. La Torre, "On a spatial Solow model with technological diffusion and nonconcave production function," *Nonlinear Analysis: Real World Applications*, vol. 11, no. 5, pp. 3858–3876, 2010.
- [26] R. J. Barro and X. Sala-Martin, *Economic Growth*, MIT Press, 2004.
- [27] C. Azariadis, "The economics of poverty traps part one: Complete markets," *Journal of Economic Growth*, vol. 1, no. 4, pp. 449–486, 1996.
- [28] W. A. Brock, A. Xepapadeas, and A. N. Yannacopoulos, "Optimal agglomerations in dynamic economics," *Journal of Mathematical Economics*, vol. 53, pp. 1–15, 2014.
- [29] C. V. Pao, *Nonlinear Parabolic and Elliptic Equations*, Plenum Press, New York, NY, USA, 1992.
- [30] O. A. Ladyzenskaja, V. A. Solonnikov, and N. N. Uralceva, *Linear and Quasilinear Equations of Parabolic Type*, American Mathematical Society, Providence, RI, USA, 1968.
- [31] K. W. Morton and D. F. Mayers, *Numerical Solution of Partial Differential Equations*, Cambridge University Press, Cambridge, UK, 1994.

## Research Article

# Research on a Triopoly Dynamic Game with Free Market and Bundling Market in the Chinese Telecom Industry

Junhai Ma , Tiantong Xu , and Wandong Lou 

*College of Management and Economics, Tianjin University, No. 92, Weijin Road, NanKai District Tianjin 300072, China*

Correspondence should be addressed to Junhai Ma; mjhtju@aliyun.com and Tiantong Xu; ttxu201608@126.com

Received 30 March 2018; Revised 31 May 2018; Accepted 3 June 2018; Published 11 July 2018

Academic Editor: Jorge E. Macias-Diaz

Copyright © 2018 Junhai Ma et al. This is an open access article distributed under the Creative Commons Attribution License, which permits unrestricted use, distribution, and reproduction in any medium, provided the original work is properly cited.

Based on the real situation of telecom industry in China, we establish a triopoly game model, which includes two competitive telecom firms and their correlative corporation which produces the complementary product. Both free market and bundling market will be concerned in this dynamic model. Moreover, we consider a one-to-many bundling way instead of two complementary products in terms of the proportion of one to one in a bundling product. By numerical simulation, we find that stable space will decrease and decision chaos appears when the degree of the competition becomes fierce between the two competitive telecom firms. Besides, increasing the amount of bundling services provided by a telecom firm can lead to different impacts on the prices of the three firms investigated. This paper enriches the decision-making for the strategy of bundling pricing and will be valuable for the telecom operators.

## 1. Introduction

As a form of marketing activity, bundling sales are widespread in operations. Since this kind of behavior may increase sales and profits, many large enterprises even small businesses should consider adopting bundling sales strategy. The form of bundling sell is varied, like bundling pricing, exchanging prizes, presenting the prizes, etc. It is worth noting that the phenomenon of bundling pricing not only occurs between tangible products but may also happen to service products; the telecommunications companies sell smart phone with their own service packages, for instance.

In this paper, we focus on two kinds of bundling products provided by two competitive oligarchies of telecom industry in China and their important partner, Apple Inc. The two telecom companies are China Mobile Communications Corporation (CMCC, for short) and China Union Communication Corporation (CUCC, for short). CMCC constitutes the majority of market share and CUCC, which also has a large market share, firstly collaborates with Apple. Both of them cooperate with Apple by the best-selling iPhone. As a high-end product in the smart phone market, iPhone, compared with other cheaper mobile phones, could be bundled with more communication services provided by the telecom firms.

On the other hand, many customers prefer to choose a package including more services instead of a package including fewer services, because the discount would become deeper under the former situation. As Table 4 shows, an extreme case is that when customers choose CUCC's bundling service package 9, which has numerous services, the price of the iPhone seems to reduce to zero. It is no doubt that this is a stratagem for attracting customers. Since each of the three firms has their own channel for marketing, we also consider three free markets.

Anyhow, the essence of bundling pricing is stimulating the demand according to the discount. Therefore, we concentrate on how the discounts provided by the three firms severally or the different degree of competition between the two telecom firms impacts the stability margin in the dynamic model. In our gaming system, a linear demand function and a constant marginal cost are supposed. In order to conform to the actual situation, we investigated all the data of the service packages for the assignment of the parameters.

## 2. Literature Review

Based on game theory and rank-dependent utility theory, Tan et al. [1] studied an incomplete information Cournot



game in an ambiguous decision environment, and they found players decision-making is affected by their behavioral characteristics and psychological preference. Many researchers have contributed much to the field of dynamic system and dynamic system bifurcation and chaos theory. Li and Chen [2] investigated some new nonlinear equations which have exact explicit parametric representations of breaking loop-solutions. Aziz-Alaoui and Chen [3] researched a new piecewise-linear continuous-time three-dimensional autonomous chaotic system and briefly discussed its complex chaotic dynamics. Zelinka et al. [4] introduced the notion of chaos synthesis and developed a new method for chaotic systems synthesis.

With the consideration of mixed bundling pricing and decision research, Shao and Li [5] studied the bundling and product strategy involving the channel competition, and they found that the retailer preferred the bundling strategy in two channel competitions. Under the consideration of the price bundle offers in the telecommunications industry, Le et al. [6] introduced a Bayesian game model. They investigated the case where operators propose substitutable offers and compete for customers, in order to maximize the operator's revenue. Based on game theory, Ma and Mallik [7] pointed out that, under the manufacturer bundling scenario, the manufacturer would not provide the full product line composed of the basic product, the premium product, and the bundle. Pan and Zhou [8] established a two-layer supply chain with bundling and pricing decisions and found that the manufacturer could earn more if he sells complementary products separately. Mantovani and Vandekerckhove [9] researched the strategies of merging and bundling decisions and showed that bundle strategy could not benefit the consumers because it brings surge in prices in their model. By calculating, R. et al. [10] discussed the optimal bundling and pricing. Chen and Wang [11] researched the pricing policies, subsidy policies, and channel selection policies of different power supply chain structures. In the perspective of the mergers producer, Gaudet and Salant [12] compared the profits of firms under different circumstances. Martin [13] studied the price pooling equilibrium under various conditions that firms produce strategic substitutes or strategic complements. Dilip and John [14] figured out that the price bundling as a usual marketing action could result in the diminution of demand. In the field of decision research, Li and Liu [15] studied the coordination of supply chain between a supplier and a retailer with price and sales effort dependent demand.

With the rise of bifurcation and chaos theory, many scholars have been interested in combining the theories to the game in the domain of economy. Agiza and Elsadany [16] built a nonlinear discrete-time duopoly game assuming the oligarchies have heterogeneous expectations. With the discussion of a 6-dimension dynamical system, Ma and Wu [17] described a triopoly game with two products. They investigated the impacts of the adjustment parameter and the reform of flexible manufacturing could decrease fluctuation risk caused by the instability in multiproduct market. By applying continuation theorem in their research, Wang et al. [18] obtained the sufficient conditions of the existence

of positive periodic solutions of a predator-prey system and improved the methods of computation on topological degree. Besides, Yassen and Agiza [19] proposed a delayed bounded rationality model and figured out that the stability region of the model with bounded rationality is reduced when the competitors use different production methods. Bischi et al. [20] showed a dynamic game model and discussed the question of whether the economic hypothesis of the "representative agent" may sometimes impact the results of research. Sarafopoulos [21] conducted the study of a duopoly game which proposes one player has limited rationality and the other uses adaptive expectations. By studying a triopoly price game model, Ma and Wu [22] found the result that the number of time-delay decision makers has no obvious relationship with stability of the system. Based on the Cournot-Bertrand duopoly model, Ma and Pu [23] studied the stability of the system and found only one Nash equilibrium point after calculation. They also showed the bifurcation diagram which could exhibit the behaviors of the system. Elsadany et al. [24] derived a dynamic system with four various firms and indicated that applying a delayed feedback control method can get the stabilization of the chaos. Srivastava and Srivastava [25] confirmed the FACTS devices could regulate the dynamic bifurcations and chaos effectively. Considering a nonlinear cost function, Du et al. [26] investigated the effects of upper and lower limiter on a duopoly game. By establishing a game model which relates to the power market, Tan et al. [27] analyzed the dynamic behaviors in different market parameters and found that the chaos could be controlled to the stable equilibrium point with the time-delayed feedback control method. As to building two different game models, Ma and Guo (2016) investigated the effect of information on the stability. As to building a Cournot model, Ma and Guo [28] investigated a game whose player's decision was based on his estimation. According to the research done by Yue et al. (2016), a point of view that information sharing may not be beneficial to the firms all through is presented. Ma and Ma [29] established a model and found that market competition could lead to bullwhip effect in a supply chain.

In the field of dynamic game, many authors have investigated the products bundled in terms of putting one product A to another product B in a package. However, the reality is often not the ratio of one to one. Therefore, we construct a model in which bundling products accord with ways of one-to-many. Furthermore, our research not only investigates the behavior of bundling pricing but also considers a competition between two monopolies. This initiate consideration enriches the previous studies of bundling pricing and makes the game more realistic.

After the literature review in Section 2, the remaining part of this paper is divided into four sections. Section 3 describes a new-type game model including five subdivided markets, with the consideration of bundling pricing. Besides, we figure out the Nash equilibrium. In Section 4, we do some numerical experiments and analyze the results of the experiments from the perspective of chaos and complexity. Finally, Section 5 is the conclusion of this paper.



### 3. The Model

#### 3.1. The Assumptions

- (a) **Assumption.** We suppose the market demand is divided into five sections, which is shown in Figure 1. Here, markets A, B, and C represent the market of CMCC's product, the market of CUCC's product, and the market of iPhone separately, and the three markets only have their own products without bundling pricing. Besides, markets AC and BC, respectively, mean the market of bundling product, which is a CMCC's product or a CUCC's product bundled a new iPhone 7. Customers would only buy products from the three free markets, like markets A, B, and C, or buy the bundling product in the bundling market, like market AC and market BC.
- (b) **Assumption.** As shown in Tables 1 and 2, the details of the service packages already fixed by the two telecom companies are presented. We consider the customers only decide which service package to choose, instead of thinking more about the costs incurred by the service out of the package.
- (c) **Assumption.** We assume the period of a service is a month. By the exhibition of Tables 1–4, we define both of the service packages, which are CM 1 and CU 1, as a unit of service, which includes 100 minutes' call and 500 M data plan. Thus, the amount of the other service packages is  $m_i$  or  $n_i$  ( $m_i, n_i$  are constants not less than 1) times as the quantity of the CM 1 or CU 1. We assume the amount of the services offered in market AC (or BC) is  $m$  (or  $n$ ), which is the expectation of  $m_i$  (or  $n_i$ ). In the same manner, the discounts of the two bundling products are  $\mu_1^I$  and  $\mu_2^I$ , and their expectations are  $\mu_1$  and  $\mu_2$ .
- (d) **Assumption.** The price of the two telecom firms refers to the price of a unit of service in one month. We also assume the price of the iPhone 7 equals the real price divided by 24, because of the research period in contrast of the services. All markets use the price list as Tables 1 and 2 show.
- (e) **Assumption.** In order to make the research feasible, we assume that all the discounts of the iPhone 7, which is bundled with one of the service packages in the two bundling markets, are the same since the exact discounts for the telecom firms are trade secret. Because of playing a leading role, we assume the discount of the iPhone 7 is a fixed value, 0.84, according to the price of the phone in Table 4, CU 1.
- (f) **Assumption.** Each of the three companies adjusts their price every period under the bounded rationality, in order to maximize their own profits.

3.2. *Variable Enactment.* A series of specification and variables in this Bertrand game model will be enacted in this section:  $p_i(t)$  ( $i = 1, 2, 3$ ) are the definitions for the three products per unit made by the three companies in the period

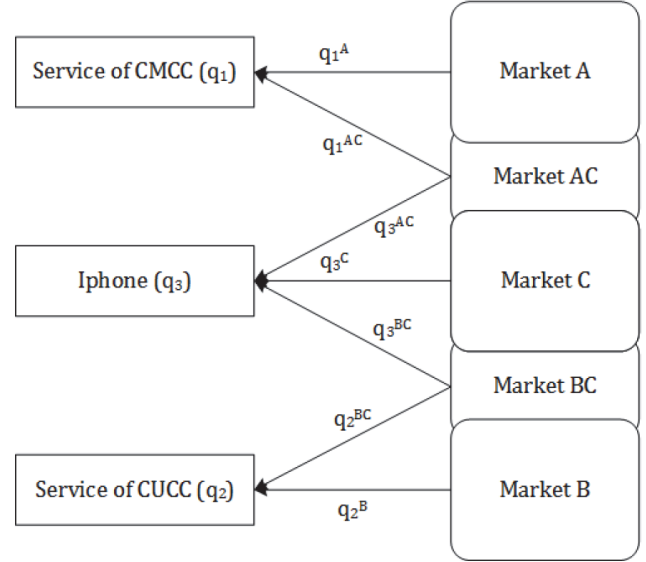


FIGURE 1: The structure of the model.

of  $t$ .  $q_1^A(t)$ ,  $q_2^B(t)$ , and  $q_3^C(t)$  are the demands of products provided by CMCC and CUCC and the demands of iPhone 7 in markets A, B, and C severally during the period of  $t$ . The linear demand functions are as follows:

$$q_1^A(t) = a_1 - b_1 p_1(t) + d_1 p_2(t). \quad (1)$$

$$q_2^B(t) = a_2 - b_2 p_2(t) + d_2 p_1(t). \quad (2)$$

$$q_3^C(t) = a_3 - b_3 p_3(t) \quad (3)$$

where  $a_i$  ( $i = 1, 2, 3$ ) are the positive parameters of potential demand in markets A, B, and C, on condition that the firms fix their prices to zero. And, then,  $b_i$  ( $i = 1, 2, 3$ ) reflect the self-price sensitive coefficients for the three kinds of products. Besides,  $d_i$  ( $i = 1, 2, 3$ ) are denoted as the mutual product substitution ratios between the two telecom firms.

And, then, the parameters  $q_3^{AC}(t)$  and  $q_3^{BC}(t)$  mean the demands of iPhone 7 in market AC and in market BC, respectively, during the period of  $t$ . The demand functions in bundling markets are given as

$$q_3^{AC}(t) = a_{31} - b_{31} \mu p_3(t) - b_{31} r_{31} \mu_1 p_1(t). \quad (4)$$

$$q_3^{BC}(t) = a_{32} - b_{32} \mu p_3(t) - b_{32} r_{32} \mu_2 p_2(t) \quad (5)$$

where the positive parameters  $a_{3i}$  ( $i = 1, 2$ ) are the potential demand for the CMCC's bundling product and the CUCC's bundling product from markets AC and BC. And  $b_{3i}$  ( $i = 1, 2$ ), which are greater than zero, are the self-price sensitive coefficients for the two bundling products. The parameters  $\mu$ ,  $\mu_1$ , and  $\mu_2$  denote the discount given by the three firms. The positive constants  $r_{3i}$  ( $i = 1, 2$ ) are the complementarity degree between two products and  $b_{3i} r_{3i}$  ( $i = 1, 2$ ) are the cross-price sensitive coefficients.

TABLE 1: The price list of CMCC.

service package	call plan (min)	data plan (M)	price of service package (RMB)	$m_i$
CM 1	100	500	58	1.00
CM 2	220	700	88	1.58
CM 3	500	1000	138	2.67
CM 4	500	2000	158	4.22
CM 5	1000	2000	238	5.35
CM 6	1000	3000	268	6.90
CM 7	2000	3000	338	9.15
CM 8	4000	6000	588	18.29

TABLE 2: The price list of CUCC.

service package	call plan (min)	data plan (M)	price of service package (RMB)	$n_i$
CM 1	100	500	56	1.00
CM 2	200	800	76	1.67
CM 3	300	1000	106	2.19
CM 4	500	1000	136	2.56
CM 5	500	2000	166	4.19
CM 6	500	3000	196	5.81
CM 7	1000	4000	296	8.37
CM 8	2000	6000	396	13.5
CM 9	3000	11000	596	23.5

TABLE 3: Details of the service package offered by CMCC.

service package	CM 1	CM 2	CM 3	CM 4	CM 5	CM 6	CM 7	CM 8
service price in the actual situation	58	88	138	158	238	268	338	588
price of the phone in bundling product	5388	5388	5388	5388	5388	5388	5388	5388
price of the phone after mathematic transaction	4540	4540	4540	4540	4540	4540	4540	4540
gift calls	348	528	828	948	1428	1608	2028	3528
service price after mathematic transaction	78.8	101.3	138.8	153.8	213.8	236.3	288.8	476.3
total cost	6432	6972	7872	8232	9672	10212	11472	15972
price ratio ( $p_{ri}^M$ )	1.0	1.29	1.76	1.95	2.71	3.00	3.66	6.04
$m_i$	1.0	1.6	2.7	4.2	5.3	6.9	9.1	18.3
$\mu_1^i$	1.00	0.81	0.66	0.46	0.51	0.43	0.40	0.33

In bundling markets AC and BC as well,  $q_1^{AC}(t)$  and  $q_2^{BC}(t)$  denote the demand of CMCC's service and CUCC's service in period  $t$ . The demand functions are demonstrated as follows:

$$q_1^{AC}(t) = mq_3^{AC}(t) \quad (6)$$

$$= m[a_{31} - b_{31}\mu p_3(t) - b_{31}r_{31}\mu_1 p_1(t)].$$

$$q_2^{BC}(t) = nq_3^{BC}(t) \quad (7)$$

$$= n[a_{32} - b_{32}\mu p_3(t) - b_{32}r_{32}\mu_2 p_2(t)]$$

where the nonintegral parameters  $m$  and  $n$  which are not less than 1 are the multiples of the unit of service.

$q_i(t)$  ( $i = 1, 2, 3$ ), the aggregate demand functions of three products offered by CMCC, CUCC, and Apple in the period  $t$ , are showed as follows:

$$q_1(t) = q_1^A(t) + q_1^{AC}(t) \quad (8)$$

$$= a_1 - b_1 p_1(t) + d_1 p_2(t)$$

$$+ m[a_{31} - b_{31}\mu p_3(t) - b_{31}r_{31}\mu_1 p_1(t)].$$

TABLE 4: Details of the service package offered by CUCC.

service package	CU 1	CU 2	CU 3	CU 4	CU 5	CU 6	CU 7	CU 8	CU 9
service price in the actual situation	56	76	106	136	166	196	296	396	596
price of the phone in bundling product	4549	4359	4069	3779	3489	3199	2239	1279	0
price of the phone after mathematic transaction	4549	4549	4549	4549	4549	4549	4549	4549	4549
gift calls	0	0	0	0	0	0	0	0	0
service price after mathematic transaction	56	68.1	86.0	103.9	121.8	139.8	199.8	259.8	406.5
total cost	5893	6183	6613	7043	7473	7903	9343	10783	14304
price ratio ( $p_{ri}^U$ )	1.00	1.22	1.54	1.86	2.18	2.50	3.57	4.64	7.26
$n_i$	1.0	1.7	2.2	2.6	4.2	5.8	8.4	13.5	15.1
$\mu_2^i$	1.00	0.73	0.70	0.72	0.52	0.43	0.43	0.34	0.48

$$\begin{aligned}
q_2(t) &= q_2^B(t) + q_2^{BC}(t) \\
&= a_2 - b_2 p_2(t) + d_2 p_1(t) \\
&\quad + n[a_{32} - b_{32} \mu p_3(t) - b_{32} r_{32} \mu_2 p_2(t)].
\end{aligned} \tag{9}$$

$$\begin{aligned}
q_3(t) &= q_3^C(t) + q_3^{AC}(t) + q_3^{BC}(t) \\
&= a_3 - b_3 p_3(t) \\
&\quad + [a_{31} - b_{31} \mu p_3(t) - b_{31} r_{31} \mu_1 p_1(t)] \\
&\quad + [a_{32} - b_{32} \mu p_3(t) - b_{32} r_{32} \mu_2 p_2(t)].
\end{aligned} \tag{10}$$

The total profit functions of the three firms are defined as  $\pi_i(t)$  ( $i = 1, 2, 3$ ) in the period of  $t$ . In addition, we suppose a fixed marginal cost greater than zero for each product.  $c_0$  is the cost per unit for the service of two telecom firms, and  $c_3$  is the cost per unit for the iPhone 7.

$$\pi_1(t) = q_1^A(t) p_1(t) + q_1^{AC}(t) \mu_1 p_1(t) - c_0 q_1(t). \tag{11}$$

$$\pi_2(t) = q_2^B(t) p_2(t) + q_2^{BC}(t) \mu_2 p_2(t) - c_0 q_2(t). \tag{12}$$

$$\begin{aligned}
\pi_3(t) &= q_3^C(t) p_3(t) + [q_3^{AC}(t) + q_3^{BC}(t)] \mu p_3(t) \\
&\quad - c_3 q_3(t).
\end{aligned} \tag{13}$$

**3.3. The Dynamic Model.** On the basis of the bounded rationality in Assumption (f), three firms treat their price as the decision variable. Meanwhile, they adjust their price according to the marginal profit  $\partial \pi_i(t) / \partial p_i(t)$  in each period. If the marginal profit is positive in period  $t$ , increasing the price in period  $t + 1$  will be profitable. Conversely, if the marginal profit is negative in period  $t$ , decreasing the price

in period  $t + 1$  will be profitable. The nonlinear functions of the marginal profit are as follows:

$$\begin{aligned}
\frac{\partial \pi_1(t)}{\partial p_1(t)} &= a_1 - b_1 p_1(t) + d_1 p_2(t) + b_1 [c_0 - p_1(t)] \\
&\quad - m \mu_1 [b_{31} \mu p_3(t) - a_{31} + b_{31} r_{31} \mu_1 p_1(t)] \\
&\quad + m b_{31} r_{31} \mu_1 [c_0 - \mu_1 p_1(t)].
\end{aligned} \tag{14}$$

$$\begin{aligned}
\frac{\partial \pi_2(t)}{\partial p_2(t)} &= a_2 - b_2 p_2(t) + d_2 p_1(t) + b_2 [c_0 - p_2(t)] \\
&\quad - n \mu_2 [b_{32} \mu p_3(t) - a_{32} + b_{32} r_{32} \mu_2 p_2(t)] \\
&\quad + n b_{32} r_{32} \mu_2 [c_0 - \mu_2 p_2(t)].
\end{aligned} \tag{15}$$

$$\begin{aligned}
\frac{\partial \pi_3(t)}{\partial p_3(t)} &= a_3 - b_3 p_3(t) - \mu [b_{31} \mu p_3(t) - a_{32} - a_{31} \\
&\quad + b_{32} \mu p_3(t) + b_{31} r_{31} \mu_1 p_1(t) + b_{32} r_{32} \mu_2 p_2(t)] + [c_3 \\
&\quad - \mu p_3(t)] (b_{31} + b_{32}) \mu + b_3 [c_3 - p_3(t)].
\end{aligned} \tag{16}$$

Hence, the dynamic equations in this model could be given by following form:

$$\begin{aligned}
p_1(t+1) &= p_1(t) + \alpha p_1(t) \frac{\partial \pi_1(t)}{\partial p_1(t)} \\
p_2(t+1) &= p_2(t) + \beta p_2(t) \frac{\partial \pi_2(t)}{\partial p_2(t)} \\
p_3(t+1) &= p_3(t) + \gamma p_3(t) \frac{\partial \pi_3(t)}{\partial p_3(t)}
\end{aligned} \tag{17}$$

$$\alpha, \beta, \gamma > 0$$

where we suppose the three companies adjust their price in the speed of  $\alpha$ ,  $\beta$ , and  $\gamma$ , which reflect the decision-making of

the three enterprises. After taking (14)–(16) into (17), we can get functions as follows:

$$\begin{aligned}
 p_1(t+1) &= p_1(t) + \alpha p_1(t) \{a_1 - b_1 p_1(t) + d_1 p_2(t) \\
 &\quad + b_1 [c_0 - p_1(t)] - m \mu_1 [b_{31} \mu p_3(t) - a_{31} \\
 &\quad + b_{31} r_{31} \mu_1 p_1(t)] + m b_{31} r_{31} \mu_1 [c_0 - \mu_1 p_1(t)]\} \\
 p_2(t+1) &= p_2(t) + \beta p_2(t) \{a_2 - b_2 p_2(t) + d_2 p_1(t) \\
 &\quad + b_2 [c_0 - p_2(t)] - n \mu_2 [b_{32} \mu p_3(t) - a_{32} \\
 &\quad + b_{32} r_{32} \mu_2 p_2(t)] + n b_{32} r_{32} \mu_2 [c_0 - \mu_2 p_2(t)]\} \\
 p_3(t+1) &= p_3(t) + \gamma p_3(t) \{a_3 - b_3 p_3(t) \\
 &\quad - \mu [b_{31} \mu p_3(t) - a_{32} - a_{31} + b_{32} \mu p_3(t) \\
 &\quad + b_{31} r_{31} \mu_1 p_1(t) + b_{32} r_{32} \mu_2 p_2(t)] + [c_3 - \mu p_3(t)] \\
 &\quad \cdot (b_{31} + b_{32}) \mu + b_3 [c_3 - p_3(t)]\}.
 \end{aligned} \tag{18}$$

In order to get the positive stable fixed points of the dynamic model, we need the condition of Nash equilibrium state which is  $p_i(t+1) = p_i(t)$  ( $i = 1, 2, 3$ ). After calculation, we obtain only one significant solution in which all the prices are positive; that is,

$$E^* = (p_1^*, p_2^*, p_3^*) \tag{19}$$

Due to the fact that the length of  $p_i^*$  ( $i = 1, 2, 3$ ) is too long to exhibit in this section, we will show the form of them which have taken the fixed parameters in Section 4.

Besides, the Jacobian matrix of dynamic equation (18) is that

$$J = \begin{pmatrix} J_{11} & \alpha d_1 p_1 & -\alpha b_{31} m p_1 \mu \mu_1 \\ \beta d_2 p_2 & J_{22} & -\beta b_{32} n p_2 \mu \mu_2 \\ -\gamma b_{31} p_3 r_{31} \mu \mu_1 & -\gamma b_{32} p_3 r_{32} \mu \mu_2 & J_{33} \end{pmatrix} \tag{20}$$

where

$$\begin{aligned}
 J_{11} &= \alpha (a_1 - b_1 p_1 + d_1 p_2 + b_1 (c_0 - p_1) \\
 &\quad - m \mu_1 (b_{31} p_3 \mu - a_{31} + b_{31} p_1 r_{31} \mu_1) + b_{31} m r_{31} \mu_1 (c_0 \\
 &\quad - p_1 \mu_1)) - \alpha p_1 (2b_{31} m r_{31} \mu_1^2 + 2b_1) + 1. \\
 J_{22} &= \beta (a_2 - b_2 p_2 + d_2 p_1 + b_2 (c_0 - p_2) - n \mu_2 (b_{32} p_3 \mu \\
 &\quad - a_{32} + b_{32} p_2 r_{32} \mu_2) + b_{32} n r_{32} \mu_2 (c_0 - p_2 \mu_2)) \\
 &\quad - \beta p_2 (2b_{32} n r_{32} \mu_2^2 + 2b_2) + 1. \\
 J_{33} &= \gamma (a_3 - b_3 p_3 - \mu (b_{31} p_3 \mu - a_{32} - a_{31} + b_{32} p_3 \mu \\
 &\quad + b_{31} p_1 r_{31} \mu_1 + b_{32} p_2 r_{32} \mu_2) + (c_3 - p_3 \mu) (b_{31} \mu \\
 &\quad + b_{32} \mu) + b_3 (c_3 - p_3)) - \gamma p_3 (2b_3 + 2\mu (b_{31} \mu \\
 &\quad + b_{32} \mu)) + 1.
 \end{aligned} \tag{21}$$

The characteristic polynomial of the matrix of (20) is as the function equation (22) shows. Consider

$$P(\lambda) = \lambda^3 + A'\lambda^2 + B'\lambda + C' \tag{22}$$

where  $A'$ ,  $B'$ , and  $C'$  will be discussed in Section 4. In addition, we can also figure out the stable region of parameters  $\alpha$ ,  $\beta$ , and  $\gamma$  by the condition of Jury criterion as follows:

$$\begin{aligned}
 \Omega_{E^*}(\alpha, \beta, \gamma) &= \{(\alpha, \beta, \gamma) : \\
 &\quad 1 + A' + B' + C' > 0 \\
 &\quad 1 - A' + B' - C' > 0 \\
 &\quad 1 - C'^2 > 0 \\
 &\quad (1 - C'^2) - (B' - A'C')^2 > 0\}.
 \end{aligned} \tag{23}$$

The stable region is the range where  $E^*$  will be stable.

## 4. The Numerical Modeling and Analysis

**4.1. The Parameter Setting.** It is worth mentioning that we investigate the service package in practice, in order to determine the values of parameters, for instance,  $m$ ,  $n$ ,  $\mu_1$ ,  $\mu_2$ , and  $\mu$ . As (A.1) and (A.2) show, the tariffs include different service packages which are posted on their official website, respectively. Based on the analysis for each of the first 8 packages, we figure out and suppose that the utility of 1.45 M data is equal to the utility of 1-minute call in CMCC, and the utility of 1.15 M data is equal to the utility of 1-minute call in CUCC. And then we could obtain all the values of the parameters  $m$  and  $n$ , which are the amount of the service. Each of  $p_{ri}^M$  and  $p_{ri}^U$  refers to each of their service package prices divided by their price of unit service, separately. We can calculate the parameters  $\mu_1^i$  and  $\mu_2^i$ , which are equal to  $p_{ri}^M/m$  and  $p_{ri}^U/n$ , respectively.

Furthermore, compared with the group clients who will be excluded in our research, most individual customers would be more likely to buy several specific service packages. The parameters  $m$ ,  $\mu_1$ ,  $n$ , and  $\mu_2$  are assigned the value of 5.5, 0.47, 6.1, and 0.46, respectively. The calculation of the values of them will be presented in Figure 9. In our research, so as to do in-depth study, we assign values for the rest of the parameters which are as follows:

$$\begin{aligned}
 a_1 &= 3.8, \\
 a_2 &= 3.8, \\
 a_3 &= 4.5, \\
 b_1 &= 0.55, \\
 b_2 &= 0.55, \\
 b_3 &= 0.6, \\
 d_1 &= 0.2, \\
 d_2 &= 0.2,
 \end{aligned}$$

$$\begin{aligned}
c_0 &= 0.0006, \\
c_3 &= 0.95, \\
a_{31} &= 1.5, \\
a_{32} &= 1.5, \\
b_{31} &= 1.15, \\
b_{32} &= 1.15, \\
r_{31} &= 0.5, \\
r_{32} &= 0.5, \\
\mu &= 0.84.
\end{aligned} \tag{24}$$

Moreover,  $\alpha = 0.16$ ,  $\beta = 0.25$ , and  $\gamma = 0.15$  when the adjustment parameter is not changed in the experiments.

**4.2. The Stable Region.** We will do some numerical modeling experiments to investigate how the parameters impact the stable region of Nash equilibrium.

*Experiment 1.* By the parameters assigned into (14)–(16) and (18)–(22), the Nash equilibrium, the Jacobian matrix, and the characteristic polynomial of the matrix are as follows, respectively.

With valuing all (14); (15); and (16) equal to 0, we can get

$$\begin{aligned}
0.2p_2 - 2.5p_1 - 2.5p_3 + 7.68 &= 0 \\
0.2p_1 - 2.58p_2 - 2.71p_3 + 8.01 &= 0 \\
9.43 - 0.222p_2 - 4.45p_3 - 0.227p_1 &= 0.
\end{aligned} \tag{25}$$

Solving (25), we can get

$$E^* = (1.181, 1.272, 1.996). \tag{26}$$

Equation (25) is the Nash equilibrium.

And, then,

$$J = \begin{pmatrix} 1 - 2.95\alpha & 0.236\alpha & -2.95\alpha \\ 0.254\beta & 1 - 3.74\beta & -3.45\beta \\ -0.453\gamma & -0.444\gamma & 1 - 8.87\gamma \end{pmatrix}. \tag{27}$$

Equation (26) is the Jacobian matrix.

Besides,

$$\begin{aligned}
P(\lambda) &= \lambda^3 + (2.95\alpha + 3.74\beta + 8.87\gamma - 3)\lambda^2 + (11\alpha\beta \\
&\quad - 7.48\beta - 17.7\gamma - 5.9\alpha + 24.8\alpha\gamma + 31.7\beta\gamma + 3)\lambda \\
&\quad + 2.95\alpha + 3.74\beta + 8.87\gamma - 11\alpha\beta - 24.8\alpha\gamma \\
&\quad - 31.7\beta\gamma + 87.2\alpha\beta\gamma - 1
\end{aligned} \tag{28}$$

where

$$\begin{aligned}
A' &= 2.95\alpha + 3.74\beta + 8.87\gamma - 3 \\
B' &= 11\alpha\beta - 7.48\beta - 17.7\gamma - 5.9\alpha + 24.8\alpha\gamma \\
&\quad + 31.7\beta\gamma + 3 \\
C' &= 3.74\beta + 8.87\gamma - 11.0\alpha\beta - 24.8\alpha\gamma - 31.7\beta\gamma \\
&\quad + 87.2\alpha\beta\gamma - 1
\end{aligned} \tag{29}$$

Equation (27) is the characteristic polynomial. Moreover, putting (29) into Jury criterion equation (23), we can obtain the system of inequalities which is the stable region. In addition, we acquire the stable region shown in Figure 2(a). As it shows, we set  $\gamma$  equal to 0.15 and calculate the stable region by Jury criterion with both  $\alpha$  and  $\beta$  changing from zero to one. The figure illustrates that the red region is the stable region, and the deep blue, green, orange, light blue, and pink region refer to the 2, 4, 8, 6, and 5 cycles' regions, severally. The rest of the regions, gray region and white region, are the variable overflow area which means the region of chaos. From this figure, we can know that the prices of the firms will have only one Nash equilibrium solution under the fixed adjusted speed in red region. Also, Figure 2(b) shows the stable region and the other regions using the same colors as  $\alpha$  and  $\gamma$  are changed from 0 to 1, on the condition that  $\beta = 0.25$  is fixed. Similarly, with  $\alpha$  assigned the value of 0.16, Figure 2(c) indicates the stable region in the same way as  $\beta$  and  $\gamma$  are changed from 0 to 1.

*Experiment 2.* In order to investigate the impacts to the stable region on conditions of different degree of competition between the two telecom firms, we did the second experiment and exhibited the result by Figure 3. Obviously, we can find that the stable region decreased when the degree of competition became fierce between the CMCC and CUCC from the picture. Under the circumstance of  $\gamma = 0.25$ , the green, the blue, and the red regions reflect the stability of  $d_1 = d_2 = 0.1$ ,  $d_1 = d_2 = 0.4$ , and  $d_1 = d_2 = 0.9$ , severally.

*Experiment 3.* By comparing the content plotted in Figure 4, the authors observed that the stable region increased when the degree of the complementarity was enhanced between the telecommunication products to the smart phones. The three regions in Figures 4(a), 4(b), and 4(c) refer to the stabilities under the circumstances of  $r_{31} = r_{32} = 0.1$ ,  $r_{31} = r_{32} = 0.5$ , and  $r_{31} = r_{32} = 0.9$ , separately.

In addition, the authors plotted the system's largest Lyapunov exponent (LLE), which was illustrated as the variation of system state, as presented in Figure 5. Note that the system was stable when the LLE was smaller than 0. If the LLE is greater than zero, the system enters into chaos. Without changing others parameters, we obtain the stability scope of  $\alpha$ ,  $\beta$ , and  $\gamma$  in Figures 5(a), 5(b), and 5(c) separately.

**4.3. The Impact of Price Adjustment Parameters.** For the sake of investigating the impact of price adjustment parameters, we plot the bifurcation diagrams by changing the adjustment

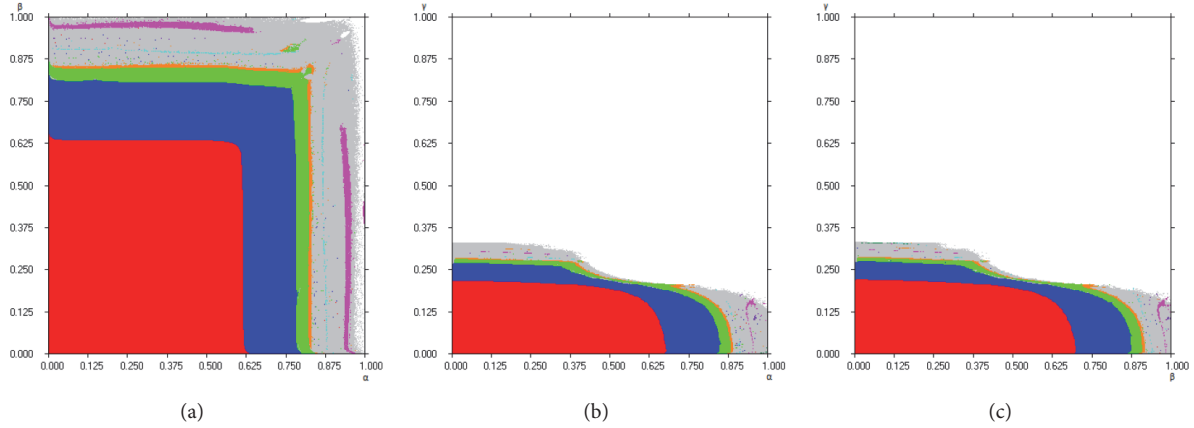


FIGURE 2: (a) The stability with  $\alpha$  and  $\beta$  is changed and  $\gamma = 0.15$ . (b) The stability with  $\alpha$  and  $\gamma$  is changed and  $\beta = 0.25$ . (c) The stability with  $\beta$  and  $\gamma$  is changed and  $\alpha = 0.16$ .

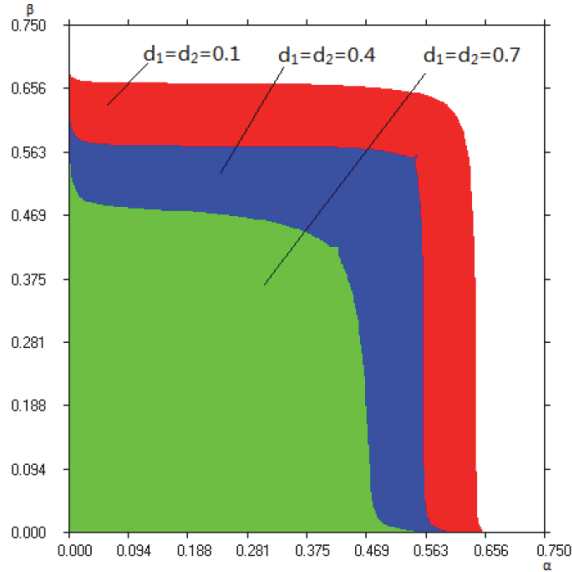


FIGURE 3: The stability of three values of  $d_1$ ,  $d_2$ , with  $\alpha$ , and  $\beta$  is changed, and  $\gamma = 0.25$ .

parameters,  $\alpha$ ,  $\beta$ , and  $\gamma$  in Figures 6(a), 6(b), and 6(c). For the three subfigures, the blue line marked  $p_1$  reflects one unit price of service package offered by CMCC, and the red line refers to one unit price of service package offered by CUCC, and finally the green line represents the price of the iPhone 7. After a period of stability, the system begins bifurcation as the parameter  $\alpha$  goes. The system goes into period four and then period eight, and afterwards it enters into chaos. When the chaos appears, it would be hard for the managers to make decision.

**4.4. The Impact of Bundling Amount.** The impact of parameter  $m$  will be investigated in this section according to Figure 7. We can see that both  $p_1$  and  $p_2$  decrease with the value of  $m$

increases in Figures 7(a) and 7(b). Conversely,  $p_3$  grows up with the increasing of  $m$  in Figure 7(c).

**4.5. The Chaos Attractor.** Figure 8 shows the chaos attractor. In Figure 8(a), the horizontal axis and vertical axis refer to the prices of the service packages of CMCC and CUCC, and then we set  $\alpha$  equal to 0.93. Similarly, in Figure 8(b), the horizontal axis and vertical axis refer to the prices of the service package of CMCC and iPhone 7, and then the authors set  $\alpha$  equal to 0.95. The chaos attractor means a little variation in the initial condition could cause a diverse and unpredictable output. Hence, the firms may suffer enormous risks with competition in the market of chaos. The fluctuations in prices, which are the decision variables made by firms every periods, exert the negative effects.

## 5. Conclusion

In this research, we build a dynamic triopoly model which includes two competitive telecom firms in China and their correlative corporation, which produces the complementary product. Both their free markets and the markets of bundling pricing products are considered in order to make the model more realistic. We do some numerical experiments to research the Nash equilibrium solution, the stable regions, bifurcation of prices, the LLE, and the chaos attractor. The valuable conclusions by our research are as follows: Firstly, we can find that the stable region will decrease when the degree of the competition becomes fierce between the two competitive firms. Secondly, the stable region will increase if the degree of the complementarity enhances between the telecommunication products to the smart phones. Thirdly, moderately increasing the amount of bundling services not only can lead to the decrease of the prices of two telecom firms when the system is stable but also can increase the price of iPhone 7. Hence, for CMCC or CUCC, moderately decreasing their services in packages without the variation of other conditions can increase their service prices. And,



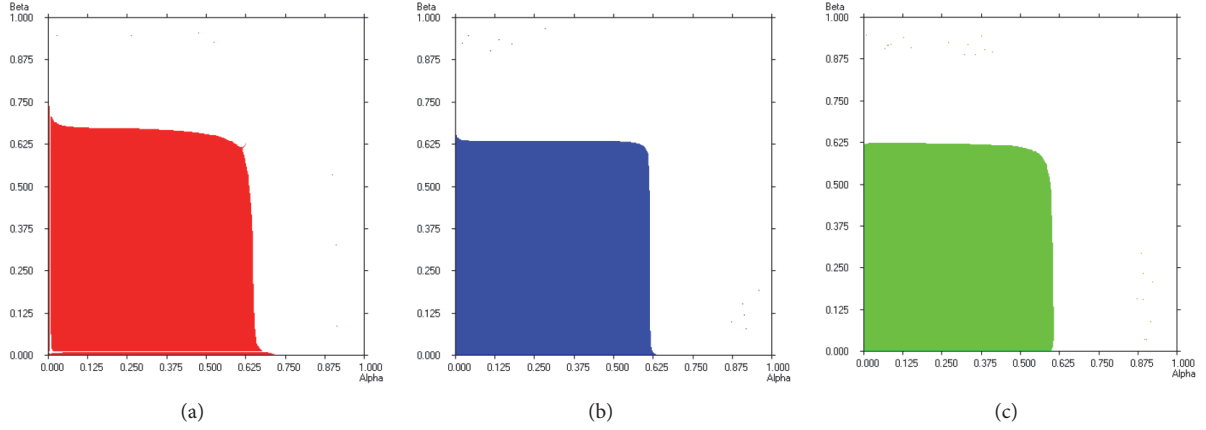


FIGURE 4: (a) The stability with  $\alpha$  and  $\beta$  is changed, and  $\gamma = 0.25$ ;  $r_{31} = r_{32} = 0.1$ . (b) The stability with  $\alpha$  and  $\beta$  is changed, and  $\gamma = 0.25$  and  $r_{31} = r_{32} = 0.5$ . (c) The stability with  $\alpha$  and  $\beta$  is changed, and  $\gamma = 0.25$  and  $r_{31} = r_{32} = 0.9$ .

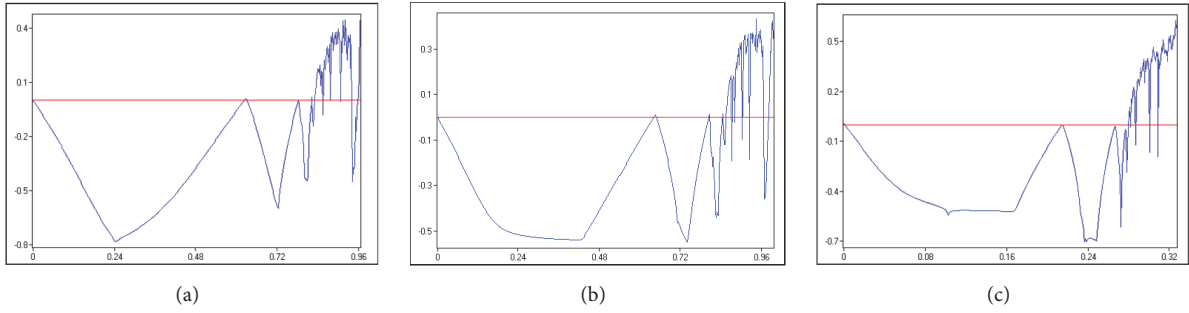


FIGURE 5: (a) The LLE as  $\alpha$  changes. (b) The LLE as  $\beta$  changes. (c) The LLE as  $\gamma$  changes.

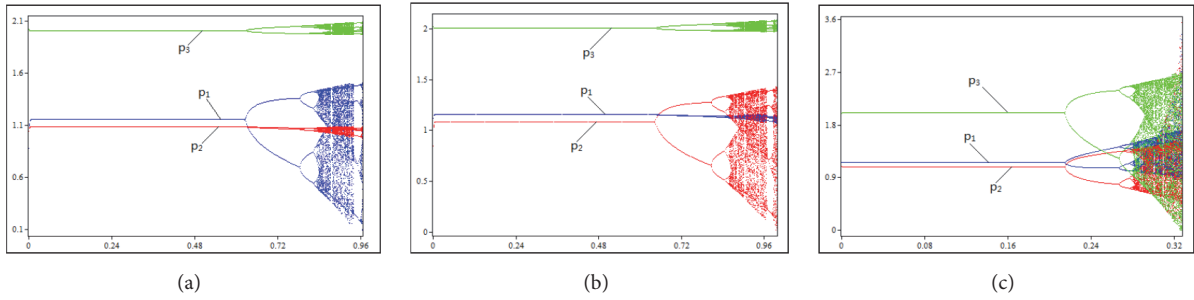


FIGURE 6: (a) Bifurcations of  $p_i$  as  $\alpha$  goes when  $\beta = 0.25$  and  $\gamma = 0.15$ , (b) bifurcations of  $p_i$  as  $\beta$  goes when  $\alpha = 0.16$  and  $\gamma = 0.15$ , and (c) bifurcations of  $p_i$  as  $\gamma$  goes when  $\alpha = 0.16$  and  $\beta = 0.25$ .

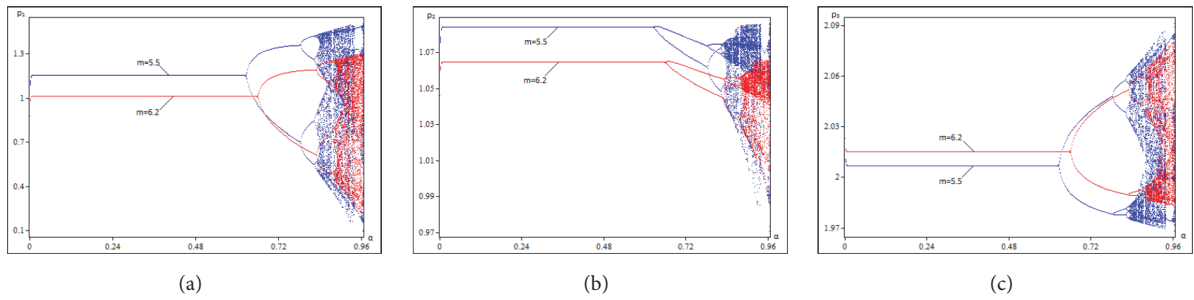


FIGURE 7: (a) Bifurcations of  $p_1$  when  $m = 5.5$  and  $6.2$ , (b) bifurcations of  $p_2$  when  $m = 5.5$  and  $6.2$ , and (c) bifurcations of  $p_3$  when  $m = 5.5$  and  $6.2$ .

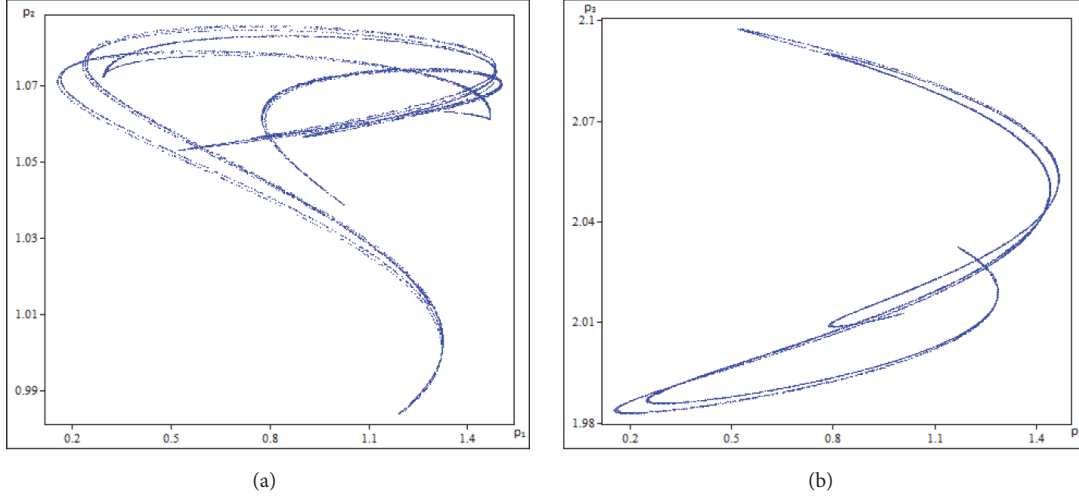


FIGURE 8: (a) The chaos attractor when  $\alpha$  is 0.93,  $\beta = 0.25$ , and  $\gamma$  is 0.15. (b) The chaos attractor when  $\alpha$  is 0.95,  $\beta = 0.25$ , and  $\gamma$  is 0.15.

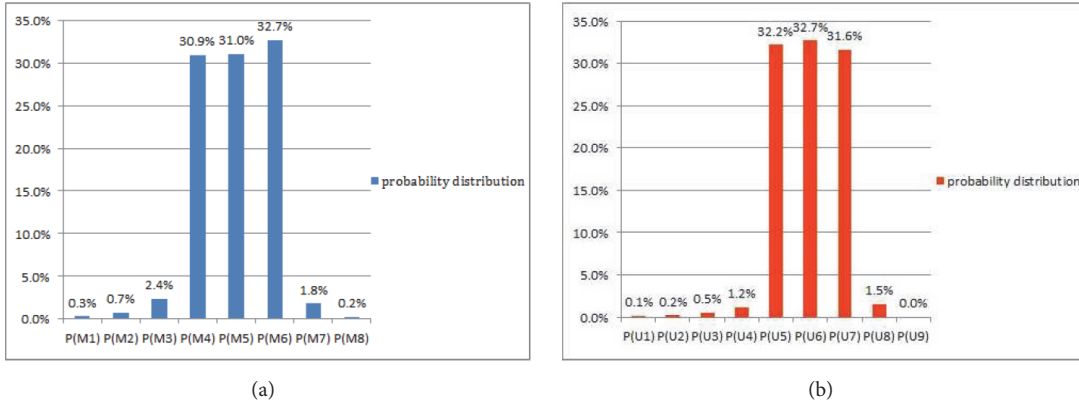


FIGURE 9: (a) The probability distribution of  $m_i$ . (b) The probability distribution of  $n_i$ .

finally, we give the regions of chaos, which should be avoided, from the perspective of economics.

Our research enriches the existing papers about bundling pricing. This research has managerial significance of not only the three firms discussed, but also the enterprises simulated to the three firms. The result of this model may help the managers adjust their decision-making with their experiences. Certainly, there are more studies that should be done in the future, such as considering the firm, which produces the complements, which has different discounts for the two firms, or the innovation of the products in the background of electronic products, etc.

## Appendix

See Tables 1, 2, 3, and 4 and Figure 9.

Based on our research, as shown in Figure 9, we investigate  $P(Mi)$ , which means the probability of the customers choosing the service package of CM  $i$  ( $i=1,2,\dots,8$ ), and also investigate the  $P(Ui)$ , which refers to the probability of the

customers choosing the service package of CU  $i$  ( $i=1,2,\dots,9$ ). So, the expectations of  $m$ ,  $\mu_1$ ,  $n$ , and  $\mu_2$  are as follows:

$$m = \sum_{i=1}^8 m_i P(Mi) \quad (A.1)$$

$$\mu_1 = \sum_{i=1}^8 \mu_1^i P(Mi) \quad (A.2)$$

$$n = \sum_{i=1}^9 n_i P(Ui) \quad (A.3)$$

$$\mu_2 = \sum_{i=1}^9 \mu_2^i P(Ui) \quad (A.4)$$

## Data Availability

The data used to support the findings of this study are available from the corresponding author upon request.

## Conflicts of Interest

The authors declare that they have no conflicts of interest.

## Acknowledgments

The research was supported by the National Natural Science Foundation of China (no. 71571131).

## References

- [1] C. Tan, Z. Liu, D. D. Wu, and X. Chen, "Cournot game with incomplete information based on rank-dependent utility theory under a fuzzy environment," *International Journal of Production Research*, pp. 1–17, 2016.
- [2] J. Li and G. Chen, "On nonlinear wave equations with breaking loop-solutions," *International Journal of Bifurcation and Chaos*, vol. 20, no. 2, pp. 519–537, 2010.
- [3] M. A. Aziz-Alaoui and G. Chen, "Asymptotic analysis of a new piecewise-linear chaotic system," *International Journal of Bifurcation and Chaos*, vol. 12, no. 1, pp. 147–157, 2002.
- [4] I. Zelinka, G. Chen, and S. Celikovskiy, "Chaos synthesis by means of evolutionary algorithms," *International Journal of Bifurcation and Chaos*, vol. 18, no. 4, pp. 911–942, 2008.
- [5] L. Shao and S. Li, "Bundling and product strategy in channel competition," *International Transactions in Operational Research*, 2017.
- [6] H. Le Cadre, M. Bouhtou, and B. Tuffin, "Consumers' preference modeling to price bundle offers in the telecommunications industry: A game with competition among operators," *NET-NOMICS: Economic Research and Electronic Networking*, vol. 10, no. 2, pp. 171–208, 2009.
- [7] M. Ma and S. Mallik, "Bundling of Vertically Differentiated Products in a Supply Chain\*," *Decision Sciences*, vol. 48, no. 4, pp. 625–656, 2017.
- [8] L. Pan and S. Zhou, "Optimal bundling and pricing decisions for complementary products in a two-layer supply chain," *Journal of Systems Science and Systems Engineering*, vol. 26, no. 6, pp. 732–752, 2017.
- [9] A. Mantovani and J. Vandekerckhove, "The strategic interplay between bundling and merging in complementary markets," *Managerial and Decision Economics*, vol. 37, no. 1, pp. 19–36, 2016.
- [10] R. Venkatesh and W. Kamakura, "Optimal Bundling and Pricing under a Monopoly: Contrasting Complements and Substitutes from Independently Valued Products," *Journal of Business*, vol. 76, no. 2, pp. 211–231, 2003.
- [11] X. Chen and X. Wang, "Free or bundled: channel selection decisions under different power structures," *Omega*, vol. 53, pp. 11–20, 2015.
- [12] G. Gaudet and S. W. Salant, "Mergers of producers of perfect complements competing in price," *Economics Letters*, vol. 39, no. 3, pp. 359–364, 1992.
- [13] S. Martin, "Oligopoly limit pricing: Strategic substitutes, strategic complements," *International Journal of Industrial Organization*, vol. 13, no. 1, pp. 41–65, 1995.
- [14] D. Soman and J. T. Gourville, "Transaction decoupling: How price bundling affects the decision to consume," *Journal of Marketing Research*, vol. 38, no. 1, pp. 30–44, 2001.
- [15] Q. Li and Z. Liu, "Supply chain coordination via a two-part tariff contract with price and sales effort dependent demand," *Decision Science Letters*, vol. 4, no. 1, pp. 27–34, 2015.
- [16] H. N. Agiza and A. A. Elsadany, "Chaotic dynamics in nonlinear duopoly game with heterogeneous players," *Applied Mathematics and Computation*, vol. 149, no. 3, pp. 843–860, 2004.
- [17] J. Ma and F. Wu, "The application and complexity analysis about a high-dimension discrete dynamical system based on heterogeneous triopoly game with multi-product," *Nonlinear Dynamics*, vol. 77, no. 3, pp. 781–792, 2014.
- [18] H. Wang, Z. Zhang, and W. Zhou, "Existence of positive periodic solutions for a nonautonomous generalized predator-prey system with time delay in two-patch environment," *Discrete Dynamics in Nature and Society*, vol. 2012, 12 pages, 2012.
- [19] M. T. Yassen and H. N. Agiza, "Analysis of a duopoly game with delayed bounded rationality," *Applied Mathematics and Computation*, vol. 138, no. 2–3, pp. 387–402, 2003.
- [20] G.-I. Bischi, M. Gallegati, and A. Naimzada, "Symmetry-breaking bifurcations and representative firm in dynamic duopoly games," *Annals of Operations Research*, vol. 89, pp. 253–272, 1999.
- [21] G. Sarafopoulos, "Chaotic effect of linear marginal cost in nonlinear duopoly game with heterogeneous players," *Journal of Engineering Science and Technology Review*, vol. 8, no. 1, pp. 19–24, 2015.
- [22] J. Ma and K. Wu, "Complex system and influence of delayed decision on the stability of a triopoly price game model," *Nonlinear Dynamics*, vol. 73, no. 3, pp. 1741–1751, 2013.
- [23] J. Ma and X. Pu, "The research on Cournot-Bertrand duopoly model with heterogeneous goods and its complex characteristics," *Nonlinear Dynamics*, vol. 72, no. 4, pp. 895–903, 2013.
- [24] H. N. Agiza, E. M. Elabbasy, and A. A. Elsadany, "Complex dynamics and chaos control of heterogeneous quadropoly game," *Applied Mathematics and Computation*, vol. 219, no. 24, pp. 11110–11118, 2013.
- [25] K. N. Srivastava, "Elimination of dynamic bifurcation and chaos in power systems using facts devices," *IEEE Transactions on Circuits and Systems I: Fundamental Theory and Applications*, vol. 45, no. 1, pp. 72–78, 1998.
- [26] J. Du, Y. Fan, Z. Sheng, and Y. Hou, "Dynamics analysis and chaos control of a duopoly game with heterogeneous players and output limiter," *Economic Modelling*, vol. 33, pp. 507–516, 2013.
- [27] T. Tan, H. Yang, and X. Deng, "Time-delayed feedback chaos control of dynamic cournot game of power market based on heterogeneous strategies," in *Proceedings of the Transmission and Distribution Exposition Conference: 2008 IEEE PES Powering Toward the Future*, PIMS 2008, usa, April 2008.
- [28] J. Ma and Z. Guo, "The parameter basin and complex of dynamic game with estimation and two-stage consideration," *Applied Mathematics and Computation*, vol. 248, pp. 131–142, 2014.
- [29] J. Ma and X. Ma, "Measure of the bullwhip effect considering the market competition between two retailers," *International Journal of Production Research*, vol. 55, no. 2, pp. 313–326, 2017.

## Research Article

# The Uniqueness Theorem of the Solution for a Class of Differential Systems with Coupled Integral Boundary Conditions

Shuman Meng<sup>1</sup> and Yujun Cui<sup>1,2</sup> 

<sup>1</sup>Department of Applied Mathematics, Shandong University of Science and Technology, Qingdao 266590, China

<sup>2</sup>State Key Laboratory of Mining Disaster Prevention and Control Co-Founded by Shandong Province and the Ministry of Science and Technology, Shandong University of Science and Technology, Qingdao 266590, China

Correspondence should be addressed to Yujun Cui; [cuj720201@163.com](mailto:cuj720201@163.com)

Received 16 April 2018; Accepted 3 July 2018; Published 11 July 2018

Academic Editor: Jorge E. Macias-Diaz

Copyright © 2018 Shuman Meng and Yujun Cui. This is an open access article distributed under the Creative Commons Attribution License, which permits unrestricted use, distribution, and reproduction in any medium, provided the original work is properly cited.

We discuss the uniqueness of the solution to a class of differential systems with coupled integral boundary conditions under a Lipschitz condition. Our main method is the linear operator theory and the solvability for a system of inequalities. Finally, an example is given to demonstrate the validity of our main results.

## 1. Introduction

In this paper, we study the following differential system with coupled integral boundary conditions:

$$\begin{aligned} -u''(t) &= f(t, u(t), v(t)), \quad t \in (0, 1), \\ -v''(t) &= g(t, u(t), v(t)), \quad t \in (0, 1), \\ u(0) &= v(0) = 0, \\ u(1) &= \alpha[v], \\ v(1) &= \beta[u], \end{aligned} \quad (1)$$

where  $\alpha[u], \beta[u]$  are bounded linear functionals on  $C[0, 1]$  given by

$$\begin{aligned} \alpha[u] &= \int_0^1 u(t) dA(t), \\ \beta[u] &= \int_0^1 u(t) dB(t), \end{aligned} \quad (2)$$

involving Riemann-Stieltjes integrals defined via positive Stieltjes measures of  $A, B$ .

Differential systems with coupled boundary conditions have some applications in various fields of sciences and

engineering, for example, the heat equation [1], reaction-diffusion phenomena [2], and interaction problems [3]. The existence of solutions for differential system with coupled boundary conditions has received a growing attention in the literature; for details, see [4–21]. For example, Asif and Khan in [4] obtained the existence of positive solution for singular sublinear system with coupled four-point boundary value conditions by using the Guo-Krasnosel'skii fixed point theorem. In [5], Cui and Sun discuss the existence of positive solutions of singular superlinear coupled integral boundary value problems by constructing a special cone and using fixed point index theory. In [7], Cui and Zou proved the existence of extremal solutions of coupled integral boundary value problems by monotone iterative method. In [10], Infante, Minhós, and Pietramala presented a general theory for existence of positive solutions for coupled systems by use of fixed point index theory.

The question of existence and uniqueness of solution of differential equations and differential systems is an age-old problem and it has a great importance, as much in theory as in applications. This problem has been investigated by use of a variety of nonlinear analyses such as fixed point theorem for mixed monotone operator [7, 15, 22–25], maximal principle [6], Banach's contraction mapping principle [26–29], and the linear operator theory [27, 30, 31].

For example, the authors [31] introduced a Banach space using the positive eigenfunction of linear operator related to differential system (1). They established the uniqueness results for differential system (1) under a Lipschitz condition. It should be noted that the Lipschitz constant is related to the spectral radius corresponding to the related linear operators. The obtained results are optimal from the viewpoint of theory. However, it is very difficult to determine the spectral radius for differential system (1) with general functions  $A(t), B(t)$ .

Motivated by the above works, we investigate the uniqueness of solutions for differential system (1) by using a system of inequalities and the linear operator theory. The main features of this paper are as follows: (1) The main results are mostly implemented to the uniqueness result for coupled boundary value problems. (2) An easy criterion to determine the uniqueness result is obtained by using a system of inequalities. (3) An example shows that the main result provides the same results with weaker conditions.

Throughout the paper, we assume that the following condition hold:

$$(H_1) \quad \alpha[t] = \int_0^1 t dA(t) > 0, \beta[t] = \int_0^1 t dB(t) > 0, \kappa = 1 - \alpha[t]\beta[t] > 0.$$

$$(H_2) \quad f, g : [0, 1] \times \mathbb{R}^2 \longrightarrow \mathbb{R} \text{ are continuous.}$$

## 2. Preliminaries

Let  $C[0, 1]$  be the Banach space with the maximal norm given by  $\|x\| = \max_{t \in [0, 1]} |x(t)|$ . Let  $E = C[0, 1] \times C[0, 1]$ ,  $\|(x, y)\|_E = \max\{\|x\|, \|y\|\}$ . Then  $(E, \|(\cdot, \cdot)\|_E)$  is a Banach space.

**Lemma 1** (see [5]). *Let  $u, v \in C[0, 1]$ , then the system of BVPs*

$$\begin{aligned} -u''(t) &= x(t), \\ -v''(t) &= y(t), \\ t &\in [0, 1], \\ u(0) &= v(0) = 0, \\ u(1) &= \alpha[v], \\ v(1) &= \beta[u] \end{aligned} \quad (3)$$

has integral representation

$$\begin{aligned} u(t) &= \int_0^1 G_1(t, s) x(s) ds + \int_0^1 H_1(t, s) y(s) ds, \\ v(t) &= \int_0^1 G_2(t, s) y(s) ds + \int_0^1 H_2(t, s) x(s) ds, \end{aligned} \quad (4)$$

where

$$\begin{aligned} G_1(t, s) &= \frac{\alpha[t] t}{\kappa} \int_0^1 k(s, \tau) dB(\tau) + k(t, s), \\ H_1(t, s) &= \frac{t}{\kappa} \int_0^1 k(s, \tau) dA(\tau), \end{aligned}$$

$$G_2(t, s) = \frac{\beta[t] t}{\kappa} \int_0^1 k(s, \tau) dA(\tau) + k(t, s),$$

$$H_2(t, s) = \frac{t}{\kappa} \int_0^1 k(s, \tau) dB(\tau),$$

$$k(t, s) = \begin{cases} t(1-s), & 0 \leq t \leq s \leq 1, \\ s(1-t), & 0 \leq s \leq t \leq 1. \end{cases} \quad (5)$$

**Lemma 2** (see [5]). *The functions  $k(t, s), G_i(t, s), H_i(t, s)$  ( $i = 1, 2$ ) satisfy the following properties:*

$$\begin{aligned} G_i(t, s) &\leq \rho t, \\ H_i(t, s) &\leq \rho t, \end{aligned} \quad (6)$$

$$\forall t, s \in [0, 1], \quad i = 1, 2,$$

$$0 < k(t, s) \leq s(1-s), \quad \forall t, s \in (0, 1), \quad (7)$$

where

$$\begin{aligned} \rho &= \max \left\{ \frac{\alpha[t]}{\kappa} \beta[1] + 1, \frac{\beta[t]}{\kappa} \alpha[1] \right. \\ &\quad \left. + 1, \frac{1}{\kappa} \beta[1], \frac{1}{\kappa} \alpha[1] \right\}. \end{aligned} \quad (8)$$

With the help of Lemma 1, BVP (1) can be viewed as a fixed point in  $E$  for the completely continuous operator

$$S(u, v) = (S_1(u, v), S_2(u, v)), \quad (u, v) \in E, \quad (9)$$

where  $S_1, S_2 : E \longrightarrow C[0, 1]$  are defined by

$$\begin{aligned} S_1(u, v)(t) &= \int_0^1 G_1(t, s) f(s, u(s), v(s)) ds \\ &\quad + \int_0^1 H_1(t, s) g(s, u(s), v(s)) ds, \\ S_2(u, v)(t) &= \int_0^1 G_2(t, s) g(s, u(s), v(s)) ds \\ &\quad + \int_0^1 H_2(t, s) f(s, u(s), v(s)) ds. \end{aligned} \quad (10)$$

In order to prove our main result, the following criterion for solving system of inequalities is needed.

**Lemma 3.** *Let  $a, b, c, d \in [0, +\infty)$  with  $a < 1, d < 1$ . Then the inequality system*

$$\begin{aligned} a + b\mu &\leq \lambda, \\ c + d\mu &\leq \lambda\mu \end{aligned} \quad (11)$$

has a solution  $(\lambda, \mu)$  with  $\lambda \in (0, 1), \mu > 0$  if and only if  $a, b, c, d$  satisfy

$$(1-d)(1-a) > bc. \quad (12)$$



*Proof.*

*Necessity.* The proof is obviously true for the case:  $bc = 0$ . So we consider the remaining case  $bc \neq 0$ . From the first inequality in (11), we get

$$\mu \leq \frac{\lambda - a}{b}. \quad (13)$$

Substituting it into the second inequality in (11), we have

$$c \leq (\lambda - d) \mu \leq (\lambda - d) \frac{\lambda - a}{b}. \quad (14)$$

Thus,

$$(1 - d)(1 - a) > (\lambda - d)(\lambda - a) \geq bc. \quad (15)$$

*Sufficiency.* For the case  $bc = 0$ , we can take  $\lambda = \max\{(d + 1)/2, (d + 1)/2\}$ . So we consider the last case  $bc \neq 0$ . Let

$$\varphi(x) = (x - d)(x - a) - bc, \quad x \in \mathbb{R}. \quad (16)$$

From the derivative of  $\varphi(x)$ , we conclude that  $\varphi(x)$  is increasing on  $[(a + d)/2, 1]$ . This together with the locally sign-preserving property of  $\varphi(x)$  implies that there exists  $\lambda \in [(a + d)/2, 1]$  such that

$$(\lambda - d)(\lambda - a) \geq bc \quad (17)$$

The above inequality can be rewritten as

$$\frac{c}{\lambda - d} \leq \frac{\lambda - a}{b}. \quad (18)$$

Hence (11) holds for  $\mu \in [c/(\lambda - d), (\lambda - a)/b]$ .  $\square$

### 3. Main Result

For notational convenience, let

$$\begin{aligned} a_{11} &= \frac{\alpha[t] \beta[\phi]}{\kappa} + \frac{1}{6}, \\ a_{12} &= \frac{\alpha[\phi]}{\kappa}, \\ a_{21} &= \frac{\alpha[\phi] \beta[t]}{\kappa} + \frac{1}{6}, \\ a_{22} &= \frac{\beta[\phi]}{\kappa}, \end{aligned} \quad (19)$$

where

$$\phi(t) = \frac{t(1-t)(1+t)}{6}. \quad (20)$$

Take  $\varphi(t) = t$ . By (7), we get

$$\begin{aligned} \int_0^1 G_1(t, s) \varphi(s) ds &= \frac{\alpha[t] t}{\kappa} \int_0^1 \int_0^1 k(s, \tau) dB(\tau) s ds + \int_0^1 k(t, s) s ds \\ &= \frac{\alpha[t] t}{\kappa} \int_0^1 \int_0^1 k(s, \tau) s ds dB(\tau) + \frac{t(1-t)(1+t)}{6} \\ &= \frac{\alpha[t] t}{\kappa} \int_0^1 \frac{\tau(1-\tau)(1-\tau)}{6} dB(\tau) \\ &\quad + \frac{t(1-t)(1+t)}{6} \leq \left( \frac{\alpha[t] \beta[\phi]}{\kappa} + \frac{1}{6} \right) \cdot t \end{aligned} \quad (21)$$

$$= a_{11}t,$$

$$\begin{aligned} \int_0^1 H_1(t, s) \varphi(s) ds &= \frac{t}{\kappa} \int_0^1 \int_0^1 k(s, \tau) dA(\tau) s ds \\ &= \frac{t}{\kappa} \int_0^1 \int_0^1 k(s, \tau) s ds dA(\tau) \\ &= \frac{t}{\kappa} \int_0^1 \frac{\tau(1-\tau)(1-\tau)}{6} dA(\tau) = \frac{\alpha[\phi]}{\kappa} \cdot t = a_{12}t, \end{aligned} \quad (22)$$

$$\begin{aligned} \int_0^1 G_2(t, s) \varphi(s) ds &= \frac{\beta[t] \alpha[\phi] t}{\kappa} \int_0^1 \int_0^1 k(s, \tau) dA(\tau) s ds \\ &\quad + k(t, s) s ds \\ &= \frac{\beta[t] t}{\kappa} \int_0^1 \frac{\tau(1-\tau)(1-\tau)}{6} dA(\tau) \\ &\quad + \frac{t(1-t)(1+t)}{6} \leq \left( \frac{\alpha[\phi] \beta[t]}{\kappa} + \frac{1}{6} \right) \cdot t \\ &= a_{21}t, \end{aligned} \quad (23)$$

$$\begin{aligned} \int_0^1 H_2(t, s) \varphi(s) ds &= \frac{t}{\kappa} \int_0^1 \int_0^1 k(s, \tau) dB(\tau) s ds \\ &= \frac{t}{\kappa} \int_0^1 \int_0^1 k(s, \tau) s ds dB(\tau) \\ &= \frac{t}{\kappa} \int_0^1 \frac{\tau(1-\tau)(1-\tau)}{6} dB(\tau) = \frac{\beta[\phi]}{\kappa} \cdot t = a_{22}t. \end{aligned} \quad (24)$$

By use of (21), (22), (23), and (24), we present the main result of this paper.

**Theorem 4.** Suppose that there exist four nonnegative constants  $a_1, b_1, c_1, d_1$  such that the following conditions hold:

$$\begin{aligned} &|f(t, u_1, v_1) - f(t, u_2, v_2)| \\ &\leq a_1 |u_1 - u_2| + b_1 |v_1 - v_2|, \\ &t \in [0, 1], \quad u_1, u_2, v_1, v_2 \in \mathbb{R}, \end{aligned}$$

$$\begin{aligned}
& |g(t, u_1, v_1) - g(t, u_2, v_2)| \\
& \leq c_1 |u_1 - u_2| + d_1 |v_1 - v_2|, \\
& t \in [0, 1], \quad u_1, u_2, v_1, v_2 \in \mathbb{R}, \\
& (1 - a_{11}a_1 - a_{12}c_1)(1 - a_{21}d_1 - a_{22}b_1) \\
& > (a_{11}b_1 + a_{12}d_1)(a_{21}c_1 + a_{22}a_1),
\end{aligned} \tag{25}$$

$$\begin{aligned}
a_{11}a_1 + a_{12}c_1 &< 1, \\
a_{21}d_1 + a_{22}b_1 &< 1.
\end{aligned} \tag{26}$$

Then differential system (1) has a unique solution in  $E$ .

*Proof.* We divide the proof into several main steps to show that the operator  $S$  has a unique point in  $E$  under the conditions of Theorem 4.

*Step 1.* It follows from (25), (26), and Lemma 3 that there exist  $\lambda \in (0, 1)$ ,  $\mu > 0$  such that

$$\begin{aligned}
(a_{11}a_1 + a_{12}c_1) + (a_{11}b_1 + a_{12}d_1)\mu &\leq \lambda, \\
(a_{21}c_1 + a_{22}a_1) + (a_{21}d_1 + a_{22}b_1)\mu &\leq \lambda\mu.
\end{aligned} \tag{27}$$

Let us introduce a linear operator  $T$  on  $E$  as

$$T(u, v) = (T_1(u, v), T_2(u, v)), \tag{28}$$

where  $T_1, T_2 : E \rightarrow C[0, 1]$  is given by

$$\begin{aligned}
T_1(u, v)(t) &= \int_0^1 G_1(t, s)(a_1 u(s) + b_1 v(s)) ds \\
&+ \int_0^1 H_1(t, s)(c_1 u(s) + d_1 v(s)) ds, \\
T_2(u, v)(t) &= \int_0^1 G_2(t, s)(c_1 u(s) + d_1 v(s)) ds \\
&+ \int_0^1 H_2(t, s)(a_1 u(s) + b_1 v(s)) ds.
\end{aligned} \tag{29}$$

Take  $\psi(t) = \mu t$ . Now, (21)-(24) and (27) show that

$$\begin{aligned}
T_1(\varphi, \psi)(t) &= \int_0^1 G_1(t, s)(a_1 \varphi(s) + b_1 \psi(s)) ds \\
&+ \int_0^1 H_1(t, s)(c_1 \varphi(s) + d_1 \psi(s)) ds \\
&\leq (a_{11}a_1 + a_{12}c_1)\varphi(t) \\
&+ (a_{11}b_1 + a_{12}d_1)\psi(t) \leq \lambda\varphi(t),
\end{aligned} \tag{30}$$

$$\begin{aligned}
T_2(\varphi, \psi)(t) &= \int_0^1 G_2(t, s)(c_1 \varphi(s) + d_1 \psi(s)) ds \\
&+ \int_0^1 H_2(t, s)(a_1 \varphi(s) + b_1 \psi(s)) ds \\
&\leq (c_1 a_{21} + a_{22} c_1)\varphi(t) \\
&+ (a_{21} d_1 + a_{22} b_1)\psi(t) \leq \lambda\psi(t),
\end{aligned} \tag{31}$$

i.e.,

$$T(\varphi, \psi)(t) \leq \lambda(\varphi(t), \psi(t)). \tag{32}$$

Then for  $p \in \mathbb{N}$ , by induction, we obtain

$$T^p(\varphi, \psi)(t) \leq \lambda^p(\varphi(t), \psi(t)). \tag{33}$$

*Step 2.* For all  $(u, v) \in E$  with  $u(t) \geq 0$  and  $v(t) \geq 0$ , there exists  $M = M(u, v) \in (0, +\infty)$  such that

$$T(u, v)(t) \leq M \cdot (\varphi(t), \psi(t)), \quad t \in [0, 1]. \tag{34}$$

Indeed, by Lemma 2, we have

$$\begin{aligned}
T_1(u, v)(t) &\leq \rho((a_1 + c_1)\|u\| + (b_1 + d_1)\|v\|)t \\
&= \rho((a_1 + c_1)\|u\| + (b_1 + d_1)\|v\|)\varphi(t) \\
T_2(u, v)(t) &\leq \rho((a_1 + c_1)\|u\| + (b_1 + d_1)\|v\|)t \\
&= \frac{\rho((a_1 + c_1)\|u\| + (b_1 + d_1)\|v\|)}{\mu}\psi(t)
\end{aligned} \tag{35}$$

So, we can take  $M = \rho \max\{1, 1/\mu\}((a_1 + c_1)\|u\| + (b_1 + d_1)\|v\|)$  such that (34) holds.

*Step 3.* For any given  $(u_0, v_0) \in E$ ,  $n = 1, 2, \dots$ , let  $(u_n, v_n) = S(u_{n-1}, v_{n-1})$ . By Step 2, there exists  $M > 0$  such that

$$\begin{aligned}
T(|u_1(t) - u_0(t)|, |v_1(t) - v_0(t)|) \\
\leq M \cdot (\varphi(t), \psi(t)), \quad t \in [0, 1].
\end{aligned} \tag{36}$$

Notice for  $p \in \mathbb{N}$  that

$$\begin{aligned}
|u_{n+p+1}(t) - u_{n+p}(t)| &= |S_1(u_{n+p}, v_{n+p})(t) \\
&- S_1(u_{n+p-1}, v_{n+p-1})(t)| \leq \int_0^1 G_1(t, s) \\
&\cdot |f(s, u_{n+p}(s), v_{n+p}(s)) \\
&- f(s, u_{n+p-1}(s), v_{n+p-1}(s))| ds \\
&+ \int_0^1 H_1(t, s) |g(s, u_{n+p}(s), v_{n+p}(s)) \\
&- g(s, u_{n+p-1}(s), v_{n+p-1}(s))| ds \\
&\leq \int_0^1 G_1(t, s) (a_1 |u_{n+p}(t) - u_{n+p-1}(t)| \\
&+ b_1 |v_{n+p}(t) - v_{n+p-1}(t)|) ds + \int_0^1 H_1(t, s) \\
&\cdot (c_1 |u_{n+p}(t) - u_{n+p-1}(t)|
\end{aligned}$$

$$\begin{aligned}
& + d_1 |v_{n+p}(t) - v_{n+p-1}(t)|) ds = T_1 (|u_{n+p}(t) \\
& - u_{n+p-1}(t)|, |v_{n+p}(t) - v_{n+p-1}(t)|)(t) \leq \dots \\
& \leq T_1^{n+p} (|u_1 - u_0|, |v_1 - v_0|)(t), \\
& |v_{n+p+1}(t) - v_{n+p}(t)| \leq T_2^{n+p} (|u_1 - u_0|, |v_1 - v_0|)(t).
\end{aligned} \tag{37}$$

Thus, by (33) and (36), we obtain that

$$\begin{aligned}
& (|u_{n+p+1}(t) - u_{n+p}(t)|, |v_{n+p+1}(t) - v_{n+p}(t)|) \\
& \leq T^{n+p} (|u_1(t) - u_0(t)|, |v_1(t) - v_0(t)|) \\
& \leq MT^{n+p-1} (\varphi, \psi)(t) \leq M\lambda^{n+p-1} (\varphi(t), \psi(t)).
\end{aligned} \tag{38}$$

Thus for  $n, m \in \mathbb{N}$ , we conclude that

$$\begin{aligned}
|u_{n+m}(t) - u_n(t)| & \leq |u_{n+m}(t) - u_{n+m-1}(t)| + \dots \\
& + |u_{n+1}(t) - u_n(t)| \\
& \leq M(\lambda^{n+m-2} + \dots + \lambda^{n-1})\varphi(t) \\
& = M \frac{\lambda^{n-1} - \lambda^{n+m-1}}{1 - \lambda} \varphi(t), \\
|v_{n+m}(t) - v_n(t)| & \leq M \frac{\lambda^{n-1} - \lambda^{n+m-1}}{1 - \lambda} \psi(t).
\end{aligned} \tag{39}$$

The above two inequalities ensure that  $\{(u_n, v_n)\}$  is a Cauchy sequence in  $E$ . Since  $E$  is complete, there exists  $(u^*, v^*) \in E$  such that  $\lim_{n \rightarrow \infty} (u_n, v_n) = (u^*, v^*)$ . Therefore,  $(u^*, v^*)$  is a fixed point of  $S$  that follows from the continuity of operator  $S$ .

*Step 4.* We show that  $S$  has a unique fixed point. Suppose there exist two elements  $(u^*, v^*), (u_*, v_*)$  with  $S(u^*, v^*) = (u^*, v^*)$  and  $S(u_*, v_*) = (u_*, v_*)$ . By Step 2, there exists  $M > 0$  such that

$$\begin{aligned}
& T(|u^*(t) - u_*(t)|, |v^*(t) - v_*(t)|) \\
& \leq M(\varphi(t), \psi(t)), \quad t \in [0, 1].
\end{aligned} \tag{40}$$

Applying the method used in Step 3 again, for  $p \in \mathbb{N}$ , we get

$$\begin{aligned}
|u^*(t) - u_*(t)| & \leq M \frac{\lambda^p}{1 - \lambda} \varphi(t), \\
|v^*(t) - v_*(t)| & \leq M \frac{\lambda^p}{1 - \lambda} \psi(t).
\end{aligned} \tag{41}$$

Hence we get the desired results.  $\square$

In the following, we give an example to illustrate our theory.

*Example 5.* Consider the differential system

$$\begin{aligned}
-x''(t) & = \sin x(t) + \ln(1 + y^2(t)) + h_1(t), \\
& t \in (0, 1), \\
-y''(t) & = 2 \arctan x(t) + \sqrt{1 + y^2(t)} + h_2(t), \\
& t \in (0, 1),
\end{aligned} \tag{42}$$

$$x(0) = y(0) = 0,$$

$$x(1) = \int_0^1 y(t) dt,$$

$$y(1) = 2 \int_0^1 x(t) dt,$$

where  $h_1, h_2 \in C[0, 1]$ . We have

$$\begin{aligned}
A(t) & = t, \\
B(t) & = 2t, \\
\alpha[t] & = \frac{1}{2}, \\
\beta[t] & = 1, \\
\kappa & = \frac{1}{2}, \\
\alpha[\phi] & = \frac{1}{24}, \\
\beta[\phi] & = \frac{1}{12}, \\
a_{11} & = \frac{\alpha[t] \beta[\phi]}{\kappa} + \frac{1}{6} = \frac{1}{4}, \\
a_{12} & = \frac{\alpha[\phi]}{\kappa} = \frac{1}{12}, \\
a_{21} & = \frac{\alpha[\phi] \beta[t]}{\kappa} + \frac{1}{6} = \frac{1}{4}, \\
a_{22} & = \frac{\beta[\phi]}{\kappa} = \frac{1}{6}.
\end{aligned} \tag{43}$$

Let

$$f(t, x, y) = \sin x + \ln(1 + y^2) + h_1(t), \tag{44}$$

$$g(t, x, y) = 2 \arctan x + \sqrt{1 + y^2} + h_2(t),$$

then

$$\begin{aligned}
|f(t, u_1, v_1) - f(t, u_2, v_2)| & \leq |u_1 - u_2| + |v_1 - v_2|, \\
|g(t, u_1, v_1) - g(t, u_2, v_2)| & \leq 2|u_1 - u_2| + |v_1 - v_2|,
\end{aligned} \tag{45}$$

where  $t \in [0, 1], u_1, u_2, v_1, v_2 \in \mathbb{R}$ . Hence, there exists a solution  $(\lambda, \mu) = (11/12, 3/2)$  of the following inequality system:

$$(a_{11}a_1 + a_{12}c_1) + (a_{11}b_1 + a_{12}d_1)\mu = \frac{5}{12} + \frac{1}{3}\mu \leq \lambda,$$

$$(a_{21}c_1 + a_{22}a_1) + (a_{21}d_1 + a_{22}b_1)\mu = \frac{2}{3} + \frac{5}{12}\mu \leq \lambda\mu. \quad (46)$$

Therefore, according to Theorem 4, the problem (42) has a unique solution.

When the nonlinearity of differential equation and differential system satisfies Lipschitz condition, the usual method to obtain the uniqueness is the well-known Banach's contraction principle. For this purpose, we should add some restriction on the Lipschitz constants to guarantee the norm of a linear operator related to differential equation and differential system less than 1. Next, we discuss the estimate of the norm of a linear operator related to differential system (42).

Take  $\sigma(t) = 1$ ,  $\varrho(t) = 3/2$ . After standard computation, we get

$$\begin{aligned} \int_0^1 G_1(t, s) \sigma(s) ds &= \int_0^1 G_2(t, s) \sigma(s) ds = \frac{4t - t^2}{6}, \\ \int_0^1 H_1(t, s) \sigma(s) ds &= \frac{t}{6}, \\ \int_0^1 H_2(t, s) \sigma(s) ds &= \frac{t}{3}. \end{aligned} \quad (47)$$

Then

$$\begin{aligned} T_1(\sigma, \varrho)(t) &= \int_0^1 G_1(t, s) (\sigma(s) + \varrho(s)) ds \\ &\quad + \int_0^1 H_1(t, s) (2\sigma(s) + \varrho(s)) ds \\ &= \frac{20t - 5t^2}{12} + \frac{7t}{12} = \frac{27t - 5t^2}{12}, \\ T_2(\sigma, \varrho)(t) &= \int_0^1 G_2(t, s) (2\sigma(s) + \varrho(s)) ds \\ &\quad + \int_0^1 H_2(t, s) (\sigma(s) + \varrho(s)) ds \\ &= \frac{28t - 7t^2}{12} + \frac{5t}{6} = \frac{38t - 7t^2}{12}. \end{aligned} \quad (48)$$

So it follows from the definition of the norm for linear operator that

$$\|T\| \geq \frac{\|T(\sigma, \varrho)\|_E}{\|(\sigma, \varrho)\|_E} = \frac{31}{18} > 1. \quad (49)$$

Thus Example 5 shows that Theorem 4 provides the same results with weaker conditions.

## Data Availability

The data used to support the findings of this study are included within the article.

## Conflicts of Interest

The authors declare that they have no conflicts of interest.

## Acknowledgments

The project is supported by the National Natural Science Foundation of China (11371221, 11571207), Shandong Natural Science Foundation (ZR2018MA011), and the Tai'shan Scholar Engineering Construction Fund of Shandong Province of China.

## References

- [1] M. Pedersen and Z. Lin, "Blow-up analysis for a system of heat equations coupled through a nonlinear boundary condition," *Applied Mathematics Letters*, vol. 14, no. 2, pp. 171–176, 2001.
- [2] A. A. Leung, "A semilinear reaction-diffusion prey-predator system with nonlinear coupled boundary conditions: equilibrium and stability," *Indiana University Mathematics Journal*, vol. 31, no. 2, pp. 223–241, 1982.
- [3] F. Ali Mehmeti and S. Nicaise, "Nonlinear interaction problems," *Nonlinear Analysis. Theory, Methods & Applications. An International Multidisciplinary Journal*, vol. 20, no. 1, pp. 27–61, 1993.
- [4] N. A. Asif and R. A. Khan, "Positive solutions to singular system with four-point coupled boundary conditions," *Journal of Mathematical Analysis and Applications*, vol. 386, no. 2, pp. 848–861, 2012.
- [5] Y. Cui and J. Sun, "On existence of positive solutions of coupled integral boundary value problems for a nonlinear singular superlinear differential system," *Electronic Journal of Qualitative Theory of Differential Equations*, vol. 41, pp. 1–13, 2012.
- [6] Y. Cui and Y. Zou, "An existence and uniqueness theorem for a second order nonlinear system with coupled integral boundary value conditions," *Applied Mathematics and Computation*, vol. 256, pp. 438–444, 2015.
- [7] Y. Cui, L. Liu, and X. Zhang, "Uniqueness and existence of positive solutions for singular differential systems with coupled integral boundary value problems," *Abstract and Applied Analysis*, vol. 2013, Article ID 340487, 9 pages, 2013.
- [8] Y. Cui and Y. Zou, "Monotone iterative method for differential systems with coupled integral boundary value problems," *Boundary Value Problems*, vol. 2013, p. 245, 2013.
- [9] Y. Cui, "Existence of solutions for coupled integral boundary value problem at resonance," *Publicationes Mathematicae*, vol. 89, no. 1-2, pp. 73–88, 2016.
- [10] G. Infante, F. M. Minhós, and P. Pietramala, "Non-negative solutions of systems of ODEs with coupled boundary conditions," *Communications in Nonlinear Science and Numerical Simulation*, vol. 17, no. 12, pp. 4952–4960, 2012.
- [11] Y. Cui and Y. Zou, "Existence of solutions for second-order integral boundary value problems," *Lithuanian Association of Nonlinear Analysts. Nonlinear Analysis: Modelling and Control*, vol. 21, no. 6, pp. 828–838, 2016.
- [12] J. Henderson, R. Luca, and A. Tudorache, "On a system of fractional differential equations with coupled integral boundary conditions," *Fractional Calculus and Applied Analysis*, vol. 18, no. 2, pp. 361–386, 2015.
- [13] J. Jiang, L. Liu, and Y. Wu, "Symmetric positive solutions to singular system with multi-point coupled boundary conditions,"

- Applied Mathematics and Computation*, vol. 220, pp. 536–548, 2013.
- [14] J. Jiang, L. Liu, and Y. Wu, “Positive solutions to singular fractional differential system with coupled boundary conditions,” *Communications in Nonlinear Science and Numerical Simulation*, vol. 18, no. 11, pp. 3061–3074, 2013.
  - [15] L. Liu, H. Li, C. Liu, and Y. Wu, “Existence and uniqueness of positive solutions for singular fractional differential systems with coupled integral boundary conditions,” *The Journal of Nonlinear Science and its Applications*, vol. 10, no. 1, pp. 243–262, 2017.
  - [16] C. Lu, C. Fu, and H. Yang, “Time-fractional generalized Boussinesq equation for Rossby solitary waves with dissipation effect in stratified fluid and conservation laws as well as exact solutions,” *Applied Mathematics and Computation*, vol. 327, pp. 104–116, 2018.
  - [17] T. Qi, Y. Liu, and Y. Zou, “Existence result for a class of coupled fractional differential systems with integral boundary value conditions,” *Journal of Nonlinear Sciences and Applications. JNSA*, vol. 10, no. 7, pp. 4034–4045, 2017.
  - [18] Q. Sun and Y. Cui, “Existence results for  $(k, n - k)$  conjugate boundary-value problems with integral boundary conditions at resonance with  $\ker L = 2$ ,” *Boundary Value Problems*, vol. 1, p. 29, 2017.
  - [19] C. Yuan, D. Jiang, D. O’Regan, and R. P. Agarwal, “Multiple positive solutions to systems of nonlinear semipositone fractional differential equations with coupled boundary conditions,” *Electronic Journal of Qualitative Theory of Differential Equations*, vol. 13, p. 17, 2012.
  - [20] Yumei Zou, Lishan Liu, and Yujun Cui, “The Existence of Solutions for Four-Point Coupled Boundary Value Problems of Fractional Differential Equations at Resonance,” *Abstract and Applied Analysis*, vol. 2014, pp. 1–8, 2014.
  - [21] Y. Zou and G. He, “A fixed point theorem for systems of nonlinear operator equations and applications to  $(p_1, p_2)$ -Laplacian system,” *Mediterranean Journal of Mathematics*, vol. 15, no. 2, Art. 74, 11 pages, 2018.
  - [22] L. Guo, L. Liu, and Y. Wu, “Uniqueness of iterative positive solutions for the singular fractional differential equations with integral boundary conditions,” *Boundary Value Problems*, vol. 2016, p. 147, 2016.
  - [23] X. Lin, D. Jiang, and X. Li, “Existence and uniqueness of solutions for singular fourth-order boundary value problems,” *Journal of Computational and Applied Mathematics*, vol. 196, no. 1, pp. 155–161, 2006.
  - [24] D. Min, L. Liu, and Y. Wu, “Uniqueness of positive solutions for the singular fractional differential equations involving integral boundary value conditions,” *Boundary Value Problems*, vol. 2018, 23 pages, 2018.
  - [25] X. Zhang, L. Liu, and Y. Wu, “Existence and uniqueness of iterative positive solutions for singular Hammerstein integral equations,” *Journal of Nonlinear Sciences and Applications. JNSA*, vol. 10, no. 7, pp. 3364–3380, 2017.
  - [26] Z. Bai, “On positive solutions of a nonlocal fractional boundary value problem,” *Nonlinear Analysis: Theory, Methods & Applications*, vol. 72, no. 2, pp. 916–924, 2010.
  - [27] Y. Cui, W. Ma, Q. Sun, and X. Su, “New uniqueness results for boundary value problem of fractional differential equation,” *Nonlinear Analysis: Modelling and Control*, pp. 31–39, 2018.
  - [28] X. Zhang and Q. Zhong, “Uniqueness of solution for higher-order fractional differential equations with conjugate type integral conditions,” *Fractional Calculus and Applied Analysis*, vol. 20, no. 6, pp. 1471–1484, 2017.
  - [29] Y. Zou and G. He, “On the uniqueness of solutions for a class of fractional differential equations,” *Applied Mathematics Letters*, vol. 74, pp. 68–73, 2017.
  - [30] Y. Cui, “Uniqueness of solution for boundary value problems for fractional differential equations,” *Applied Mathematics Letters*, vol. 51, pp. 48–54, 2016.
  - [31] Y. Cui, W. Ma, X. Wang, and X. Su, “Uniqueness theorem of differential system with coupled integral boundary conditions,” *Electronic Journal of Qualitative Theory of Differential Equations*, vol. 9, pp. 1–10, 2018.



## Research Article

# Applications of General Residual Power Series Method to Differential Equations with Variable Coefficients

Bochao Chen,<sup>1</sup> Li Qin,<sup>1</sup> Fei Xu,<sup>1,2</sup> and Jian Zu <sup>1,3</sup>

<sup>1</sup>*School of Mathematics and Statistics and Center for Mathematics and Interdisciplinary Sciences, Northeast Normal University, Changchun 130024, China*

<sup>2</sup>*College of Mathematics, Jilin University, Changchun 130012, China*

<sup>3</sup>*Key Laboratory of Symbolic Computation and Knowledge Engineering of Ministry of Education, Jilin University, Changchun 130012, China*

Correspondence should be addressed to Jian Zu; [zuj100@nenu.edu.cn](mailto:zuj100@nenu.edu.cn)

Received 21 March 2018; Revised 24 May 2018; Accepted 11 June 2018; Published 9 July 2018

Academic Editor: Jorge E. Macias-Diaz

Copyright © 2018 Bochao Chen et al. This is an open access article distributed under the Creative Commons Attribution License, which permits unrestricted use, distribution, and reproduction in any medium, provided the original work is properly cited.

This paper is devoted to studying the analytical series solutions for the differential equations with variable coefficients. By a general residual power series method, we construct the approximate analytical series solutions for differential equations with variable coefficients, including nonhomogeneous parabolic equations, fractional heat equations in 2D, and fractional wave equations in 3D. These applications show that residual power series method is a simple, effective, and powerful method for seeking analytical series solutions of differential equations (especially for fractional differential equations) with variable coefficients.

## 1. Introduction

In the field of science and engineering, many physical phenomena can be described by differential equations with variable coefficients. For example, some physical problems in inhomogeneous media [1–3]. In the past, many assumptions on integral order differential equations were applied artificially to describe the systems with memory properties and hereditary properties. Some significant information will be lost by such assumptions. Generally, fractional calculus provides an effective tool to describe memory properties and hereditary properties of different materials and processes without extra assumptions. Now the fractional differential equation has attracted a great deal of interest in several areas including chemistry, physics, engineering, and even finance and social sciences [4, 5]. Some recent progress in fractional calculus can be found in [6–8].

The analytical series solutions of differential equations are of fundamental importance in applied science. Various numerical and analytical methods are proposed such as Adomian decomposition method [9, 10], Fractional complex transform method [11], and Laplace transform method [12].

Although lots of methods are put forward, scientists are still looking for more effective ways to solve specific problems, especially for the fractional equations with variable coefficients.

The residual power series method (RPS), proposed by Abu Arqud in [13], is an efficient and easy method for constructing power series solutions of differential equations without linearization, perturbation, or discretization. Different from the classical power series method, RPS does not need to compare the coefficients of the corresponding terms. This method computes the coefficients of the power series by a chain of equations with one or more variables. One advantage is that RPS is not affected by computational round-off errors and also does not require large computer memory and extensive time. In [14], power series solutions of higher-order ordinary differential equations are obtained by RPS. Inspired by this approach, we present a general residual power series method (GRPS) for constructing power series solutions of time-space fractional differential equations with variable coefficients:

$$D_t^{\alpha} u(x, t) + P(x)G(u) = F(x, t),$$

$$D_t^{i\alpha} u(\mathbf{x}, 0) = a_i(\mathbf{x}), \quad i = 0, \dots, m-1, \quad (1)$$

where  $\mathbf{x} = (x_1, x_2, \dots, x_d) \in \mathbb{R}^d$ ,  $\alpha \in ((m-1)/m, 1]$ ,  $m \in \mathbb{N}^+$ , and

$$G(u) := G(u, D_t^\alpha u, \dots, D_t^{(m-1)\alpha} u, D_{x_1}^{\beta_{11}} u, \dots, D_{x_d}^{\beta_{1d}} u, \dots, D_{x_1}^{\beta_{l1}} u, \dots, D_{x_d}^{\beta_{ld}} u), \quad (2)$$

with  $p-1 < \beta_{pj} \leq p$ ,  $p = 1, \dots, l$ ;  $j = 1, \dots, d$ . Here  $D_t^{i\alpha}$  and  $D_{x_j}^{\beta_{pj}}$  mean the Caputo fractional derivative with respect to  $t$  of order  $i\alpha$  and  $x_j$  of order  $\beta_{pj}$ , respectively. Such type of differential equation provides an exact description of some physical phenomena in fluid dynamics, electrodynamics, and elastic mechanics.

RPS has been extended to many partial differential equations (PDE), especially to fractional partial differential equations (FPDE), such as time-fractional dispersive PDE [15, 16], time-fractional KdV-Burgers equations [17], homogeneous time-fractional wave equation [18], and time-space fractional Boussinesq equations [19]. In the present paper, we will apply GRPS to a series of PDE with variable coefficients, including fourth-order parabolic equations, fractional heat equation, and fractional wave equation. For other approximation and numerical techniques for FPDE, we refer to finite difference methods [20, 21], differential transform method [22, 23], wavelet method [24], Adomian's decomposition method [25], variational iteration method [26, 27], homotopy analysis method [28], homotopy perturbation method [29], tau method [30, 31], and so on.

The paper is organized as follows: some necessary definitions and theorems will be presented in Section 2. In Section 3, we propose the main steps of GRPS for the general time-space fractional equations with variable coefficients. In Section 4, the applications of GRPS to some different equations with variable coefficients are given, including fourth-order parabolic equations, fractional heat equations, and fractional wave equations. Finally, conclusions are presented in Section 5.

## 2. Concepts on Fractional Calculus Theory

There are several definitions of the fractional integration with order  $\alpha \geq 0$ , and they are not necessarily equivalent to each other. The two most common ones are Riemann-Liouville's definition and Caputo's definition; see [32, 33].

**Definition 1.** The Mittag-Leffler function is defined as follows:

$$E_\alpha(x) := \sum_{k=0}^{\infty} \frac{x^k}{\Gamma(\alpha k + 1)}, \quad \alpha > 0. \quad (3)$$

**Definition 2.** A real function  $u(x, t)$ ,  $x \in I$ ,  $t > 0$  is said to be in the space  $C_\mu(I \times \mathbb{R}^+)$ ,  $\mu \in \mathbb{R}$ , if there exists a real number  $p > \mu$  such that  $u(x, t) = t^p f(x, t)$ , where  $f(x, t) \in C(I \times \mathbb{R}^+)$ ,

and it is said to be in the space  $C_\mu^n$ , if  $(\partial^n / \partial t^n)u(x, t) \in C_\mu$ ,  $n \in \mathbb{N}$ .

**Definition 3.** Let  $u(x, t) \in C_\mu(I \times \mathbb{R}^+)$ ,  $\mu \geq -1$ . The Riemann-Liouville fractional integral operator of order  $\alpha \geq 0$  of  $u(x, t)$  is defined as follows:

$$J_t^\alpha u(x, t) := \begin{cases} \frac{1}{\Gamma(\alpha)} \int_0^t (t-\tau)^{\alpha-1} u(x, \tau) d\tau, & \alpha > 0, \quad x \in I, \quad t > \tau \geq 0, \\ u(x, t), & \alpha = 0. \end{cases} \quad (4)$$

**Definition 4.** The Caputo time-fractional derivative operator of order  $\alpha$  of  $u(x, t)$  is defined as follows:

$$D_t^\alpha u(x, t) := \begin{cases} J_t^{n-\alpha} \left( \frac{\partial^n u(x, t)}{\partial t^n} \right), & n-1 < \alpha < n, \quad n \in \mathbb{N}^+, \\ \frac{\partial^n u(x, t)}{\partial t^n}, & \alpha = n. \end{cases} \quad (5)$$

**Definition 5.** The Caputo space fractional derivative operator of order  $\beta$  is defined as follows:

$$D_{x_j}^\beta u(x, t) := \begin{cases} J_x^{n-\beta} \left( \frac{\partial^n u(x, t)}{\partial x^n} \right), & n-1 < \beta < n, \quad n \in \mathbb{N}^+, \\ \frac{\partial^n u(x, t)}{\partial x^n}, & \alpha = n. \end{cases} \quad (6)$$

**Definition 6.** A power series representation of the form

$$\sum_{n=0}^{\infty} c_n (t-t_0)^{n\alpha} := c_0 + c_1 (t-t_0)^\alpha + c_2 (t-t_0)^{2\alpha} + \dots \quad (7)$$

is called a fractional power series (FPS) about  $t_0$ , where  $t$  is a variable and  $c_n$  are the coefficients of the series.

**Theorem 7** (see [34]). Suppose that  $f$  has a FPS representation at  $t_0$  of the form

$$f(t) = \sum_{n=0}^{\infty} c_n (t-t_0)^{n\alpha}, \quad t_0 \leq t < t_0 + R, \quad (8)$$

where  $R$  is the radius of convergence of the FPS. If  $D_t^{n\alpha} f(t) \in C(t_0, t_0 + R)$  for  $n = 0, 1, 2, \dots$ , then the coefficients  $c_n$  will take the form of

$$c_n = \frac{D_t^{n\alpha} f(t)|_{t=t_0}}{\Gamma(n\alpha + 1)}, \quad (9)$$

where  $D_t^{n\alpha} = D_t^\alpha \cdot D_t^\alpha \cdots D_t^\alpha$  ( $n$ -times).

## 3. Algorithm of GRPS

In this section, we give a general RPS to obtain fractional power series solutions for any-order time-space fractional

differential equations with variable coefficients (1). The analytic function  $u(\mathbf{x}, t)$  can be expanded as follows:

$$u(\mathbf{x}, t) = \sum_{n=0}^{\infty} u_n(\mathbf{x}, t) := \sum_{n=0}^{\infty} C_n(\mathbf{x}) t^{n\alpha}, \quad (10)$$

$$\mathbf{x} \in I \subset \mathbb{R}^d, \quad |t| < R,$$

where  $R$  is the radius of convergence of above series. Substitute the initial conditions in (1); we have

$$a_i(\mathbf{x}) = C_i(\mathbf{x}) \Gamma(i\alpha + 1), \quad i = 0, 1, \dots, m-1, \quad (11)$$

which implies

$$u_i(\mathbf{x}, t) = C_i(\mathbf{x}) t^{i\alpha} = \frac{a_i(\mathbf{x})}{\Gamma(i\alpha + 1)} t^{i\alpha}, \quad (12)$$

$$i = 0, 1, \dots, m-1.$$

So we have the initial guess approximation of  $u(\mathbf{x}, t)$  in the following form:

$$\begin{aligned} u^{\text{initial}}(\mathbf{x}, t) &:= u_0(\mathbf{x}, t) + u_1(\mathbf{x}, t) + \dots + u_{m-1}(\mathbf{x}, t) \\ &= a_0(\mathbf{x}) + \frac{a_1(\mathbf{x})}{\Gamma(\alpha + 1)} t^\alpha + \dots \\ &\quad + \frac{a_{m-1}(\mathbf{x})}{\Gamma((m-1)\alpha + 1)} t^{(m-1)\alpha}. \end{aligned} \quad (13)$$

Define the approximate solution of (1) by the  $k$ th truncated series:

$$u^k(\mathbf{x}, t) := u^{\text{initial}}(\mathbf{x}, t) + \sum_{i=m}^k C_i(\mathbf{x}) t^{i\alpha}, \quad (14)$$

$$k = m, m+1, m+2, \dots.$$

Before applying GRPS to solve (1), we give some notations

$$\text{Res}(u, \mathbf{x}, t) := D_t^{m\alpha} u(\mathbf{x}, t) + P(\mathbf{x}) G(u) - F(\mathbf{x}, t). \quad (15)$$

Substituting the  $k$ th truncated approximate solutions  $u^k(\mathbf{x}, t)$  into (1), we obtain the  $k$ th residual function

$$\begin{aligned} \text{Res}^k(u, \mathbf{x}, t) &:= D_t^{m\alpha} u^k(\mathbf{x}, t) + P(\mathbf{x}) G^k(u) \\ &\quad - F(\mathbf{x}, t), \end{aligned} \quad (16)$$

where

$$\begin{aligned} G^k(u) &= G(u^k, D_t^\alpha u^k, \dots, D_t^{(m-1)\alpha} u^k, D_{x_1}^{\beta_{11}} u^k, \dots, D_{x_d}^{\beta_{1d}} u^k, \\ &\quad \dots, D_{x_1}^{\beta_{1n}} u^k, \dots, D_{x_d}^{\beta_{1d}} u^k). \end{aligned} \quad (17)$$

Then we have the following facts:

- (1)  $\lim_{k \rightarrow \infty} u^k(\mathbf{x}, t) = u(\mathbf{x}, t)$ ;
- (2)  $\text{Res}(u, \mathbf{x}, t) = 0$ ;
- (3)  $\lim_{k \rightarrow \infty} \text{Res}^k(u, \mathbf{x}, t) = \text{Res}(u, \mathbf{x}, t)$ ,  $\mathbf{x} \in I \subseteq \mathbb{R}^d$ ,  $|t| < R$ .

Assume that

$$D_t^{(k-m)\alpha} \text{Res}^k(u, \mathbf{x}, t) \Big|_{t=0} = 0. \quad (18)$$

Since

$$\begin{aligned} D_t^{(k-m)\alpha} \text{Res}^k(u, \mathbf{x}, t) \Big|_{t=0} \\ = C_k(\mathbf{x}) \Gamma(k\alpha + 1) \\ + D_t^{(k-m)\alpha} [P(\mathbf{x}) G^k(u) - F(\mathbf{x}, t)] \Big|_{t=0}, \end{aligned} \quad (19)$$

we have

$$C_k(\mathbf{x}) = -\frac{D_t^{(k-m)\alpha} [P(\mathbf{x}) G^k(u) - F(\mathbf{x}, t)] \Big|_{t=0}}{\Gamma(k\alpha + 1)}, \quad (20)$$

$$k = m, m+1, m+2, \dots.$$

In fact, this relation is a fundamental rule in GRPS. So the FPS solution of (1) is

$$\begin{aligned} u(\mathbf{x}, t) &= u^{\text{initial}}(\mathbf{x}, t) + \sum_{i=m}^{\infty} C_i(\mathbf{x}) t^{i\alpha} \\ &= \sum_{i=0}^{m-1} \frac{a_i(\mathbf{x})}{\Gamma(i\alpha + 1)} t^{i\alpha} + \sum_{i=m}^{\infty} \frac{f_i(\mathbf{x})}{\Gamma(i\alpha + 1)} t^{i\alpha}, \end{aligned} \quad (21)$$

where

$$\begin{aligned} f_k(\mathbf{x}) &= -D_t^{(k-m)\alpha} [P(\mathbf{x}) G^k(u) - F(\mathbf{x}, t)] \Big|_{t=0}, \\ k &= m, m+1, m+2, \dots. \end{aligned} \quad (22)$$

## 4. Applications of GRPS to PDEs with Variable Coefficients

**4.1. Fourth-Order Parabolic Equation with Variable Coefficients in  $\mathbb{R}^1$ .** Let us consider the fourth-order parabolic differential equation

$$\frac{\partial^2 u}{\partial t^2} + \left( \frac{x}{\sin x} - 1 \right) \frac{\partial^4 u}{\partial x^4} = 0, \quad 0 < x < 1, \quad t > 0, \quad (23)$$

where  $x/\sin x - 1 > 0$  is the ratio of flexural rigidity of the beam to its mass per unit length; see [35]. In [35], the initial conditions and the boundary conditions of (23) are

$$\begin{aligned} u(x, 0) &= x - \sin x, \\ \frac{\partial}{\partial t} u(x, 0) &= -x + \sin x, \end{aligned} \quad (24)$$

and

$$\begin{aligned} u(0, t) &= 0, \\ u(1, t) &= e^{-t} (1 - \sin 1), \end{aligned}$$

$$\begin{aligned} \frac{\partial^2}{\partial x^2} u(0, t) &= 0, \\ \frac{\partial^2}{\partial x^2} u(1, t) &= e^{-t} \sin 1, \end{aligned} \quad (25)$$

respectively. According to (10),  $u$  can be written in the following form:

$$u(x, t) = C_0(x) + C_1(x)t + C_2(x)t^2 + C_3(x)t^3 + \dots \quad (26)$$

The initial approximation is

$$u^{\text{initial}}(x, t) = (x - \sin x) - (x - \sin x)t. \quad (27)$$

Now by (15), denote

$$\begin{aligned} \text{Res}(x, t) &= \frac{\partial^2 u(x, t)}{\partial t^2} + \left( \frac{x}{\sin x} - 1 \right) \frac{\partial^4 u(x, t)}{\partial x^4}, \\ u^k(x, t) &= u^{\text{initial}} + \sum_{i=2}^k f_i(x) t^i, \end{aligned} \quad (28)$$

$$\text{Res}^k(x, t) = \frac{\partial^2 u^k(x, t)}{\partial t^2} + \left( \frac{x}{\sin x} - 1 \right) \frac{\partial^4 u^k(x, t)}{\partial x^4}.$$

By (16) and (18), we assume that

$$D_t^{k-2} \text{Res}^k(x, 0) = 0, \quad k = 2, 3, 4, \dots \quad (29)$$

Letting  $k = 2$  in (29), it shows

$$2!C_2(x) + \left( \frac{x}{\sin x} - 1 \right) (-\sin x) = 0, \quad (30)$$

which implies

$$C_2(x) = \frac{x - \sin x}{2!}. \quad (31)$$

So the 2nd truncated approximate solution of (23) is

$$u^2(x, t) = (x - \sin x) - (x - \sin x)t + \frac{x - \sin x}{2!}t^2. \quad (32)$$

Similarly,  $C_k(x)$  can be constructed as follows:

$$C_k(x) = \frac{(-1)^k}{k!} (x - \sin x), \quad k = 2, 3, 4, \dots \quad (33)$$

So the  $k$ th truncated approximate solution of (23) is

$$u^k(x, t) = (x - \sin x) \sum_{i=0}^k \frac{(-1)^i}{i!} t^i. \quad (34)$$

Finally, if we define

$$u(x, t) := \lim_{k \rightarrow \infty} u^k(x, t) = (x - \sin x) e^{-t}, \quad (35)$$

it is easy to verify that  $u(x, t)$  in (35) is the exact solution of (23) with boundary value condition (25).

Numerical comparisons are studied next. Figure 1 shows the exact solution  $u$  of (23) with  $0 \leq t \leq 5$ . In Figure 2,  $u^9, u^{10}, u^{11}$ , and  $u^{12}$  represent the 9th-, 10th-, 11th-, and 12th-order truncated approximate solution of  $u$  with  $0 \leq t \leq 5$ . It shows that these GRPS approximate solutions are convergent to the exact solution  $u$ .

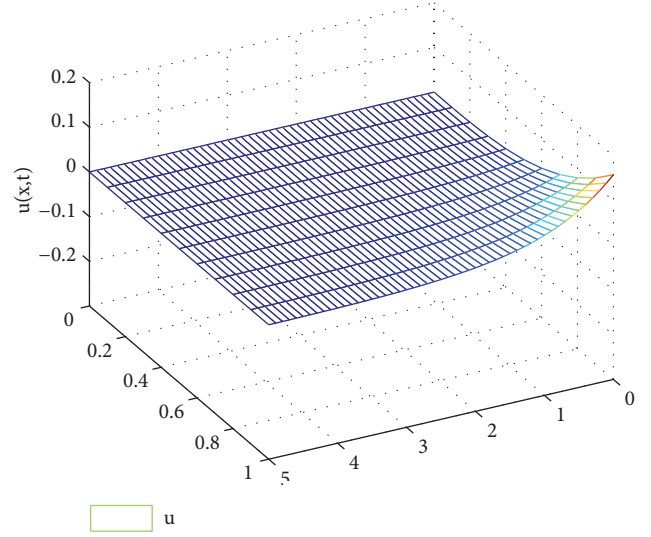


FIGURE 1: The exact solution  $u$  of (23).

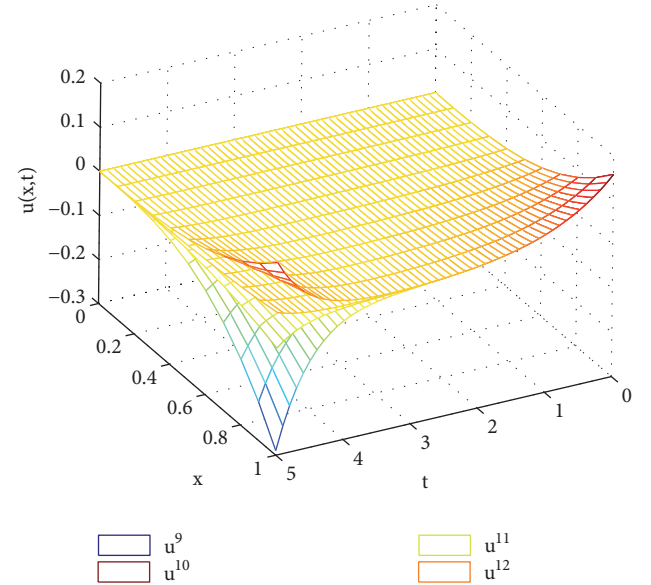


FIGURE 2: The approximate solutions  $u^9, u^{10}, u^{11}$ , and  $u^{12}$  of (23).

**4.2. Nonhomogeneous Parabolic Equation with Source Term in  $\mathbb{R}^1$ .** Let us consider the nonhomogeneous parabolic equation (see [35]):

$$\begin{aligned} \frac{\partial^2 u}{\partial t^2} + (1+x) \frac{\partial^4 u}{\partial x^4} &= \left( x^4 + x^3 - \frac{6}{7!} x^7 \right) \cos t, \\ 0 < x < 1, \quad t > 0, \end{aligned} \quad (36)$$

with the initial conditions

$$\begin{aligned} u(x, 0) &= \frac{6}{7!} x^7, \\ \frac{\partial}{\partial t} u(x, 0) &= 0, \end{aligned} \quad (37)$$

and the boundary conditions

$$\begin{aligned} u(0, t) &= 0, \\ u(1, t) &= \frac{6}{7!} \cos t, \\ \frac{\partial^2}{\partial x^2} u(0, t) &= 0, \\ \frac{\partial^2}{\partial x^2} u(1, t) &= \frac{1}{20} \cos t. \end{aligned} \quad (38)$$

Assume that  $u(x, t)$  is an analytical function with  $t > 0$ . The initial approximation is

$$u^{\text{initial}}(x, t) = \frac{6}{7!} x^7. \quad (39)$$

Denote

$$\begin{aligned} \text{Res}^k(x, t) &= \frac{\partial^2 u^k(x, t)}{\partial t^2} + (1+x) \frac{\partial^4 u^k(x, t)}{\partial x^4} \\ &\quad - \left( x^4 + x^3 - \frac{6}{7!} x^7 \right) \cos t, \end{aligned} \quad (40)$$

where

$$u^k(x, t) = u^{\text{initial}}(x, t) + C_2(x)t^2 + \cdots + C_k(x)t^k. \quad (41)$$

Let  $k = 2$  in (40); it yields

$$\begin{aligned} \text{Res}^2(x, t) &= 2C_2(x) + (1+x) \left( \frac{6}{3!} x^3 + C_2^{(4)}(x) t^2 \right) \\ &\quad - \left( x^4 + x^3 - \frac{6}{7!} x^7 \right) \cos t. \end{aligned} \quad (42)$$

Using the fact that

$$D_t^{k-2} \text{Res}^k(x, 0) = 0, \quad k = 2, 3, 4, \dots, \quad (43)$$

we have

$$C_2(x) = -\frac{6}{2!7!} x^7. \quad (44)$$

Thus the 2nd truncated series have the following form:

$$u^2(x, t) = \frac{6}{7!} x^7 - \frac{6}{2!7!} x^7 t^2. \quad (45)$$

Similarly, taking  $k = 3, 4, 5, 6$  in (40) we obtain

$$\begin{aligned} C_3(x) &= 0, \\ C_4(x) &= \frac{6}{4!7!} x^7, \\ C_5(x) &= 0, \\ C_6(x) &= -\frac{6}{6!7!} x^7. \end{aligned} \quad (46)$$

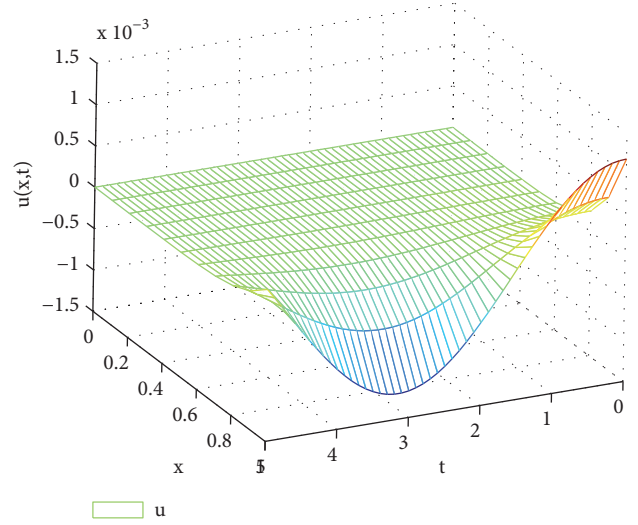


FIGURE 3: The exact solution  $u$  of (36).

Then 6th truncated approximate solution of (36) is

$$u^6(x, t) = \frac{6}{7!} x^7 - \frac{6}{2!7!} x^7 t^2 + \frac{6}{4!7!} x^7 t^4 - \frac{6}{6!7!} x^7 t^6. \quad (47)$$

By (21), we can obtain the solution of (36):

$$u(x, t) = \lim_{k \rightarrow \infty} u^k(x, t) = \frac{6}{7!} x^7 \cos t, \quad (48)$$

which is consistent with the solution obtained by Adomian decomposition method [35].

Some numerical comparisons are given next. Figure 3 shows the exact solution  $u$  of (36) with  $0 \leq t \leq 5$ . In Figure 4,  $u^{19}$ ,  $u^{20}$ ,  $u^{21}$ , and  $u^{22}$  represent the 19th-, 20th-, 21st-, and 22nd-order GRPS solution of  $u$  with  $0 \leq t \leq 5$ . It shows that these approximate solutions are convergent to the exact solution  $u$ .

**4.3. Fractional Heat Equation with Variable Coefficients in  $\mathbb{R}^2$ .** Consider the two-dimensional heat equation with variable coefficients

$$\begin{aligned} D_t^\alpha u(x, y, t) &= \frac{1}{2} y^2 u_{xx}(x, y, t) + \frac{1}{2} x^2 u_{yy}(x, y, t), \\ (x, y, t) &\in (\mathbb{R}^+)^3, \quad 0 < \alpha \leq 1, \end{aligned} \quad (49)$$

with the initial conditions

$$u(x, y, 0) = y^2. \quad (50)$$

Assume that  $u(x, y, t)$  is an analytical function on  $t > 0$  and the initial approximation solution has the following form:

$$u^{\text{initial}}(x, y, t) = y^2. \quad (51)$$

Then the  $k$ th truncated series and  $k$ th residual function will be

$$\begin{aligned} u^k(x, y, t) &= u^{\text{initial}}(x, y, t) + \sum_{m=1}^k C_m(x, y) t^{m\alpha} \\ &= y^2 + C_1(x, y) t^\alpha + \cdots + C_k(x, y) t^{k\alpha}, \end{aligned} \quad (52)$$



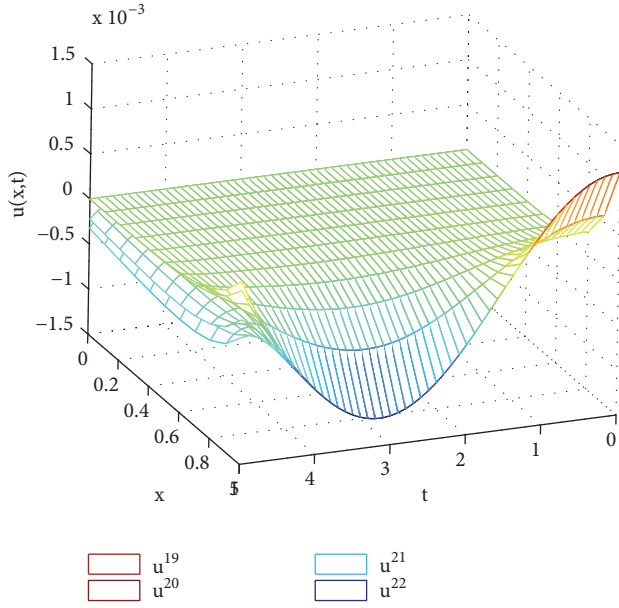


FIGURE 4: The approximate solutions  $u^{19}$ ,  $u^{20}$ ,  $u^{21}$ , and  $u^{22}$  of (36).

and

$$\begin{aligned} \text{Res}^k(x, y, t) &= D_t^\alpha u^k(x, y, t) - \frac{1}{2} y^2 \frac{\partial^2 u^k(x, y, t)}{\partial x^2} \\ &\quad - \frac{1}{2} x^2 \frac{\partial^2 u^k(x, y, t)}{\partial y^2}, \end{aligned} \quad (53)$$

respectively. By (18), we have

$$D_t^{(k-1)\alpha} \text{Res}^k(x, y, 0) = 0, \quad 0 < \alpha < 1, \quad k = 1, 2, 3, \dots \quad (54)$$

When  $k = 1$  in (54), we obtain

$$C_1(x, y) = \frac{x^2}{\Gamma(\alpha + 1)}. \quad (55)$$

Thus, the 1st truncated approximate solution of (49)-(50) is

$$u^1(x, y, t) = y^2 + \frac{x^2}{\Gamma(\alpha + 1)} t^\alpha. \quad (56)$$

Let  $k=2$  in (54); it yields that

$$C_2(x, y) = \frac{y^2}{\Gamma(2\alpha + 1)}. \quad (57)$$

Therefore, the 2nd truncated approximate solution of (49)-(50) is

$$u^2(x, y, t) = y^2 + \frac{x^2}{\Gamma(\alpha + 1)} t^\alpha + \frac{y^2}{\Gamma(2\alpha + 1)} t^{2\alpha}. \quad (58)$$

In the similar way, taking  $k = 3, 4, 5, 6$  in (54), we can obtain that

$$\begin{aligned} C_3(x, y) &= \frac{x^2}{\Gamma(3\alpha + 1)}, \\ C_4(x, y) &= \frac{y^2}{\Gamma(4\alpha + 1)}, \\ C_5(x, y) &= \frac{x^2}{\Gamma(5\alpha + 1)}, \end{aligned} \quad (59)$$

and

$$C_6(x, y) = \frac{y^2}{\Gamma(6\alpha + 1)}. \quad (60)$$

Thus 6th truncated approximate solution of (49)-(50) can be obtained

$$\begin{aligned} u^6(x, y, t) &= y^2 + \frac{x^2}{\Gamma(\alpha + 1)} t^\alpha + \frac{y^2}{\Gamma(2\alpha + 1)} t^{2\alpha} \\ &\quad + \frac{x^2}{\Gamma(3\alpha + 1)} t^{3\alpha} + \frac{y^2}{\Gamma(4\alpha + 1)} t^{4\alpha} \\ &\quad + \frac{x^2}{\Gamma(5\alpha + 1)} t^{5\alpha} + \frac{y^2}{\Gamma(6\alpha + 1)} t^{6\alpha}. \end{aligned} \quad (61)$$

Following the same step, we have the exact analytical solutions of (49)-(50):

$$\begin{aligned} u(x, y, t) &= y^2 \left( 1 + \frac{1}{\Gamma(2\alpha + 1)} t^{2\alpha} + \frac{1}{\Gamma(4\alpha + 1)} t^{4\alpha} \right. \\ &\quad \left. + \frac{1}{\Gamma(6\alpha + 1)} t^{6\alpha} + \dots \right) + x^2 \left( \frac{1}{\Gamma(\alpha + 1)} t^\alpha \right. \\ &\quad \left. + \frac{1}{\Gamma(3\alpha + 1)} t^{3\alpha} + \frac{1}{\Gamma(5\alpha + 1)} t^{5\alpha} + \dots \right) = y^2 \\ &\quad \cdot \cosh(t^\alpha, \alpha) + x^2 \sinh(t^\alpha, \alpha). \end{aligned} \quad (62)$$

Particularly, if  $\alpha = 1$ , we obtain the following form:

$$u(x, y, t) = y^2 \frac{e^t + e^{-t}}{2} + x^2 \frac{e^t - e^{-t}}{2}, \quad (63)$$

which is the solution of the integer order heat equation with variable coefficients.

Some numerical simulation are presented next. In Figures 5 and 6,  $u^9$ ,  $u^{10}$ ,  $u^{11}$ , and  $u^{12}$  represent the 9th-, 10th-, 11th-, and 12th-order GRPS solution of (49) at time  $t = 3$  with  $\alpha = 1/2$  and  $\alpha = 1$ , respectively. In Figures 7 and 8,  $u^9$ ,  $u^{10}$ ,  $u^{11}$ , and  $u^{12}$  represent the 9th-, 10th-, 11th-, and 12th-order GRPS solution of (49) at time  $t = 5$  with  $\alpha = 1/2$  and  $\alpha = 1$ , respectively. It shows that the speed of convergence of truncated approximate solution of (49) with  $\alpha = 1$  is better than the one with  $\alpha = 1/2$ .

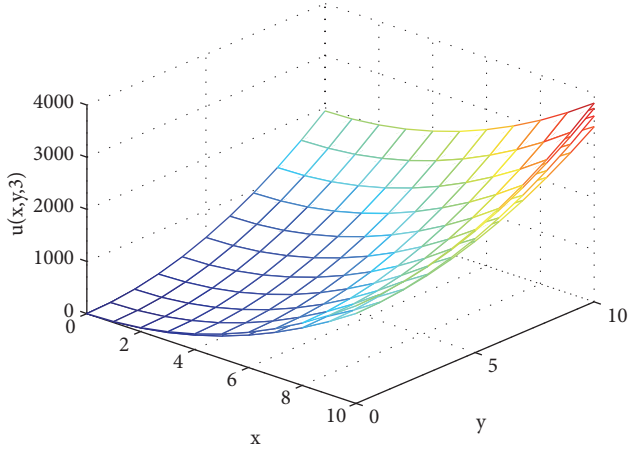


FIGURE 5: The approximate solutions  $u^9, u^{10}, u^{11}$ , and  $u^{12}$  of (49) at  $t = 3$  with  $\alpha = 1/2$ .

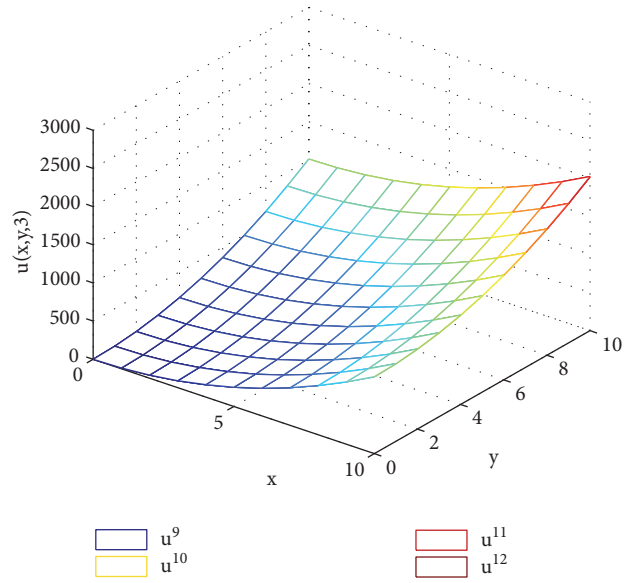


FIGURE 6: The approximate solutions  $u^9, u^{10}, u^{11}$ , and  $u^{12}$  of (49) at  $t = 3$  with  $\alpha = 1$ .

4.4. *Fractional Wave Equation in  $\mathbb{R}^3$ .* Consider the three-dimensional wave equation with variable coefficients

$$\begin{aligned} D_t^{2\alpha} u(x, y, z, t) &= \frac{1}{2} (x^2 u_{xx}(x, y, z, t) \\ &+ y^2 u_{yy}(x, y, z, t) + z^2 u_{zz}(x, y, z, t)) + x^2 + y^2 \\ &+ z^2, \quad (x, y, z) \in (\mathbb{R}^+)^3, \quad t > 0, \quad 0 < \alpha \leq 1, \end{aligned} \quad (64)$$

with the initial conditions

$$\begin{aligned} u(x, y, z, 0) &= 0, \\ D_t^\alpha u(x, y, z, 0) &= x^2 + y^2 - z^2. \end{aligned} \quad (65)$$

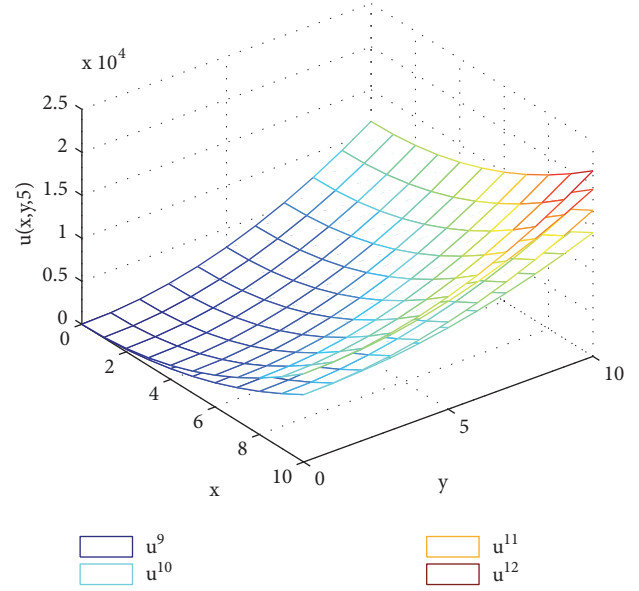


FIGURE 7: The approximate solutions  $u^9, u^{10}, u^{11}$ , and  $u^{12}$  of (49) at  $t = 5$  with  $\alpha = 1/2$ .

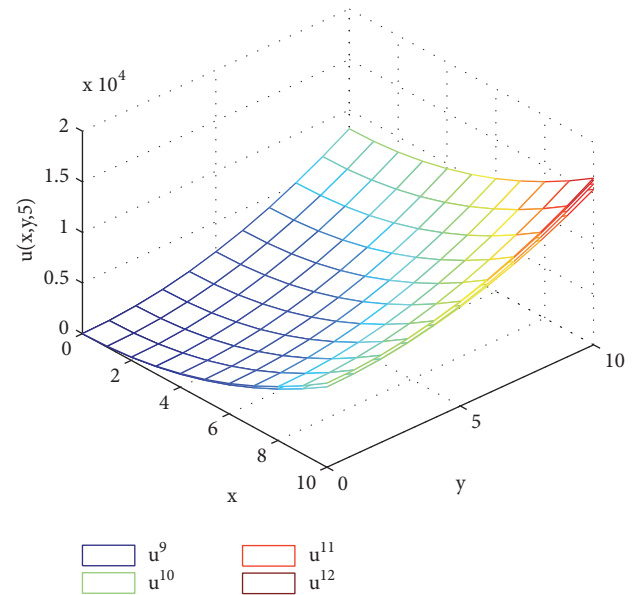


FIGURE 8: The approximate solutions  $u^9, u^{10}, u^{11}$ , and  $u^{12}$  of (49) at  $t = 5$  with  $\alpha = 1$ .

First, we construct the initial approximation solution:

$$u^{\text{initial}}(x, y, z, t) = \frac{x^2 + y^2 - z^2}{\Gamma(\alpha + 1)} t^\alpha. \quad (66)$$

Secondly, construct the  $k$ th truncated series and  $k$ th residual function of (64)-(65) as follows:

$$\begin{aligned} u^k(x, y, z, t) &= u^{\text{initial}}(x, y, z, t) \\ &+ \sum_{m=2}^k C_m(x, y, z) t^{m\alpha}, \end{aligned}$$

$$\begin{aligned} \text{Res}^k(x, y, z, t) &= D_t^{2\alpha} u^k(x, y, z, t) - (x^2 + y^2 + z^2) \\ &\quad - \frac{1}{2} (x^2 u_{xx}^k(x, y, z, t) + y^2 u_{yy}^k(x, y, z, t) \\ &\quad + z^2 u_{zz}^k(x, y, z, t)). \end{aligned} \quad (67)$$

By (18), we have

$$\begin{aligned} D_t^{(k-2)\alpha} \text{Res}^k(x, y, z, 0) &= 0, \\ 0 < \alpha < 1, \quad k &= 2, 3, 4, \dots \end{aligned} \quad (68)$$

Taking  $k = 2$  in (68), it yields

$$C_2(x, y, z) = \frac{x^2 + y^2 + z^2}{\Gamma(2\alpha + 1)}. \quad (69)$$

Then the 2nd truncated approximate solution will be

$$\begin{aligned} u^2(x, y, z, t) &= \frac{1}{\Gamma(\alpha + 1)} (x^2 + y^2 - z^2) t^\alpha \\ &\quad + \frac{1}{\Gamma(2\alpha + 1)} (x^2 + y^2 + z^2) t^{2\alpha}. \end{aligned} \quad (70)$$

In a similar way, taking  $k = 3, 4, 5, 6$  in (68), we have

$$\begin{aligned} C_3(x, y, z) &= \frac{1}{\Gamma(3\alpha + 1)} (x^2 + y^2 - z^2), \\ C_4(x, y, z) &= \frac{1}{\Gamma(4\alpha + 1)} (x^2 + y^2 + z^2), \\ C_5(x, y, z) &= \frac{1}{\Gamma(5\alpha + 1)} (x^2 + y^2 - z^2), \\ C_6(x, y, z) &= \frac{1}{\Gamma(6\alpha + 1)} (x^2 + y^2 + z^2). \end{aligned} \quad (71)$$

Then the 6th-order truncated approximate solution of (64)-(65) can be obtained as follows:

$$\begin{aligned} u^6(x, y, z, t) &= \frac{1}{\Gamma(\alpha + 1)} (x^2 + y^2 - z^2) t^\alpha \\ &\quad + \frac{1}{\Gamma(2\alpha + 1)} (x^2 + y^2 + z^2) t^{2\alpha} \\ &\quad + \frac{1}{\Gamma(3\alpha + 1)} (x^2 + y^2 - z^2) t^{3\alpha} \\ &\quad + \frac{1}{\Gamma(4\alpha + 1)} (x^2 + y^2 + z^2) t^{4\alpha} \\ &\quad + \frac{1}{\Gamma(5\alpha + 1)} (x^2 + y^2 - z^2) t^{5\alpha} \\ &\quad + \frac{1}{\Gamma(6\alpha + 1)} (x^2 + y^2 + z^2) t^{6\alpha}. \end{aligned} \quad (72)$$

Finally, the exact analytical solution of (64)-(65) can be obtained:

$$\begin{aligned} u(x, y, t) &= (x^2 + y^2 - z^2) \left( \frac{1}{\Gamma(\alpha + 1)} t^\alpha \right. \\ &\quad + \frac{1}{\Gamma(3\alpha + 1)} t^{3\alpha} + \frac{1}{\Gamma(5\alpha + 1)} t^{5\alpha} + \dots \Big) + (x^2 + y^2 \\ &\quad + z^2) \left( \frac{1}{\Gamma(2\alpha + 1)} t^{2\alpha} + \frac{1}{\Gamma(4\alpha + 1)} t^{4\alpha} \right. \\ &\quad + \frac{1}{\Gamma(6\alpha + 1)} t^{6\alpha} + \dots \Big) = (x^2 + y^2 - z^2) \\ &\quad \cdot \sinh(t^\alpha, \alpha) + (x^2 + y^2 + z^2) [\cosh(t^\alpha, \alpha) - 1]. \end{aligned} \quad (73)$$

## 5. Conclusions

This paper concerns the analytical series solutions of the differential equations with variable coefficients (integer order or fractional order). By a general residual power residual series method, we construct the analytical approximate solutions and the analytical exact solutions of the differential equations with variable coefficients, for example, nonhomogeneous parabolic equations, fractional heat equations in 2D, and fractional wave equations in 3D. It shows that GRPS is a direct, simple, and efficient method which could be widely applied to many other PDEs with variable coefficients.

## Data Availability

The Matlab data used to support the findings of this study are included within the supplementary information file.

## Conflicts of Interest

The authors declare that they have no conflicts of interest regarding the publication of this paper.

## Acknowledgments

This work is supported in part by NSFC Grant [11401089, 11671071] and Jilin Province's Education Department [JJKH20170535KJ, JJKH20180006KJ], JLSTDP 20160520094JH, and FRFCU2412017FZ005.

## Supplementary Materials

The Matlab codes of examples 1, 2, and 3 are presented in Supplementary Material. The Matlab code of GRPS method is presented in section "Supplementary Material", which can help readers follow our simulation. (*Supplementary Materials*)

## References

- [1] V. Barbu and N. H. Pavel, "Periodic solutions to nonlinear one dimensional wave equation with  $x$ -dependent coefficients," *Transactions of the American Mathematical Society*, vol. 349, no. 5, pp. 2035–2048, 1997.

- [2] P. Gérard, "Nonlinear Schrödinger equations in inhomogeneous media: wellposedness and illposedness of the Cauchy problem," in *International Congress of Mathematicians*, pp. 157–182, 2006.
- [3] S. Ji and Y. Li, "Periodic solutions to one-dimensional wave equation with  $x$ -dependent coefficients," *Journal of Differential Equations*, vol. 229, no. 2, pp. 466–493, 2006.
- [4] K. Diethelm, *The Analysis of Fractional Differential Equations. An Application-Oriented Exposition Using Differential Operators of Caputo Type*, vol. 2004 of *Lecture Notes in Mathematics*, Springer, Berlin, Germany, 2010.
- [5] J. T. Machado, V. Kiryakova, and F. Mainardi, "Recent history of fractional calculus," *Communications in Nonlinear Science and Numerical Simulation*, vol. 16, no. 3, pp. 1140–1153, 2011.
- [6] D. Baleanu, G.-C. Wu, and S.-D. Zeng, "Chaos analysis and asymptotic stability of generalized Caputo fractional differential equations," *Chaos, Solitons & Fractals*, vol. 102, pp. 99–105, 2017.
- [7] V. E. Tarasov, *Fractional Dynamics: Application of Fractional Calculus to Dynamics of Particles, Fields and Media*, Springer, 2010.
- [8] V. V. Uchaikin, "Fractional derivatives for physicists and engineers. Volume I," in *Nonlinear Physical Science*, Higher Education Press, Berlin, Germany, 2013.
- [9] G. Adomian, "A review of the decomposition method in applied mathematics," *Journal of Mathematical Analysis and Applications*, vol. 135, no. 2, pp. 501–544, 1988.
- [10] G. Adomian, *Solving Frontier Problems of Physics: The Decomposition Method*, Kluwer Academic, Dordrecht, The Netherlands, 1994.
- [11] J. He, S. K. Elagan, and Z. B. Li, "Geometrical explanation of the fractional complex transform and derivative chain rule for fractional calculus," *Physics Letters A*, vol. 376, no. 4, pp. 257–259, 2012.
- [12] S. A. Khuri, "A new approach to Bratu's problem," *Applied Mathematics and Computation*, vol. 147, no. 1, pp. 131–136, 2004.
- [13] O. Abu Arqub, "Series solution of fuzzy differential equations under strongly generalized differentiability," *Journal of Advanced Research in Applied Mathematics*, vol. 5, no. 1, pp. 31–52, 2013.
- [14] O. Abu Arqub, Z. Abo-Hammour, R. Al-Badarnah, and S. Momani, "A reliable analytical method for solving higher-order initial value problems," *Discrete Dynamics in Nature and Society*, vol. 2013, Article ID 673829, 12 pages, 2013.
- [15] O. Abu Arqub, "Application of residual power series method for the solution of time-fractional Schrödinger equations in one-dimensional space," *Fundamenta Informaticae*, 2018.
- [16] O. A. Arqub, A. El-Ajou, and S. Momani, "Constructing and predicting solitary pattern solutions for nonlinear time-fractional dispersive partial differential equations," *Journal of Computational Physics*, vol. 293, pp. 385–399, 2015.
- [17] A. El-Ajou, O. Abu Arqub, and S. Momani, "Approximate analytical solution of the nonlinear fractional KdV-Burgers equation: a new iterative algorithm," *Journal of Computational Physics*, vol. 293, pp. 81–95, 2015.
- [18] A. El-Ajou, O. Abu Arqub, S. Momani, D. Baleanu, and A. Alsaedi, "A novel expansion iterative method for solving linear partial differential equations of fractional order," *Applied Mathematics and Computation*, vol. 257, pp. 119–133, 2015.
- [19] F. Xu, Y. Gao, X. Yang, and H. Zhang, "Construction of fractional power series solutions to fractional boussinesq equations using residual power series method," *Mathematical Problems in Engineering*, vol. 2016, 15 pages, 2016.
- [20] L. Su, W. Wang, and Q. Xu, "Finite difference methods for fractional dispersion equations," *Applied Mathematics and Computation*, vol. 216, no. 11, pp. 3329–3334, 2010.
- [21] C. Tadjeran, M. M. Meerschaert, and H. Scheffler, "A second-order accurate numerical approximation for the fractional diffusion equation," *Journal of Computational Physics*, vol. 213, no. 1, pp. 205–213, 2006.
- [22] Z. Odibat and S. Momani, "A generalized differential transform method for linear partial differential equations of fractional order," *Applied Mathematics Letters*, vol. 21, no. 2, pp. 194–199, 2008.
- [23] S. Z. Rida, A. M. El-Sayed, and A. A. Arafa, "On the solutions of time-fractional reaction-diffusion equations," *Communications in Nonlinear Science and Numerical Simulation*, vol. 15, no. 12, pp. 3847–3854, 2010.
- [24] Y. Chen, Y. Wu, Y. Cui, Z. Wang, and D. Jin, "Wavelet method for a class of fractional convection-diffusion equation with variable coefficients," *Journal of Computational Science*, vol. 1, no. 3, pp. 146–149, 2010.
- [25] S. S. Ray, "Analytical solution for the space fractional diffusion equation by two-step Adomian decomposition method," *Communications in Nonlinear Science and Numerical Simulation*, vol. 14, no. 4, pp. 1295–1306, 2009.
- [26] M. Dehghan, S. A. Yousefi, and A. Lotfi, "The use of He's variational iteration method for solving the telegraph and fractional telegraph equations," *International Journal for Numerical Methods in Biomedical Engineering*, vol. 27, no. 2, pp. 219–231, 2011.
- [27] M. Inc, "The approximate and exact solutions of the space- and time-fractional Burgers equations with initial conditions by variational iteration method," *Journal of Mathematical Analysis and Applications*, vol. 345, no. 1, pp. 476–484, 2008.
- [28] M. Dehghan, J. Manafian, and A. Saadatmandi, "Solving nonlinear fractional partial differential equations using the homotopy analysis method," *Numerical Methods for Partial Differential Equations*, vol. 26, no. 2, pp. 448–479, 2010.
- [29] S. Momani and Z. Odibat, "Comparison between the homotopy perturbation method and the variational iteration method for linear fractional partial differential equations," *Computers & Mathematics with Applications*, vol. 54, no. 7-8, pp. 910–919, 2007.
- [30] S. K. Vanani and A. Aminataei, "Tau approximate solution of fractional partial differential equations," *Computers & Mathematics with Applications*, vol. 62, no. 3, pp. 1075–1083, 2011.
- [31] A. Saadatmandi and M. Dehghan, "A tau approach for solution of the space fractional diffusion equation," *Computers & Mathematics with Applications*, vol. 62, no. 3, pp. 1135–1142, 2011.
- [32] A. A. Kilbas, H. M. Srivastava, and J. J. Trujillo, *Theory and Applications of Fractional Differential Equations*, New York, NY, USA, Elsevier, 2006.
- [33] K. S. Miller and B. Ross, *An Introduction to the Fractional Calculus and Fractional Differential Equations*, A Wiley-Interscience Publication, John Wiley & Sons, New York, NY, USA, 1993.
- [34] O. A. Arqub, A. El-Ajou, Z. A. Zhour, and S. Momani, "Multiple solutions of nonlinear boundary value problems of fractional order: a new analytic iterative technique," *Entropy*, vol. 16, no. 1, pp. 471–493, 2014.
- [35] A.-M. Wazwaz, "Analytic treatment for variable coefficient fourth-order parabolic partial differential equations," *Applied Mathematics and Computation*, vol. 123, no. 2, pp. 219–227, 2001.

## Research Article

# Asymptotic Properties of Solutions to Second-Order Difference Equations of Volterra Type

Janusz Migda,<sup>1</sup> Małgorzata Migda ,<sup>2</sup> and Magdalena Nockowska-Rosiak<sup>3</sup>

<sup>1</sup>Faculty of Mathematics and Computer Science, A. Mickiewicz University, Umultowska 87, 61-614 Poznań, Poland

<sup>2</sup>Institute of Mathematics, Poznań University of Technology, Piotrowo 3A, 60-965 Poznań, Poland

<sup>3</sup>Institute of Mathematics, Lodz University of Technology, Ul. Wólczajska 215, 90-924 Łódź, Poland

Correspondence should be addressed to Małgorzata Migda; [malgorzata.migda@put.poznan.pl](mailto:malgorzata.migda@put.poznan.pl)

Received 26 April 2018; Accepted 21 June 2018; Published 9 July 2018

Academic Editor: Jorge E. Macias-Diaz

Copyright © 2018 Janusz Migda et al. This is an open access article distributed under the Creative Commons Attribution License, which permits unrestricted use, distribution, and reproduction in any medium, provided the original work is properly cited.

We consider the discrete Volterra type equation of the form  $\Delta(r_n \Delta x_n) = b_n + \sum_{k=1}^n K(n, k) f(x_k)$ . We present sufficient conditions for the existence of solutions with prescribed asymptotic behavior. Moreover, we study the asymptotic behavior of solutions. We use  $o(n^s)$ , for given nonpositive real  $s$ , as a measure of approximation.

## 1. Introduction

In this paper we consider the nonlinear Volterra sum-difference equation of nonconvolution type:

$$\Delta(r_n \Delta x_n) = b_n + \sum_{k=1}^n K(n, k) f(x_k), \quad (\text{E})$$

$$r_n, b_n \in \mathbb{R}, \quad r_n > 0, \quad f: \mathbb{R} \longrightarrow \mathbb{R}, \quad K: \mathbb{N} \times \mathbb{N} \longrightarrow \mathbb{R}. \quad (1)$$

Here  $\mathbb{N}$ ,  $\mathbb{R}$  denote the set of positive integers and the set of real numbers, respectively. By a solution of (E) we mean a sequence  $x: \mathbb{N} \longrightarrow \mathbb{R}$  satisfying (E) for large  $n$ .

Discrete Volterra equations of different types are widely used in the process of modeling of some real phenomena or by applying a numerical method to a Volterra integral equation. Let  $m \in \mathbb{N}$ . The general form of a Volterra sum-difference autonomous equation is

$$\Delta^m x_n = a_n + \sum_{k=1}^n K(n, k) f(x_k). \quad (2)$$

Such equations can be regarded as the discrete analogue of Volterra integrodifferential equations of the form

$$x^{(m)}(t) = f(t) + \int_0^t K(t, s) f(x(s)) ds. \quad (3)$$

There are relatively few works devoted to the study of equations of type (2); see, for example, [1–4]. In [5], the asymptotic behaviors of nonoscillatory solutions of the higher-order integrodynamical equation on time scales are presented.

In most papers, the following special case of (2) is considered:

$$x_{n+1} = a_n x_n + b_n + \sum_{k=1}^n K(n, k) x_k; \quad (4)$$

see, e.g., [6–9], [10–13], [14], [15], or [16]. For some recent results devoted to nonlinear Volterra equations we refer to [5, 17–22] and references therein.

Note, that equation (E) generalizes the second-order discrete Volterra difference equation of type (2):

$$\Delta^2 x_n = b_n + \sum_{k=1}^n K(n, k) f(x_k). \quad (5)$$

On the other hand, if  $K(n, k) = 0$  for  $k \neq n$ , then denoting  $a_n = K(n, n)$  equation (E) takes the form

$$\Delta(r_n \Delta x_n) = a_n f(x_n) + b_n. \quad (6)$$

Hence second-order difference equation (6) is a special case of (E). The results on asymptotic properties and oscillation of equations of type (6) can be found, i.e., in [23–26].



Our main goal is to present sufficient conditions for the existence of a solution  $x$  to equation (E) such that

$$x_n = \sum_{k=1}^{n-1} \frac{c}{r_k} + d + o(n^s), \quad (7)$$

where  $c, d \in \mathbb{R}$  and  $s \in (-\infty, 0]$ . We give also sufficient conditions for a given solution  $x$  of equation (E) to have an asymptotic property (7). Moreover, in Section 5 we show applications of the obtained results to linear Volterra equation of type (E). We present also some results for the case when  $(r_n)$  is a potential sequence.

## 2. Preliminaries

We will denote by SQ the space of all sequences  $x : \mathbb{N} \rightarrow \mathbb{R}$ . If  $x, y$  in SQ, then  $xy$  and  $|x|$  denote the sequences defined by  $xy(n) = x_n y_n$  and  $|x|(n) = |x_n|$ , respectively. Moreover,

$$\|x\| = \sup \{|x_n| : n \in \mathbb{N}\}. \quad (8)$$

If  $x \in \text{SQ}$ ,  $s \in \mathbb{R}$ , and  $\lim_{n \rightarrow \infty} n^{-s} x_n = 0$ , then we write  $x_n = o(n^s)$ . Analogously,  $x_n = O(n^s)$  denotes the boundedness of the sequence  $(n^{-s} x_n)$ .

The following two lemmas will be useful in the proof of our main results.

**Lemma 1.** Assume  $u \in \text{SQ}$ ,  $n \in \mathbb{N}$ , and

$$\sum_{j=1}^{\infty} \frac{1}{r_j} \sum_{i=j}^{\infty} |u_i| < \infty. \quad (9)$$

Then

$$\sum_{j=n}^{\infty} \frac{1}{r_j} \sum_{i=j}^{\infty} |u_i| \leq \sum_{j=n}^{\infty} \sum_{i=1}^j \frac{|u_j|}{r_i} < \infty. \quad (10)$$

*Proof.* We have

$$\begin{aligned} \sum_{j=n}^{\infty} \frac{1}{r_j} \sum_{i=j}^{\infty} |u_i| &= \frac{1}{r_n} (|u_n| + |u_{n+1}| + |u_{n+2}| + \dots) \\ &\quad + \frac{1}{r_{n+1}} (|u_{n+1}| + |u_{n+2}| + \dots) + \dots \\ &= \frac{1}{r_n} |u_n| + \left( \frac{1}{r_n} + \frac{1}{r_{n+1}} \right) |u_{n+1}| \\ &\quad + \left( \frac{1}{r_n} + \frac{1}{r_{n+1}} + \frac{1}{r_{n+2}} \right) |u_{n+2}| + \dots \\ &\leq \sum_{j=n}^{\infty} \sum_{i=1}^j \frac{|u_j|}{r_i} \leq \sum_{j=1}^{\infty} \sum_{i=1}^j \frac{|u_j|}{r_i} \\ &= \frac{1}{r_1} |u_1| + \left( \frac{1}{r_1} + \frac{1}{r_2} \right) |u_2| + \dots \\ &= \frac{1}{r_1} (|u_1| + |u_2| + \dots) \end{aligned}$$

$$\begin{aligned} &+ \frac{1}{r_2} (|u_2| + |u_3| + \dots) + \dots \\ &= \sum_{j=1}^{\infty} \frac{1}{r_j} \sum_{i=j}^{\infty} |u_i| < \infty. \end{aligned} \quad (11)$$

□

**Lemma 2** ([27, Lemma 4.7]). Assume  $y, \rho \in \text{SQ}$ , and  $\lim_{n \rightarrow \infty} \rho_n = 0$ . In the set

$$X = \{x \in \text{SQ} : |x - y| \leq |\rho|\} \quad (12)$$

we define a metric by the formula

$$d(x, z) = \|x - z\|. \quad (13)$$

Then any continuous map  $H : X \rightarrow X$  has a fixed point.

## 3. Solutions with Prescribed Asymptotic Behavior

In this section we present sufficient conditions for the existence of a solution  $x$  to equation (E) such that

$$x_n = \sum_{k=1}^{n-1} \frac{c}{r_k} + d + o(n^s), \quad (14)$$

where  $c, d \in \mathbb{R}$  and  $s \in (-\infty, 0]$ .

**Theorem 3.** Assume  $s \in (-\infty, 0]$ ,  $t \in [s, \infty)$ ,  $c, d \in \mathbb{R}$ ,  $y : \mathbb{N} \rightarrow \mathbb{R}$ ,  $q \in \mathbb{N}$ ,  $\alpha \in (0, \infty)$ ,

$$r_n^{-1} = O(n^t),$$

$$\sum_{n=1}^{\infty} n^{1+t-s} \sum_{i=1}^n |K(n, i)| < \infty,$$

$$\sum_{n=1}^{\infty} n^{1+t-s} |b_n| < \infty, \quad (15)$$

$$y_n = d + c \sum_{k=1}^{n-1} \frac{1}{r_k},$$

$$U = \bigcup_{n=q}^{\infty} [y_n - \alpha, y_n + \alpha],$$

and  $f$  is continuous and bounded on  $U$ . Then there exists a solution  $x$  of (E) such that

$$x_n = y_n + o(n^s). \quad (16)$$

*Proof.* For  $n \in \mathbb{N}$  and  $x \in \text{SQ}$  let

$$F(x)(n) = b_n + \sum_{k=1}^n K(n, k) f(x_k). \quad (17)$$

There exists  $L > 0$  such that

$$|f(u)| \leq L \quad \text{for any } u \in U. \quad (18)$$

Let

$$Y = \{x \in \text{SQ} : |x - y| \leq \alpha\}. \quad (19)$$

If  $x \in Y$  and  $n \geq q$ , then

$$x_n \in [y_n - \alpha, y_n + \alpha] \subset U. \quad (20)$$

Choose a positive number  $Q$  such that  $r_n^{-1} \leq Qn^t$  for any  $n$ . Then

$$\sum_{n=1}^{\infty} \frac{1}{n^s r_n} \sum_{j=n}^{\infty} \sum_{k=1}^j |K(j, k)| \leq Q \sum_{n=1}^{\infty} n^{t-s} \sum_{j=n}^{\infty} \sum_{k=1}^j |K(j, k)| \quad (21)$$

Since  $t - s \geq 0$ , we have

$$\sum_{n=1}^{\infty} n^{t-s} \sum_{j=n}^{\infty} \sum_{k=1}^j |K(j, k)| \leq \sum_{n=1}^{\infty} \sum_{j=n}^{\infty} j^{t-s} \sum_{k=1}^j |K(j, k)|. \quad (22)$$

For  $j \in \mathbb{N}$  let

$$z_j = j^{t-s} \sum_{k=1}^j |K(j, k)|. \quad (23)$$

Then we have

$$\begin{aligned} \sum_{n=1}^{\infty} \sum_{j=n}^{\infty} z_j &= (z_1 + z_2 + \cdots) + (z_2 + z_3 + \cdots) + \cdots \\ &= z_1 + 2z_2 + 3z_3 + \cdots = \sum_{n=1}^{\infty} n z_n \\ &= \sum_{n=1}^{\infty} n n^{t-s} \sum_{k=1}^n |K(n, k)| \\ &= \sum_{n=1}^{\infty} n^{1+t-s} \sum_{k=1}^n |K(n, k)| < \infty. \end{aligned} \quad (24)$$

Hence, using (21) and (22), we get

$$\sum_{n=1}^{\infty} \frac{1}{n^s r_n} \sum_{j=n}^{\infty} \sum_{k=1}^j |K(j, k)| < \infty. \quad (25)$$

Analogously, replacing  $\sum_{k=1}^j |K(j, k)|$  by  $|b_j|$ , we obtain

$$\sum_{n=1}^{\infty} \frac{1}{n^s r_n} \sum_{j=n}^{\infty} |b_j| < \infty. \quad (26)$$

Using (25) and (26) we get

$$\sum_{j=1}^{\infty} \frac{1}{j^s r_j} \sum_{i=j}^{\infty} \left( |b_i| + L \sum_{k=1}^i |K(i, k)| \right) < \infty. \quad (27)$$

Since  $s \leq 0$ , we have

$$\sum_{j=1}^{\infty} \frac{1}{j^s r_j} \sum_{i=j}^{\infty} \left( |b_i| + L \sum_{k=1}^i |K(i, k)| \right) < \infty. \quad (28)$$

Define a sequence  $\rho \in \text{SQ}$  by

$$\rho_n = \sum_{j=n}^{\infty} \frac{1}{r_j} \sum_{i=j}^{\infty} \left( |b_i| + L \sum_{k=1}^i |K(i, k)| \right). \quad (29)$$

Define  $w, g \in \text{SQ}$  by

$$\begin{aligned} w_n &= |b_n| + L \sum_{k=1}^n |K(n, k)|, \\ g_n &= \sum_{j=n}^{\infty} \frac{1}{j^s r_j} \sum_{i=j}^{\infty} w_i. \end{aligned} \quad (30)$$

By (27),  $g_n = o(1)$ . We have

$$\begin{aligned} n^{-s} \rho_n &= n^{-s} \sum_{j=n}^{\infty} \frac{1}{r_j} \sum_{i=j}^{\infty} w_i = \sum_{j=n}^{\infty} \frac{1}{n^s r_j} \sum_{i=j}^{\infty} w_i \leq \sum_{j=n}^{\infty} \frac{1}{j^s r_j} \sum_{i=j}^{\infty} w_i \\ &= g_n. \end{aligned} \quad (31)$$

Hence  $n^{-s} \rho_n = o(1)$  and we get

$$\rho_n = n^s o(1) = o(n^s). \quad (32)$$

Hence there exists an index  $p \geq q$  such that

$$\rho_n \leq \alpha \quad (33)$$

for  $n \geq p$ . Let

$$X = \{x \in \text{SQ} : |x - y| \leq \rho, x_n = y_n \text{ for } n < p\},$$

$$H : Y \longrightarrow \text{SQ},$$

$$H(x)(n) = \begin{cases} y_n & \text{for } n < p \\ y_n + \sum_{j=n}^{\infty} \frac{1}{r_j} \sum_{i=j}^{\infty} F(x)(i) & \text{for } n \geq p. \end{cases} \quad (34)$$

We define a metric on  $X$  by formula (13). Note that  $X \subset Y$ . Let  $x \in X$ . By (33) and (20) we have  $x_i \in U$  for any  $i \geq p$ . Hence, by (18),  $|f(x_i)| \leq L$  for  $i \geq p$ . Using (17) and (29) we obtain

$$|H(x)(n) - y_n| = \left| \sum_{j=n}^{\infty} \frac{1}{r_j} \sum_{i=j}^{\infty} F(x)(i) \right| \quad (35)$$

$$\leq \sum_{j=n}^{\infty} \frac{1}{r_j} \sum_{i=j}^{\infty} |F(x)(i)| \leq \rho_n$$

for  $n \geq p$ . Therefore  $HX \subset X$ . Now we show that the map  $H$  is continuous. Using (25) and the assumption  $s \leq 0$ , we have

$$\sum_{n=1}^{\infty} \frac{1}{r_n} \sum_{j=n}^{\infty} \sum_{k=1}^j |K(j, k)| < \infty. \quad (36)$$

Hence, by Lemma 1, we get

$$\sum_{n=1}^{\infty} \sum_{j=1}^n \frac{1}{r_j} \sum_{k=1}^n |K(n, k)| < \infty. \quad (37)$$

Let  $\varepsilon > 0$ . Choose an index  $m \geq p$  and a positive constant  $\gamma$  such that

$$\begin{aligned} L \sum_{n=m}^{\infty} \sum_{j=1}^n \frac{1}{r_j} \sum_{k=1}^n |K(n, k)| &< \varepsilon, \\ \gamma \sum_{n=1}^m \sum_{j=1}^n \frac{1}{r_j} \sum_{k=1}^n |K(n, k)| &< \varepsilon. \end{aligned} \quad (38)$$

Let

$$C = \bigcup_{n=1}^m [y_n - \alpha, y_n + \alpha]. \quad (39)$$

Choose a positive  $\delta$  such that if  $t_1, t_2 \in C$  and  $|t_1 - t_2| < \delta$ , then

$$|f(t_1) - f(t_2)| < \gamma. \quad (40)$$

Choose  $x, z \in X$  such that  $\|x - z\| < \delta$ . Then we have

$$\begin{aligned} \|Hx - Hz\| &= \sup_{n \geq p} \left| \sum_{j=n}^{\infty} \frac{1}{r_j} \sum_{i=j}^{\infty} (F(x)(i) - F(z)(i)) \right| \\ &\leq \sup_{n \geq p} \sum_{j=n}^{\infty} \frac{1}{r_j} \sum_{i=j}^{\infty} |F(x)(i) - F(z)(i)| \\ &= \sum_{j=p}^{\infty} \frac{1}{r_j} \sum_{i=j}^{\infty} |F(x)(i) - F(z)(i)| \\ &\leq \sum_{j=p}^{\infty} \frac{1}{r_j} \sum_{i=j}^{\infty} \sum_{k=1}^i |K(i, k)| |f(x_k) - f(z_k)|. \end{aligned} \quad (41)$$

Using Lemma 1 we obtain

$$\|Hx - Hz\| \leq \sum_{j=p}^{\infty} \sum_{i=1}^j \frac{1}{r_i} \sum_{k=1}^j |K(j, k)| |f(x_k) - f(z_k)|. \quad (42)$$

Note that  $|f(x_j) - f(z_j)| \leq 2L$  for  $j \geq p$  and

$$|f(x_j) - f(z_j)| \leq \gamma \quad \text{for } j \in \{p, p+1, \dots, m\}. \quad (43)$$

Hence we obtain

$$\begin{aligned} \|Hx - Hz\| &\leq \gamma \sum_{n=1}^m \sum_{j=1}^n \frac{1}{r_j} \sum_{k=1}^n |K(n, k)| \\ &\quad + 2L \sum_{n=m}^{\infty} \sum_{j=1}^n \frac{1}{r_j} \sum_{k=1}^n |K(n, k)| < 3\varepsilon. \end{aligned} \quad (44)$$

Therefore  $H : X \rightarrow X$  is continuous. By Lemma 2 there exists a point  $x \in X$  such that  $x = Hx$ . Then, for  $n \geq p$ , we have

$$x_n = y_n + \sum_{j=n}^{\infty} \frac{1}{r_j} \sum_{i=j}^{\infty} F(x)(i). \quad (45)$$

Note that

$$\begin{aligned} \Delta(r_n \Delta y_n) &= \Delta \left( r_n \Delta \left( d + c \sum_{k=1}^{n-1} \frac{1}{r_k} \right) \right) \\ &= c \Delta \left( r_n \Delta \left( \sum_{k=1}^{n-1} \frac{1}{r_k} \right) \right) = c \Delta 1 = 0 \end{aligned} \quad (46)$$

for any  $n$ . Hence, for  $n \geq p$ , we get

$$\begin{aligned} \Delta(r_n \Delta x_n) &= \Delta \left( r_n \Delta \left( \sum_{j=n}^{\infty} \frac{1}{r_j} \sum_{i=j}^{\infty} F(x)(i) \right) \right) \\ &= -\Delta \left( r_n \frac{1}{r_n} \sum_{i=n}^{\infty} F(x)(i) \right) = F(x)(n) \\ &= b_n + \sum_{k=1}^n K(n, k) f(x_k). \end{aligned} \quad (47)$$

Therefore  $x$  is a solution of (E). Since  $x \in X$  we have  $x_n = y_n + o(n^s)$ .  $\square$

If the function  $f$  is continuous, then from Theorem 3 we get the following two results.

**Corollary 4.** Assume  $s \in (-\infty, 0]$ ,  $t \in [s, \infty)$ ,  $f$  is continuous, and

$$r_n^{-1} = O(n^t),$$

$$\sum_{n=1}^{\infty} n^{1+t-s} \sum_{i=1}^n |K(n, i)| < \infty, \quad (48)$$

$$\sum_{n=1}^{\infty} n^{1+t-s} |b_n| < \infty.$$

Then for any  $d \in \mathbb{R}$  there exists a solution  $x$  of (E) such that  $x_n = d + o(n^s)$ .

*Proof.* Taking  $c = 0$ ,  $q = 1$ , and  $\alpha = 1$  in Theorem 3, we obtain the result.  $\square$

**Corollary 5.** Assume  $t \in (-\infty, -1)$ ,  $s \in (-\infty, t]$ ,  $f$  is continuous, and

$$r_n^{-1} = O(n^t),$$

$$\sum_{n=1}^{\infty} n^{1+t-s} \sum_{i=1}^n |K(n, i)| < \infty, \quad (49)$$

$$\sum_{n=1}^{\infty} n^{1+t-s} |b_n| < \infty.$$

Then for any  $c, d \in \mathbb{R}$  there exists a solution  $x$  of (E) such that

$$x_n = d + c \sum_{k=1}^{n-1} \frac{1}{r_k} + o(n^s). \quad (50)$$

*Proof.* Assume  $c, d \in \mathbb{R}$  and a sequence  $y \in \text{SQ}$  is defined by

$$y_n = d + c \sum_{k=1}^{n-1} \frac{1}{r_k}. \quad (51)$$

Since  $r_n^{-1} = O(n^t)$  and  $t < -1$ , we see that  $y$  is bounded. Now, taking  $q = 1$  and  $\alpha = 1$  in Theorem 3, we obtain the result.  $\square$

Note that Corollaries 4 and 5 concern convergent solutions. However, Theorem 3 includes also divergent solutions. For example, if  $f(x) = x^{-1}$  for  $x \neq 0$ ,  $s \in (-\infty, 0]$ ,  $t = 0$ ,  $r_n^{-1} = O(1)$ , and

$$\begin{aligned} \sum_{k=1}^{\infty} r_k^{-1} &= \infty, \\ \sum_{n=1}^{\infty} n^{1-s} \sum_{i=1}^n |K(n, i)| &< \infty, \\ \sum_{n=1}^{\infty} n^{1-s} |b_n| &< \infty. \end{aligned} \quad (52)$$

then, by Theorem 3, for any nonzero  $c \in \mathbb{R}$  and any  $d \in \mathbb{R}$  there exists a solution  $x$  of (E) such that

$$x_n = d + c \sum_{k=1}^{n-1} \frac{1}{r_k} + o(n^s). \quad (53)$$

Now we present an example that proves the assumption

$$\sum_{n=1}^{\infty} n^{1+t-s} \sum_{i=1}^n |K(n, i)| < \infty, \quad (54)$$

in Theorem 3, is essential.

*Example 6.* Assume  $r_n = n$ ,  $b_n = 0$ ,

$$K(n, k) = \frac{1}{n^2}, \quad (55)$$

$$f(x) = \frac{1}{|x| + 1} + 1,$$

$s = 0$ , and  $t = 0$ . Then equation (E) takes the form

$$\Delta(n\Delta x_n) = \frac{1}{n^2} \sum_{k=1}^n \left( \frac{1}{|x_k| + 1} + 1 \right). \quad (56)$$

Let  $c, d \in \mathbb{R}$  and

$$y_n = d + c \sum_{k=1}^{n-1} \frac{1}{r_k} = d + c \sum_{k=1}^{n-1} \frac{1}{k}. \quad (57)$$

Notice that  $f$  is continuous and bounded on  $\mathbb{R}$ . Moreover,

$$\sum_{n=1}^{\infty} n^{1+t-s} \sum_{k=1}^n K(n, k) = \sum_{n=1}^{\infty} n \frac{1}{n} = \infty, \quad (58)$$

and

$$\begin{aligned} \Delta y_n &= \frac{c}{n}, \\ \Delta(n\Delta y_n) &= 0. \end{aligned} \quad (59)$$

Assume  $x$  is a solution of (56) such that

$$\begin{aligned} x_n &= y_n + z_n, \\ z_n &= o(n^s) = o(1). \end{aligned} \quad (60)$$

Since  $\Delta(n\Delta y_n) = 0$ , we have

$$\Delta(n\Delta x_n) = \Delta(n\Delta y_n) + \Delta(n\Delta z_n) = \Delta(n\Delta z_n). \quad (61)$$

Hence

$$\Delta(n\Delta z_n) = \Delta(n\Delta x_n) = \sum_{k=1}^n \frac{1}{n^2} \left( \frac{1}{|x_k| + 1} + 1 \right) > 0 \quad (62)$$

for large  $n$ . Therefore, the sequence  $n\Delta z_n$  is eventually increasing and there exists the limit

$$\lambda = \lim_{n \rightarrow \infty} n\Delta z_n > -\infty. \quad (63)$$

If  $\lambda < \infty$ , then the sequence  $n\Delta z_n$  is convergent in  $\mathbb{R}$ . Hence the series

$$\sum_{n=1}^{\infty} \Delta(n\Delta x_n) = \sum_{n=1}^{\infty} \Delta(n\Delta z_n) \quad (64)$$

is convergent. On the other hand

$$\Delta(n\Delta x_n) = \sum_{k=1}^n \frac{1}{n^2} \left( \frac{1}{|x_k| + 1} + 1 \right) > \frac{1}{n} \quad (65)$$

for large  $n$ . Hence  $\lambda = \infty$ . Therefore  $n\Delta z_n > 1$  for large  $n$  and we get

$$\sum_{n=1}^{\infty} \Delta z_n \geq \sum_{n=1}^{\infty} \frac{1}{n} = \infty. \quad (66)$$

But since  $z_n \rightarrow 0$ , the series  $\sum_{n=1}^{\infty} \Delta z_n$  is convergent.

#### 4. Asymptotic Behavior of Solutions

In this section we present sufficient conditions for a given solution  $x$  of equation (E) to have an asymptotic property

$$x_n = \sum_{k=1}^{n-1} \frac{c}{r_k} + d + o(n^s), \quad (67)$$

where  $c, d \in \mathbb{R}$  and  $s \in (-\infty, 0]$ .

**Theorem 7.** Assume  $s \in (-\infty, 0]$ ,  $t \in [s, \infty)$ ,

$$r_n^{-1} = O(n^t),$$

$$\sum_{n=1}^{\infty} n^{1+t-s} \sum_{i=1}^n |K(n, i)| < \infty, \quad (68)$$

$$\sum_{n=1}^{\infty} n^{1+t-s} |b_n| < \infty,$$

and  $x$  is a solution of (E) such that the sequence  $(f(x_n))$  is bounded. Then there exist  $c, d \in \mathbb{R}$  such that

$$x_n = \sum_{k=1}^{n-1} \frac{c}{r_k} + d + o(n^s). \quad (69)$$

*Proof.* We have

$$\Delta(r_n \Delta x_n) = b_n + \sum_{k=1}^n K(n, k) f(x_k) \quad (70)$$

for large  $n$ . Using boundedness of the sequence  $(f(x_n))$  and (68) we get

$$\sum_{n=1}^{\infty} n^{1+t-s} |\Delta(r_n \Delta x_n)| < \infty. \quad (71)$$

Define  $w, u \in \text{SQ}$  by

$$\begin{aligned} w_n &= \Delta(r_n \Delta x_n), \\ u_n &= n^{t-s} |w_n|. \end{aligned} \quad (72)$$

Choose a positive  $L$  such that  $r_n^{-1} \leq Ln^t$  for any  $n$ . Since  $t-s \geq 0$ , we have

$$\begin{aligned} \sum_{n=1}^{\infty} \frac{1}{n^s r_n} \sum_{j=n}^{\infty} |w_j| &\leq L \sum_{n=1}^{\infty} n^{t-s} \sum_{j=n}^{\infty} |w_j| = L \sum_{n=1}^{\infty} \sum_{j=n}^{\infty} n^{t-s} |w_j| \\ &\leq L \sum_{n=1}^{\infty} \sum_{j=n}^{\infty} j^{t-s} |w_j|. \end{aligned} \quad (73)$$

Moreover,

$$\begin{aligned} \sum_{n=1}^{\infty} n^{1+t-s} |w_n| &= \sum_{n=1}^{\infty} n u_n \\ &= u_1 + (u_2 + u_2) + (u_3 + u_3 + u_3) + \cdots \\ &= \sum_{j=1}^{\infty} u_j + \sum_{j=2}^{\infty} u_j + \sum_{j=3}^{\infty} u_j + \cdots = \sum_{n=1}^{\infty} \sum_{j=n}^{\infty} u_j \\ &= \sum_{n=1}^{\infty} \sum_{j=n}^{\infty} j^{t-s} |w_j|. \end{aligned} \quad (74)$$

Hence, by (73)

$$\sum_{n=1}^{\infty} \frac{1}{n^s r_n} \sum_{j=n}^{\infty} |w_j| < \infty. \quad (75)$$

Since  $s \leq 0$ , we have

$$\sum_{n=1}^{\infty} \frac{1}{r_n} \sum_{j=n}^{\infty} |w_j| < \sum_{n=1}^{\infty} \frac{1}{n^s r_n} \sum_{j=n}^{\infty} |w_j| < \infty. \quad (76)$$

Let

$$z_n = \sum_{j=n}^{\infty} \frac{1}{r_j} \sum_{i=j}^{\infty} w_i. \quad (77)$$

Then

$$\begin{aligned} n^{-s} |z_n| &= n^{-s} \left| \sum_{j=n}^{\infty} \frac{1}{r_j} \sum_{i=j}^{\infty} w_i \right| \leq n^{-s} \sum_{j=n}^{\infty} \frac{1}{r_j} \sum_{i=j}^{\infty} |w_i| \\ &= \sum_{j=n}^{\infty} \frac{1}{n^s r_j} \sum_{i=j}^{\infty} |w_i| \leq \sum_{j=n}^{\infty} \frac{1}{j^s r_j} \sum_{i=j}^{\infty} |w_i| = o(1). \end{aligned} \quad (78)$$

Thus  $z_n = o(n^s)$ . Let

$$y_n = x_n - z_n. \quad (79)$$

Then

$$\Delta y_n = \Delta x_n - \Delta z_n = \Delta x_n + \frac{1}{r_n} \sum_{i=n}^{\infty} w_i. \quad (80)$$

Hence

$$r_n \Delta y_n = r_n \Delta x_n + \sum_{i=n}^{\infty} w_i \quad (81)$$

and we get

$$\begin{aligned} \Delta(r_n \Delta y_n) &= \Delta(r_n \Delta x_n) - w_n \\ &= \Delta(r_n \Delta x_n) - \Delta(r_n \Delta x_n) = 0 \end{aligned} \quad (82)$$

for any  $n \in \mathbb{N}$ . Therefore, there exists a real constant  $c$  such that  $r_n \Delta y_n = c$ . Thus

$$y_n - y_1 = \Delta y_1 + \cdots + \Delta y_{n-1} = \frac{c}{r_1} + \cdots + \frac{c}{r_{n-1}}. \quad (83)$$

Hence

$$x_n = y_n + z_n = \sum_{k=1}^{n-1} \frac{c}{r_k} + d + o(n^s) \quad (84)$$

where  $d = y_1$ .  $\square$

**Corollary 8.** Assume  $s \in (-\infty, 0]$ ,  $t \in [s, \infty)$ ,  $r_n^{-1} = O(n^t)$ ,  $f$  is locally bounded,

$$\begin{aligned} \sum_{n=1}^{\infty} n^{1+t-s} \sum_{i=1}^n |K(n, i)| &< \infty, \\ \sum_{n=1}^{\infty} n^{1+t-s} |b_n| &< \infty, \end{aligned} \quad (85)$$

and  $x$  is a bounded solution of (E). Then there exist  $c, d \in \mathbb{R}$  such that

$$x_n = \sum_{k=1}^{n-1} \frac{c}{r_k} + d + o(n^s). \quad (86)$$

*Proof.* Since  $x$  is bounded and  $f$  is locally bounded, the sequence  $(f(x_n))$  is bounded. Hence the assertion is a consequence of Theorem 7.  $\square$



**Corollary 9.** Assume  $t \in [0, \infty)$ ,  $r_n^{-1} = O(n^t)$ ,  $f$  is locally bounded, and

$$\begin{aligned} \sum_{n=1}^{\infty} n^{1+t} \sum_{i=1}^n |K(n, i)| &< \infty, \\ \sum_{n=1}^{\infty} n^{1+t} |b_n| &< \infty. \end{aligned} \quad (87)$$

Then any bounded solution of (E) is convergent.

*Proof.* Assume  $x$  is a bounded solution of (E). Let  $s = 0$ . By Corollary 8, there exist  $c, d \in \mathbb{R}$  such that

$$x_n = c \sum_{k=1}^{n-1} \frac{1}{r_k} + d + o(1). \quad (88)$$

Define a sequence  $u \in \text{SQ}$ , by  $u_n = r_1^{-1} + r_2^{-1} + \dots + r_{n-1}^{-1}$ . Then  $u$  is increasing and bounded. Hence  $u$  is convergent. Therefore  $x_n = cu_n + d + o(1)$  is convergent.  $\square$

**Corollary 10.** Assume  $s \in (-\infty, 0]$ ,  $t \in [s, \infty)$ ,  $r_n^{-1} = O(n^t)$ ,  $f$  is bounded,

$$\begin{aligned} \sum_{n=1}^{\infty} n^{1+t-s} \sum_{i=1}^n |K(n, i)| &< \infty, \\ \sum_{n=1}^{\infty} n^{1+t-s} |b_n| &< \infty, \end{aligned} \quad (89)$$

and  $x$  is an arbitrary solution of (E). Then there exist  $c, d \in \mathbb{R}$  such that

$$x_n = \sum_{k=1}^{n-1} \frac{c}{r_k} + d + o(n^s). \quad (90)$$

*Proof.* The assertion is an immediate consequence of Theorem 7.  $\square$

## 5. Additional Results

In this section we present some additional results. First, we give some applications of our results to linear discrete Volterra equations of type (E). From Corollary 4 we get the following result.

**Corollary 11.** Assume  $s \in (-\infty, 0]$ ,  $t \in [s, \infty)$ ,

$$\begin{aligned} r_n^{-1} &= O(n^t), \\ \sum_{n=1}^{\infty} n^{1+t-s} \sum_{i=1}^n |K(n, i)| &< \infty, \\ \sum_{n=1}^{\infty} n^{1+t-s} |b_n| &< \infty. \end{aligned} \quad (91)$$

Then for any  $d \in \mathbb{R}$  there exists a solution  $x$  of equation

$$\Delta(r_n \Delta x_n) = b_n + \sum_{k=1}^n K(n, k) x_k \quad (92)$$

such that  $x_n = d + o(n^s)$ .

From Corollary 5 we get the following.

**Corollary 12.** Assume  $t \in (-\infty, -1)$ ,  $s \in (-\infty, t]$ , and

$$\begin{aligned} r_n^{-1} &= O(n^t), \\ \sum_{n=1}^{\infty} n^{1+t-s} \sum_{i=1}^n |K(n, i)| &< \infty, \\ \sum_{n=1}^{\infty} n^{1+t-s} |b_n| &< \infty. \end{aligned} \quad (93)$$

Then for any  $c, d \in \mathbb{R}$  there exists a solution  $x$  of (92) such that

$$x_n = d + c \sum_{k=1}^{n-1} \frac{1}{r_k} + o(n^s). \quad (94)$$

*Example 13.* Assume  $s = 0$ ,  $t = 1$ , and

$$\begin{aligned} r_n &= \frac{1}{n-1}, \\ b_n &= -\frac{3}{(n+2)(n+1)n(n-1)} - \frac{1}{n^4}, \end{aligned} \quad (95)$$

$$K(n, k) = \frac{2k}{n^6}.$$

Then (92) takes the form

$$\begin{aligned} \Delta\left(\frac{1}{n-1} \Delta x_n\right) &= -\frac{3}{(n+2)(n+1)n(n-1)} - \frac{1}{n^4} \\ &\quad + \sum_{k=1}^n \frac{2k}{n^6} x_k. \end{aligned} \quad (96)$$

It is easy to check that all assumptions of Corollary 11 hold. Indeed, we have

$$\sum_{n=1}^{\infty} n^2 \sum_{k=1}^n |K(n, k)| = \sum_{n=1}^{\infty} n^2 \sum_{k=1}^n \frac{2k}{n^6} = \sum_{n=1}^{\infty} \frac{n+1}{n^3} < \infty, \quad (97)$$

and

$$\sum_{n=1}^{\infty} n^2 |b_n| < \infty. \quad (98)$$

So, for every  $d \in \mathbb{R}$ , there exists a solution  $x$  of (96) such that  $\lim_{n \rightarrow \infty} x_n = d$ . One such solution is  $x_n = 1 - 1/n$ .

In our investigations the condition

$$\sum_{n=1}^{\infty} n^{1+t-s} \sum_{i=1}^n |K(n, i)| < \infty \quad (99)$$

plays an important role. In practice, this condition can be difficult to verify. In the following remark we present the condition, which is a little stronger but easier to check.

*Remark 14.* Assume  $s \in (-\infty, 0]$ ,  $t \in \mathbb{R}$ ,  $\lambda \in (-\infty, s - t - 2)$ , and  $u_n = O(n^\lambda)$ . Let  $\varepsilon = s - t - 2 - \lambda$ ,  $L > 0$ ,  $|u_n| \leq Ln^\lambda$  for any  $n$ . Then  $\lambda = s - t - 2 - \varepsilon$  and

$$\sum_{n=1}^{\infty} n^{1+t-s} |u_n| \leq L \sum_{n=1}^{\infty} n^{1+t-s} n^\lambda = \sum_{n=1}^{\infty} \frac{1}{n^{1+\varepsilon}} < \infty. \quad (100)$$

Applying this remark to Corollaries 4, 5, 8, and 9, respectively, we obtain following results.

**Corollary 15.** Assume  $s \in (-\infty, 0]$ ,  $t \in [s, \infty)$ ,  $\lambda \in (-\infty, s - t - 2)$ ,  $f$  is continuous, and

$$\begin{aligned} r_n^{-1} &= O(n^t), \\ \sum_{i=1}^n |K(n, i)| &= O(n^\lambda), \end{aligned} \quad (101)$$

$$b_n = O(n^\lambda).$$

Then for any  $d \in \mathbb{R}$  there exists a solution  $x$  of (E) such that  $x_n = d + o(n^s)$ .

**Corollary 16.** Assume  $t \in (-\infty, -1)$ ,  $s \in (-\infty, t]$ ,  $\lambda \in (-\infty, s - t - 2)$ ,  $f$  is continuous, and

$$\begin{aligned} r_n^{-1} &= O(n^t), \\ \sum_{i=1}^n |K(n, i)| &= O(n^\lambda), \end{aligned} \quad (102)$$

$$b_n = O(n^\lambda).$$

Then for any  $c, d \in \mathbb{R}$  there exists a solution  $x$  of (E) such that

$$x_n = d + c \sum_{k=1}^{n-1} \frac{1}{r_k} + o(n^s). \quad (103)$$

**Corollary 17.** Assume  $s \in (-\infty, 0]$ ,  $t \in [s, \infty)$ ,  $\lambda \in (-\infty, s - t - 2)$ ,  $f$  is locally bounded,

$$\begin{aligned} r_n^{-1} &= O(n^t), \\ \sum_{i=1}^n |K(n, i)| &= O(n^\lambda), \end{aligned} \quad (104)$$

$$b_n = O(n^\lambda),$$

and  $x$  is a bounded solution of (E). Then there exist  $c, d \in \mathbb{R}$  such that

$$x_n = \sum_{k=1}^{n-1} \frac{c}{r_k} + d + o(n^s). \quad (105)$$

**Corollary 18.** Assume  $t \in [0, \infty)$ ,  $\lambda \in (-\infty, -t - 2)$ ,  $f$  is locally bounded, and

$$\begin{aligned} r_n^{-1} &= O(n^t), \\ \sum_{i=1}^n |K(n, i)| &= O(n^\lambda), \end{aligned} \quad (106)$$

$$b_n = O(n^\lambda).$$

Then any bounded solution of (E) is convergent.

Now we present some results for the case when the series

$$\begin{aligned} \sum_{n=1}^{\infty} n^{1+t-s} \sum_{i=1}^n |K(n, i)|, \\ \sum_{n=1}^{\infty} n^{1+t-s} |b_n| \end{aligned} \quad (107)$$

are strongly convergent.

**Remark 19.** If  $u : \mathbb{N} \rightarrow \mathbb{R}$  and  $\limsup_{n \rightarrow \infty} \sqrt[n]{|u_n|} < 1$ , then, by the root test,

$$\sum_{n=1}^{\infty} n^\lambda |u_n| < \infty \quad (108)$$

for any  $\lambda \in \mathbb{R}$ .

**Corollary 20.** Assume  $t \in \mathbb{R}$ ,  $f$  is continuous, and

$$\begin{aligned} r_n^{-1} &= O(n^t), \\ \limsup_{n \rightarrow \infty} \sqrt[n]{\sum_{i=1}^n |K(n, i)|} &< 1, \\ \limsup_{n \rightarrow \infty} \sqrt[n]{|b_n|} &< 1. \end{aligned} \quad (109)$$

Then for any  $d \in \mathbb{R}$  and any  $\lambda \in (-\infty, 0]$  there exists a solution  $x$  of (E) such that

$$x_n = d + o(n^\lambda). \quad (110)$$

*Proof.* Let  $d \in \mathbb{R}$ . Choose  $s \in (-\infty, \min\{t, \lambda\})$ . By Remark 19, we have

$$\begin{aligned} \sum_{n=1}^{\infty} n^{1+t-s} \sum_{i=1}^n |K(n, i)| &< \infty, \\ \sum_{n=1}^{\infty} n^{1+t-s} |b_n| &< \infty. \end{aligned} \quad (111)$$

By Corollary 4, there exists a solution  $x$  of (E) such that

$$x_n = d + o(n^s) = d + o(n^\lambda). \quad (112)$$

□

Analogously, using Corollary 5, we get the following.

**Corollary 21.** Assume  $t \in (-\infty, -1)$ ,  $f$  is continuous, and

$$\begin{aligned} r_n^{-1} &= O(n^t), \\ \limsup_{n \rightarrow \infty} \sqrt[n]{\sum_{i=1}^n |K(n, i)|} &< 1, \\ \limsup_{n \rightarrow \infty} \sqrt[n]{|b_n|} &< 1. \end{aligned} \quad (113)$$

Then for any  $c, d \in \mathbb{R}$  and any  $\lambda \in (-\infty, 0]$  there exists a solution  $x$  of (E) such that

$$x_n = d + \sum_{k=1}^{n-1} \frac{c}{r_k} + o(n^\lambda). \quad (114)$$

To the end we consider the case when  $(r_n)$  is a potential sequence.

**Lemma 22.** If  $\omega \in (1, \infty)$ , then

$$\sum_{k=1}^{n-1} \frac{1}{k^\omega} = \sum_{n=1}^{\infty} \frac{1}{n^\omega} + O(n^{1-\omega}). \quad (115)$$

*Proof.* Define  $u \in \text{SQ}$  and  $\lambda \in \mathbb{R}$  by

$$\begin{aligned} u_n &= \sum_{k=1}^{n-1} \frac{1}{k^\omega}, \\ \lambda &= \sum_{k=1}^{\infty} \frac{1}{k^\omega}. \end{aligned} \quad (116)$$

By [28, Theorem 2.2], we have

$$\Delta n^{1-\omega} = (1-\omega)n^{-\omega} + o(n^{-\omega}). \quad (117)$$

Since  $\Delta u_n = n^{-\omega}$ , we get

$$\begin{aligned} \frac{\Delta(u_n - \lambda)}{\Delta n^{1-\omega}} &= \frac{n^{-\omega}}{(1-\omega)n^{-\omega} + o(n^{-\omega})} \\ &= \frac{1}{(1-\omega) + o(1)} \rightarrow \frac{1}{1-\omega}. \end{aligned} \quad (118)$$

Note that  $n^{1-\omega} \rightarrow 0$  and  $(u_n - \lambda) \rightarrow 0$ . Hence, by discrete L'Hospital's Rule,

$$\frac{u_n - \lambda}{n^{1-\omega}} = \frac{1}{1-\omega} + o(1). \quad (119)$$

Therefore

$$\begin{aligned} u_n &= \lambda + \frac{1}{1-\omega} n^{1-\omega} + o(n^{1-\omega}) \\ &= \sum_{k=1}^{\infty} \frac{1}{k^\omega} + O(n^{1-\omega}). \end{aligned} \quad (120)$$

□

**Corollary 23.** Assume  $t \in (-\infty, -1)$ ,  $s \in (-\infty, t]$ ,  $f$  is continuous, and

$$\begin{aligned} r_n &= n^{-t}, \\ \sum_{n=1}^{\infty} n^{1+t-s} \sum_{i=1}^n |K(n, i)| &< \infty, \\ \sum_{n=1}^{\infty} n^{1+t-s} |b_n| &< \infty. \end{aligned} \quad (121)$$

Then for any  $\mu \in \mathbb{R}$  there exists a solution  $x$  of (E) such that

$$x_n = \mu + O(n^{t+1}). \quad (122)$$

*Proof.* Assume  $\mu \in \mathbb{R}$ . Let

$$\begin{aligned} d &= 0, \\ \lambda &= \sum_{n=1}^{\infty} n^t, \\ c &= \frac{\mu}{\lambda}. \end{aligned} \quad (123)$$

By Corollary 5, there exists a solution  $x$  of (E) such that

$$x_n = d + c \sum_{k=1}^{n-1} k^t + o(n^s). \quad (124)$$

By Lemma 22

$$\sum_{k=1}^{n-1} k^t = \lambda + O(n^{t+1}). \quad (125)$$

Hence

$$x_n = \mu + O(n^{t+1}) + o(n^s) = \mu + O(n^{t+1}). \quad (126)$$

□

**Corollary 24.** Assume  $t \in (-\infty, -1)$ ,  $s \in (-\infty, t]$ ,  $f$  is locally bounded, and

$$\begin{aligned} r_n &= n^{-t}, \\ \sum_{n=1}^{\infty} n^{1+t-s} \sum_{i=1}^n |K(n, i)| &< \infty, \\ \sum_{n=1}^{\infty} n^{1+t-s} |b_n| &< \infty. \end{aligned} \quad (127)$$

Then for any bounded solution  $x$  of (E) there exists a real number  $\mu$  such that

$$x_n = \mu + O(n^{t+1}). \quad (128)$$

*Proof.* By Corollary 8 there exist  $c, d \in \mathbb{R}$  such that

$$x_n = d + c \sum_{k=1}^{n-1} k^t + o(n^s). \quad (129)$$

By Lemma 22 we obtain

$$\begin{aligned} x_n &= d + c \left( \sum_{k=1}^{\infty} k^t + O(n^{t+1}) \right) + o(n^s) \\ &= \mu + O(n^{t+1}), \quad \text{where } \mu = d + c \sum_{k=1}^{\infty} k^t. \end{aligned} \quad (130)$$

□

## Data Availability

No data were used to support this study.

## Conflicts of Interest

The authors declare that there are no conflicts of interest regarding the publication of this paper.

## Acknowledgments

The second author was supported by the Ministry of Science and Higher Education of Poland (04/43/DSPB/0095).

## References

- [1] R. Medina, "The asymptotic behavior of the solutions of a Volterra difference equation," *Computers & Mathematics with Applications. An International Journal*, vol. 34, no. 1, pp. 19–26, 1997.
- [2] R. Medina, "Asymptotic behavior of Volterra difference equations," *Computers & Mathematics with Applications*, vol. 41, no. 5–6, pp. 679–687, 2001.
- [3] J. Migda and M. g. Migda, "Asymptotic behavior of solutions of discrete Volterra equations," *Opuscula Mathematica*, vol. 36, no. 2, pp. 265–278, 2016.
- [4] J. Migda and M. g. Migda, "Qualitative approximation of solutions to discrete Volterra equations," *Electronic Journal of Qualitative Theory of Differential Equations*, vol. 3, pp. 1–27, 2018.
- [5] M. Bohner, S. Grace, and N. Sultana, "Asymptotic behavior of nonoscillatory solutions of higher-order integro-dynamic equations," *Opuscula Mathematica*, vol. 34, no. 1, pp. 5–14, 2014.
- [6] J. Diblik and E. Schmeidel, "On the existence of solutions of linear Volterra difference equations asymptotically equivalent to a given sequence," *Applied Mathematics and Computation*, vol. 218, no. 18, pp. 9310–9320, 2012.
- [7] S. Elaydi, "Stability and asymptoticity of Volterra difference equations: a progress report," *Journal of Computational and Applied Mathematics*, vol. 228, no. 2, pp. 504–513, 2009.
- [8] K. Gajda, T. Gronek, and E. Schmeidel, "On the existence of weighted asymptotically constant solutions of Volterra difference equations of nonconvolution type," *Discrete and Continuous Dynamical Systems - Series B*, vol. 19, no. 8, pp. 2681–2690, 2014.
- [9] T. Gronek and E. Schmeidel, "Existence of bounded solution of Volterra difference equations via Darbo's fixed-point theorem," *Journal of Difference Equations and Applications*, vol. 19, no. 10, pp. 1645–1653, 2013.
- [10] I. Györi and L. Horvath, "Asymptotic representation of the solutions of linear Volterra difference equations," *Advances in Difference Equations*, 22 pages, article 932831, 2008.
- [11] I. Györi and D. W. Reynolds, "Sharp conditions for boundedness in linear discrete Volterra equations," *Journal of Difference Equations and Applications*, vol. 15, no. 11–12, pp. 1151–1164, 2009.
- [12] I. Györi and D. W. Reynolds, "On asymptotically periodic solutions of linear discrete Volterra equations," *Fasciculi Mathematici*, no. 44, pp. 53–67, 2010.
- [13] V. Kolmanovskii and L. Shaikhet, "Some conditions for boundedness of solutions of difference volterra equations," *Applied Mathematics Letters*, vol. 16, no. 6, pp. 857–862, 2003.
- [14] E. Messina and A. Vecchio, "Boundedness and asymptotic stability for the solution of homogeneous Volterra discrete equations," *Discrete Dynamics in Nature and Society*, vol. 2018, Article ID 6935069, 8 pages, 2018.
- [15] M. Migda and J. Morchał, "Asymptotic properties of solutions of difference equations with several delays and Volterra summation equations," *Applied Mathematics and Computation*, vol. 220, pp. 365–373, 2013.
- [16] D. W. Reynolds, "On asymptotic constancy for linear discrete summation equations," *Computers & Mathematics with Applications. An International Journal*, vol. 64, no. 7, pp. 2335–2344, 2012.
- [17] C. T. Baker and Y. Song, "Periodic solutions of non-linear discrete Volterra equations with finite memory," *Journal of Computational and Applied Mathematics*, vol. 234, no. 9, pp. 2683–2698, 2010.
- [18] L. Berezansky, M. Migda, and E. Schmeidel, "Some stability conditions for scalar Volterra difference equations," *Opuscula Mathematica*, vol. 36, no. 4, pp. 459–470, 2016.
- [19] I. Györi and E. Awwad, "On the boundedness of the solutions in nonlinear discrete Volterra difference equations," *Advances in Difference Equations*, vol. 2, 20 pages, 2012.
- [20] I. Györi and F. Hartung, "Asymptotic behaviour of nonlinear difference equations," *Journal of Difference Equations and Applications*, vol. 18, no. 9, pp. 1485–1509, 2012.
- [21] M. g. Migda and J. Migda, "Bounded solutions of nonlinear discrete Volterra equations," *Mathematica Slovaca*, vol. 66, no. 5, pp. 1169–1178, 2016.
- [22] Y. Song and C. T. Baker, "Linearized stability analysis of discrete Volterra equations," *Journal of Mathematical Analysis and Applications*, vol. 294, no. 1, pp. 310–333, 2004.
- [23] M. Migda, "Asymptotic behaviour of solutions of nonlinear delay difference equations," *Fasciculi Mathematici*, no. 31, pp. 57–62, 2001.
- [24] P. Rehák, "Asymptotic formulae for solutions of linear second-order difference equations," *Journal of Difference Equations and Applications*, vol. 22, no. 1, pp. 107–139, 2016.
- [25] Z. a. Szafranski and B. a. Szmanda, "Oscillation of solutions of some nonlinear difference equations," *Publicacions Matemàtiques*, vol. 40, no. 1, pp. 127–133, 1996.
- [26] E. Thandapani, M. M. Manuel, J. R. Graef, and P. W. Spikes, "Monotone properties of certain classes of solutions of second-order difference equations," *Computers & Mathematics with Applications. An International Journal*, vol. 36, no. 10–12, pp. 291–297, 1998.
- [27] J. Migda, "Approximative solutions of difference equations," *Electronic Journal of Qualitative Theory of Differential Equations*, vol. 13, pp. 1–26, 2014.
- [28] J. Migda, "Asymptotically polynomial solutions of difference equations," *Advances in Difference Equations*, vol. 92, pp. 1–16, 2013.

## Research Article

# Nonsmooth Vibration Characteristic of Gear Pair System with Periodic Stiffness and Backlash

Minjia He,<sup>1,2</sup> Shuo Li ,<sup>2</sup> Zhenjun Lin,<sup>2</sup> Jinjin Wang,<sup>1,2</sup> Shuang Liu ,<sup>1,2</sup> and Ruolan Hao <sup>2</sup>

<sup>1</sup>Liren College of Yanshan University, Qinhuangdao, China

<sup>2</sup>College of Electrical Engineering, Yanshan University, Qinhuangdao, China

Correspondence should be addressed to Shuang Liu; [shliu@ysu.edu.cn](mailto:shliu@ysu.edu.cn)

Received 8 March 2018; Accepted 24 May 2018; Published 8 July 2018

Academic Editor: Jorge E. Macias-Diaz

Copyright © 2018 Minjia He et al. This is an open access article distributed under the Creative Commons Attribution License, which permits unrestricted use, distribution, and reproduction in any medium, provided the original work is properly cited.

As the most widely used power transmission device in mechanical equipment, the vibration characteristics of gears have a very important influence on the working performance. It is of great theoretical and practical significance to study the vibration characteristics of gear system. In this paper, a gear transmission system model is set up in a forcefully nonlinear form; the continuity mapping and discontinuity mapping are utilized to analyze the nonsmooth vibration. Then, the sliding dynamics of separation boundaries is studied by using the perturbation method and the differential inclusion theory. In addition, the periodic response of gear pair system is illustrated and Floquet's theory is presented to confirm the stability and bifurcation of periodic response. Concurrently, the maximal Lyapunov exponent is obtained to accurately determine the chaotic state in gear pair system, which is consistent with the bifurcation diagram and Poincare section. Finally, a reasonable explanation is given for the jump phenomenon in bifurcation diagram.

## 1. Introduction

The gear system is widely used in various mechanical systems and equipment because of its compact structure and high transmission efficiency. Its own vibration characteristics can directly affect the performance and reliability of the whole system. Therefore, the study of its vibration characteristics has great significance.

Dating back to 1980s, many researchers had carried out experiments on the nonlinear vibration of gear system [1–5]; besides a certain number of complicated phenomena such as bifurcation and chaos had been observed. In [6], the nonlinear frequency response characteristics of a gear transmission system with backlash had been studied by the harmonic balance method. In [7], some experiments had been carried out on a gear pair transmission system. In addition several phenomena such as chaotic behaviors of subharmonic resonance and superharmonic resonance had been studied. In [8], a nonlinear rotor-bearing system was observed; bifurcations and the periodic responses were also investigated. Moreover, the chaotic response was checked as well through using the Lyapunov exponent and numerical

methods. In [9], a research on a nonlinear model of gear transmission system including backlash, friction, and time-varying stiffness was achieved. On the contrary, the existence of bifurcation, periodic responses, and chaotic motions were studied numerically. In [10], the frequency responses of a nonlinear geared rotor-bearing system with time-varying mesh stiffness were inspected by the methods of multiple-scales and mathematical simulation. In [11], the vibration dynamic responses of a gear transmission system supported by journal bearing were studied; besides the subharmonic, periodic, and chaotic states were examined.

What is more, plenty of valuable research had been commenced on gear transmission system. But they rarely involved the nonsmooth dynamics of gear system. More precisely, the gear transmission system is a typical system with segmented properties, caused by the presence of backlash. Moreover, with the presence of backlash, the gear transmission system can be considered as one of vibration shock systems. At the beginning of this century, considerable researchers were interested in this system, especially in segmented linear systems that were stimulated by external periodic forces. In [12], the earliest research for a segmented linear system without



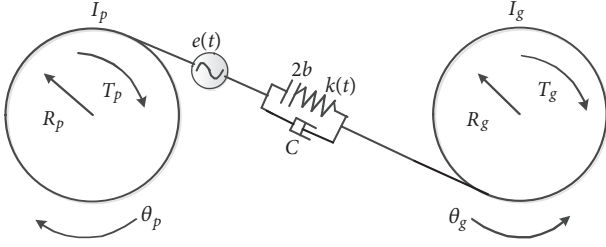


FIGURE 1: The gear transmission model.

damping was made and a closed solution of the periodic response was obtained. In [13], a mapping technique was developed to investigate a discrete linear system; besides the chaotic behavior was presented in numerical representation. In [14], a mapping approach was adopted to observe the periodic response and bifurcation of a segmented linear oscillator. In [15], a mapping structure for discontinuous system was initially proposed; the idea of mapping structure was used to investigate a periodic segmented linear system. In addition, the investigations can serve as examples in [16–18].

In all those works, a continuous mapping method was applied to transform nonsmooth gear system into segmented linear system, which can not explain the nonsmooth dynamic behavior of gear system completely. A large number of common problems can be described by discrete dynamic systems even if the problems are described by continuous dynamic systems. In this paper, the Poincare section and bifurcation diagram are obtained by numerical simulation, and the dynamic performance of gear transmission system is studied. In this paper, we construct discontinuous mapping, and combining with Floquet theory, we study the local dynamic characteristics of clearance and its front and rear, which reveal the vibration mechanism of gear transmission system in the gap nonsmooth state. The organization of this paper is as follows. Firstly, this paper briefly introduces a gear drive model with the basic dynamic response of a typical gear drive system. Then, the continuity mapping and discontinuity mapping are set up systematically. What is more, the differential inclusion theory and the method of perturbation are adopted to investigate the singularity of the sliding dynamics on separation boundaries, and the periodic response is analyzed by the mapping method. In addition, the discretization is a very important tool for analyzing the stability of the periodic motion in the gear system. The discrete-time shooting method is adopted to calculate the change of the Floquet multiplier. Then, the Floquet theory and the idea of mapping are introduced to give the methods and conditions for judging the periodic response of the system. At last, a summary of this work is presented.

## 2. The Mechanical Model

When both the bearing support of the entire system and the stiffness of the drive shaft are large for the gears in the transmission system, the torsional vibration model can be simplified as the form shown in Figure 1.

If the vibration between teeth is ignored in the gear system, the time-varying stiffness and static transmission

error of the basic oscillation frequency are equal to the gear meshing frequency:

$$\omega_h = n_p \omega_p = n_g \omega_g \quad (1)$$

$n_p$  and  $n_g$  represent the number of teeth in the driving wheel and the driven wheel, respectively. This means that the time-varying stiffness and static transmission error of the system can be expressed in a form of Fourier to Fourier series:

$$k(t) = k_0 + \sum_{m=1}^{\infty} k_m \cos(m\omega_h t + \varphi_m t) \quad (2)$$

Through Newton's theorem, the balance equation of driving wheel and driven wheel can be written as

$$I_p \ddot{\theta}_p + CR_p [R_p \dot{\theta}_p - R_g \dot{\theta}_g - \dot{e}(t)] + K(t) R_p f [R_p \theta_p - R_g \theta_g - e(t)] = T_p \quad (3)$$

$$I_g \ddot{\theta}_g - CR_g [R_p \ddot{\theta}_p - R_g \dot{\theta}_g - \dot{e}(t)] - K(t) R_g f [R_p \theta_p - R_g \theta_g - e(t)] = -T_g \quad (4)$$

$I_p$  and  $I_g$  are, respectively, the rotational inertia of the driving gear and the driven gear,  $\theta_p$  and  $\theta_g$  are, respectively, the angular displacement of driving gear and driven gear,  $R_p$  and  $R_g$  are, respectively, the radius of base circle of driving gear and the driven gear, and  $T_p$  and  $T_g$  are, respectively, the load torque of driving wheel and wheel. In addition,  $k(t)$  is the time-varying meshing stiffness,  $e(t)$  is the transmission error, and  $c$  is the mesh damping.

By assuming that  $x = R_p \theta_p - R_g \theta_g - e(t)$ , (3) and (4) can be transformed as

$$m_e \ddot{x} + c \dot{x} + k(t) f(x) = F_{av} + F_e \quad (5)$$

$$m_e = I_p I_g / (I_g R_p^2 + I_p R_g^2); F_e = -m_e \ddot{e}(t); F_{av} = m_e * (R_p T_p / I_p + R_g T_g / I_g).$$

Because the time-varying stiffness and static transmission error of the basic oscillation frequency are equal to the gear meshing frequency  $\omega_h$ , the mesh stiffness and the static transmission error terms can be expressed in the form of Fourier series. Taking the first harmonic,

$$\begin{aligned} k(t) &= k_0 + k_1 \cos(\omega_h t), \\ e(t) &= e_m \cos(\omega_h t + \varphi_e) \end{aligned} \quad (6)$$

$k_0$  is the average stiffness, and  $k_1$  is the fluctuation amplitude. Assuming that  $\tau = \omega_0 t$ ,  $\omega_0 = \sqrt{k_0/m_e}$ ,  $\xi = c/2\sqrt{m_e k_0}$ ,  $k(\tau) = k(t)/k_0$ ,  $\omega = \omega_h/\omega_0$ ,  $u(\tau) = x(t)/b$ , and replacing  $\tau$  with  $t$ , then the dynamic model can be simplified as follows:

$$\begin{aligned} \ddot{u} + 2\xi \dot{u} + k(t) f(u) &= f_{av} + f_e \omega^2 \cos(\omega t + \varphi), \\ e(t) &= e_m \cos(\omega_h t + \varphi_e) \end{aligned} \quad (7)$$

And  $f_{av} = F_{av}/bk_0$ ,  $f_e = e_m/b$ ,  $k(t) = 1 + k_1 \cos(\omega t)$ ,

$$f(u) = \begin{cases} u-1 & u \geq 1 \\ 0 & -1 \leq u \leq 1 \\ u+1 & u \leq -1 \end{cases} \quad (8)$$

From (7), the mechanical model is set up. Because the gear system is a typical nonsmooth system, the previous method about smooth is not applicable. Therefore, a mapping method is utilized to analyze the nonsmooth system.

### 3. The Construction of Mapping

For the gear model in this paper, due to the backlash, time-varying stiffness, and static transmission error, a variety of complex motion patterns may occur between the driving wheel and the driven wheel, so it is necessary to establish different mappings to study each movement. There are three main cases and corresponding mapping methods.

(1) *The Meshing State.* In this case, the system flow does not pass through the constraint surface. But in a smooth area, the operating state of the system is continuous and smooth, and it can be analyzed by continuous smooth theory.

(2) *The Collision State.* In this case, the system flow moves from one subinterval through the constraint surface to another subinterval. The Jacobi matrix of the system has a jump when the flow crosses over the constraint surface. A discontinuous mapping is necessary to compensate for the system flow jump, and then the composite mapping method can be used to analyze the whole system.

(3) *The Edge State.* In this case, the teeth of driving wheel are in contact with the teeth of driven wheel at a relative zero speed, which is a critical situation. The system flow is tangent to a constraint in a subinterval. Edge theory can be used to study this condition; besides the discontinuous mapping is used to analyze the local characteristics.

**3.1. The Basic Mapping.** For the gear pair system (7), the phase space is divided into three subdomains by two separation boundaries and the corresponding phase space is defined as

$$\begin{aligned} D_1 &= \{(u, \dot{u}) \mid u \in (1, \infty), \dot{u} \in (-\infty, +\infty)\} \\ D_2 &= \{(u, \dot{u}) \mid u \in (-1, 1), \dot{u} \in (-\infty, +\infty)\} \\ D_3 &= \{(u, \dot{u}) \mid u \in (-\infty, -1), \dot{u} \in (-\infty, +\infty)\} \end{aligned} \quad (9)$$

The two constraint surfaces are defined as

$$\begin{aligned} D_{12} &= \{(u, \dot{u}) \mid u = 1, \dot{u} \in (-\infty, +\infty)\} \\ D_{23} &= \{(u, \dot{u}) \mid u = -1, \dot{u} \in (-\infty, +\infty)\} \end{aligned} \quad (10)$$

In order to establish the mapping, the two constraints can be further divided,  $D_{12} = \partial D_{12} \cup \partial D_{21} \cup (1, 0)$ ,  $D_{23} = \partial D_{23} \cup \partial D_{32} \cup (-1, 0)$ , and the four subsets are defined as

$$\begin{aligned} \partial D_{12} &= \{(u, \dot{u}) \mid u = 1, \dot{u} < 0\} \\ \partial D_{21} &= \{(u, \dot{u}) \mid u = 1, \dot{u} > 0\} \\ \partial D_{23} &= \{(u, \dot{u}) \mid u = -1, \dot{u} < 0\} \\ \partial D_{32} &= \{(u, \dot{u}) \mid u = -1, \dot{u} > 0\} \end{aligned} \quad (11)$$

From the four subsets, all the six basic mappings are defined as shown in Figure 2.

$$\begin{aligned} P_1: \partial D_{21} &\longrightarrow \partial D_{12}, \\ P_2: \partial D_{21} &\longrightarrow \partial D_{23}, \\ P_3: \partial D_{23} &\longrightarrow \partial D_{32}, \\ P_4: \partial D_{32} &\longrightarrow \partial D_{21}, \\ P_5: \partial D_{12} &\longrightarrow \partial D_{21}, \\ P_6: \partial D_{32} &\longrightarrow \partial D_{23} \end{aligned} \quad (12)$$

**3.2. Discontinuous Mapping.** Discontinuous mapping is a conversion relationship that represents the flow of the system between two adjacent subintervals. This transformation is to compensate for the discontinuity of the system flow at the constraint surface. Considering the gear pair system in this paper, it is used to compensate for the discontinuity of the teeth during the transition between the disengaged state and the meshing state. The motion between the driving wheel teeth and the driven wheel teeth mainly includes three cases; the relationship between the system flow and the constraint surface is different from the cases (2) and (3), which are the collision state and the edge state. Therefore, it is necessary to introduce two types of discontinuous mappings, which are noncritical discontinuous mapping and critical discontinuous mapping.

The noncritical discontinuous mapping is to compensate for the discontinuity of the system's flow through the constraint surface. The figure is shown in Figure 3.

$t_p$  is the time that the undamaged line  $x(t)$  reaches the interface  $S$ ;  $\bar{t}$  is the time that the disturbed trajectory reaches the constraint surface  $S$ ;  $\delta x_0 = \bar{x}_0 - x_0$  is the initial disturbance value;  $\delta x_{p-} = \bar{x}(\bar{t}_p) - x(\bar{t}_p)$  represents the disturbance value in the subspace before crossing the boundary  $D_-$ ;  $\delta x_{p+} = \bar{x}(\bar{t}_p) - x(\bar{t}_p)$  is the disturbance value in the subspace after crossing the boundary  $D_-$ . Assuming that  $\delta x_{p+} = S_{21} \delta x_{p-}$ ,  $S_{21}$  represents the transition from the subspace  $D_-$  across the

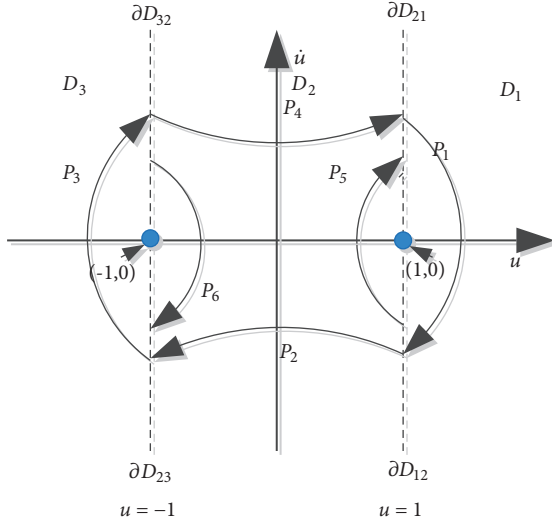


FIGURE 2: The basic mapping.

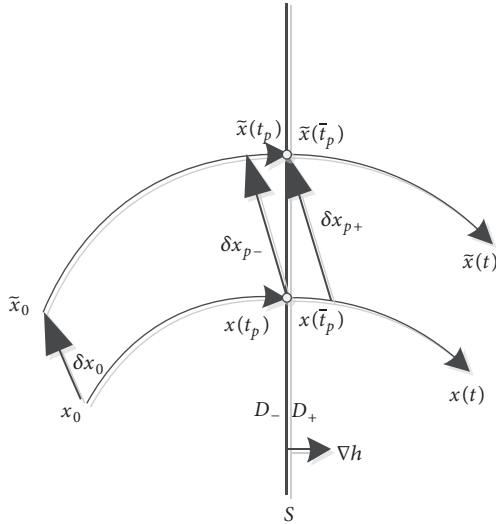


FIGURE 3: The noncritical discontinuous mapping.

interface to the subspace  $D_+$ . Make the trajectory  $\delta x_{p+}$  in front of  $t_p$  the first-order Taylor expansion.

$$\begin{aligned}
 \delta x_{p+} &= \tilde{x}(\bar{t}_p) - x(\bar{t}_p) \\
 &\approx (\tilde{x}(t_p) + f_{p-}\delta t) - (x(t_p) + f_{p+}\delta t) \\
 &\approx (\tilde{x}(t_p) - x(t_p)) + (f_{p-}\delta t - f_{p+}\delta t) \\
 &\approx \delta x_{p-} + (f_{p-} - f_{p+})\delta t
 \end{aligned} \tag{13}$$

$\delta t = \bar{t}_p - t_p$  is the time which  $\tilde{x}(t)$  reaches the constraint surface after the trajectory  $x(t)$  reaches the interface. According to the analysis of the transition point conditions  $h(x) = 0$ ,

$$\delta t = -\frac{\nabla h \delta x_{p-}}{\nabla h f_{p-}} \tag{14}$$

From (13) and (14),

$$\begin{aligned}
 \delta x_{p+} &= \delta x_{p-} + (f_{p-} - f_{p+})\delta t \\
 &= \delta x_{p-} + (f_{p-} - f_{p+})\left(-\frac{\nabla h \delta x_{p-}}{\nabla h f_{p-}}\right) \\
 &= \left(I + \frac{(f_{p+} - f_{p-})\nabla h}{\nabla h f_{p-}}\right)\delta x_{p-}
 \end{aligned} \tag{15}$$

Then

$$S_{21} = I + \frac{(f_{p+} - f_{p-})\nabla h}{\nabla h f_{p-}} \tag{16}$$

If it is reversible, then

$$S_{21} = I + \frac{(f_{p+} - f_{p-})\nabla h}{\nabla h f_{p-}} \tag{17}$$

Equations (16) and (17) are the noncritical discontinuous mapping. When the state of motion of the gear system transitions between teeth and meshing happens, it is necessary to introduce the above discontinuous mapping.

The critical discontinuous mapping is to compensate for discontinuities when the system flow near the edge of the wipe traverses the interface.

The discontinuous mapping of the critical situation is the discontinuous mapping when the edge is bifurcated. For the vector field segmented smooth system, the vector field is given as follows:

$$\dot{X} = \begin{cases} F_1(x), & H(x) < 0 \\ F_2(x), & H(x) > 0 \end{cases} \tag{18}$$

$$X \in \mathbb{R}^n, F_i : \mathbb{R}^n \mapsto \mathbb{R}^n, H : \mathbb{R}^n \mapsto \mathbb{R}$$

$i = 1, 2$ . Define the switching plane or interface as follows:  $\Sigma = \{x \in \mathbb{R}^n \mid H(x) = 0\}$ . The switching surface corresponds to the constraint surface of the model. The interface divides the phase space of the system into two parts,  $S^- = \{x \in \mathbb{R}^n \mid H(x) < 0\}$ ,  $S^+ = \{x \in \mathbb{R}^n \mid H(x) > 0\}$ . Assuming that, in  $S^-$ , the motion is determined by the flow  $\Phi_1(t)$ ; in  $S^+$ , the motion is determined by the flow  $\Phi_2(t)$ . The phase space is shown in Figure 4.

If bifurcation occurs in the system at the edge of  $(x^*, t^*)$ , it should meet the analytical conditions:

$$H(x^*) = 0,$$

$$\nabla H(x^*) \neq 0$$

$$\left\langle \nabla H(x^*), \frac{\partial \phi_i}{\partial t}(x^*, t^*) \right\rangle = \langle \nabla H, F_i \rangle = 0 \tag{19}$$

$$\begin{aligned}
 &\left. \frac{d^2}{dt^2} H(\phi_i(x^*, t^*)) \right|_{X=X^*, t=t^*} \\
 &= \left\langle \nabla H, \frac{\partial H}{\partial x} F_i \right\rangle + \left\langle \frac{\partial^2 H}{\partial x^2} F_i, F_i \right\rangle > 0
 \end{aligned}$$

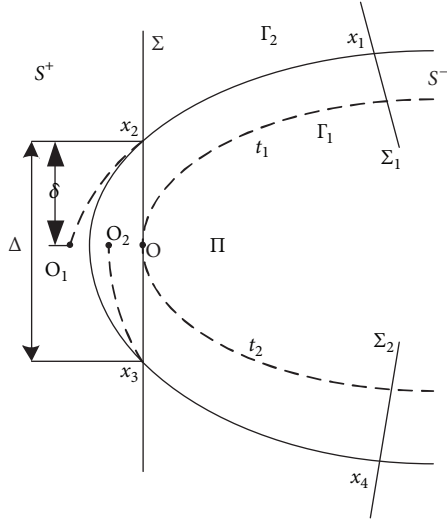


FIGURE 4: The critical discontinuous mapping.

In general, the bifurcation point can be converted to by coordinate transformation. In this paper, the analytical form of the discontinuity map is ignored. We just give the conclusion that the local mapping in the neighborhood of grazing point has a 3/2-type singularity.

**3.3. Local Singularity.** The sliding dynamics along the separation boundaries will be investigated in this section by using the perturbation method and the differential inclusion theory.

For (7), suppose  $x_1 = u$ ,  $x_2 = \dot{u}$ , then

$$\begin{aligned} \dot{x}_1 &= x_2 \\ \dot{x}_2 &= -2\xi x_2 - (1 + k_1 \cos(\omega t)) * f(x_1) + f_{av} \\ &\quad + f_e \omega^2 \cos(\omega t) \end{aligned} \quad (20)$$

where

$$f(x_1) = \begin{cases} x_1 - 1 & x_1 \geq 1 \\ 0 & -1 \leq x_1 \leq 1 \\ x_1 + 1 & x_1 \leq -1, \end{cases} \quad (21)$$

and the system can also be expressed as a uniform

$$\dot{X} = F^{(i)}(x, t, \mu_i), \quad i \in \{1, 2, 3\} \quad (22)$$

where  $F^{(1)}(x, t, \mu_1) = (x_2, -2\xi x_2 - (1 + k_1 \cos(\omega t))(x_1 - 1) + f_{av} + f_e \omega^2 \cos(\omega t))^T$ ,  $F^{(2)}(x, t, \mu_2) = (x_2, -2\xi x_2 + f_{av} + f_e \cos(\omega t))^T$ ,  $F^{(3)}(x, t, \mu_3) = (x_2, -2\xi x_2 - (1 + k_1 \cos(\omega t))(x_1 + 1) + f_{av} + f_e \omega^2 \cos(\omega t))^T$ .

$\mu_i$ ,  $i = 1 \sim 3$ , represent system parameters. In order to obtain the sliding dynamics along the separation boundaries, the differential inclusion theory will be introduced.

For (22), it can also be expressed as

$$\dot{X} \in F(x, t, \lambda), \quad X = (X_1, X_2)^T \in D_i \cup D_j \cup D_{ij} \quad (23)$$

The set-valued vector field  $F(X, t, \lambda)$  is convex and continuous with respect to the parameter  $\lambda$  contained in the closed interval  $[0, 1]$ . The following property holds for the convex set of the vector field.

$$F(x, t, \lambda) = \begin{cases} F^\alpha(x, t, \mu_\alpha) & \lambda = 0 \\ F^0(x, t) & \exists \lambda \in (0, 1) \\ F^\beta(x, t, \mu_\beta) & \lambda = 1 \end{cases} \quad (24)$$

$\alpha, \beta \in \{i, j\}$ ,  $\alpha \neq \beta$ , and  $F^\alpha(x, t, \mu_\alpha)$  and  $F^\beta(x, t, \mu_\beta)$  are the input and output vector fields, respectively.  $F^0(x, t)$  is a vector field along the separation boundary.

From the convexity of the set-valued vector field, we have

$$F^0(x, t) = \lambda F^\beta(x, t, \mu_\beta) + (1 - \lambda) F^\alpha(x, t, \mu_\alpha) \quad (25)$$

The sliding motion is along the separation boundary, which indicates the vector field is along the boundary. So  $n_{D_{ij}}^T F^0(x, t) = 0$  from which we have

$$\lambda = \frac{n_{D_{ij}}^T F^\alpha(x, t, \mu_\alpha)}{n_{D_{ij}}^T [F^\alpha(x, t, \mu_\alpha) - F^\beta(x, t, \mu_\beta)]} \quad (26)$$

For our system, the separation boundaries are  $x_1 \pm 1 = 0$ , so the normal vector of separation boundaries is  $n_{D_{12}} = n_{D_{23}} = (1, 0)^T$ ; then we get

$$\begin{aligned} n_{D_{12}}^T F^{(1)}(x, t, \mu_1) &= n_{D_{12}}^T F^{(2)}(x, t, \mu_2) = x_2 \\ n_{D_{23}}^T F^{(2)}(x, t, \mu_1) &= n_{D_{23}}^T F^{(3)}(x, t, \mu_3) = x_2 \end{aligned} \quad (27)$$

From (26) and (27), we can obtain  $\lambda \rightarrow \infty$ . However, from the convexity, the parameter  $0 < \lambda < 1$  is required. Therefore, a perturbation parameter  $\delta$  is introduced for a new separation boundary  $(x_1 + \delta x_2 = \pm 1)$  near the original boundaries  $x_1 \pm 1 = 0$ ; then

$$n_{D_{12}} = n_{D_{23}} = (1, \delta)^T \quad (28)$$

$$\begin{aligned} n_{D_{12}}^T F^{(1)}(x, t, \mu_1) &\neq n_{D_{12}}^T F^{(2)}(x, t, \mu_2) = x_2 \\ n_{D_{23}}^T F^{(2)}(x, t, \mu_1) &\neq n_{D_{23}}^T F^{(3)}(x, t, \mu_3) = x_2 \end{aligned} \quad (29)$$

Finally, the vector field on the new separation boundaries can be determined as  $F^{(0)}(x, t) = (x_2, -x_2/\delta)^T$ , so the sliding dynamics along the separation boundaries can be investigated by

$$\begin{pmatrix} \dot{x}_1 \\ \dot{x}_2 \end{pmatrix} = \begin{pmatrix} 0 & 1 \\ 0 & -1/\delta \end{pmatrix} \begin{pmatrix} x_1 \\ x_2 \end{pmatrix} \quad (30)$$

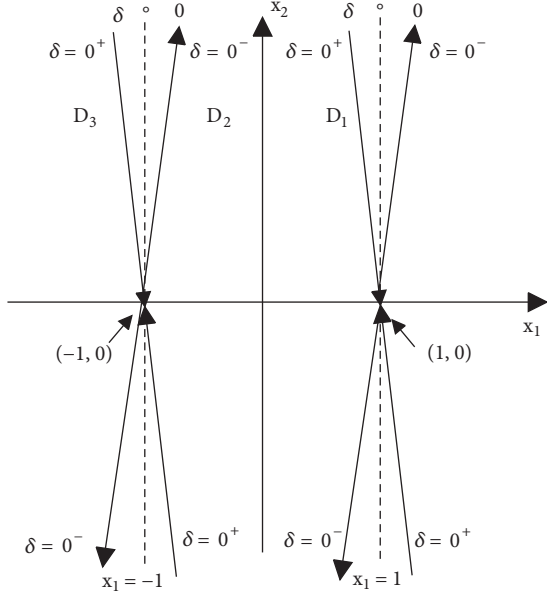


FIGURE 5: Sliding dynamics.

With initial condition  $(\pm 1, x_{20})$  at  $t = 0$ , the foregoing equation gives

$$\begin{aligned} x_1 &= \pm 1 - \delta x_{20} e^{-t/\delta}, \\ x_2 &= x_{20} e^{-t/\delta} \end{aligned} \quad (31)$$

Since  $\delta$  is very small, (31) can approximately describe the sliding dynamics along the separation boundaries. From (30), if  $\delta \rightarrow 0^+$ , all the sliding motions on the two boundaries, respectively, approach the two static balance points (i.e.,  $(\pm 1, 0)$ ) as  $t \rightarrow \infty$ . However, for given  $\delta \rightarrow 0^-$ , the sliding motions on the two boundaries, respectively, go away from the two static balance points. So the two balance points are like saddles as shown in Figure 5. But for  $\delta \equiv 0$ , the sliding dynamics along the separation boundaries  $x_1 \pm 1 = 0$  are undetermined.

From the analytical conditions for grazing motions, the grazing bifurcation conditions on the separation boundaries for the flows of this nonsmooth system are

$$\begin{aligned} x_2 &= 0, \\ \dot{x}_2 &\neq 0 \end{aligned} \quad (32)$$

for  $x_1 = \pm 1$

Therefore, in the neighborhoods of the two equilibrium points, the local topological structures can be sketched in Figure 6.

In order to verify the rationality of the topology, several grazing trajectories will be obtained. Herein, we make use of these grazing trajectories to approximately describe the sliding dynamics along the separation boundaries.

Choose the system parameters as  $\xi = 0.024$ ,  $k_1 = 0.06$ ,  $\omega = 0.61$ ,  $f_e = 0.25$ , where  $f_{av}$  represents the constant forcing parameter and  $\varphi$  denotes the initial phase.

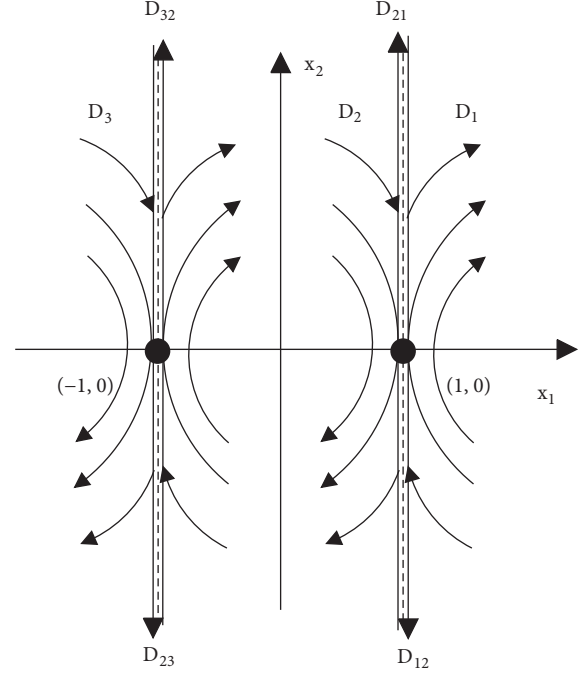


FIGURE 6: Topological structures of the flows.

Consider the parameters  $f_{av} = 0.075$ ,  $\varphi = 4.47$ , initial state  $(1, 0.3)$ ;  $f_{av} = 0.596$ ,  $\varphi = 4.21$ , initial state  $(1, 0.4)$ , respectively. Two grazing trajectories can be obtained as shown in Figure 7. The grazing points are both  $(1, 0)$ . In the neighborhoods of  $(1, 0)$ , the system trajectories conform to the topology above.

Suppose  $f_{av} = 0.075$ ,  $\varphi = 4.47$ , initial state  $(1, 0.3)$ ;  $f_{av} = 0.596$ ,  $\varphi = 4.21$ , initial state  $(1, -0.3)$ , respectively. We can also obtain two grazing trajectories in the points  $(-1, 0)$ ,  $(1, 0)$ , respectively. As shown in Figure 8, they both conform to the topology above.

As shown in Figure 9, several grazing trajectories are obtained to draw on the same coordinates to approximately describe the sliding motions along the separation boundaries and to verify the topology in the neighborhood of grazing points.

#### 4. Analysis of Periodic Response

For the gear transmission system, due to the existence of time-varying period stiffness and periodic excitation, the system must have periodic motion under certain system parameters' combination. Therefore, the external load is used as the conversion parameter, and the periodic response of the system is analyzed by the mapping method.

**4.1. The First Case Periodic Motions.** The system parameter adopts common parameter, which can be accessed from [2, 18]. Select the system parameters as follows:  $\xi = 0.024$ ,  $k_1 = 0.06$ ,  $\omega = 0.61$ ,  $f_e = 0.25$ ,  $f_{av} = 0.25$ . The system flow is always within the range  $u \geq 1$  of intervals  $D_1$  (Figure 2).



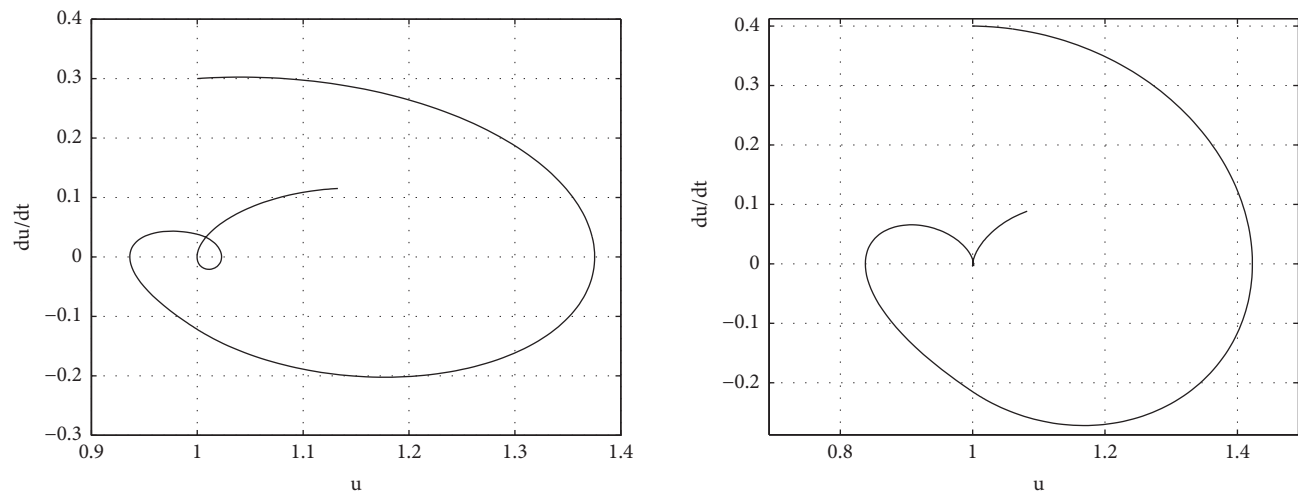


FIGURE 7: Grazing trajectories at (1,0).

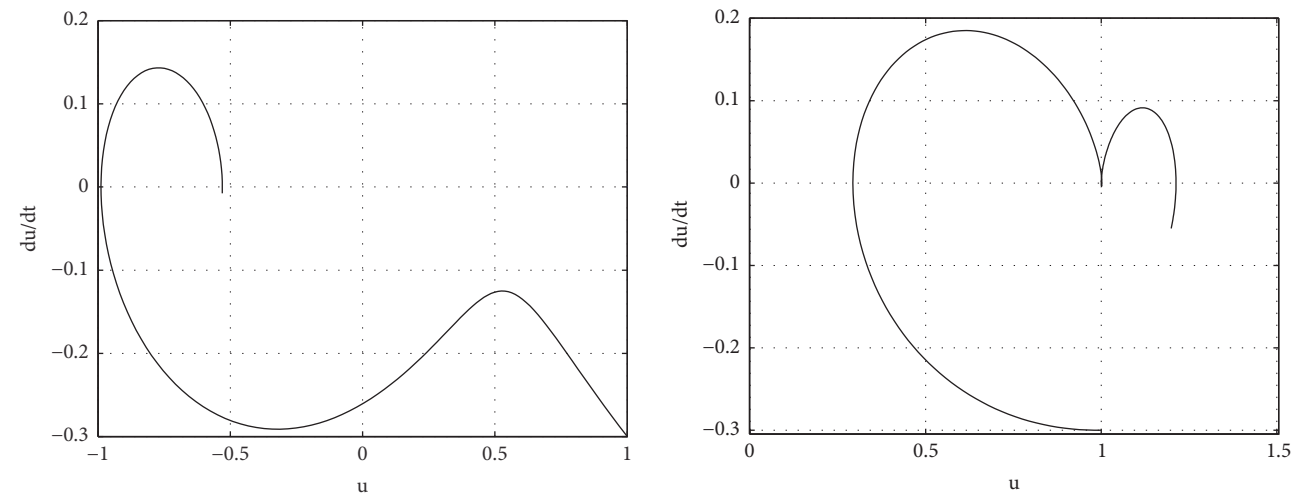


FIGURE 8: Grazing trajectories at (-1,0) and (1,0).

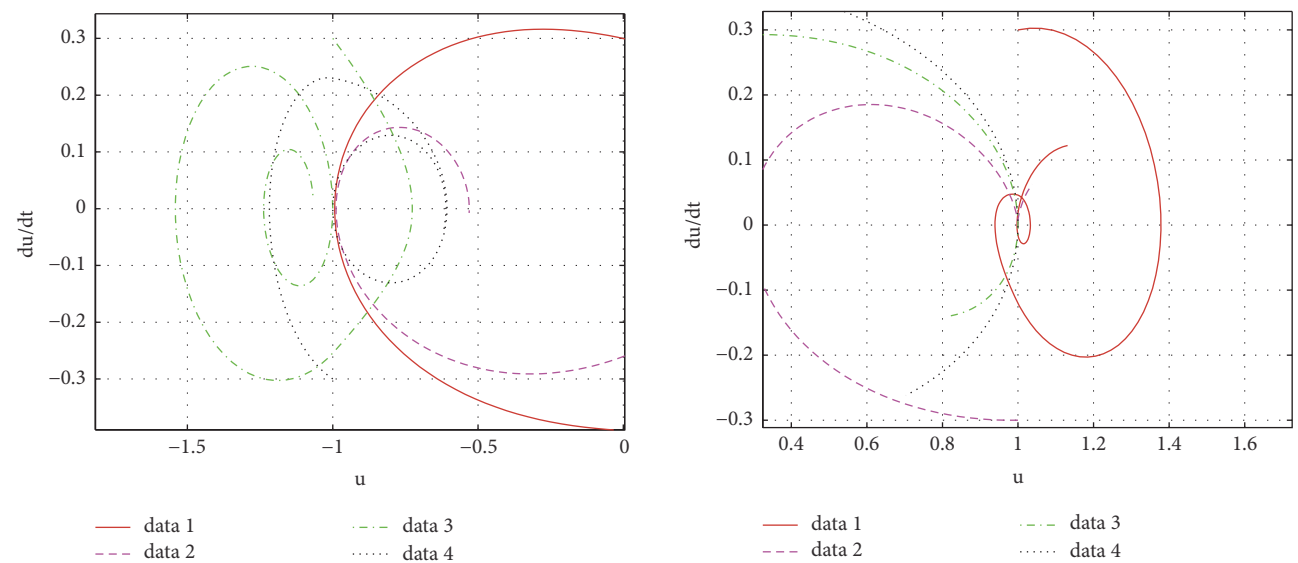


FIGURE 9: Combination of grazing trajectories.

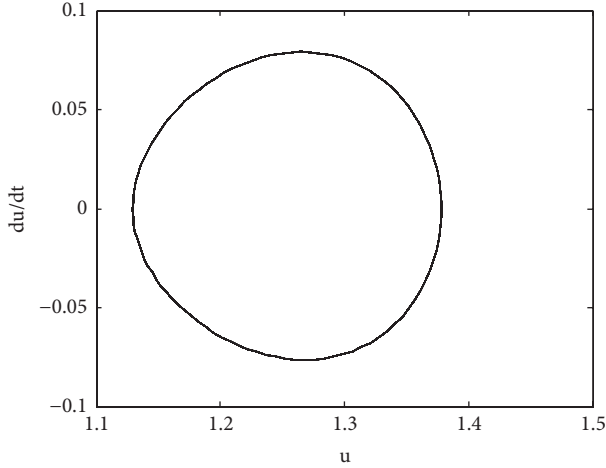


FIGURE 10: Phase diagram of meshing state.

The phase diagram is shown in Figure 10. The dynamics is constrained by the equation:

$$\ddot{u} + 2\xi\dot{u} + k(t)(u - 1) = f_{av} + f_e\omega^2 \cos(\omega t) \quad (33)$$

where  $k(t) = 1 + k_1 \cos(\omega t)$ ;  $f_{av} = F_{av}/bk_0$ ;  $f_e = e_m/b$ .

**4.2. The Second Case Periodic Motion.** For the gear transmission system, the second case periodic motion that corresponds to the collision state of the gear can be divided into

$$f_{p+} : \begin{cases} \dot{x}_1 = x_2 \\ x_2 = -2\xi x_2 - (1 + k_1 \cos(\omega t)) * (x_1 - 1) + f_{av} + f_e\omega^2 \cos(\omega t) \end{cases} \quad (35)$$

In interval  $D_2$ ,

$$f_{p-} : \begin{cases} \dot{x}_1 = x_2 \\ \dot{x}_2 = -2\xi x_2 + f_{av} + f_e\omega^2 \cos(\omega t) \end{cases} \quad (36)$$

According to the noncritical discontinuous mapping,

$$S_{21} = I + \frac{(f_{p+} - f_{p-}) \nabla h}{\nabla h f_{p-}} = I \quad (37)$$

$$S_{12} = S_{21}^{-1} = I \quad (38)$$

Therefore, the periodic mapping is

$$PT = S_{21} \cdot P_5 \cdot S_{12} \cdot P_1 = P_5 \cdot P_1 \quad (39)$$

**4.2.2. Double-Sided Impact Periodic Motions.** When  $f_{av} = 0.233$ , other parameters remain the same. A steady periodic state can be obtained as shown in Figure 13. In this case, the maximum value is bigger than 1 and the minimum value is

two cases: single-sided impact periodic motions and double-sided impact periodic motions.

**4.2.1. Single-Sided Impact Periodic Motions.** When  $f_{av} = 0.223$ , other parameters remain the same. In this case, the maximum value of the corresponding periodic flow is bigger than 1, the minimum value is between the two constraint surfaces  $u = \pm 1$ . The gear system operates in a single-sided impact periodic motions, and the teeth are transitioning between the two states of disengagement and engagement. The phase diagram is shown in Figure 11.

For the convenience of research, assuming the initial state of the periodic motion is a fixed point on the interface  $\partial D_{21}$ , as shown in Figure 12. At this point the system flow consists of two parts; one is in the interval  $D_1$  and the other is in the interval  $D_2$ . For the trajectory in  $D_1$ , the dynamic is constrained by (33), and the corresponding basic mapping is  $P_1$ ; for the trajectory in  $D_2$ , the dynamic is determined by (34), and the corresponding basic mapping is  $P_5$ .

$$\ddot{u} + 2\xi\dot{u} = f_{av} + f_e\omega^2 \cos(\omega t) \quad (34)$$

In this case, the system flow moves through the constraint surface. In order to establish the periodic mapping corresponding to periodic motion, it is necessary to introduce discontinuous mappings  $S_{21}$  and  $S_{12}$  to compensate for the discontinuity of the system flow and then use the mapping compound rule to obtain the periodic mapping  $PT$ .

Suppose  $x_1 = u$ ,  $x_2 = \dot{u}$ ; then the system (7) can be expressed as follows:

In interval  $D_1$ ,

smaller than -1. This state corresponds to the double-sided impact.

As shown in Figure 14, the initial state still selects the fixed point on interface  $\partial D_{21}$ . Adopting the similar method above, the periodic mapping could be obtained as

$$PT = S_{12} \cdot P_4 \cdot P_{23} \cdot P_3 \cdot S_{32} \cdot P_2 \cdot S_{21} \cdot P_1 \quad (40)$$

As  $S_{12} = S_{21} = S_{23} = S_{32} = I$ , then

$$PT = P_4 \cdot P_3 \cdot P_2 \cdot P_1 \quad (41)$$

## 5. Stability Analysis

In this section, these mapping structures will be used to analyze the periodic motion stability of the system through Floquet theory. At the same time, in order to judge whether the system enters the chaotic state, the maximum Lyapunov exponent spectrum of the system is obtained. That paper takes the double-sided impact case as an example to demonstrate the mapping method of stability analysis. Its

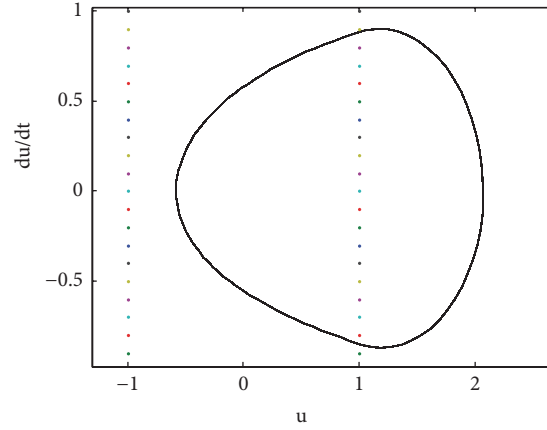


FIGURE 11: Single-sided impact.

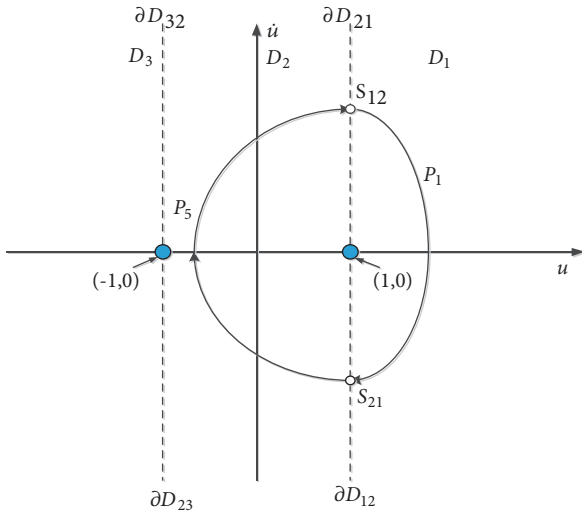


FIGURE 12: The mapping structures.

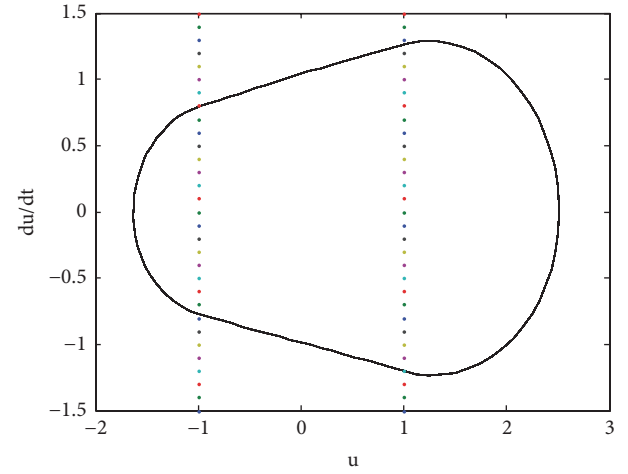


FIGURE 13: Double-sided impact.

corresponding periodic mapping is  $PT = P_4 \cdot P_3 \cdot P_2 \cdot P_1$ . The stability and bifurcation for periodic motion can also be confirmed through the periodic mapping  $PT$  which is corresponding to Jacobi matrix. By the chain rule, the Jacobi matrix can be expressed as follows:

$$DP = DP_4 \cdot DP_3 \cdot DP_2 \cdot DP_1 \quad (42)$$

For  $DP_i$ ,  $i = 1 \sim 4$ , due to the time-varying stiffness of the gear system and backlash,  $DP_i$  has difficulty in getting the analytical form of its system flow, so the analysis of each mapping form can not be got. But they can be obtained through numerical method, such as the shooting method. At the same time, the corresponding Jacobi matrix can be yielded.

Suppose that the Jacobi matrix  $DP$  of periodic motion has been obtained, then the eigenvalues of a fixed point for this periodic mapping can be demonstrated as

$$\lambda_{1,2} = \frac{1}{2} [\text{Tr}(DP) \pm \sqrt{\Delta}] \quad (43)$$

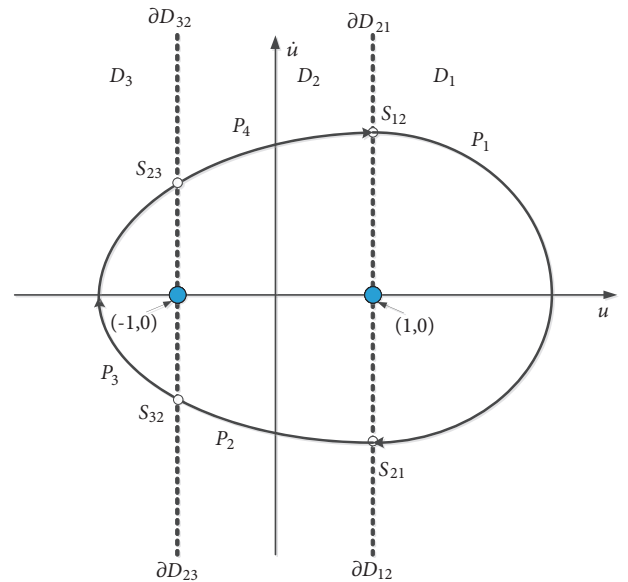


FIGURE 14: The mapping structure.

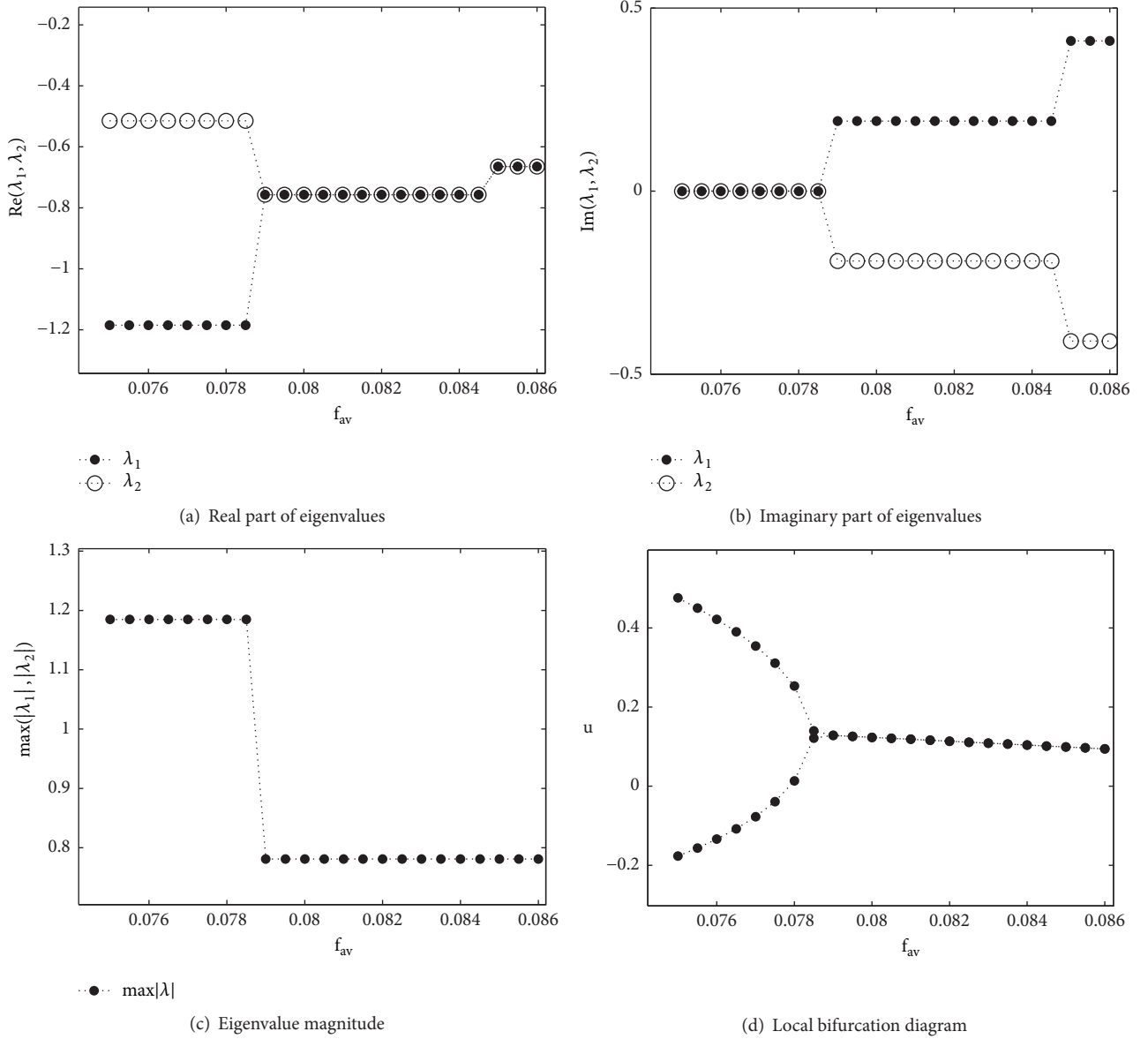


FIGURE 15: Floquet multiplier map and bifurcation diagram.

$\text{Tr}(DP)$  represents the trace of  $DP$ ;  $\text{Det}(DP)$  denotes the determinant of  $DP$ .

$\Delta = [\text{Tr}(DP)]^2 - 4\text{Det}(DP)$ . If  $\Delta < 0$ , (43) can be demonstrated through

$$\lambda_{1,2} = \text{Re}(\lambda) \pm j\text{Im}(\lambda) \quad (44)$$

$$j = \sqrt{-1}; \text{Re}(\lambda) = (1/2)\text{Tr}(DP); \text{Im}(\lambda) = (1/2)\sqrt{|\Delta|}.$$

For  $\lambda_{1,2}$ , the period-1 motion will be stable if they are located in the unit circle. But if one of them is located outside the unit circle, then the period-1 motion will be unstable. This means that only if  $|\lambda_{1,2}| < 1$ , the periodic motion of the system is stable.

If one eigenvalue is -1 and the other is within the unit circle, the periodic doubling bifurcation is going to occur.

If one eigenvalue is +1 and the other is within the unit circle, the saddle-node bifurcation is going to occur.

Therefore, an improved shooting method is adopted to calculate the variation of the Floquet multiplier when the system changes with the external load parameters. The principle of the shooting method is to convert the two-point boundary value problem into the initial value problem. When the shooting method is used to calculate the Floquet multiplier, the Floquet multiplier is discrete and parameterized in the time domain. According to the change of Floquet multiplier, the stability of the system's periodic motion and the way of instability are predicted. The Floquet multiplier map and the corresponding bifurcation diagram in the interval [0.075, 0.086] are also presented as shown in Figure 15.

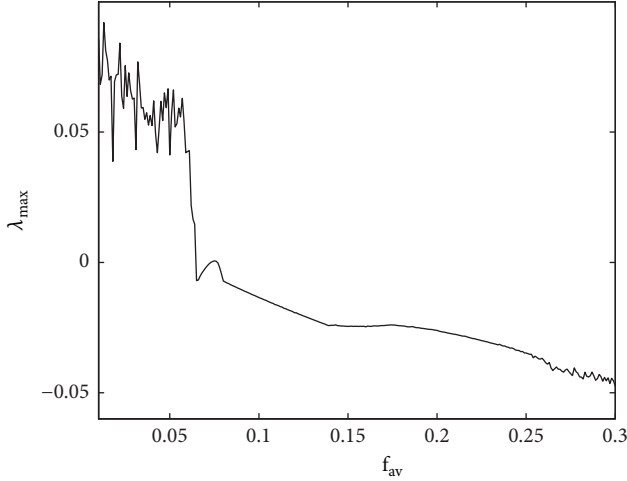


FIGURE 16: The maximum Lyapunov exponent spectrum.

From Figure 15, we can deduce that when  $f_{av} \geq 0.079$  both eigenvalues are located in the unit circle, which implies that corresponding period-1 motion is stable. When  $f_{av}$  is at the vicinity of 0.0785, one of the two eigenvalues jump out the unit circle from -1. Meanwhile the other is still within the unit circle, which indicated the period doubling bifurcation takes place.

By using the Floquet theory, we can merely get the stability and bifurcation of periodic motions. For judging the chaos state, other effective methods need to be introduced. As the Lyapunov exponent spectrum is one of the most precise tools to determine the chaos state, therefore, the maximum Lyapunov exponent spectrum is presented in Figure 16.

From Figure 16, we can deduce that when  $f_{av} \geq 0.06$ , the maximum Lyapunov exponents are negative, which implies the system does not enter the chaos state. When  $f_{av} \leq 0.06$ , the maximum Lyapunov exponents are positive, which implies the system is under chaos state. By comparing the result with the bifurcation diagram and Poincare section, consistent conclusions can be obtained. For the sake of demonstrating this system and ensuring the conclusion above, the system bifurcation of the gear system with external load parameters  $f_{av}$  is shown in Figure 17. Enlarging the 0.06 - 0.08 part of bifurcation diagram, we can get the local bifurcation diagram as demonstrated in Figure 18.

The bifurcation diagram is used in the process of simulation. Bifurcation refers to small and continuous changes in the parameters of the system. As a result, the nature or topological structure of the system suddenly changes.

Poincare is a method for discretizing continuous systems and the Poincare map can replace the  $n$  order continuous system by using the discrete mapping of order  $n - 1$ . The Poincare map is used to reduce the order of the system, and the Poincare map builds a bridge between the continuous system and the discrete system.

In order to demonstrate the transition process in detail, suppose  $f_{av} = 0.08, 0.078, 0.064, 0.0624, 0.058$ , respectively; both the Poincare section and the corresponding phase diagram are gained as demonstrated in Figure 19.

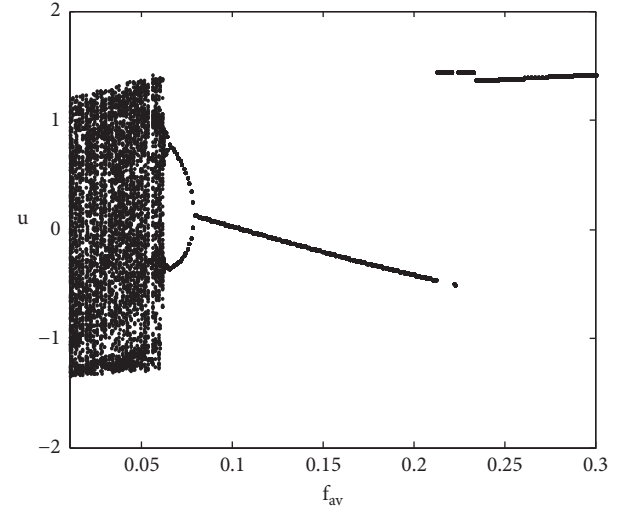


FIGURE 17: Bifurcation diagram.

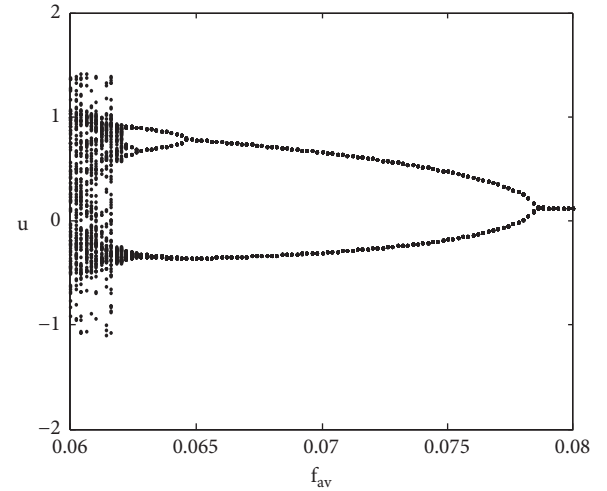


FIGURE 18: Local bifurcation diagram.

## 6. Conclusions

Firstly, for common gear systems, a nonlinear vibration model with backlash, time-varying stiffness, and static transmission error is established. The nonsmooth characteristics of the system are analyzed theoretically. According to the model, the state of motion is summarized into three main cases. For the period motion, the corresponding Poincare mapping is established. In order to analyze the stability of the periodic motion of the system, the discrete-time shooting method was adopted to calculate the variation of the Floquet multiplier. Then, the Floquet theory and the idea of mapping are used to give methods and conditions for judging the stability of the system's periodic response. At the same time, to judge the chaotic state of the system, the maximum Lyapunov exponent of the system is obtained. Finally, in order to verify the rationality of the above method, the global bifurcation diagram of the system is gained. Through the comparison, the same conclusion can be got, the whole process of the system

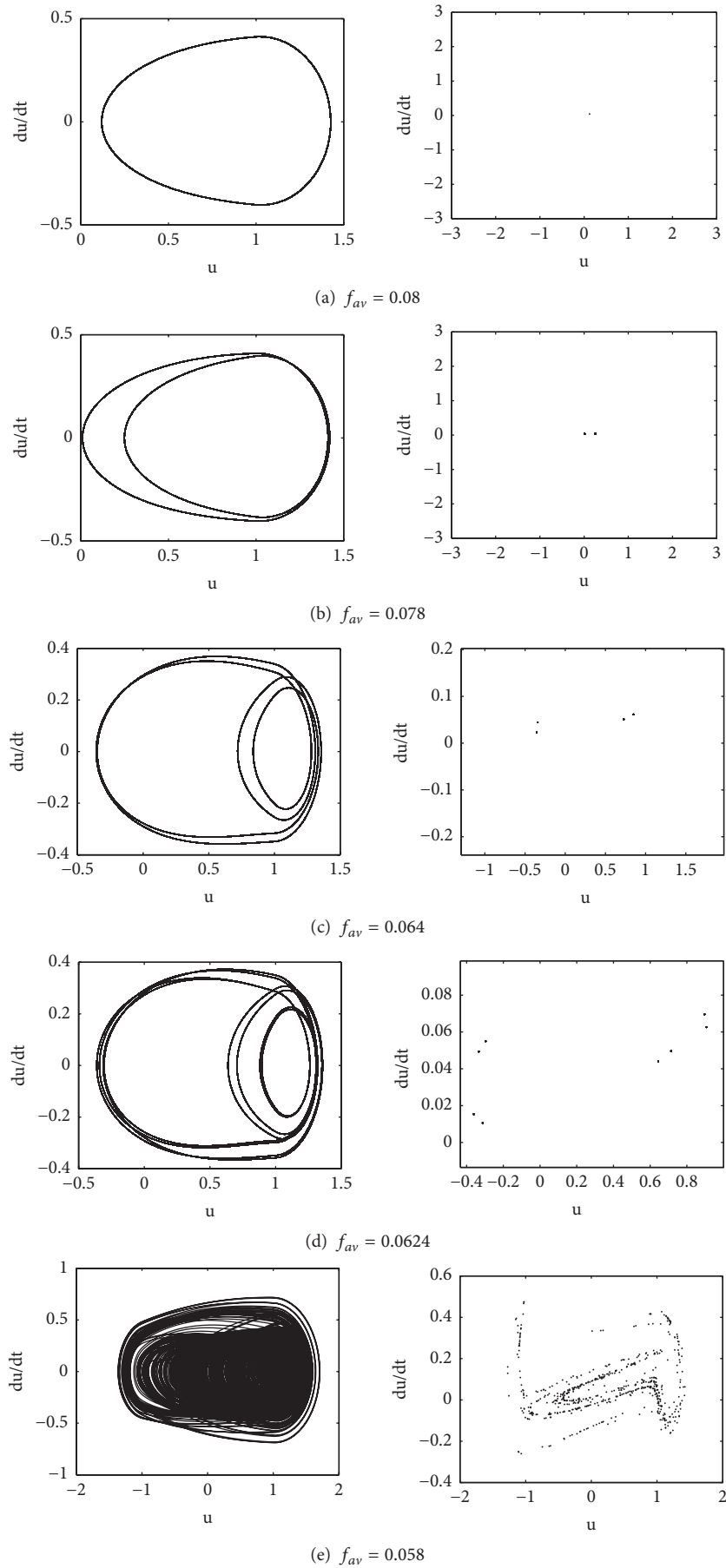


FIGURE 19: Phase diagrams and Poincaré sections.



from the periodical bifurcation to the chaos is given, and a reasonable explanation for the jumping phenomenon in the bifurcation diagram is given.

Through the study of the gear system we can get the following conclusions. When the external load of the gear system is large, it is in a fully engaged state; as the load decreases, the state of motion changes from full meshing to unilateral collisions and bilateral collisions. In addition unilateral collisions and bilateral collisions occur alternately. As the load continues to decrease, the stable periodic motion of the system begins to lose its stability, and the motion state enters chaotic state through periodic bifurcation. This conclusion has important practical value, which can guide us in the actual project to select reasonable load parameters.

As a complex nonlinear system, the gear system not only includes backlash, time-varying stiffness, and static transmission error of these nonsmooth factors, but also includes many other nonsmooth factors. Therefore, how to improve the system's nonsmooth characteristics in the further is an important research direction. In addition, how to avoid chaos by taking effective measures is also a future research tendency.

## Data Availability

The data used to support the findings of this study are available from the corresponding author upon request.

## Conflicts of Interest

The authors declare that they have no conflicts of interest.

## Acknowledgments

This work was supported by Proceedings of the 2017 International Conference on Advances in Construction Machinery and Vehicle Engineering, the China Postdoctoral Science Foundation funded project (Grant no. 2017M620096), and the Natural Science Foundation of Hebei Province, China (Grant no. E2017203144).

## References

- [1] S. Theodossiades and S. Natsiavas, "Non-linear dynamics of gear-pair systems with periodic stiffness and backlash," *Journal of Sound and Vibration*, vol. 229, no. 2, pp. 287–310, 2000.
- [2] S. Wang, Y. Shen, and H. Dong, "Chaos and bifurcation analysis of a spur gear pair with combined friction and clearance," *Jixie Gongcheng Xuebao/Chinese Journal of Mechanical Engineering*, vol. 38, no. 9, pp. 8–11, 2002.
- [3] X.-S. Wang, S.-J. Wu, X.-H. Zhou, and Q.-L. Li, "Bifurcation and chaos in a nonlinear dynamic model of spur gear with backlash," *Zhendong yu Chongji*, vol. 27, no. 1, pp. 53–56, 2008.
- [4] Y. Shen, S. Yang, and X. Liu, "Nonlinear dynamics of a spur gear pair with time-varying stiffness and backlash based on incremental harmonic balance method," *International Journal of Mechanical Sciences*, vol. 48, no. 11, pp. 1256–1263, 2006.
- [5] J.-Y. Tang, W.-T. Chen, S.-Y. Chen, and W. Zhou, "Wavelet-based vibration signal denoising with a new adaptive thresholding function," *Journal of Vibration and Shock*, vol. 28, no. 7, pp. 118–121, 2009 (Chinese).
- [6] A. Kahraman and R. Singh, "Non-linear dynamics of a spur gear pair," *Journal of Sound and Vibration*, vol. 142, no. 1, pp. 49–75, 1990.
- [7] G. W. Blankenship and A. Kahraman, "Steady state forced response of a mechanical oscillator with combined parametric excitation and clearance type non-linearity," *Journal of Sound and Vibration*, vol. 185, no. 5, pp. 743–765, 1995.
- [8] A. Raghothama and S. Narayanan, "Bifurcation and chaos in geared rotor bearing system by incremental harmonic balance method," *Journal of Sound and Vibration*, vol. 226, no. 3, pp. 469–492, 1999.
- [9] J. Wang, J. Zheng, and A. Yang, "An analytical study of bifurcation and chaos in a spur gear pair with sliding friction," *Procedia Engineering*, vol. 31, no. 1, pp. 563–570, 2012.
- [10] A. Kahraman and R. Singh, "Nonlinear dynamic of geared rotor-bearing system with multiple clearances," *Journal of Sound and Vibration*, vol. 144, no. 3, pp. 469–506, 1991.
- [11] C.-W. Chang-Jian, "Strong nonlinearity analysis for gear-bearing system under nonlinear suspension-bifurcation and chaos," *Nonlinear Analysis: Real World Applications*, vol. 11, no. 3, pp. 1760–1774, 2010.
- [12] J. Hartog and S. Mikina, "Forced vibrations with non-linear spring constants," *Journal of Applied Mechanics*, vol. 58, pp. 157–164, 1932.
- [13] S. W. Shaw and P. J. Holmes, "A periodically forced piecewise linear oscillator," *Journal of Sound and Vibration*, vol. 90, no. 1, pp. 129–155, 1983.
- [14] M. Kleczka, E. Kreuzer, and W. Schiehlen, "Local and global stability of a piecewise linear oscillator," *Philosophical Transactions Physical Sciences & Engineering*, vol. 338, no. 1651, pp. 533–546, 1992.
- [15] A. C. J. Luo, "Analytical modeling of bifurcations, chaos and multifractals in nonlinear dynamics," 1996.
- [16] A. B. Nordmark, "Non-periodic motion caused by grazing incidence in an impact oscillator," *Journal of Sound & Vibration*, vol. 145, no. 2, pp. 279–297, 1991.
- [17] B. Blazejczyk, "Dynamics of a two-degree-of-freedom cantilever beam with impacts," *Chaos Solitons & Fractals*, vol. 40, no. 4, pp. 1991–2006, 2009.
- [18] G. W. Luo, X. H. Lv, and Y. Q. Shi, "Vibro-impact dynamics of a two-degree-of freedom periodically-forced system with a clearance: diversity and parameter matching of periodic-impact motions," *International Journal of Non-Linear Mechanics*, vol. 65, no. 4, pp. 173–195, 2014.